1-1-2018

Functional Study Of Smyd2 Glutathionylation In Cardiomyocytes

Dhanushka Nalin Perera Munkanatta Godage
Wayne State University,

FUNCTIONAL STUDY OF SMYD2 GLUTATHIONYLATION IN CARDIOMYOCYTES

by

DHANUSHKA MUNKANATTA GODAGE

DISSERTATION

Submitted to the Graduate School

of Wayne State University,

Detroit, Michigan

in partial fulfillment of the requirements

for the degree of

DOCTOR OF PHILOSOPHY

2018

MAJOR: CHEMISTRY (Biochemistry)

Approved By:

_____

Advisor Date

_____

_____

_____

DEDICATION

This dissertation is dedicated to my parents, Chandrawathie Perera and Banduwardana Perera, my wife Sachini and daughter Sanaya for their enormous love, support and commitments

ACKNOWLEDGEMENTS

First I would like to thank my advisor Prof. Young-Hoon Ahn, for his guidance and support given during my graduate studies. I was fortunate to spend several years under his mentorship and I am grateful to him for giving me the opportunity to work on different projects, learn many new techniques and broaden my knowledge.

I would like to thank my departmental committee members, Prof. Ashok Bhagwat and Prof. Stanislav Groysman, for being helpful all the time and giving valuable critique on my work. I would also like to thank my non-departmental committee member Prof. Zhe Yang for inspiring me to start my dissertation project and for his feedbacks and suggestions.

I would like to thank all the current members of Ahn lab, Harshani Sewvandi, Maheeshi Abeywardana, Garret VanHecke, Shima Nagi, Adeleye Adwale, Dhanushika Kukulage and Iftekher Mahmud for their great friendship and always being supportive. I would also like to thank past members of Ahn lab, Dr. Kusal Samarasinghe, Dr. Dilini Kekulandara and Dr. Fidelis Ndombera for helping me in several ways during my PhD.

I would like to thank the staff of Department of Chemistry for their support and would like to convey my special gratitude to Melissa Barton who helped me during a tough time in the start of my PhD. I am grateful to Prof. Phillip Pellet, Prof. Jian-Ping Jin, Prof. Karin Przyklenk, Dr. Charles Chung and Dr.Hanzhong Feng at Wayne State University, School of Medicine for allowing me to work in their labs and use their equipment. I would like to thank the staff of the Lumigen instrument center and MICR core, especially Daniel DeSantis and Linda Mayernik for training me and for their help

given and also Dr. Bhagwat's lab and Dr. Honn’s lab for sharing equipment and material.

None of my success would have been possible without my beloved mother Mrs. Chandrawathie Perera. I would like to thank her for the endless love and for the sacrifices she made to shape me who I am today. Also I would like to thank my father Mr. Banduwardana Perera and brother Mr. Buddhike Prabath Perera for their continuous love and support given. I am grateful to my father-in-law Mr. Hemantha Siriwardena for helping me during my graduate studies by taking care of my daughter. I am grateful to my wife Sachini Siriwardena for her endless love, support and encouragement. Her continuous motivation has helped me to achieve the best in my life. Also I would like to thank my daughter Sanaya, for giving me happiness and invaluable love during stressful periods in my life. Finally, I would like to thank all my relatives, teachers and friends for their love, support and encouragement.

TABLE OF CONTENTS

LIST OF FIGURES

LIST OF ABBREVIATIONS

mROS : Mitochondrial reactive oxygen species

GSH : Glutathione

Cys : Cysteine

ATP : Adenosine triphosphate

Fn-3 domain : Fibronectin type III-like domain

Ig domain : Immunoglobulin-like domains

CARP : Cardiac ankyrin repeat protein

DARP : Diabetes-related ankyrin repeat protein

Ankrd2 : Ankyrin repeat domain-containing protein 2

SMYD2 : SET and MYND-containing lysine methyltransferase 2

SAM : S-adenosylmethionine

SAH : S-adenosylhomocysteine

TPR : Tetratricopeptide like domain

HSP90 : Heat shock protein 90

pRb : Retinoblastoma protein

ERα : Estrogen receptor α

TnC : Troponin C

TnI : Troponin I

TnT : Troponin T

NADPH : Nicotinamide adenine dinucleotide phosphate

ROS : Reactive oxygen species

MMP-2 : Matrix metalloproteinases 2

TCA : Tricarboxylic acid (TCA) cycle

ANT : Adenine nucleotide translocator

NADH : Nicotinamide adenine dinucleotide

FADH : Flavin adenine dinucleotide

ETC : Electron transport chain

OXPHOS : Oxidative phosphorylation

MnSOD : Manganese superoxide dismutase

SOD : Superoxide dismutase

GPx : Glutathione peroxidase

H_2O_2 : Hydrogen peroxide

PARP : Poly (ADP-ribose) polymerase

GSK-3β : glycogen synthase kinase-3β

RNS : Reactive nitrogen species

GSSG : Oxidized glutathione

GSNO : S-nitrosoglutathione

GSTP1 : Glutathione s-transferase pi 1

GSTO1 : Glutathione s-transferase omega-1

Grx : Glutaredoxin

GR : Glutathione reductase

PTP1B : Protein-tyrosine phosphatase 1B

Srx : Sulfiredoxin

PON1 : HDL-associated paraoxonase 1

PKA : Protein kinase A

DTT : Dithiothreitol

LC/MS : Liquid chromatography mass spectrometry

CDNB : 1-Chloro-2,4-dinitrobenzene

G-SDNB : Glutathione-2, 4-Dinitrobenzene

MRM : Multiple reaction mode

I-AM : Iodoacetamide

THPTA : Tris (3-hydroxypropyltriazolylmethyl) amine

CHCA : α-cyano-hydroxycinnamic acid

AMA : Antimycin A

MHC : Myosin heavy chain

PEG : Polyethyleneglycol

Ag II : Angiotensin II

GAPDH : Glyceraldehyde 3-phosphate dehydrogenase

CHAPTER 1: INTRODUCTION

Heart failure is a leading cause of mortality in America, accounting for 375,000 annual deaths (Figure 1.1)[1]. Heart failure frequently results from coronary artery disease with myocardial ischemia in which mitochondrial reactive oxygen species (mROS) strongly contribute to cardiac dysfunction[2, 3]. Notably, mROS are emerging as important signaling molecules that strongly influence the sarcomere, which is a key structural and functional unit of muscle[4]. A high level of mROS is a strong contributor for cardiac hypertrophy while a low level of mROS regulates calcium signaling and muscle contraction[5]. This complex role of mROS is largely mediated by protein oxidative modifications, including glutathionylation that is disulfide bond formation of protein Cys residue with intracellular glutathione (GSH)[6]. However, the identity of proteins that are susceptible to glutathionylation in response to mROS and their roles in regulating sarcomere stability and integrity remain largely unknown, which is crucial for understanding the complex role of mROS in cardiac muscle.

1.1 The structure of the cardiac muscle

Human body contains three major muscles including skeletal, smooth and cardiac muscle. Cardiac muscle forms the wall of the heart and it is a striated muscle known as myocardium. Cardiac muscle contains bundles of muscle fibers and numerous myofibrils join together to form a muscle fiber. Structural organization of Myosin thick and actin thin filaments in myofibrils provides the characteristic striation pattern for the cardiac muscle fibers (Figure 1.1a)[7].

a

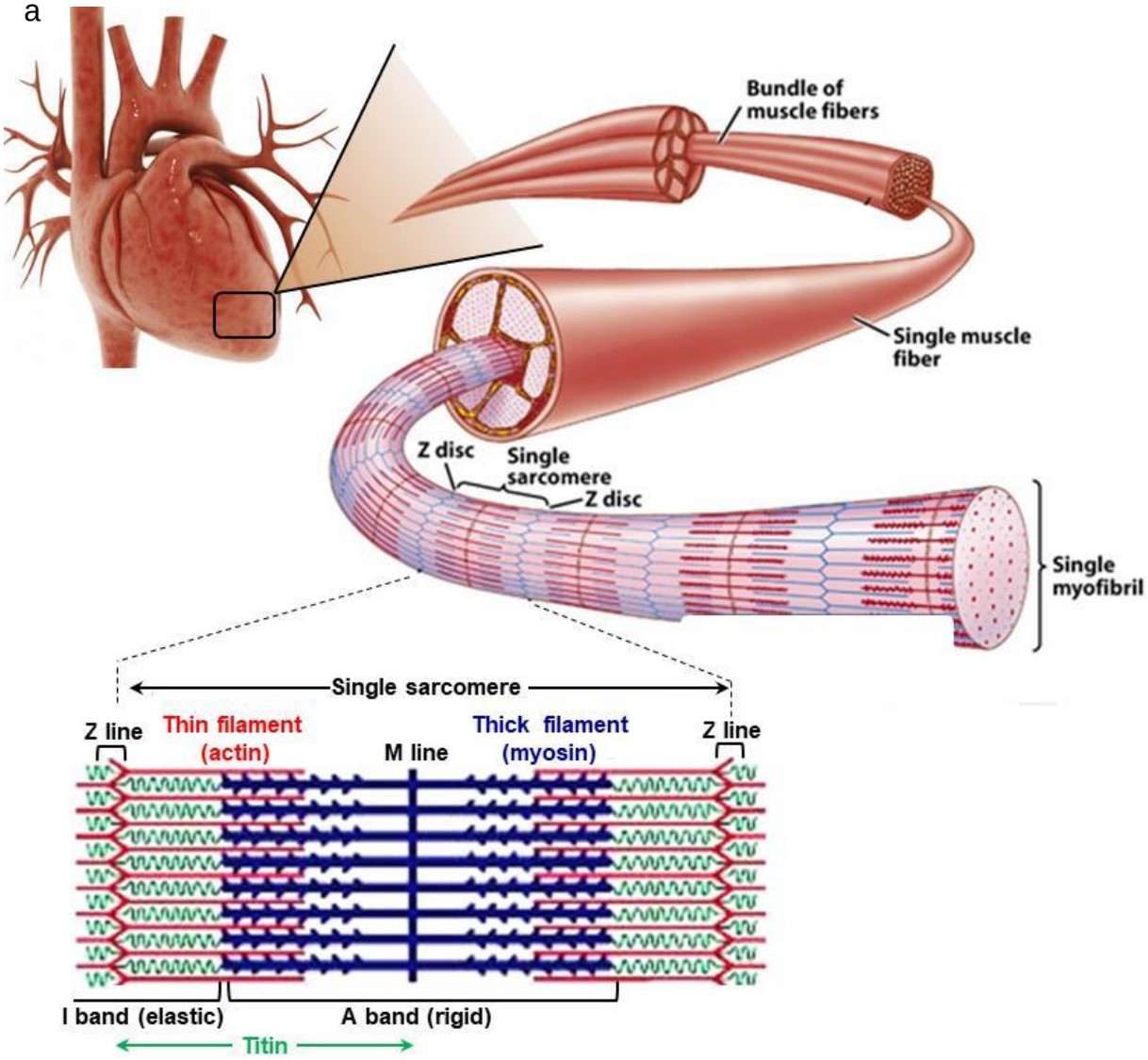
Bundle of muscle fibers
Single muscle fiber
Z disc
Single sarcomere
Z disc
Single myofibril
Single sarcomere
Z line
Thin filament (actin)
M line
Thick filament (myosin)
Z line
I band (elastic)
A band (rigid)
Titin

b

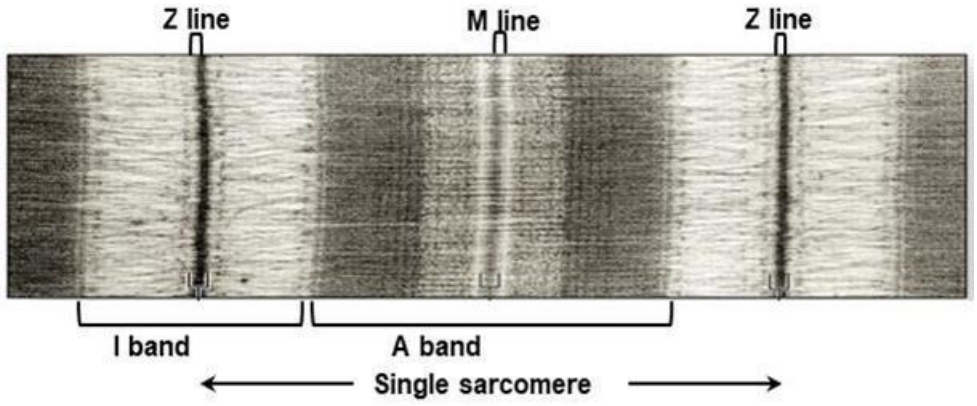
Z line
M line
Z line
I band
A band
Single sarcomere

Figure 1.1. Composition and functional subunits in cardiac muscle. (**a**) Organization of cardiac muscle from muscle fibers and myofibrils. (**b**) A basic contractile unit of striated muscle known as sarcomere which is made up with mainly from actin, myosin and titin proteins. Highly organized sarcomere includes several important regions including Z line which represents the edges of one sarcomere, M line which forms the middle point of sarcomere, elastic I band region which includes mainly actin thin filaments and rigid A band mostly comprise with myosin thick filaments. (**c**) Electron micrograph picture of a myofibril. Light color region of sarcomere includes actin thin filament and dark color region is an overlap of both actin and myosin filaments. Figure adapted from reference (10) with permission from copyright clearance center.

1.2 Sarcomere: the basic contractile unit of the cardiac muscle

Muscle fiber (myocytes) is composed of linear and cylindrical contractile myofibrils that are made of repeated sarcomeres, a basic contractile unit of striated muscle[8]. Sarcomere has a highly organized structure that is assembled by multiple sarcomeric proteins, including actin, myosin, and titin (Figure 1.1a). Notably, multiple proteins are assembled to form the remarkably regular architecture of sarcomeres. I-band (light color area in myofibrils) (Figure 1.1b) is an elastic region mostly comprised of actin thin filament that alters the sarcomere length during contraction and relaxation[9, 10]. Specifically, A-band (dark color area in myofibrils) (Figure 1.1b) is a segment where myosin (thick) filaments slide over actin (thin) filaments for contraction. Titin extends from Z line to the M line of the sarcomere and interacts with multiple sarcomeric proteins in both A-band and I-band for elastic, architectural and signaling function. Z-disk forms the border in sarcomere while crosslinking titin and actin filaments (Figure 1.1a). Alpha actinin is a key structural protein, important for stability of Z disk in sarcomere and holds the N terminal region of titin. Myomesin and C-protein are major components in M line, a middle point of sarcomere, holds the both myosin thick filament as well as C-terminal region of titin protein[11]. Creatine kinase on M line is important for

ATP production by consuming ADP and phosphocreatine while providing energy needed for sarcomere shortening or myofibril contraction[12].

1.3 Sarcomere shortening and cardiac muscle contraction

According to the actin myosin sliding filament theory, when Ca^{+} concentrations increases up to a certain level, Ca^{+} ions will bind to Troponin and it will induce a morphological change in the troponin structure[13]. This change in shape makes tropomyosin move away from the active site of actin. As a result, myosin filaments form a cross-bridge with actin.

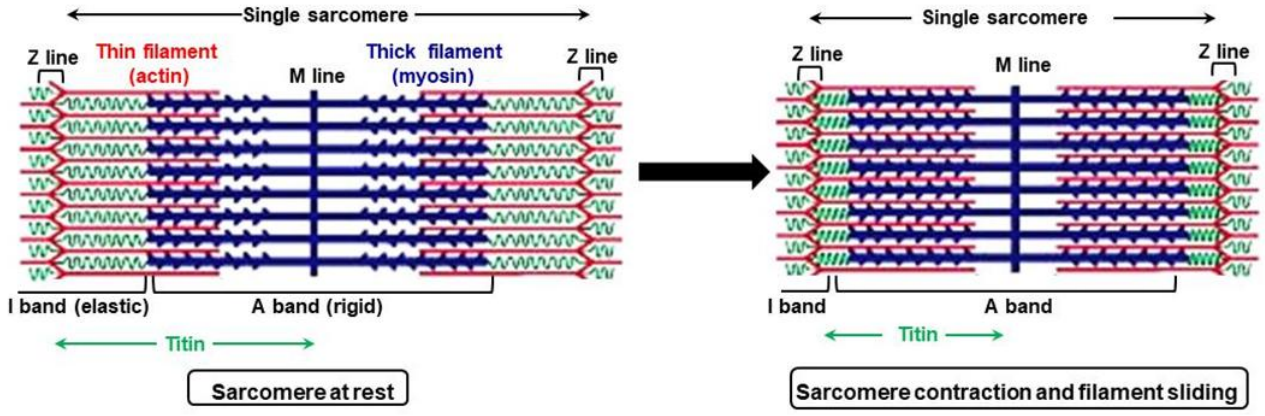

Figure 1.2. Sarcomere shortening caused by Actin myosin sliding filament theory. Myosin (thick) filaments (blue) in A band region of sarcomere slide over actin (thin) filaments (red) in elastic I band region for contraction. Cellular calcium concentration and mitochondrial ATP production is important for this mechanism. Elastic nature of titin protein (green) is important for movement of actin filament on rigid myosin filament.

ATP hydrolysis provides enough energy for myosin to bring the actin filament inwards and consequently muscle will contract (Figure 1.2). This process occurs on the entire myofibril in a muscle cell. Upon the attachment of an ATP molecule to the myosin head, actin bound myosin will detach and the cross-bridge will be broken. Upon hydrolysis of ATP myosin can reattach to the actin binding site further along the actin

filament repeating the continues cycle of “power stroke”[14]. This is also classified as the ratchet mechanism[15]. This actin movement over myosin will continue until there is an enough amount of ATP and calcium[16]. After the impulse stops, actin comes to its’ resting position by lengthening and relaxing the muscle.

1.4 Intrasarcomeric protein

1.4.1 Structural features of titin

Titin, which was initially referred to as connectin, is a giant protein found only in cardiac and skeletal muscles. Titin plays an important role in striated muscle action, especially in cardiac muscles. Located within the sarcomeres, titin binds to and interact with myofilament proteins such as actin and myosin. Therefore, titin is important to maintain structure and architecture of the sarcomere by enabling the correct alignment of actin and myosin. Also it allows the regulation of the length and distensibility of the sarcomere by providing elasticity and this has an impact on both cardiac diastolic and systolic functions[17].

Titin is the largest protein found in mammals. The single gene encoding titin has 363 exons and is located on the long arm of chromosome 2 in the 2q31 region[18]. There are two isoforms of titin found in the heart, which are generated by alternative splicing. Isoforms N2B and N2BA vary in size ranging from 2970 and 3700 kDa. Titin has two major domains, fibronectin type III-like (called Fn-3 domains) domains and immunoglobulin-like (Ig) domains (Ig domains)[19]. It also has an additional kinase domain close to the carboxyl-terminal and several unique-sequence regions.

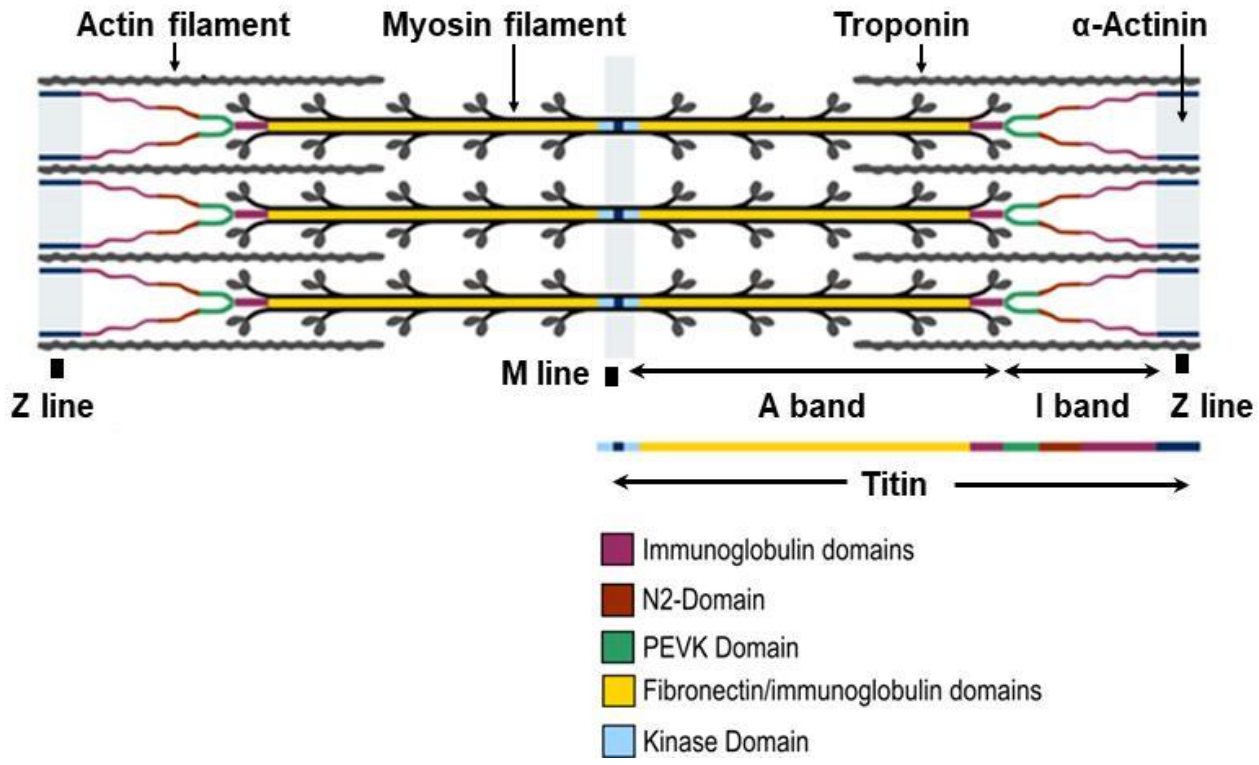

Figure 1.3. Localization of titin within the sarcomere and its domain composition. Titin is an intrasarcomeric protein extending from Z-line to M-line and it has a length around 1 µm. One titin molecule travel over the four sarcomere zones called M-line region, A-band region, I-band region and Z-line region. The amino-terminal is located in the Z-line region and carboxyl-terminal of titin is located in the M line of sarcomere. Titin protein comprise of several domains including Ig domain, N2 domain and PEVK domain are localized in I band region of sarcomere, while largest fibronectin domain is localized in rigid A band region. Figure adapted from reference (20) with permission from copyright clearance center.

Titin is an intrasarcomeric protein extending from Z-line to M-line and it has a length around 1 µm[20]. Therefore it can encompass four sarcomere zones called M-line region, A-band region, I-band region and Z-line region (Figure 1.3). The amino-terminal is located in the Z-line region, whereas the M-line region is in the carboxyl- terminal of the protein. In addition to interacting with other proteins in the Z-line, titin is involved in intracellular signaling, functioning as a biomechanical sensor (Figure 1.3)[21]. The A-band

region, containing a large proportion of titin protein, has a similar composition in the different isoforms (N2B and N2BA). This region of titin is not extensible and it is formed by single repeats of Ig and Fn3 domains representing a component that constitutes the thick filament. In contrast, the very extensible I-band region provides ability to elongate or coil. Therefore it functions as an "elastic" binding between the thick region and the Z-line (Figure 1.4)[22].

There are number of structural elements in the I-band region of titin including Ig domains, PEVK segment and N2 region (Figure 1.3). The sub-region N2 in I-band region can have either N2A or N2B elements creating the two titin isoforms (Figure 1.4)[23]. These 2 elements are considered as signaling hubs which are important to control the mechanical properties of titin protein and N2A element also important for stress-sensing as well. The N2A domain is composed of four immunoglobulin domains (Ig80-83, figure 1.4b red) and a unique sequence region, called N2A-Us (also called UN2A, figure 1.4b blue), between Ig80 and Ig81[24, 25].

N2A domain interacts with several proteins including MARP family protein (CARP, DARP and Ankrd2)[26, 27], calpains and calcium dependent proteases[28, 29]. Recently it was found that UN2A region of N2A domain is important for the interaction with SMYD2 as well[30, 31]. The UN2A element contains 106 amino acid residues. The N2B element has three Ig domains and a unique 572-residue region. The N2A elements are found in both the cardiac and skeletal muscles but the presence of N2B is confined only to cardiac muscles. Both isoforms of titin, N2B and N2BA, are present in cardiac muscle[32] (Figure 1.5a and b) and N2A isoform of titin 9 (Figure 1.5c) is predominant in skeletal muscle[33]. The smaller N2B isoform is 2970 kDa and has only the N2B element.

The larger N2BA consists of both N2B and N2A elements and has a molecular weight ranging from 3200 to 3400 kDa (Figure 1.6b).

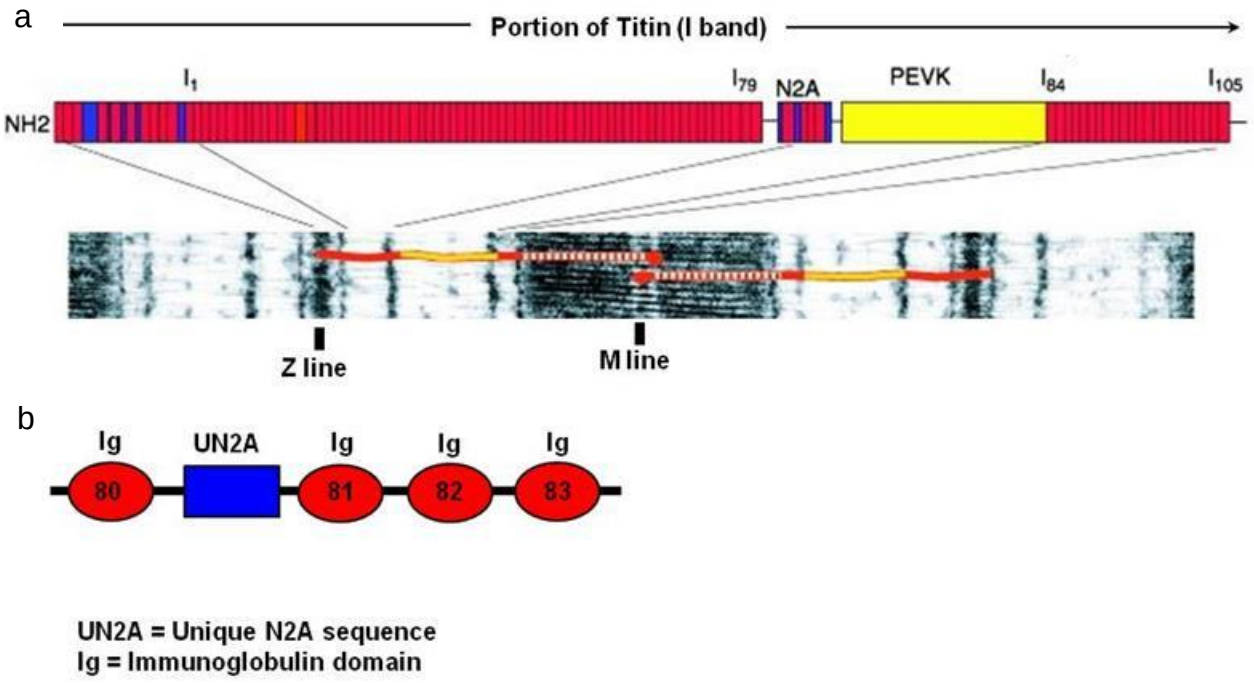

Figure 1.4. Localization of N2A domain in I band region of sarcomere and its domain composition. N2A domain of titin protein is localized in I band region of sarcomere and it is considered as a signaling hub which is important to regulate mechanical properties of sarcomere. The N2A domain, is composed of four immunoglobulin domains (Ig80-83) and a unique sequence region, called N2A-Us (also called UN2A), between Ig80 and Ig81[34, 35]. N2A domain interacts with several proteins including MARP family protein (CARP, DARP and Ankrd2) and calcium dependent proteases. Recently found that UN2A region of N2A domain is important for the interaction with SMYD2 as well. Figure adapted from reference (34) with permission from copyright clearance center.

In humans, both isoforms are present in each half of the sarcomere with a ratio of 30:70 (N2BA:N2B)[36]. Due to the presence of an additional extensible element in the I-band region, N2BA isoform is more distensible and less rigid compared to the N2B isoform (Figure 1.5b). This causes increased rigidity in cardiomyocytes expressing high levels of N2B isoforms than those that express larger amounts of N2BA isoform[37].

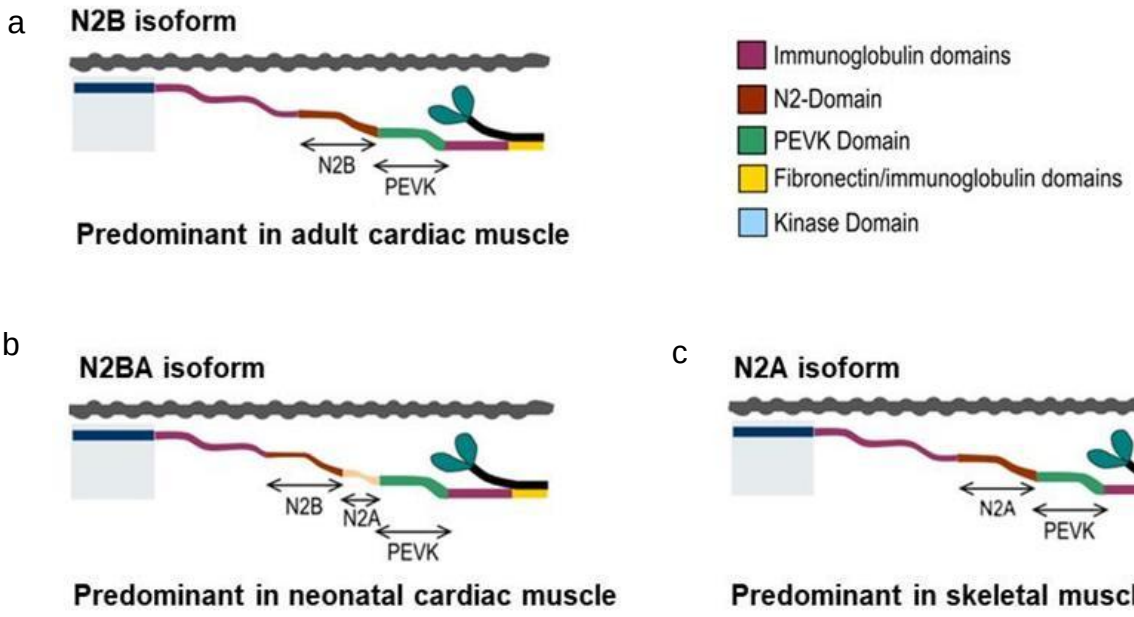

Figure 1.5. Major titin isoforms. The sub-region N2 in I-band region can have either N2A or N2B elements. N2BA contains both N2A and N2B elements and its predominant in neonatal cardiac muscle. N2B predominant in adult cardiac muscle and N2A isoform of titin is confined only to skeletal muscle. Figure adapted from reference (20) with permission from copyright clearance center.

1.4.2 Functional importance of titin

Titin is the main determinant of passive tension of cardiomyocytes. Due to its elastic nature, which is caused mainly due to the I-band region, titin protein involves in regulation of the sarcomere length and muscle function. Ig segments, PEVK segments and N2 region mainly contribute to elasticity of titin protein (Figure 1.6)[38]. A complex set of events are involved in the development of passive tension during muscle stretching. The behavior of different segments in I-band region has different passive tension-length relationships. Depending on the sarcomere length, each one stretches at different moments. Sarcomeres maintain 1.9 µm long, when titin is in contracted form, during the resting state of cardiomyocytes[39]. During the progressive stretching of the sarcomere Ig

sequences are first stretched due to the elongation of the binding between different Ig domains (Figure 1.6). At 2.15 µm the PEVK segments start elongating, followed by the N2 segments (Figure 1.6)[40].

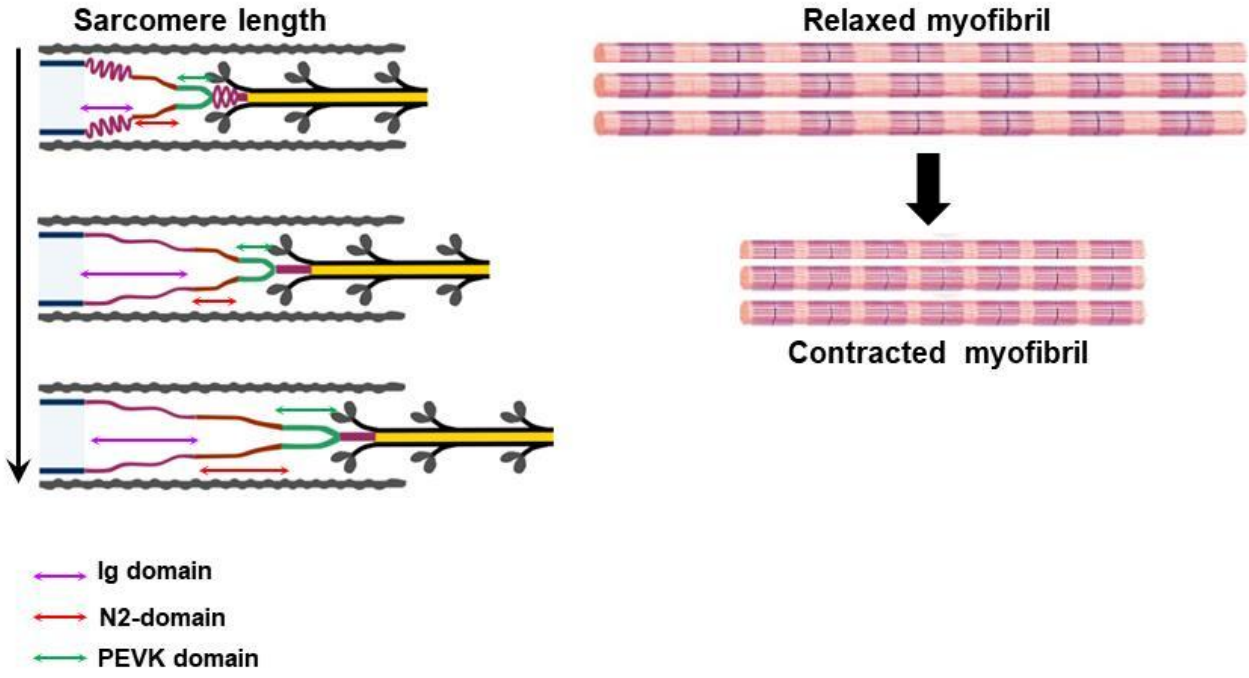

Figure 1.6. Mechanism of sarcomere elongation. Titin protein involves in regulation of sarcomere length and muscle function. Ig segments, PEVK segments and N2 region are mainly contributed to elasticity of titin protein to facilitate the myofibril contraction and relaxation. Figure adapted from reference (20) with permission from copyright clearance center.

1.4.3 Structural and functional importance of SMYD2

SMYD2 is one of the SET and MYND-containing lysine methyltransferases (SMYD). SMYD is a family of five members which includes SMYD (1-5) (Figure 1.7a and b)[41]. Catalytically important SET domain of SMYD family catalyzes the mono methylation of protein lysine residues using S-adenosylmethionine (SAM) as the methyl donor and release the S-adenosylhomocysteine (SAH) as a byproduct (Figure 1.7c).

Cysteine-rich zinc finger containing MYND domain was initially found in **My**eloid translocation protein 8, **N**ervy, and **D**EAF-1. This domain is mainly important for protein-protein interaction and it shows a preference towards the proteins with a proline rich motif[41].

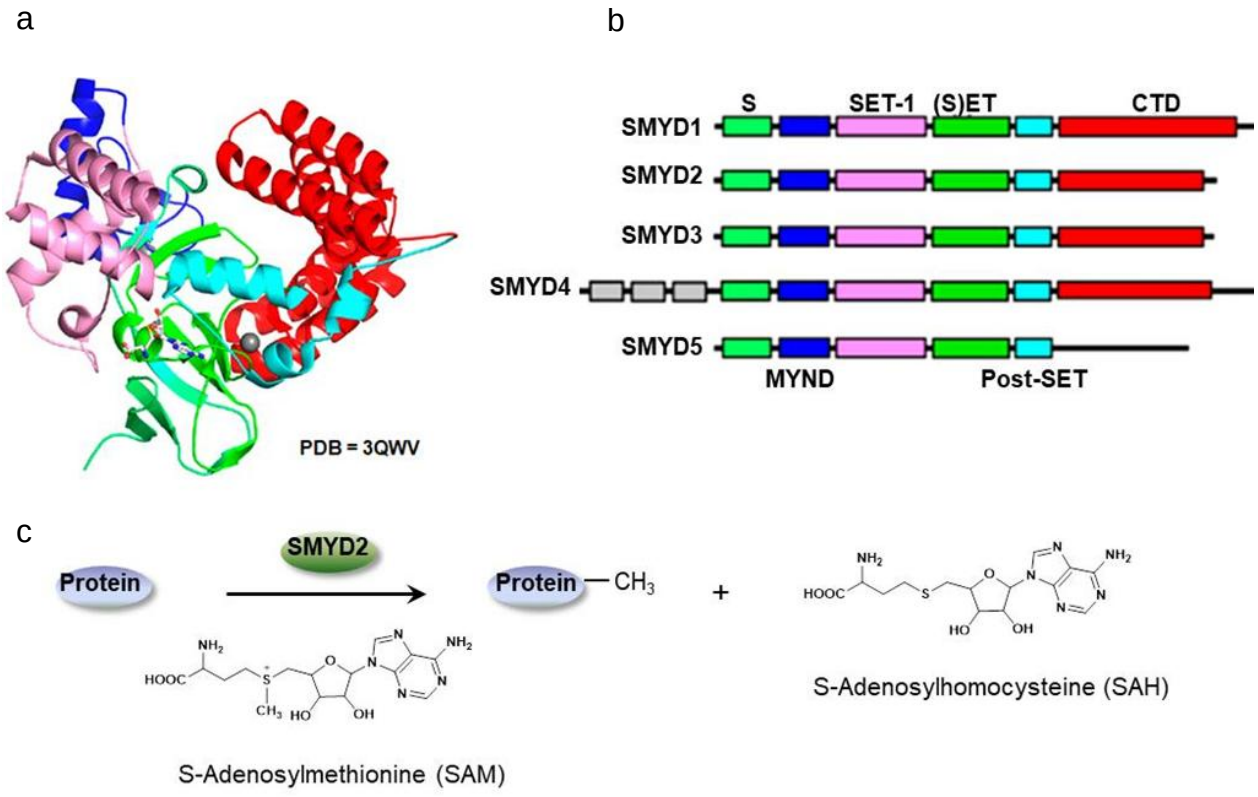

Figure 1.7. Domain organization and catalytic activity of SMYD2. (**a**) Ribbon diagram of SMYD2 protein with SAH molecule in catalytically important SET domain (PDB = 3QWV). (**b**) Schematic presentation of SMYD family and their domain composition. Catalytically important SET domain (green), MYND domain which is important for protein-protein interaction (blue) and C-terminal region with TPR domain (red). (**c**) Mono methylation of lysine residues catalyzes by SMYD protein using SAM as the methyl donor and production of SAH as the byproduct. Figure adapted from reference (41) with permission from copyright clearance center.

C-terminal region of SMYD1-4 has a tetratricopeptide (TPR) like domain which is also involved in protein-protein interactions and HSP90 mainly binds to the TPR domains of

SMYD2 (Figure 1.7b)[41, 42]. SMYD2 has 17 cysteine residues, ten of which are bound to three zinc ions in the MYND and Post-SET domains. SMYD2 is mostly cytoplasmic[43] where it catalyzes mono-methylation of p53 to suppress apoptosis[44], retinoblastoma protein (pRb) to enhance cell cycle progression[45], estrogen receptor α (ERα) to suppress its transactivation[46], and heat shock protein 90 (Hsp90) to enhance its chaperone activity and cell proliferation[47]. Recent proteomic analysis found over 200 substrate proteins, suggesting its roles in diverse cellular processes[48].

1.4.4 Importance of SMYD2 for sarcomere integrity

Importantly, both SMYD1 and SMYD2 are abundant in cardiac and skeletal muscle, playing an important role in myofibril assembly. SMYD1 is important for heart development[49]. Thus, SMYD1 null mice embryos do not survive due to failure in right ventricle formation of heart[50]. On the other hand, an early study showed that cardiac SMYD2 knockout mice have no detrimental effect on heart development, suggesting that SMYD2 is dispensable for heart development[51]. But, recently mice with conditional knockout of SMYD2 showed an enhanced level of cardiomyocyte apoptosis upon myocardial infarction by proving its cardioprotective function in pathophysiological conditions of heart muscle[52]. Recently, it was found that zebrafish with SMYD2 knockdown forms a disorganized I-band and Z-disks in sarcomere in heart and skeletal muscle, suggesting its potential role in sarcomere organization or stabilization[31].

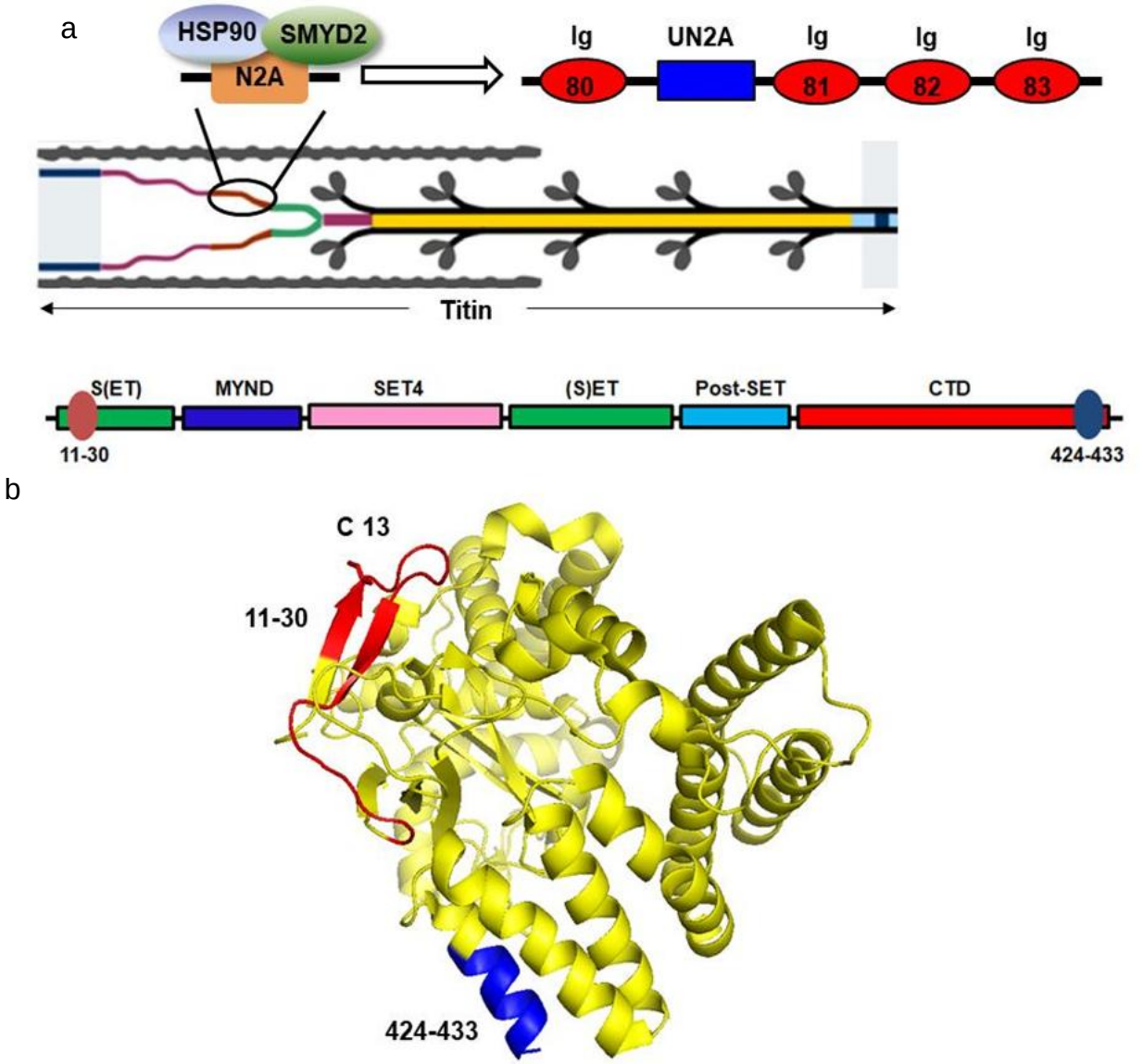

Figure 1.8. Protein complex of SMYD2: HSP90: N2A domain on sarcomere and binding surfaces of SMYD2 and N2A domain. (**a**) In a molecular level, SMYD2 forms a complex with Hsp90. This complex binds to N2A domain of titin at I-band of sarcomere. UN2A region of N2A domain is important for the interaction with SMYD2 (**b**) ribbon diagram of SMYD2 with cysteine 13. N-terminal region (11-30 aa) and C-terminal region (424-433 aa) of SMYD2 are important to interact with the N2A domain of titin protein. Figure adapted from reference (20) with permission from copyright clearance center.

In myocytes, SMYD2 is involved in mono-methylation of Hsp90, which increases Hsp90 chaperone activity. SMYD2 then forms a complex with mono-methylated Hsp90 (Figure 1.8a). This complex binds to N2A, a domain of titin, which has been implicated to be important for sarcomere stabilization[31]. The N2A domain is composed of four immunoglobulin domains (Ig80-83, figure 1.8a red) and a unique sequence region, called N2A-Us (also called UN2A, figure 1.8a blue), between Ig80 and Ig81 (Figure 1.8a). UN2A region of N2A domain is important for the interaction with SMYD2[30]. N-terminal region (11-30 aa) and C-terminal region (424-433 aa) of SMYD2 are important to interact with the N2A domain of titin protein (Figure 1.8b). SMYD2-methyl HSP90-N2A complex has shown to be important for sarcomere organization especially in I-band region (Figure 1.8a). Notably, SMYD2 knockdown decreases the level of N2A (a domain of titin) and induces disorganization of sarcomere structure in zebrafish, showing the importance of SMYD2 for the integrity and stability of sarcomere[31].

1.4.5 Importance of α-actinin for sarcomere integrity

α-Actinin belongs to a family of actin binding proteins and a part of the spectrin superfamily which includes two other major proteins known as spectrin and dystrophin[53]. Alpha actinin is important for cytoskeleton framework in non-muscle cells and it is a key structural protein important to stabilize the Z-disk of sarcomere in striated cardiac and skeletal myocytes (Figure 1.9). Alpha actinin forms a lattice like structure at the Z-disk and supports the contractile nature of sarcomere (Figure 1.9)[53]. The ABD domain of alpha actinin holds the antiparallel actin filaments to support the filament sliding mechanism between the actin and myosin. Meanwhile a CaM like domain of

muscle related α-actinin interacts with the Z-repeats on N-terminal region of titin protein in striated muscle[54].

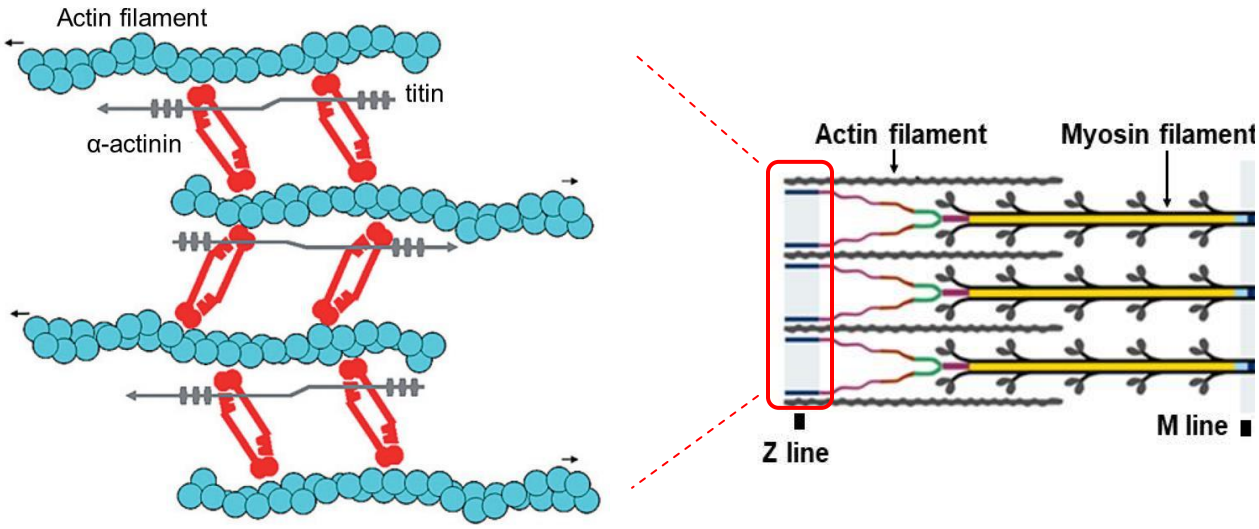

Figure 1.9. Localization of alpha actinin in Z-disk of sarcomere. Alpha actinin (red color), actin filament (pale blue color), titin (ash color). The α-actinin maintains the interaction between antiparallel actin filaments and holds the N-terminal region of titin protein. Figure adapted from reference (53) with permission from copyright clearance center.

1.4.6 Structural and functional importance of troponin

A basic contractile unit in striated muscle (sarcomere) includes two filaments known as myosin thick filament and actin thin filament. F-actin and G-actin combination forms the actin thin filament. Troponin complex made of troponin C, troponin T and troponin I is localized on the groove of the F-actin filament interacting with the tropomyosin protein (Figure 1.10a)[55]. Mainly, intracellular calcium concentration regulates the muscle contraction and relaxation. Binding of calcium onto troponin complex triggers the muscle contraction (Figure 1.10b).

During relaxation period, tropomyosin blocks the accessibility of myosin head into active site of actin in order to generate the muscular force. Binding of calcium to TnC produces structural changes in TnI and disrupt the interaction between actin thin filament and tropomyosin (Figure 1.11b)[56]. Disruption of this complex facilitates the interaction between myosin head and actin active site in order to produce the muscle contraction or shortening of sarcomere[57]. In addition to involvement in muscle contraction and relaxation, troponins are considered as a biomarker in cardiac muscle disorders including myocardial infarction, heart failure and cardiomyopathy[55].

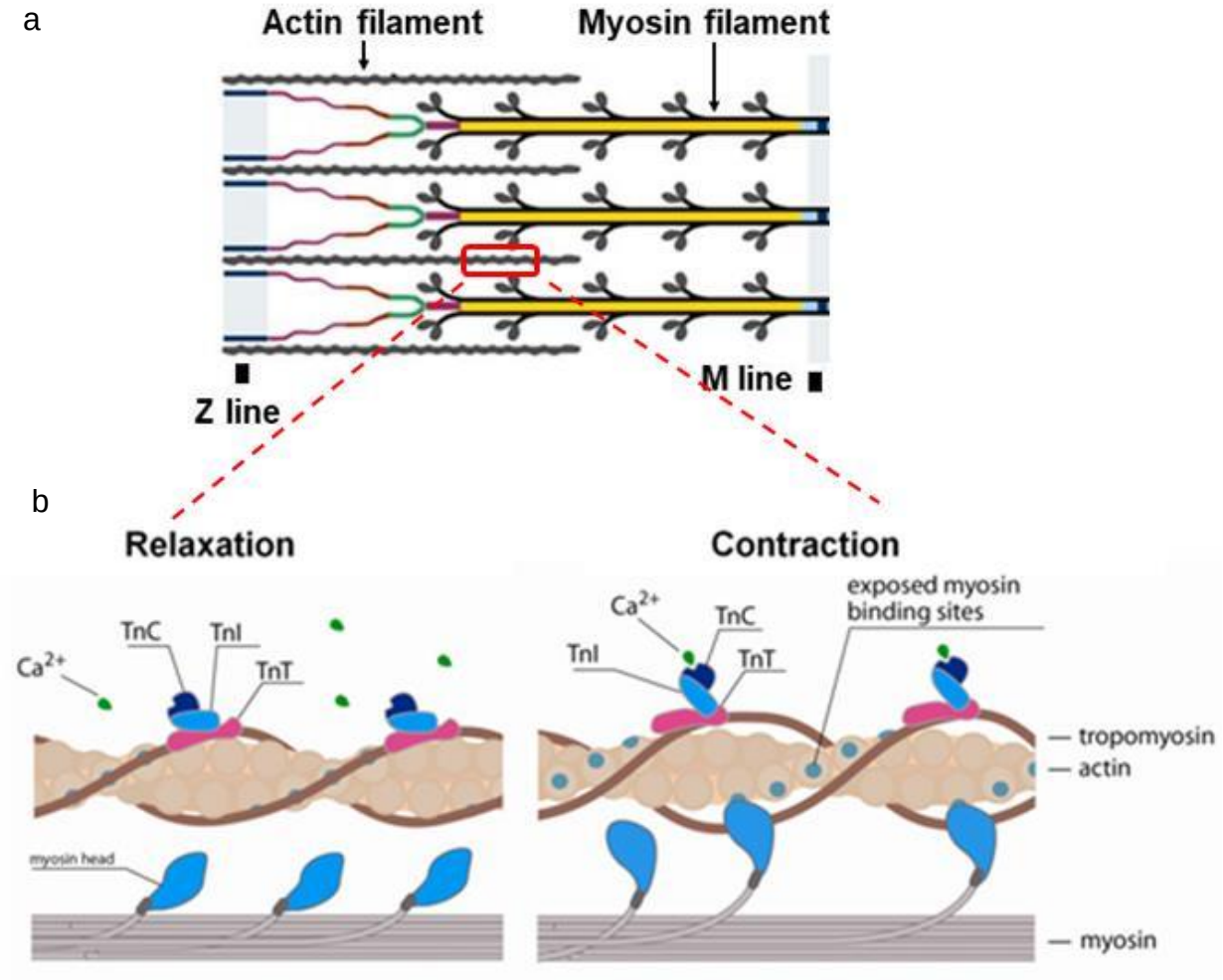

Figure 1.10. Localization and functional importance of troponins. (**a**) Localization of troponin complex in groove of the actin thin filament. (**b**) During muscle relaxation tropomyosin blocks the active site of actin (blue color dots on actin filament are covered by brown color tropomyosin). Calcium binding to TnC induces disruption of tropomyosin and actin filament complex (blue color dots are exposed to myosin heads) while facilitating myosin: actin interaction in order to activate the muscle contraction. Figure adapted from reference (56) with permission from copyright clearance center.

1.5. Mitochondria is important for cardiac metabolism

Mitochondria are one of the major organelles which govern the lifetime of cardiac myocytes. Healthy cells of the beating heart meet their high energy demand by the ATP derived from mitochondria via oxidative phosphorylation. Thus, mitochondria often categorized as the “Powerhouse of the cell”. This highly efficient and localized supply of ATP helps to sustain basic functions such as metabolism, contraction and ion homeostasis in cardiac myocytes (Figure 1.11). Mitochondria are primarily localized in between the myofibrils and below the sarcolemma in each myocyte. Furthermore, it plays a vital role in regulating apoptosis in response to stress signals such as hypoxia and oxidative stress (Figure 1.11)[58].

1.5.1 Mitochondria are the major energy source in cardiac muscle

Energy-demanding cardiac tissues are rich in mitochondria accounting for 20-40% of cellular volume. Energy production in mitochondria depends on several factors including enzyme activity, availability of cofactors, oxygen and fuels such as sugars and fatty acids (Figure 1.11)[58]. Number of bioenergetic pathways contributes to energy production in mitochondria. They include pyruvate oxidation, the tricarboxylic acid (TCA) cycle, the mitochondrial β-oxidation of fatty acids and oxidative phosphorylation.

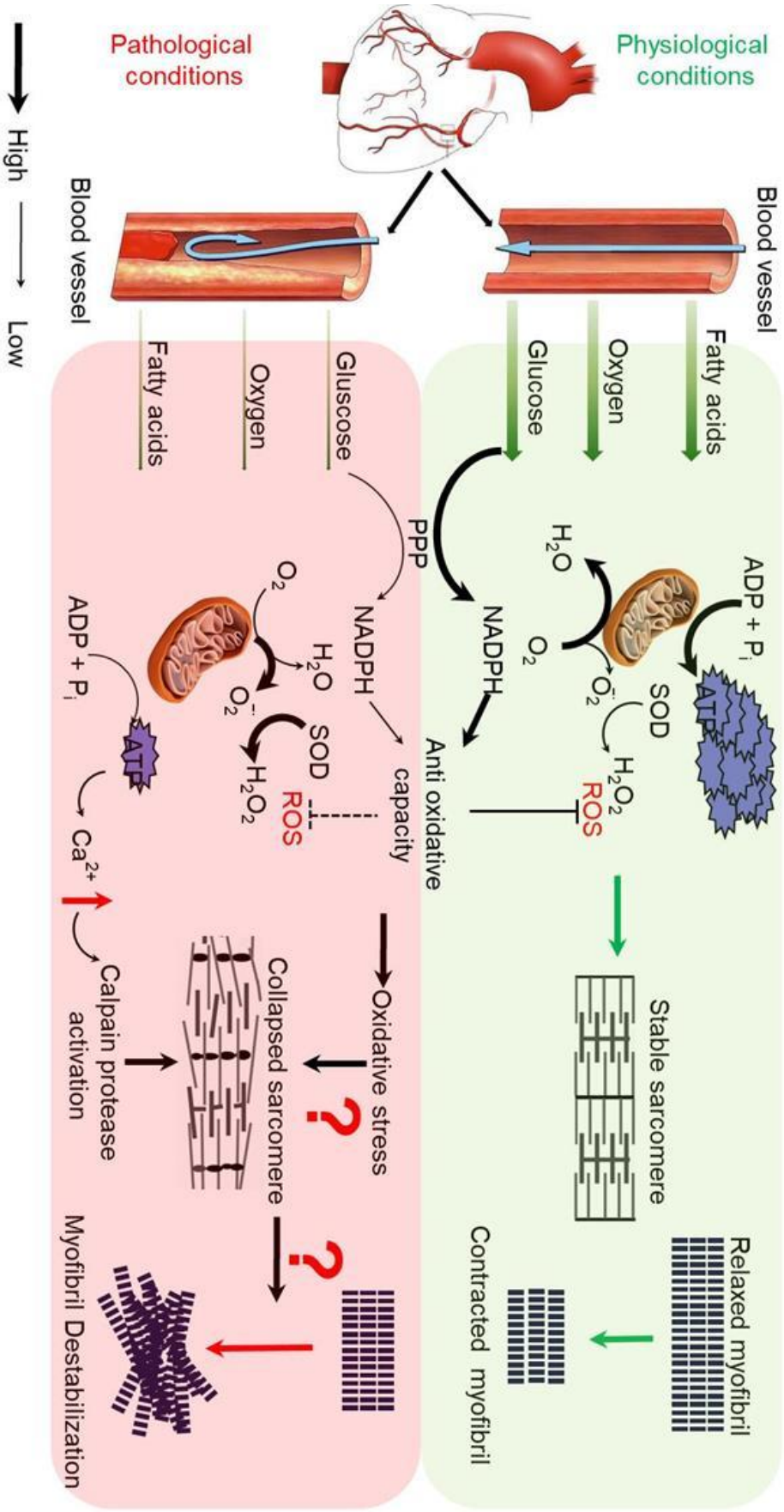
Pathological conditions
Physiological conditions
High
Low
Blood vessel
Blood vessel
Fatty acids
Oxygen
Glucose
Glucose
Oxygen
Fatty acids
PPP
NADPH
Anti oxidative
capacity
ADP + Pi
ATP
H2O
O2
O2·-
SOD
H2O2
ROS
Stable sarcomere
Relaxed myofibril
Contracted myofibril
Ca2+
Calpain protease activation
Oxidative stress
?
Collapsed sarcomere
?
Myofibril Destabilization

Figure 1.11. Mitochondrial behavior in physiological and pathological conditions of cardiac muscle. In physiological conditions where sufficient level of glucose, fatty acid and oxygen are present, mitochondria produce satisfactory level of ATP molecule to facilitate the muscle contraction and relaxation. In pathological conditions depletion of nutrition and oxygen result higher level of ROS production through dysfunctional mitochondria. When antioxidant capacity coming from NADPH (electron carrier) or redox enzymes may not be able to counteract the effects of ROS creates an oxidative stress *in-vivo*. Myocardial stress lowers the ATP production and activates the proteases including calpain and MMP-2 which are involved in sarcomeric protein degradation. Degradation of proteins in sarcomere affects the myofibril integrity and cardiac muscle contraction.

About 80-90% of cellular ATP is produced by oxidative phosphorylation occurring in the proteins at the mitochondrial inner membrane including complexes I-IV, ATP synthase (complex V) and adenine nucleotide translocator (ANT). In cardiac muscles, ATP is generated primarily by fatty acid β-oxidation[59]. In normal cardiac tissue, there is limited ATP supply from other sources such as glycolytic metabolism. Several transport proteins are required to efficiently transport fatty acids into cardiomyocytes and then into mitochondria. The major sources of electrons for the electron transport chain are the intramitochondrial NADH and FADH. They are generated primarily by fatty acid β-oxidation and the oxidation of carbohydrates via the TCA cycle. Additionally, the heart stores high energy phosphates such as phosphocreatine which is produced by mitochondrial creatine kinase using ATP[60].

1.6 Ischemia-reperfusion induces mitochondrial ROS production

Complex I and complex III in mitochondria convert about 0.2-2% of molecular oxygen into superoxide during cellular respiration which is important to synthesize an energy molecule “ATP”. Therefore mitochondria are considered as a major source of ROS in intracellular environment. During mitochondrial electron transfer, O_2 captures an

electron from Complex I or from the ubisemiquinone located in Complex III and produce superoxide (Figure 1.11)[61].

Myocardial ischemia, obstruction of a blood flow caused by a plaque in coronary arteries prevents the supply of both nutrition and oxygen into the heart muscle. Low level of oxygen as well as nutrition affects the metabolism of cardiomyocytes by lowering the capacity of oxidative phosphorylation and mitochondrial ETC flux[60, 62]. Furthermore, upon depletion of creatine phosphate levels, impaired oxidation of fatty acids and pyruvate along with reduced ATP production can also be seen. Accumulation of lactate during breakdown of ATP derived via TCA cycle leads to drop of intracellular pH causing acidosis which has a direct effect on the contractile function of cardiac muscle[61].

In reperfusion conditions, where there is a high oxygen concentration, mitochondrial ROS production is elevated. Also increased level of superoxide occurs when there is a reduction in Complex I activity. In cardiac muscles there is a high density of mitochondria and during ischemia-reperfusion injury significant amount of superoxide is produced due to high rate of oxidative phosphorylation (Figure 1.12)[63].

Moreover, at the onset of reperfusion, mitochondria can aggravate the ischemic damage. During reperfusion, high acetyl CoA levels can form via increased fatty acid intake and unregulated fatty acid oxidation thus saturating the TCA cycle. This eventually causes an inhibition of the glycolysis and pyruvate oxidation. Furthermore, increase of OXPHOS tends to accumulate more ROS with respect to elevated levels of lipid peroxidation (Figure 1.12)[64].

In general, there are antioxidant enzymes in mitochondria to detoxify superoxide by converting it to water and oxygen. They include manganese superoxide dismutase (MnSOD), catalase, and glutathione peroxidase (GPx). But when these antioxidant systems fail to neutralize excess amounts of ROS, oxidative stress occurs inside the cell (Figure 1.11)[4].

1.6.1 Antimycine A induces mROS production

Complex I and complex III in mitochondria are known to produce superoxide from molecular oxygen during cellular respiration. Complex I is localized in the inner membrane of mitochondria and it is known to be the entry point of electron carriers. During cellular respiration, ROS production in complex I will be minimal but, binding of rotenone, inhibitor of complex I, generates ROS production by blocking the electron transfer from ion-sulfur center to the CoQ site[65]. Complex III is also localized in inner membrane of mitochondria and is important for transfer electron from $CoQH_2$ to cytochrome c (Figure 1.12)[66]. Antimycin A is a known inhibitor of complex III and produces ROS by blocking the shuttle of electron from Q_O site to Q_I site by binding to Q_i site. Blockage of electron transfer at complex III[67] induce ROS production through superoxide generation by molecular oxygen (Figure 1.12)[68]. But, during physiological conditions, superoxide generation by complex III will be minimum.

1.7 ROS induce oxidative stress

Having unpaired electrons in the outer orbit, reactive oxygen species such as superoxide ($O_2^{-\cdot}$), peroxynitrite ($ONOO^{\cdot-}$) and hydroxyl radicals ($^{\bullet}OH$) are highly reactive. $O_2^{-\cdot}$ is generated through reduction of molecular O_2 by one electron. Due to its poor membrane permeability, it has a limited capacity to diffuse and therefore generally

restricted to intracellular compartments where it is produced. The half-life of $O_2^{\cdot-}$ is only a few seconds as it is rapidly dismutated to H_2O_2 and oxygen .

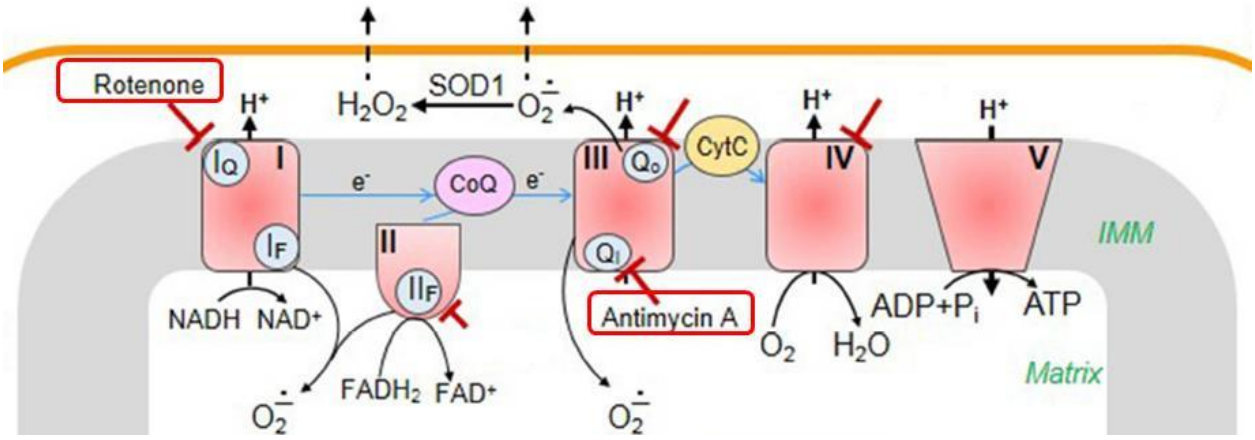

Figure 1.12. Antimycin A induces mROS production by blocking complex III in mitochondria. Antimycin A is a known inhibitor of complex III and produces ROS by blocking the shuttle of electron from Q_0 site to Q_1 site by binding to Q_i site. Blockage of electron transfer at complex III, induce ROS production through superoxide generation by molecular oxygen. Figure adapted from reference (67) with permission from copyright clearance center.

But H_2O_2 is more stable and membrane permeable[69]. Therefore it can act at more remote sites. $^{\bullet}OH$ is the most reactive oxygen free radical and it is formed from H_2O_2. In normal cells the level of $^{\bullet}OH$ is negligible. But in pathological conditions such as ischemia-reperfusion, there is an elevated level of $^{\bullet}OH$. This may contribute to cellular damage associated with oxidative stress. $ONOO^{\cdot-}$ is produced when O_2 reacts with NO. This occurs at high nanomolar range of NO and results in its inactivation (Figure 1.13)[70].

There are number of potential sources of ROS in major cardiac cell types; cardiac myocytes, fibroblasts and endothelial cells[71, 72]. They include mitochondrial

respiratory chain[72], NADPH oxidases[73], xanthine oxidase (XO)[74], NO synthases[75], lipoxygenase[76], peroxidases, cytochrome P-450s and other hemoproteins[77]. Among these sources, mitochondria, NADPH oxidases and XO are considered as major contributors to heart failure (Figure 1.13).

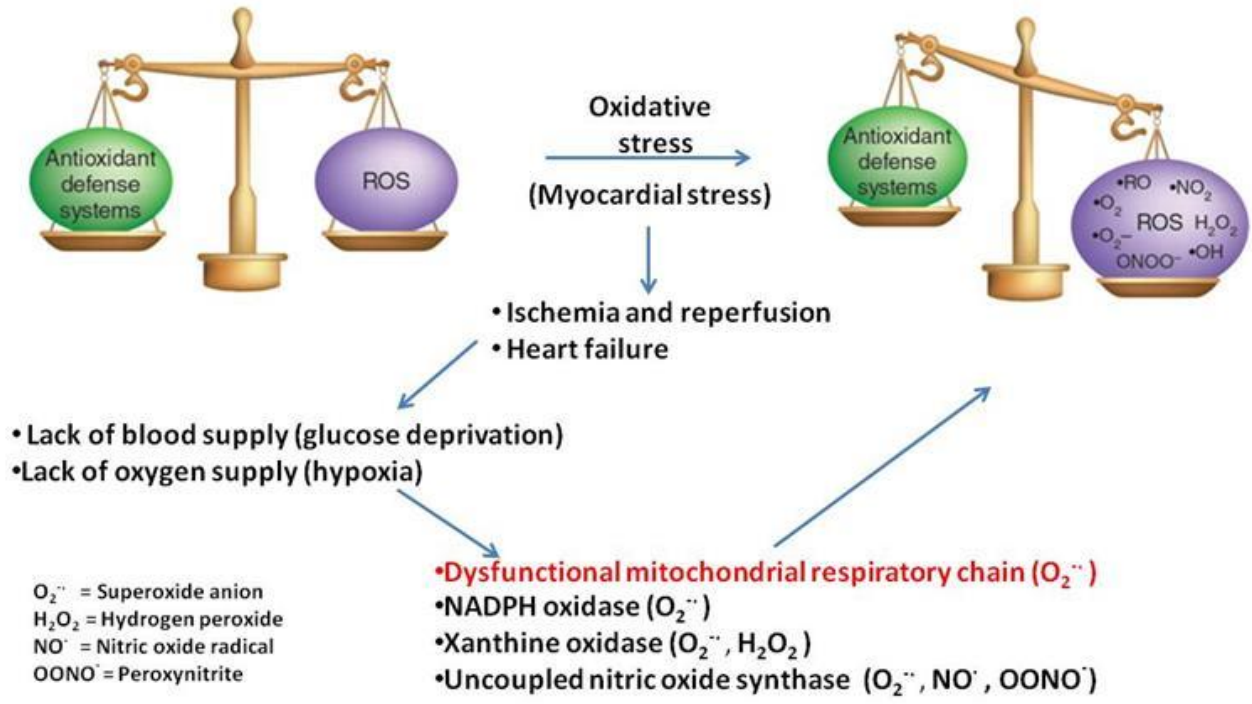

Figure 1.13. ROS sources and species contribute to oxidative stress. Imbalance between antioxidant defense system and ROS generation cause oxidative stress[78]. Numerous ROS and RNS species including superoxide, hydrogen peroxide, nitric oxide and peroxynitrite contribute for myocardial stress induce by ischemia/ reperfusion injury. Dysfunctional mitochondria, NADPH oxidase, xanthine oxidase and uncoupled nitric oxide synthase are major sources of ROS and accumulation of these reactive molecule cause cardiac muscle dysfunction and heart failure[78]. Figure adapted from reference (78) with permission from copyright clearance center.

There are number of enzymatic and non-enzymatic pathways in normal cells to counterbalance these ROS. Superoxide dismutases (SODs), glutathione peroxidase

and catalase enzymes are the major endogenous antioxidant pathways[79]. SOD converts $O_2^{-\cdot}$ into H_2O_2 and oxygen. Several different SOD enzymes are present in different cellular compartments. Manganese SOD (Mn SOD), copper/zinc (Cu/Zn) SOD and extracellular SOD are present in mitochondria, cytosol and plasma membrane respectively. By converting H_2O_2 to water and O_2 , cellular catalases and glutathione peroxidase maintain the H_2O_2 levels in the cells where glutathione acts as a reducing substrate during the enzymatic activity of glutathione peroxidase[80]. Another important antioxidant defense is provided by thioredoxin and thioredoxin reductase; they catalyze generation of ubiquinone (Q10), ascorbic acid and lipoic acid which are antioxidant molecules[81]. These and other intracellular antoioxidants including vitamins E, C and β-carotene, urate and glutathione provide non-enzymatic mechanisms to counter balance ROS[82]. But, the imbalance between this antioxidant capacity and ROS generation cause an oxidative stress in intracellular environment.

1.8 Oxidative stress induce protease activation

It is emerging that a highly ordered structure of sarcomere is maintained in a dynamic process that involve an intricate balance between assembly and degradation of sarcomeric proteins by the action of many chaperones and proteases. In particular, an ischemia-reperfusion injury leads to an increased activity of several proteases, including matrix-metalloprotease 2 (MMP-2) and calpain 1/3 (Figure 1.14)[83]. Activated MMP2 is involved in degradation of several sarcomeric proteins, including titin, α-actinin, troponin, and myosin-light chains[84, 85]. Activated calpain is also responsible for degradation of titin and troponin.

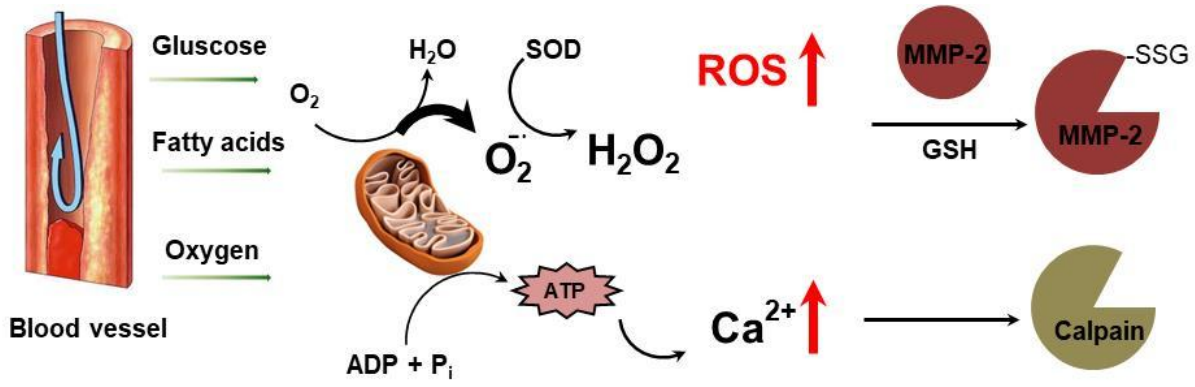

Figure 1.14. Sarcomere associated protease activation by ischemia-reperfusion injury. Dysfunctional mitochondria cause higher level mROS production and accumulation of intracellular calicium. Oxidative stress induce protein glutathionylation activates MMP2 and overload of calcium cause by malfunction of ion-channels activates calcium dependent calpain protease.

1.8.1 Structural features and functional importance of MMP-2

MMP-2 is a zinc-dependent protease involved in cardiac remodeling and has shown its increased activity during myocardial ischemia and reperfusion injury. Mainly, MMP-2 is localized on I band region of sarcomere (sarcomeric MMP-2) and two other forms known as cytoskeletal and nuclear MMP-2[86] has been reported. It includes several domains including N-terminal signal sequence (Pre domain), propeptide domain, catalytic site with zinc ion binding site, and C-terminal haemopexin domain (Figure 1.15a). A cysteine amino acid in the highly conserved PRCGVPD sequence within the auto inhibitory pro-peptide domain prevents the accessibility of substrate by making an interaction with a catalytically important zinc ion[85]. Because of this, MMP-2 is considered as a latent enzyme which can be activated by either oxidative stress or proteolytic cleavage. Oxidative stress induces S-glutathionylation of critical cysteine residue in the pro-domain, disrupts the interaction between thiolate and zinc ion resulting an active full length MMP2 enzyme (Figure 1.15b). Active MMP-2 plays a role

in sarcomeric protein degradation[87]. Meanwhile, activation of MMP2 involves in myocardial apoptosis via activation of β-adrenergic receptors. MMP-2 mediated regulation of poly (ADP-ribose) polymerase (PARP) or glycogen synthase kinase-3b (GSK-3β) are involved in cardiomyocyte apoptosis (Figure 1.15c)[88].

a

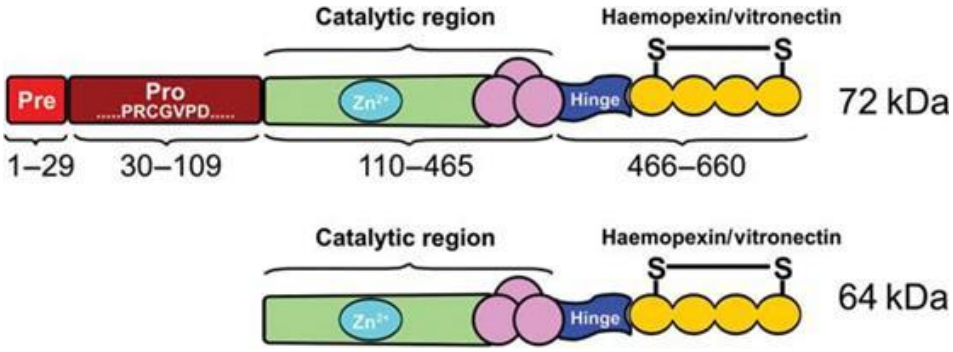

b

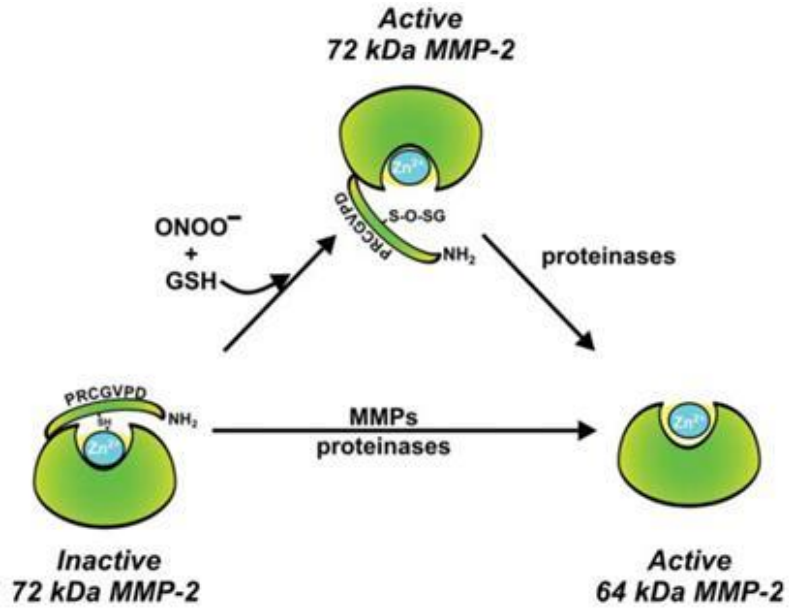

c

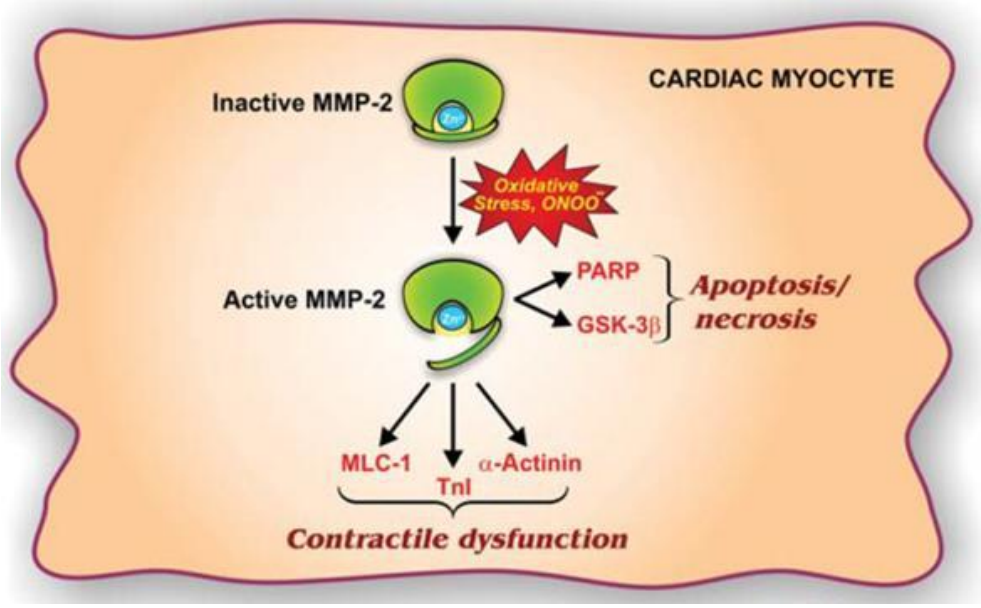

Figure 1.15. Composition and activation of MMP-2. (**a**) Schematic presentation of full length (72 kDa) and proteolytically cleaved MMP-2 (64k Da). (**b**) Activation of full length MMP2 by glutathionylation under oxidative stress conditions. Proteolytic cleavage of 72 kDa MMP2 by MMP-14 and tissue inhibitor of metalloproteinase-2(TIMP-2) to produce active 64 kDa MMP-2. (**c**) Active MMP-2 degrades sarcomeric protein including MLC-1, TnI and α-actinin. MMP-2 plays a role on cardiomyocyte apoptosis through regulation of PARP or GSK-3β[85]. Figure adapted from reference (85) with permission from copyright clearance center.

1.8.2 Structural features and functional importance of calpain 1

Calpain is a cysteine protease which is dependent on calcium ion availability for its activation and mostly localized on cytoplasm[89]. Mainly, there are two conventional calpains in mammalian cells which differ by the calcium sensitivity. One is μ-calpain sensitive to μM concentrations of calcium and m-calpain needs mM concentration of calcium for its activation. There are two major domains in calpain including 80 kDa catalytic subunit and 30 kDa regulatory subunit. Disruption of calpains into subunits in the presence of calcium results in the substrate cleavage by 80 kDa catalytic subunit

(Figure 1.16a)[90]. Oxidative stress or mitochondrial damage negatively regulates calcium homeostasis, and the resulting calcium overload activates cellular calpains. Cleavage of calpastatin, p35 or calcineurin leads to induction of apoptosis through caspase activation (Figure 1.16b)[91, 92].

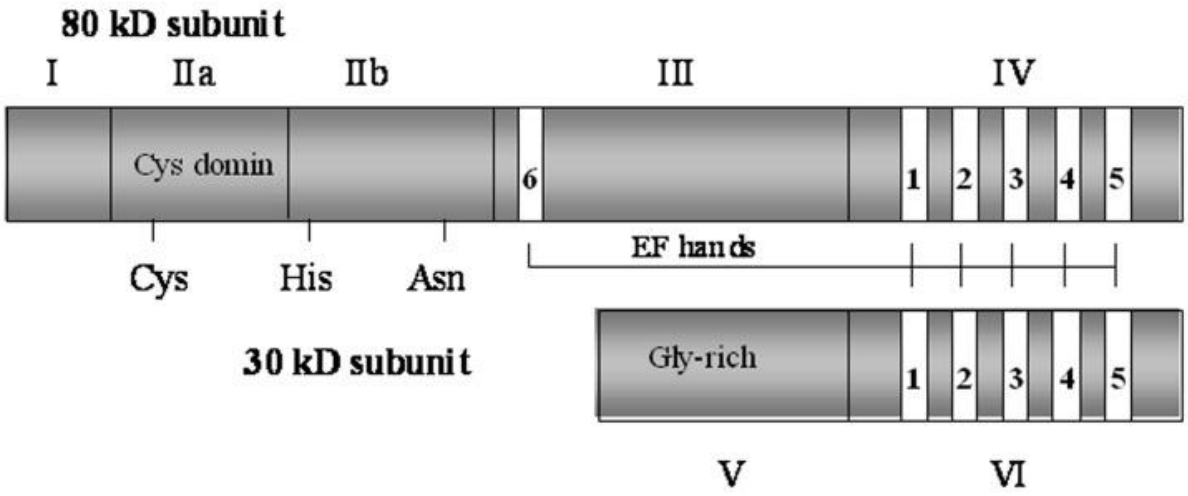

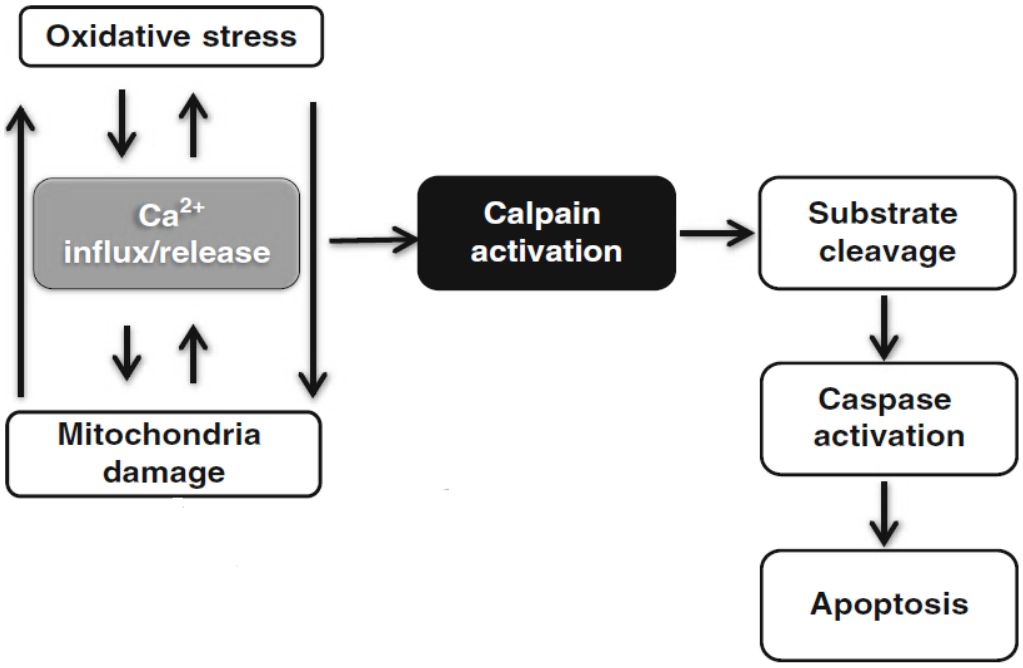

Figure 1.16. Composition and activation of calpain 1. (a) Schematic presentation of 80 kDa catalytic subunit and 30 kDa regulatory subunit. (**b**) Impairs calcium homeostasis cause by oxidative stress and mitochondrial damage leads to calpain activation. Active calpain degrades calpastatin, p35 or calcineurin to activate caspase which involves in apoptosis[91]. Figure adapted from reference (91) with permission from copyright clearance center.

1.9 Protein S-glutathionylation

High level of reactive oxygen/nitrogen species (ROS/RNS) or failure in antioxidant defenses in the cells cause oxidative stress due to changes in cellular homeostasis. This can cause reversible or irreversible damage to proteins when they undergo oxidative modifications. Specifically, the thiol groups in proteins are more susceptible to oxidative modifications in response to changes in cellular ROS/NOS levels. Cysteine is an amino acid with nucleophilic sulfhydryl group, found in active sites of proteins and plays an important functional role.

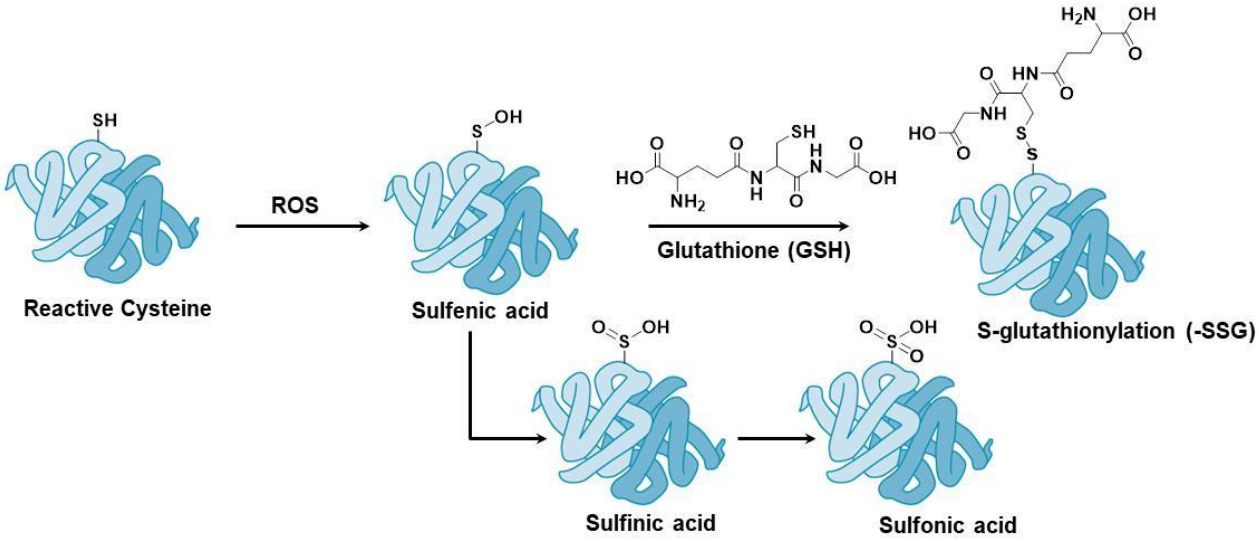

Figure 1.17. Protein thiol oxidative modifications. A Reaction between a reactive thiol and ROS produces a sulfenic acid moiety which can be further modified by GSH to make the glutathionylated proteins. Redox enzymes or reducing agents restores the protein thiol by reducing the glutathionylated protein. Higher level of oxidative stress can further modify these sulfenic acids into sulfinic or sulfonic moieties which are

recognize as irreversible modification. The consequences of this irreversible protein modification include inactivation of the protein as well as degradation of the protein.

When a functionally important cysteine sulfhydryl group is modified, this can affect the protein activity[93]. Even if the cysteines are not in the active site, oxidative modifications can cause conformational changes in the protein and its activity[94]. However, in the cells, there are mechanisms which reverse the redox alterations in protein thiols. Glutathionylation is one such important mechanism to regulate protein oxidation.

1.9.1 Mechanism of protein S-glutathionylation

Maintaining an optimal GSH/GSSG ratio in the cell is essential to regulate the redox state of protein thiols and continue cell survival. In physiological conditions, the cell has a reducing environment with a GSH/GSSG ratio around 100[95]. Changes in this ratio can cause oxidation of protein cysteinyl residues and therefore even a slight shifting of this equilibrium could promote protein S-glutathionylation. There are several ways protein glutathionylation can occur including direct interaction between GSH and partially oxidized cysteine thiols in proteins (sulfenic acid moieties or S-nitrosothiol)[96], thiol/disulfide exchange reactions between oxidized glutathione and thiol groups in proteins, and reaction between S-nitrosoglutathione (GSNO) and protein reactive thiols (Figure 1.17)[97, 98]. In addition, glutathione sulfenic acid and glutathione disulfide S-monoxide can contribute for protein glutathionylation[99].

1.9.2 Cycle of protein S-glutathionylation

Glutathione S-transferases (GST's) are a class of enzymes which mediate enzymatic formation and removal of S-glutathionylation. They decrease the pKa of thiol group in GSH and therefore increase its nucleophilicity and the reactivity promoting S-glutathionylation. One of the GST family members, GSTP, is known to increase glutathionylation in specific substrates such as peroxiredoxin[100, 101]. When the catalytic cysteine in peroxiredoxin is oxidized to sulfenic acid, its peroxidase activity is inhibited. But S-glutathionylation of the active site cysteine mediated by GSTP restores the catalytic activity[102].

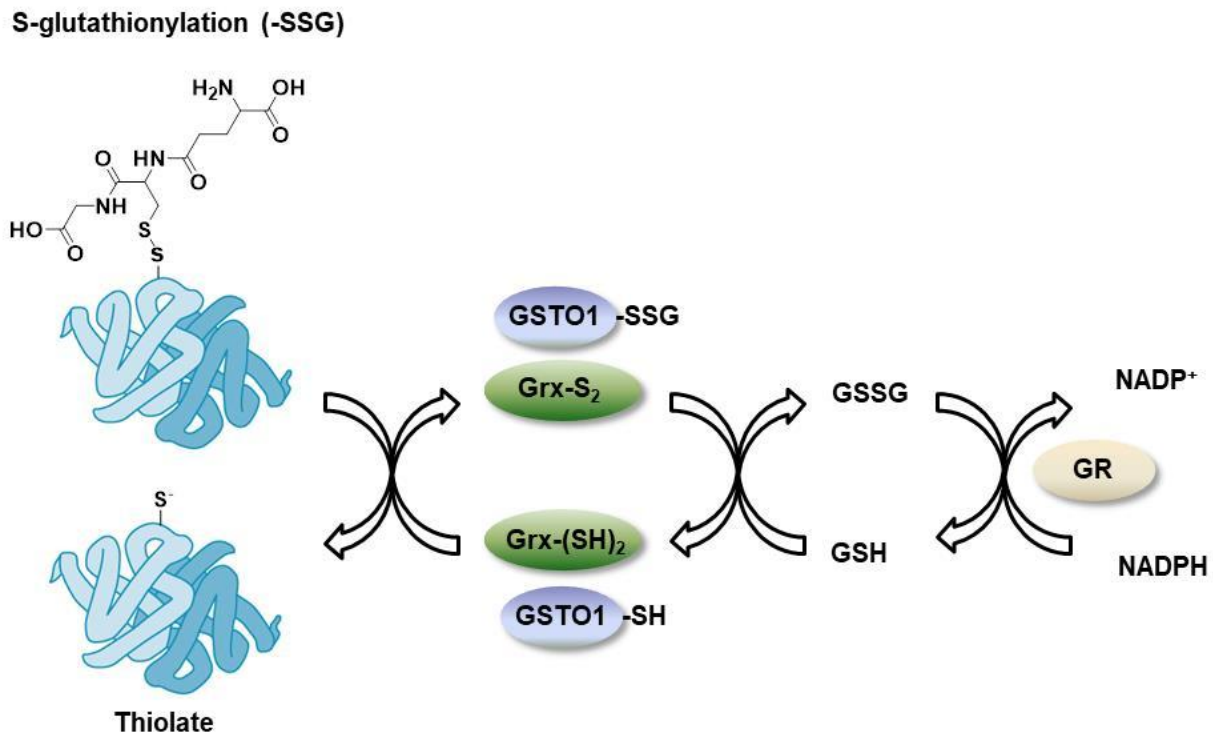

Figure 1.18. Redox enzymes induce Protein glutathionylation and deglutathionylation. Glutathione S-transferases (GST's) are a class of enzymes which mediate enzymatic formation and removal of S-glutathionylation. GSTP1 known to involve in protein glutathionylation and GSTO1 mainly catalyze deglutathionylation of proteins. Oxidation of Grx1 also involves in protein deglutathionylation. Oxidation of

GSH reduces oxidized Grx1 and GSTO1 enzymes. Meanwhile GR brings oxidized GSH back to reduced form by consuming NADPH which is a well-known electron carrier important to maintain the redox potential *in-vivo*.

There are several other enzymes which play a role in S-glutathionylation such as glutaredoxin 1 (Grx1)[103], glutaredoxin 2 (Grx2) and gamma-glutamyl transpeptidase. Grx catalyzes glutathionylation of many proteins including GAPDH, actin and protein-tyrosine phosphatase 1B (PTP1B)[104]. On the other hand, Grx has a role in deglutathionylation of proteins by catalyzing the removal of GSH from cysteine residues by disulfide-exchange mechanism (Figure 1.18). The Grx-catalyzed deglutathionylation involves both monothiol and dithiol mechanisms and release of GSSG which is reduced back to GSH by GR (Figure 1.18). There are several other enzymes involved in deglutathionylation. Sulfiredoxin (Srx) deglutathionylates many proteins, such as PRX1, actin and PTP1B[104]. Deglutathionylation of catalytic cysteine in PTP1B activates its phosphatase activity and therefore plays a crucial role in regulating important signaling pathways[103].

1.9.3 Regulation of protein function through S-glutathionylation

When cells undergo oxidative stress, the thiol groups in proteins can get oxidized into sulfinic and sulfonic acids. The consequences of this irreversible protein modification include inactivation of the protein as well as degradation of the protein[105, 106]Therefore under oxidative stress, where there is a high level of ROS or RNS production, protein S-glutathionylation plays an important role in protecting the protein thiols from permanent oxidation. This may also has a regulatory function in different cellular processes as evident by the glutathionylation of cysteines in some proteins even at basal conditions[102].

Since S-glutathionylation is reversible, it enables the restoration of protein function by reducing the protein thiols back to the native sulfhydryl form[107]. As examples, reversible inactivation of γ-glutamyl transpeptidase, α-ketoglutarate dehydrogenase and HDL-associated paraoxonase 1 (PON1)[108] by S-glutathionylation protect these enzymes from irreversible oxidative damage caused by oxidative stress including hydrogen peroxide, alterations in mitochondrial GSH status etc[109].

Nevertheless, modification of a functionally critical cysteine by S-glutathionylation may affect the protein function and compromise its cellular activities, especially in the case of enzymes and transcription factors[110]. Also it can effect ROS/RNS production and is evident in Cu/Znsuperoxide dismutase, thioredoxin, glutaredoxin and 1-Cys peroxiredoxin when they undergo S-glutathionylation[111-113]. In some instances, protein function is inhibited by glutathionylation as seen with some of the metabolic enzymes, including tyrosine hydroxylate, aldose reductase, creatine kinase and GAPDH[114].

Glutathionylation of different cysteine residues in the same protein can have different biological significances. When Cys67 in HIV-1 protease is glutathionylated, it stabilizes the protein and activates protease activity. In contrast, glutathionylation of Cys95 is involved in inhibiting the protease activity. As another example, in carbonic anhydrase III, glutathionylation of Cys186 activates its phosphatase activity whereas Cys181 glutathionylation inhibits it.

S-glutathionylation regulates many kinases and phosphatases and therefore it plays an important role in cellular signaling pathways during cell proliferation, differentiation, apoptosis and immunity[115]. S-glutathionylation of Ras, a small GTPase is

induced by angiotensin II and is involved in hypotrophy in both smooth muscles and cardiac myocytes[116]. Glutathionylated Ras activates downstream signal transduction pathways involving ERK and AKT, and also inhibits insulin signaling in endothelial cells[117]. S-glutathionylation can inhibit most of the kinases[118]. For instance, when Cys199 in the active site of protein kinase A (PKA) undergoes glutathionylation, the kinase activity is inhibited in a reversible manner[119]. Protein glutathionylation can regulate several transcription factors by altering protein-DNA interactions. Glutathionylation of p65 and p50 subunits in NF- kB interferes with DNA binding and therefore inhibits transcription of target genes[120].

Previous studies have shown ROS induced oxidative modifications of several sarcomeric proteins[99]. Myosin heavy chain is oxidized at C697 and C707, which reduce its ATPase activity, thus decreasing the sliding force during sarcomere contraction[121]. Actin is glutathionylated at C374, which decreases the maximum contractile force[122]. Titin is glutathionylated at cryptic cysteine residues or oxidized at N2B domain, which decreases sarcomere elasticity and increases stiffness of sarcomere during contraction[123]. Previous global analysis found relatively a few number of proteins (e.g. actin, tropomyosin, and troponin) glutathionylated in sarcomere, muscle, or myocytes[124]. However, the identity of proteins that are susceptible to glutathionylation in response to mROS and their roles in regulating sarcomere stability and integrity remain largely unknown, which is crucial for understanding the complex role of mROS in muscle.

1.10 Clickable glutathione approach in cardiomyocyte cell line

A direct consequence of ROS in the sarcomere includes oxidative protein modifications, including disulfide, sulfenylation, and glutathionylation.[125, 126] In particular,

glutathionylation is one of the significant oxidative protein modifications in response to ROS.[127] We recently developed a clickable glutathione approach to identify protein glutathionylation.[128, 129] In this approach, we mutated one of the enzymes involved in glutathione biosynthesis pathway. The γ-glutamylcysteine synthetase, the first and rate limiting enzyme, catalyzes the reaction between glutamic acid and cysteine in order to synthesize the γ-glutamylcysteine (Figure 1.19). Glutathione synthetase, the second enzyme of GSH biosynthesis pathway, catalyzes the reaction glycine with γ-glutamylcysteine to produce GSH (γGlu-Cys-Gly) *in-vivo* (Figure 1.19a)[130, 131].

Azido-glutathione (γGlu-Cys-azido-Ala) is in situ biosynthesized in cells expressing a glutathione synthetase mutant (GS M4) that efficiently catalyzes an incorporation of azido-Ala in place of Gly in glutathione (γGlu-Cys-Gly) (Figure 1.19a).[128]

a

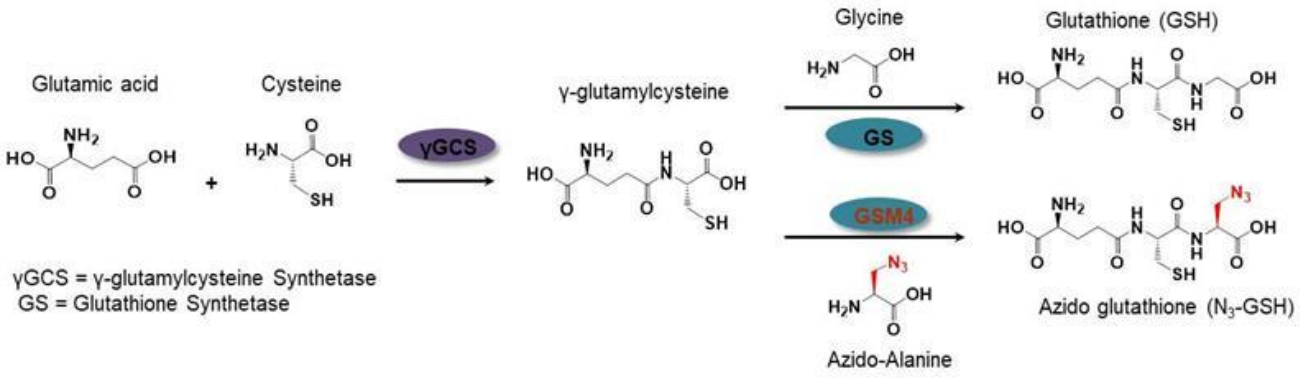

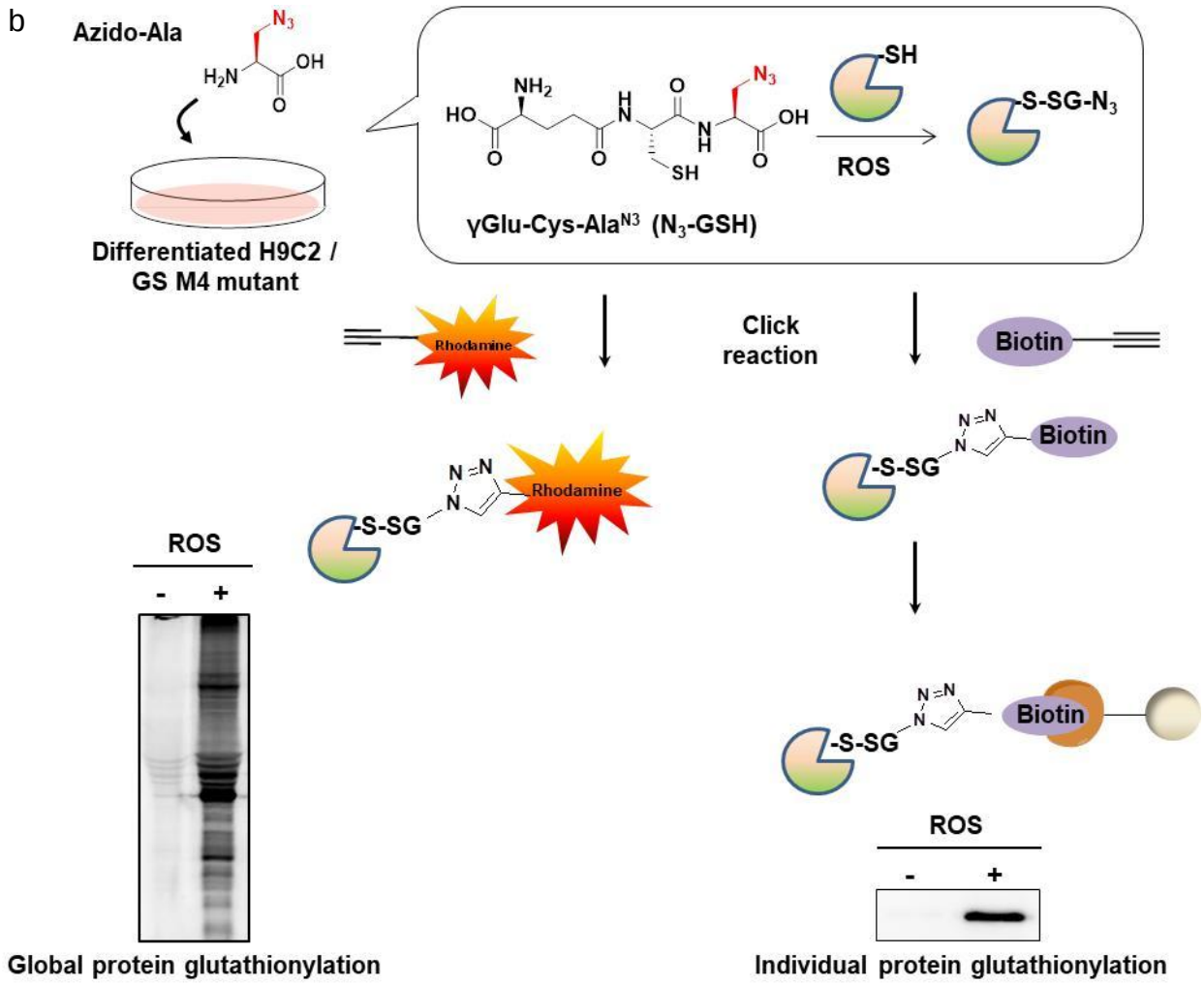

Figure 1.19. Clickable glutathione approach in H9c2 myocytes to detect protein glutathionylation. Mutant form of a glutathione synthetase, second enzyme of glutathione biosynthesis pathway, catalyzes the incorporation of azido alanine onto γ-glutamylcysteine more effectively than glycine synthesizes a glutathione derivative *in vivo* with a azido clickable handle. During oxidative stress (ROS stimuli) labeled proteins with clickable glutathione detects by in-gel fluorescence (global protein glutathionylation) or biotin-streptavidin analysis (individual protein glutathionylation).

Importantly, a clickable functionality on glutathione serves as an efficient chemical tag for identifying and characterizing glutathionylated proteins. During oxidative stress (ROS stimuli), labeled proteins with clickable glutathione (global protein

glutathionylation) are detected by in-gel fluorescence analysis using a fluorophore alkyne and individual protein glutathionylation can be detected by streptavidin-biotin pulldown (Figure 1.19b).

With this approach, we recently found that glucose depletion or a treatment of mitochondrial electron transport chain blockers strongly induces global protein glutathionylation in which glucose availability was an important factor for induction of glutathionylation.[132] Further mass spectrometry analysis identified multiple glutathionylated proteins, including SET and MYND domain-containing protein 2 (SMYD2).[132]

1.11 Specific goals and significant findings of the dissertation work

ROS play an essential role in redox signaling, but also cause detrimental effects under oxidative stress, especially in cardiac and skeletal muscle[133]. For example, low levels of ROS are produced in muscle or increased during exercise, regulating intracellular calcium release and contractile force[134]. Hydrogen peroxide (H_2O_2) derived from the endothelium and myocardial mitochondria serves as a vasodilator that regulates the coronary collateral flow[135]. In contrast, high levels of ROS induce abnormal calcium regulation, a loss of contractile force, contractile dysfunction, and hypertrophy. Indeed, elevated levels of ROS are associated with muscle-related pathological conditions, including myocardial ischemia-reperfusion injury[136], heart failure[71], and muscular dystrophy[137].

The basic contractile unit of striated muscle is a sarcomere. Sarcomeres are composed of multiple sarcomeric proteins, including actin, myosin, and titin, that are assembled in a highly organized structure[8]. Many of these ROS effects partially result

from oxidative modifications of sarcomeric or myofibrillar proteins. For example, ROS elevated during ischemic reperfusion cause glutathionylation and carbonylation of actin[138], glutathionylation of troponin subunits[139], and disulfide formation in tropomyosin[140], nitration of myosin[141], many of which result in the reduced contractile force of myofilaments. Titin is also oxidized in multiple regions. For example, the N2B domain of titin forms disulfide, which increases muscle stiffness[142]. The cryptic cysteine residues in Ig-domains of titin at the I-band are also glutathionylated, which reduces passive stiffness[123].

One major consequence of ischemic reperfusion injury that induces mitochondrial ROS or during autophagy under nutrition-deprivation is degradation of sarcomeric proteins, which reduces the contractile force of muscle[143-145]. For example, an ischemia-reperfusion injury leads to an increased activity of several proteases, including MMP-2 and calpain 1/3[83]. Activated MMP-2 and calpains are involved in degradation of several sarcomeric proteins, including titin, α-actinin, troponin, and myosin-light chains[84, 85]. In particular, titin serves as an integral part for a stress-sensing network. The elastic region of titin binds with chaperones, proteases, and signaling complexes of which interactions are altered in response to the mechanical and chemical stress, ultimately causing muscle degradation, remodeling or adaptation to stress[3, 146]. The molecular link between sarcomeric protein oxidative modification and the action of the protease system is not well-characterized. In order to address these unanswered questions, I started to analyze the functional importance of SMYD2 glutathionylation in cardiomyocytes as my dissertation work.

Glutathionylation plays an important role in regulating protein function in cellular stress[127]. In this report, we used our clickable glutathione approach to detect glutathionylation of multiple proteins, including SMYD2, under stressed conditions. A key idea of our approach is routing glutathione biosynthesis to clickable glutathione by using a mutant of a glutathione biosynthetic enzyme[147]. A modified clickable glutathione is an efficient substrate of glutathione disulfide reductase (GR), glutathione transferase omega (GSTO), and glutaredoxin 1 (Grx1), and is tolerated in cells without significant disturbance of the redox system[129, 148], all of which support that our approach is suitable for investigating glutathionylation in response to cellular stress.

We confirmed glutathionylation of SMYD2 in various stressed conditions and found selective glutathionylation at Cys13. While there are 17 Cys residues in SMYD2, many of them are bound to zinc atoms or buried inside SMYD2, thus may not be accessible for glutathionylation.

A key observation in my dissertation is that myofibril integrity is significantly lost in cells expressing SMYD2 WT in response to ROS, whereas SMYD2 C13S protects myofibrils from degradation, showing a critical role of SMYD2 glutathionylation in myofibril integrity or sarcomere stability.

Another important finding is that protein interaction between SMYD2 and the N2A domain of titin contributes to modulating myofibril or sarcomere degradation. Indeed, protein-protein interactions at titin's extensible domains, including N2B, PEVK, and N2A at the I-band, play a central role in stress-signaling[149]. The N2A domain has four Ig-domains and one extensible unique sequence (N2A-Us) [150]. Hsp90-SMYD2 chaperone complex binds to N2A, mainly with N2A-Us. Our data showed that the SMYD2-N2A

interaction protects N2A from degradation by MMP-2 and calpain 1, and SMYD2 also protect titin in myofibrils from MMP-2 mediated cleavage.

Therefore, our data support the concept that N2A is an important domain of titin where the SMYD2-Hsp90 chaperone complex interacts for stabilization or protection of sarcomeres. Notably, it is interesting to find that N2A can be cleaved by MMP-2 and calpain 1 in our data. While titin is known to be degraded by MMP-2 and calpain 1, the exact cleavage sites of titin are unknown and difficult to confirm due to a large size of titin (>3 MD). Our data suggest that titin can be cleaved at the N2A domain that interacts with SMYD2.

Overall, our study discussed in this dissertation provides evidence, that SMYD2 can be selectively glutathionylated at Cys13, and SMYD2 Cys13 glutathionylation serves as a key molecular event that leads degradation of sarcomeric proteins in response to ROS.

CHAPTER 2: MATERIALS AND METHODS

2.1 Materials

All chemicals were purchased from Sigma unless otherwise stated. Amaxa Cell Line Nucleofector™ Kit L for H9c2 cell line was purchased from Lonza. All cell culture reagents, media and Alexa-Fluor 647 goat anti-mouse IgG (H+L) secondary antibody (Cat# A21235) were purchased from Life Technologies. Human Heart QUICK-CLONE™ cDNA library was purchased from Clontech (Cat# 637213). ProLong Gold Antifade Mountant with DAPI, high capacity streptavidin-agarose beads, chemiluminescent substrates, HRV 3C Protease Solution Kit (2 units/µL) and Protein G Agarose beads were purchased from Thermo Scientific. HRP-conjugated anti-mouse (Cat# NA931), anti-rabbit secondary antibodies (Cat# NA934) and Glutathione Sepharose 4 Fast Flow beads were purchased from GE healthcare. EDTA-free protease inhibitor cocktail tablets were purchased from Roche. Polyethyleneimine-MAX was purchased from Polysciences, Inc (USA). Ni-NTA agarose was purchased from QIAGEN. Oxidized glutathione and 2, 2-dithiodipyridine were purchased from Acros Organics. S-Adenosylhomocysteine-D4 was purchased from Cayman chemicals. Human Active Matrix Metalloproteinase 2 (MMP-2) was purchased from EMD Milipore and Human Calpain 1 was purchased from Sigma. Trypsin Gold, Mass Spectrometry Grade was purchased from Promega. SeaKem Gold Agarose (Cat# 50152) was purchased from Lonza. SUMO Protease 1 was purchased from LifeSensors. ARP 100 (MMP-2 inhibitor) and Acetyl-Calpastatin (184-210) (calpain 1 inhibitor) were purchased from Tocris Bioscience. Actin-EGFP [151] (pEGFP-C1 beta actin) and myosin heavy chain-mCherry [152] (pCMV-mCherry-MHC-IIA) mammalian vectors were obtained from Addgene.

2.2 Synthesis of glutathione derivatives

2.2.1 Synthesis of azido-glutathione using GSM4 enzyme

Clickable GSH containing L-azido-Ala (azido-glutathione, ^{N3}GSH) was synthesized using GS M4 enzyme. 3.5 mM azidoalanine, 3.0 mM γ-glutamyl-cystein, 10 mM ATP, 50 mM $MgCl_2$, 300 mM NaCl, 200 mM Tris buffer (pH = 7.4) and GSM4 (80 ng) were mixed together in 10 mL final reaction mixture and incubated overnight in 37^{o}C. After acidification of the aqueous solution it was subjected to HPLC purification and oxidized form of azido-glutathione (Figure 2.1) was obtained as a white solid after lyophilization.

Purity and mass were confirmed by ESI-MS and LC/MS. Calculated mass: 722. ESI m/z 723 (M+H), 362 (M+2H), 761 (M+ K^+) and 381 (M+ K^++H). Oxidized azido-glutathione was reduced using dithiothreitol (DTT) (2 equivalent) in 100 mM PBS (pH = 7.4) at room temperature for 2 hrs. Then acidified aqueous sample was subjected to HPLC purification and reduced azido-glutathione (Figure 2.2) was obtained as a white solid after lyophilization. Purity and mass were confirmed by ESI-MS and LC/MS. Calculated mass: 362. ESI m/z 363 (M+H) 725 (2M+H).

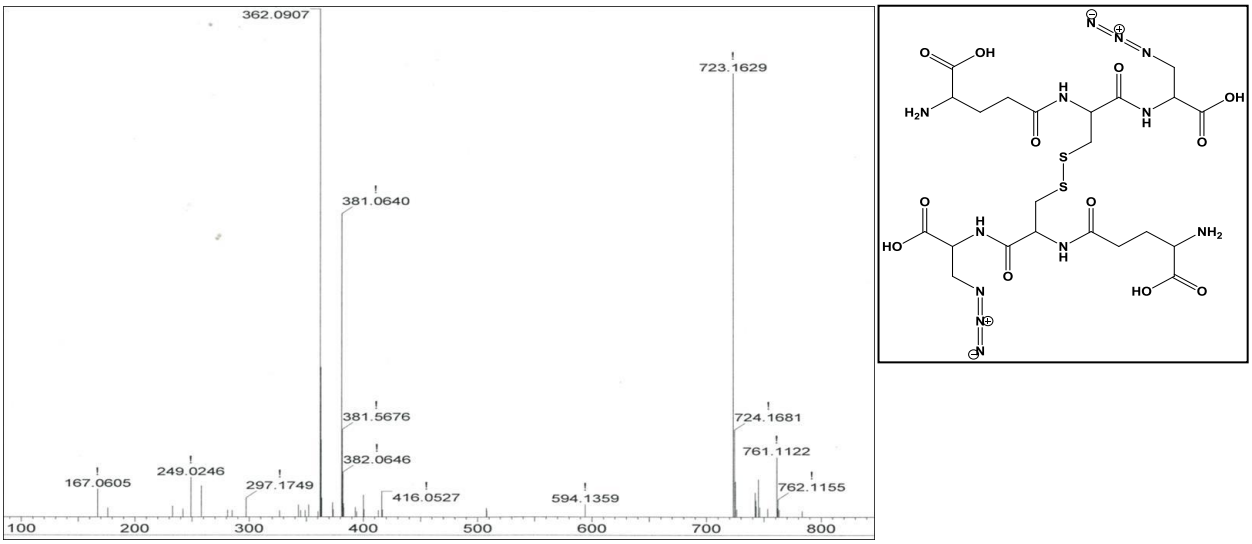

Figure 2.1. ESI mass spectrum of oxidized azido-glutathione (^{N3}GSSG ^{N3})

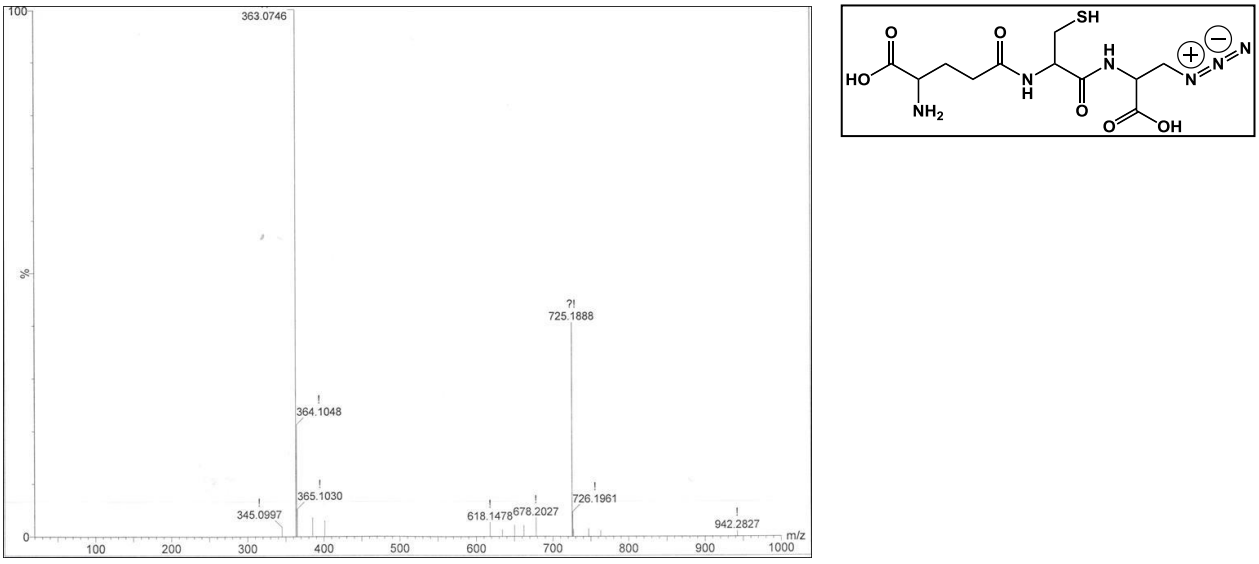

Figure 2.2. ESI mass spectrum of azido-glutathione (^{N3}GSH)

2.2.2 Synthesis of mixed oxidized form of ^{N3}GS-SG, ^{N3}GS-8mer, GS-8mer

Mixed oxidized glutathione (^{N3}GS-SG, ^{N3}GS-8mer, GS-8mer) was synthesized by using 2,2'- dithiopyridine. Glutathione (1 equivalent) and 2, 2-dithiodipyridine (2 equivalant) were mixed in water: methanol (1:1) mixture and stirred for 15-20 hrs at

room temperature. After completion of the reaction, methanol was removed by rotary evaporation and the aqueous layer was extracted several times with dichloromethane[153, 154]. Then the aqueous portion was subjected to HPLC purification and S-(2-thiopyridyl) GSH (Figure 2.3) and ^{N3}GSH (Figure 2.4) was obtained as a white

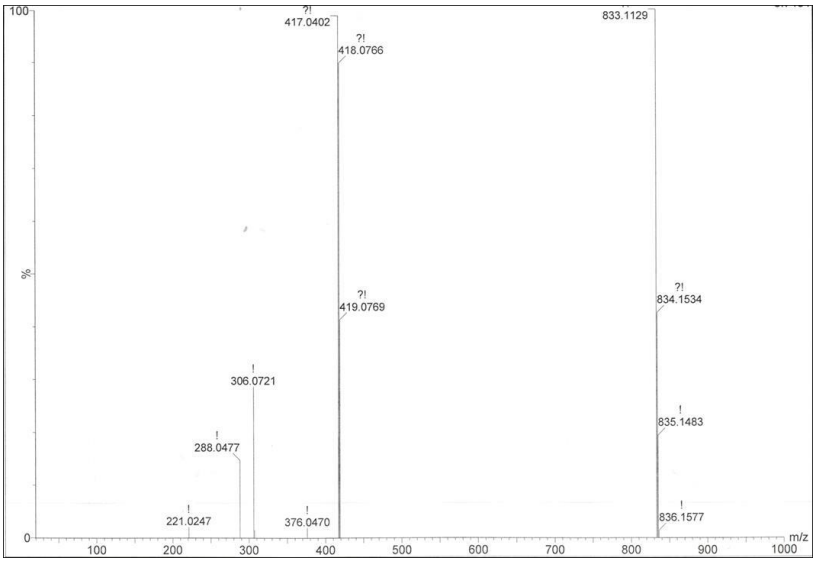

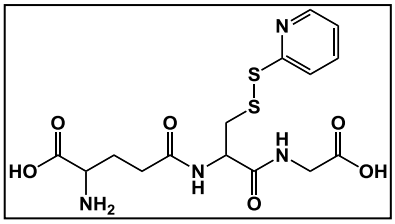

Figure 2.3. ESI mass spectrum of S-(2-thiopyridyl) GSH

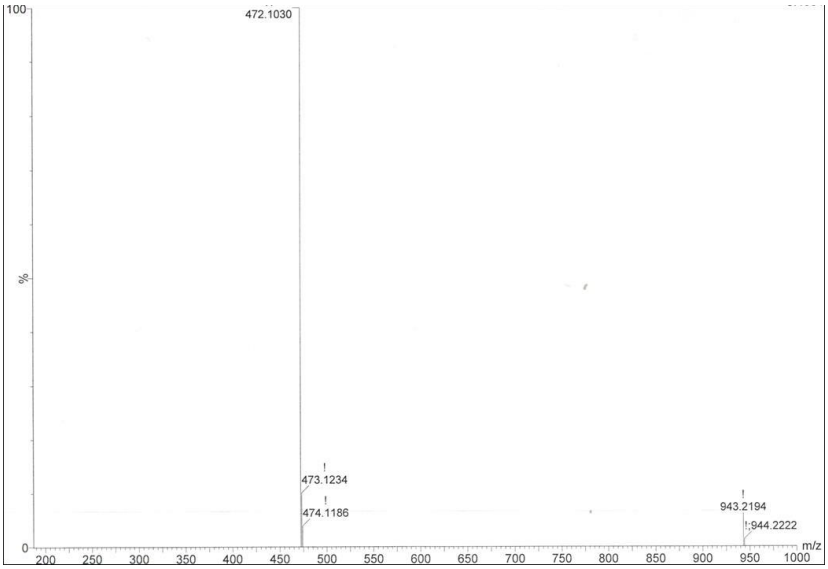

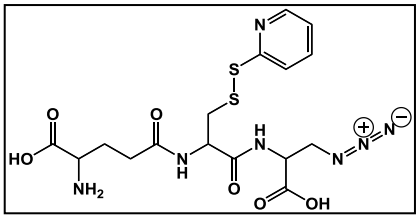

Figure 2.4. ESI mass spectrum of S-(2-thiopyridyl) ^{N3}GSH

solid after lyophilization. Purity and mass were confirmed by ESI-MS and LC/MS. Calculated mass for S-(2-thiopyridyl) GSH : 416. ESI m/z 417 (M+H) 833 (2M+H). Calculated mass for S-(2-thiopyridyl) ^{N3}GSH: 471. ESI m/z 471 (2M+2H), 943(2M+H).

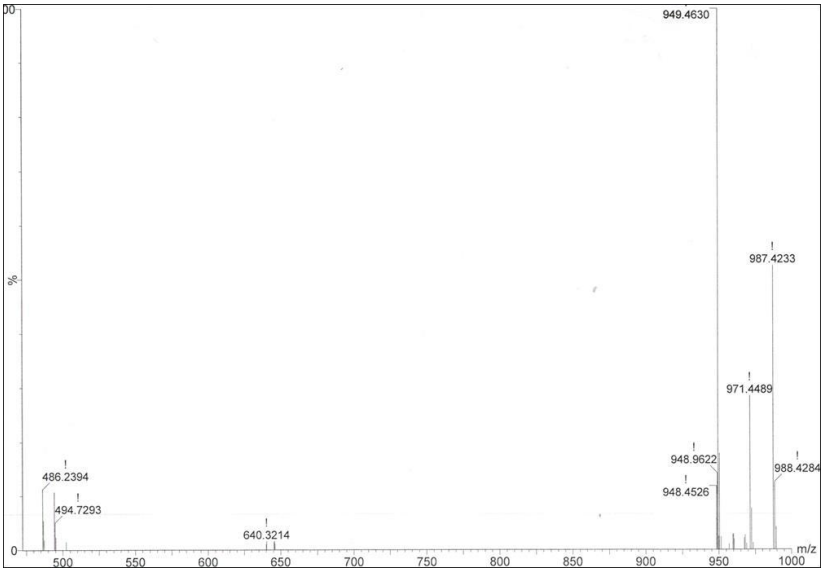

Figure 2.5. ESI mass spectrum of 8mer peptide (SQLWCLSN)

S-(2-thiopyridyl) ^{N3}GSH (1 equivalent) and GSH (1 equivalent) were dissolved in 100 mM PBS buffer (pH = 7.4) and the reaction mixture was stirred for 2 hrs at room temperature for the synthesis of ^{N3}GS-SG (Figure 2.6). S-(2-thiopyridyl) ^{N3}GSH (1 equivalent) or S-(2-thiopyridyl) GSH (1 equivalent) was mixed with 8-mer peptide (SQLWCLSN) (Figure 2.5) (this peptide was synthesized by using Fmoc solid phase peptide synthesis) in 100 mM PBS buffer (pH = 7.4) with 20% acetonitrile and stirred for 2 hrs at room temperature for the synthesis of ^{N3}GS-8mer (Figure 2.7) and GS-8mer (Figure 2.8). After completion of the reaction, aqueous layer was extracted with dichloromethane for five times to remove the thione by-product.

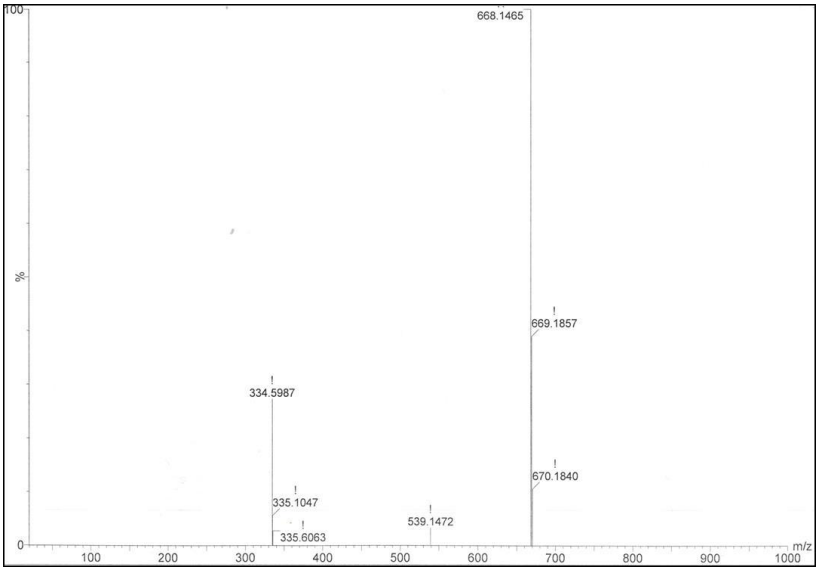

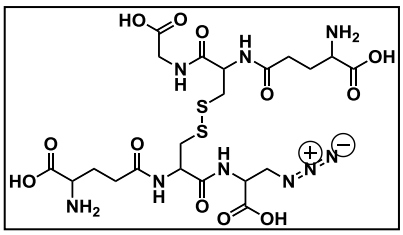

Figure 2.6. ESI mass spectrum of ^{N3}GS-SG

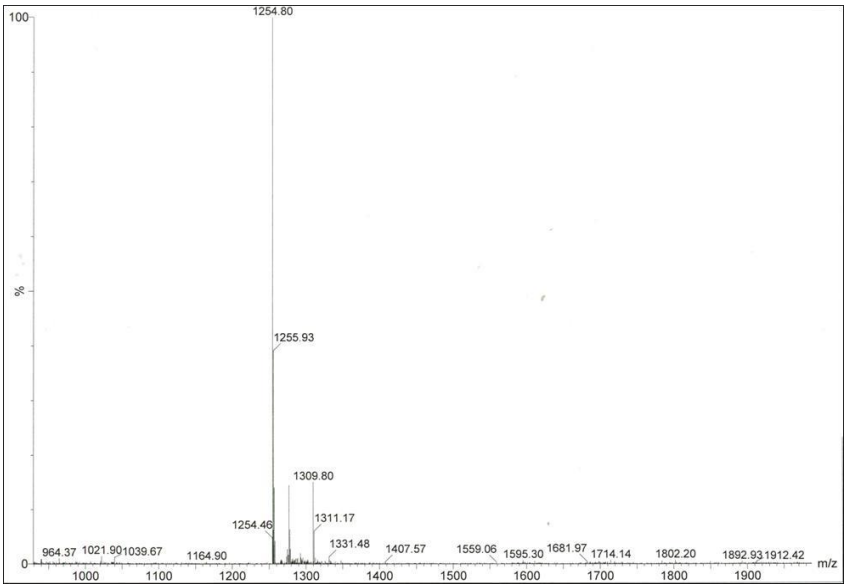

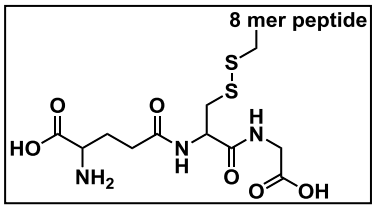

Figure 2.7. ESI mass spectrum of GS-8mer

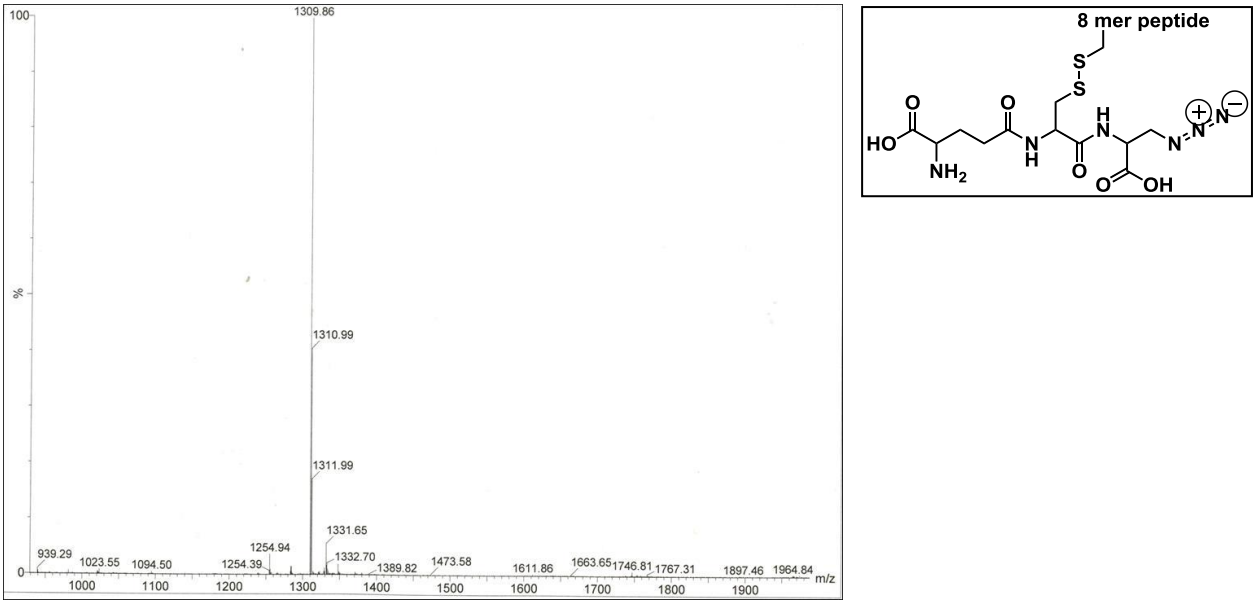

Figure 2.8. ESI mass spectrum of ^{N3}GS-8mer

Then aqueous portion was subjected to HPLC purification and white solids were obtained after lyophilization. Calculated mass for ^{N3}GS-SG: 667. ESI m/z 668 (M+H) 334 (M+2H). Calculated mass for ^{N3}GS-8mer : 1308. ESI m/z 1309 (M+H) 655 (M+2H). Calculated mass for ^{N3}GS-8mer: 1254. ESI m/z 628 (M+2H).

2.3 Spectrophotometric assay of GSTP1 Activity

Enzyme assay was carried out in 0.1 M PBS (phosphate buffer saline) (pH 6.5) with 1 mM EDTA and1 mM CDNB. In this assay condition generation of G-SDNB was monitored by measuring absorbance at 340 nm using DU730-Beckman coulter UV-VIS Spectrophotometer. The rate of spontaneous conjugation of GSH to CDNB was subtracted from the rates of GSTP1 catalyzed reactions[155]. The extinction coefficient (9.6 $mM^{-1}cm^{-1}$) for the G-SDNB at 340 nm was used to calculate the enzyme kinetics[156]. Initial velocity versus substrate concentration plots were fitted to the Michaelis-Menten equation using Graphpad prism 5.01 and apparent kinetic constants (K_m, K_{cat} and V_{max}) for GSH, GSH (L) alkyne and GSH (L) azide were calculated accordingly.

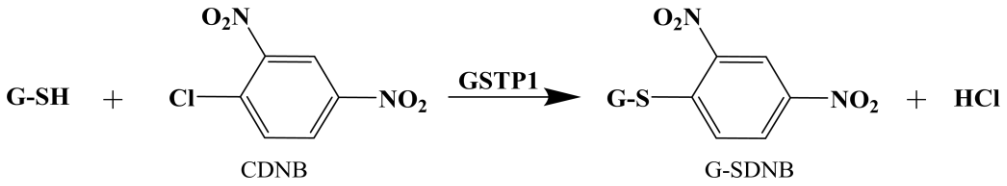

Figure 2.9. Gstp1 catalyzes conjugation of GSH and CDNB

CDNB = 1-Chloro-2, 4-Dinitrobenzene

G-SDNB = Glutathione-2, 4-Dinitrobenzene

2.4 Spectrophotometric assay of Grx1/ GSTO1 Activity

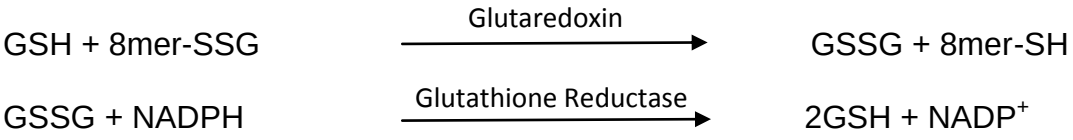

Figure 2.10. NADPH dependent deglutathionylation by GRX1 and GSTO1.

The coupled spectrophotometric assay was performed in 0.1 M PBS (pH 7.4) with 1 mM EDTA, 0.2 mM NADPH, GR (4 units per mL), GSH 0.25 mM and Grx1 (23 nM) or GSTO1 (0.19 µM) and was incubated for 7 min at 25^0C[157]. The reactions were initiated by adding the substrate and oxidation of NADPH was monitored at 340 nm using DU730-Beckman coulter UV-VIS spectrophotometer[158]. Non-enzymatic reaction was subtracted from the GRX1 (glutaredoxin) catalyzed reaction and extinction coefficient (6.2 $mM^{-1}cm^{-1}$) for the NADPH was used to calculate the enzyme kinetics[159]. Initial velocity versus substrate concentration plots were fitted to the Michaelis-Menten equation using Graphpad prism 5.01 and apparent kinetic constants (K_m, K_{cat} and V_{max})

for 8mer-SSG, 8mer-SSG (L, D) alkyne and 8mer-SSG (L) azide were calculated accordingly.

2.5 Spectrophotometric assay of GR Activity

$$GSSG + NADPH \xrightarrow{\text{Glutathione Reductase}} 2\,GSH + {}^{+}NADP$$

Figure 2.11. NADPH dependent reduction of oxidized GSH by GR.

Kinetic parameters for GR were determined by measuring consumption of NADPH in different substrate concentrations (0.01-0.5 mM). NADPH consumption was monitored at 25^{O}C by UV absorbance at 340 nm[160]. The reaction mixture (0.2 mL) contains 100 mM PBS (pH 7.4), 1 mM EDTA, 0.2 mM NADPH and 50 ng of GR. The extinction coefficient (6.2 $mM^{-1}cm^{-1}$) for the NADPH was used to calculate the enzyme kinetics. Initial velocity versus substrate concentration plots were fitted to the Michaelis-Menten equation using Graphpad prism 5.01 and apparent kinetic constants (K_m, K_{cat} and V_{max}) for GSSG, GSSG (L) alkyne and GSSG (L) azide were calculated accordingly.

2.6 Cloning and mutagenesis

PCR and cloning techniques were applied to construct the pcDNA3.1 (+)-HA-SMYD2 WT/C13S/C13D/Y24F, pGEX-6p-2 GST-N2A, pET-28a N2A and pcDNA3.1 (+)-N2A-FLAG. Human titin N2A domain (exon 102-109 or Ig 80-83) (UniProtKB - Q8WZ42 (TITIN_HUMAN)) region was amplified by PCR from human cardiac cDNA library (Clontech), and cloned into pGEX-6p2 bacterial expression vector: N2A region was amplified by using a forward primer (5'-CG CCG CGA ATT CTC ATG GTG GCT

GGA AGT GAC ACT ACC AAA TCA AAA GTG ACC-3') with EcoR1 restriction site, and a reverse primer (5'- GCG CGC CTC GAG TCA GGA GTC AGG AAT ATC AGG AGG CTT CAG CTC AAG -3') with Xho1 restriction site, as reported previously [31]. PGEX-6p-2 plasmid and PCR product were double digested with EcoR1 and Xho1. Ligation was then performed using T4 DNA ligase. Human GSTP1 cDNA clone (OriGene) and Human GSTO1 cDNA clone (gift from Dr. YoungTae Chang, National University of Singapore) were subcloned in to pET-28a (+) bacterial expression vector using NheI/XhoI (GSTP1) and NdeI/XhoI (GSTO1) restriction sites. PCR reaction was performed using forward primer (5'- GCG CGC GCT AGC ATG CCG CCC TAC ACC GTG GTC TAT TTC -3') with NheI and reverse primer (5'- GCG CGC CTCGAG TCA CTG TTT CCC GTT GCC ATT GAT GGG -3') with XhoI for human GSTP1 cDNA clone. Forward primer (5'- GCG CGC CAT ATG ATG TCC GGG GAG TCA GCC AGG-3') with NdeI and reverse primer (5'-GCG CGC CTC GAG TCA GAG CCC ATA GTC ACA GGC C-3') with XhoI were used for the PCR reaction of human GSTO1 cDNA clone. Both PCR product and the empty pET-28a (+) vector were double digested with above restriction enzymes accordingly and ligated using T4 DNA ligase. For mammalian expression vectors, human SMYD2 gene was amplified by PCR with a forward primer (5'-GCG CGC GCT AGC ACC ATG AGG GCC GAG GGC CTC -3') with Kozak sequence and Nhe1 restriction site and reverse primer (5'-GCG CGC CTC GAG TCA GGC ATA GTC GGG CAC GTC ATA CGG ATA GTG GCT TTC AAT TTC CTG TTT GAT CTC AG-3') with C-terminal HA-tag and Xho1 restriction site. A PCR product of SMYD2 gene was sub-cloned into pcDNA3.1/hygro (+) mammalian vector using Nhe1/Xho1 sites. For mammalian expression, N2A domain was amplified by PCR with a

forward primer containing Kozak sequence, N-terminal FLAG-tag, and BamH1 restriction site (5’-GCC GCC GGA TCC ACC ATG GAC TAC AAA GAC GAT GAC GAC AAG GTG GCT GGA AGT GAC AC-3’) and a reverse primer with Xho1 restriction site (5’-CGC CGC CTC GAG TCA GGA GTC AGG AAT ATC AGG AG-3’). All bacterial and mammalian mutant vectors of SMYD2 were constructed using quick change mutagenesis with following primers: SMYD2 C13S mutation (forward: 5’-GGC CTG GAG CGC TTC AGC AGC CCG GGC AAA GGC-3’ and reverse: 5'-GCC TTT GCC CGG GCT GCT GAA GCG CTC CAG GCC -3'), C13D mutation (forward: 5’-GGC CTG GAG CGC TTC GAC AGC CCG GGC AAA GGC-3’ and reverse: 5’-GCC TTT GCC CGG GCT GTC GAA GCG CTC CAG GCC-3’), Y240F mutation (forward: 5’-G GAG GTT TTT ACC AGC TTT ATT GAT CTC CTG TAC CC-3’ and reverse: 5’-GG GTA CAG GAG ATC AAT AAA GCT GGT AAA AAC CTC C-3’). The entire open reading frame (ORF) of all prepared plasmids was confirmed by DNA sequencing and agarose gel electrophoresis after digestion with appropriate restriction enzymes.

2.7 Bacterial expression and purification of proteins

BL21 (DE3) cells were transformed with pCDF-SUMO-SMYD2 (WT, C13S, or C13D). Transformants were grown in LB medium (2 L) at 37^{o}C until OD_{600} reached about 0.5. The protein expression was induced with 0.1 mM IPTG and was incubated overnight at 15^{o}C. Cells were harvested by centrifugation at 5,000 rpm for 20 min, and lysed by passing French Press three times. Cell lysate was centrifuged at 15,000 rpm for 30 min, and the soluble fraction was subjected to Ni^{2+}-NTA affinity column. The eluted protein was incubated with SUMO Protease 1 at 4^{o}C for 10 h in a buffer (50 mM Tris pH 7.4, 150 mM NaCl and 6 mM β-mercaptoethanol). The mixture was then

incubated with Ni^{2+}-NTA beads to remove His6-SUMO tag and His-SUMO protease. Cleaved SMYD2 was collected in the flow-through. SMYD2 protein was finally purified by anion exchange column [Mono Q^{TM} 5/50 GL cation column (GE Healthcare) with a buffer A (50 mM Tris-HCl pH 8.0) and a buffer B (50 mM Tris-HCl, pH 8.0, and 1 M NaCl) to homogeneity and concentrated to 4-5 mg/ml. The purified protein was stored in a buffer with 50 mM Tris–HCl pH 8.0, 150 mM NaCl, 0.2 mM β-mercaptoethanol and 5% glycerol. The same approach was applied to express the GST-Hsp90 and GST-N2A where proteins were incubated with glutathione beads for purification, and proteins were stored in a buffer with 50 mM Tris–HCl pH 8.0, 150 mM NaCl, 0.2 mM β-mercaptoethanol and 5% glycerol. GST on N2A domain was cleaved using HRV 3C Protease Solution Kit (2 units/µL). Initially, GST-N2A was incubated with the HRV 3C protease (enzyme/substrate ratio = 1/50) overnight at 4^{o}C in the supplied 1X HRV 3C protease reaction buffer. The cleaved mixture was incubated with pre-washed GSH beads (three times with 1X HRV 3C protease reaction buffer) for 2 hr at 4^{o}C. The cleaved N2A domain was then collected in the flow-through and stored in the same buffer (50 mM Tris–HCl pH 8.0, 150 mM NaCl, 0.2 mM β-mercaptoethanol and 5% glycerol). GST (S.japonicum) was expressed using pGEX-6P-2 plasmid and purified as described elsewhere. All the bacterial expression constructs (pET-HisGSTP1 and pET-HisGSTO1) were transformed in to BL21 (DE3) cells and transformants were grown at 37^{O}C until OD_{600} reached about 0.6 in 1 L LB medium. The protein expression (GSTP1 and GSTO1) was induced with 1 mM isopropyl-1-thio-β-D-galactopyranoside (IPTG) and was incubated 4-5 hr at 37 ^{O}C. The expression of PTP1B was induced with 0.2 mM IPTG and was incubated 14 hr at 23 ^{O}C The Cells were harvested by

centrifugation at 5000 rpm for 20 min and lysed by French Press. Then cell-free lysate was centrifuged at 15 000 rpm for 20 min and soluble fraction was purified by Ni^{2+}-NTA affinity column. The eluted proteins were dialyzed (50 mM Tris–HCl (pH 8.0), 150 mM NaCl, 0.1 mM DTT and 5% glycerol) and concentrated. Protein concentrations were determined by Bradford assay.

2.8 Preparation of glutathionylated SMYD2 in vitro

SMYD2 WT protein was incubated in a buffer (100 mM Tris-HCl pH 7.4 and 150 mM NaCl) with and without 1 mM oxidized glutathione at 4^{o}C for 4 h, respectively. These two samples were then purified by anion exchange column chromatography using Mono Q^{TM} 5/50 GL cation column (GE healthcare). A linear gradient between a buffer A (50 mM Tris-HCl, pH 8.0) and a buffer B (50 mM Tris-HCl, pH 8.0 and 1 M NaCl) was used to elute bound proteins while monitoring absorbance at 280 nm. Glutathionylation of SMYD2 was confirmed using glutathione antibody (Virogen, Cat# 101-A-100) (1:1000) by Western blotting. Purified proteins were dialyzed in a buffer (50 mM Tris–HCl pH 8.0, 150 mM NaCl and 10% glycerol), concentrated, flash-frozen in liquid-nitrogen, and stored at -80^{o}C. Protein concentration was determined by Bradford assay (BioRad) using bovine serum albumin as the standard.

2.9 Partial trypsin digestion of SMYD2

The same amount of purified SMYD2-SH and SMYD2-SSG (5 µg) were mixed with trypsin (1 µg) at 37^{o}C. Digestion was quenched in different time points (15, 30, 60 and 120 min) by an addition of a SDS loading dye and heating at 95^{o}C for 5 min. Digested samples were separated on a SDS-PAGE gel, and protein bands were visualized by Coomassie stain.

2.10 In vitro SMYD2 methyl transferase activity assay

To evaluate the SMYD2 methyl transferase activity, the level of S-adenosylhomocysteine (SAH) generated by the enzymatic reaction was quantified through the multiple reactions monitoring (MRM) mode in LC-MS/MS with SAH-d4 as an internal standard. In MRM mode, the mass transition from the precursor to product was used to detect SAH (*m/z* 385 to 136) and SAH-d4 (*m/z* 389 to 136) with peak quantification [161]. The UV absorbance at 260 nm and a molar extinction coefficient of 15,400 $M^{-1}cm^{-1}$ [162] were used to determine the concentartion of SAM and SAH. The calibration curve was made by plotting the integrated peak size versus SAH concentrations (10, 50, 100, 250 and 1000 nM). The activity assay was carried out at room temperature using 200 nM SMYD2 in a buffer (25 mM Tris-HCl, pH 8.0, and 0.01% Tween 20). For p53 peptide substrate, SAM (25 μM) and p53 peptide (25 μM) were used. For Hsp90 substrate, SAM (5 μM) and Hsp90 (4 μM) were used. For N2A and GST, SMYD2 was incubated with Hsp90-GST (4 μM), N2A (4 μM) or GST(4 μM), followed by additon of SAM (5 μM) for 10 min at room temperature. In each experiment, methylation reaction was quenched at different time points using 5% TCA.

2.11 GST pull-down assay

N-terminal GST-tagged Hsp90 was incubated with glutathione beads at 4^{o}C in a buffer (Tris-HCl pH 7.4, 150 mM NaCl) for 1 h. Beads were then washed 3 times with the same buffer to remove any unbound protein. Then, an equal amount of SMYD2-SH and SMYD2-SSG (purified by ion exchange chromatography) was incubated with immobilized Hsp90 on glutathione agarose for 1 h at 4^{o}C. In control, SMYD2 was incubated with immobilized GST (S.Japonicum) on glutathione agarose. Beads were

then washed with Tris-HCl (pH 7.4) buffer, and bound proteins were eluted with 1x SDS loading dye, and separated on the SDS-PAGE gel. GST-N2A or GST-Hsp90 interaction with SMYD2 or SMYD2 C13D was analyzed in the same manner

2.12 *In vitro* glutathionylation of SMYD2 with azido-glutathione

Glutathionylation of purified SMYD2 WT (10 µg) and C13S (10 µg) was induced in 50 mM PBS buffer containing 1 mM azido-glutathione by adding different concentrations of H_2O_2 or diamide (0, 1, 10, 50 and 100 µM) for 5 min at room temperature. Glutathionylation was quenched by addition of iodoacetamide (20 mM) for 15 min at 37^{o}C in the presence of 1% SDS. Proteins were pelleted by adding cold acetone (-20^{o}C for 30 min). Proteins were re-suspended in 50 mM PBS with 1% SDS, and were subjected to click reaction using 0.2 mM rhodamine-alkyne, 0.8 mM Tris (3-hydroxypropyltriazolylmethyl) amine (THPTA), 1 mM CuBr for 1 h at 37^{o}C. A dose-dependent signal of protein glutathionylation was monitored in a protein gel by fluorescence. To monitor the extent of glutathionylation in SMYD2 WT compared to C13S, the similar approach was used by adding 1 mM oxidized azido-glutathione (^{N3}GSSG^{N3}) for the induction. Proteins were then precipitated by cold acetone treatment, and washed with cold methanol to remove unreacted rhodamine. Proteins were then dissolved in a PBS buffer, and absorbance was taken at 550 nm and used to calculate the bound concentration of rhodamine with a molar extinction coefficient (65,000 $M^{-1}cm^{-1}$) (a sample without oxidized azido-glutathione was used as a control). SMYD2 concentration was quantified in gel analysis by using ImageJ program in comparison to a standard curve made of BSA. A ratio of SMYD2 to rhodamine concentration was plotted versus time to analyze the level of modification.

An *In vitro* mass-tag approach was performed with SMYD2 WT and C13S in a similar condition using 2-kD PEG-alkyne (0.4 mM). The gel-shift of SMYD2 was analyzed by SDS-PAGE gel electrophoresis. The synthesis of reduced and oxidized forms of azido glutathione is described previously.

2.13 Mass identification of the cysteine site of glutathionylation in SMYD2

To a PBS solution (45 µL) containing SMYD2 (100 µg) and azido-glutathione (1.25 mM) was added diamide (100 µM). The solution was allowed to sit at room temperature for 1 hour after which SDS (final 1%) and iodoacetamide (final 20 mM) were added. The solution was incubated at 37^0C for 20 minutes and then cold acetone (4 volumes) was added. The solution was kept at -20^oC for 20 minutes, followed by centrifugation at 7,000 RPM for 5 minutes. The acetone was removed and the protein pellet was suspended in 1% SDS in PBS (36 µL). The samples were briefly sonicated until all of the proteins had been dissolved, and subjected to click reaction by adding biotin-DDE-alkyne (4 µL of a 5 mM stock solution in DMSO), and a premixed solution of THPTA (5 µL of a 20 mM solution in water, final 2 mM) and Cu(I)Br (5 µL of a 20 mM solution in 3:1 DMSO and tert-butanol, final 2 mM). This reaction was allowed to sit at 37^oC for 1 hour, after which EDTA was added (1 µL of 100 mM solution) and kept at room temperature for 15 minutes. The proteins were precipitated by adding cold acetone (4 volumes) for 20 minutes at -20^oC. The solutions were centrifuged at 7,000 RPM for 5 minutes and the supernatant removed. Cold methanol was added to the pellet and briefly sonicated. The resulting suspension was kept at –20^oC for 20 minutes. The protein was pelleted by centrifugation at 7,000 RPM for 5 minutes, and the supernatant was removed. To the pellet was added a 50 µL of denaturation buffer (8 M

urea, 4 mM $CaCl_2$ in 1x PBS). The solution was briefly sonicated and kept at 37^{o}C for 1 hour. The solution was diluted with 150 µL of 1x PBS to make the final concentrations of urea (2 M) and $CaCl_2$ (1 mM), and allowed to digest by trypsin (3 µg) overnight at 37^{o}C. The solution containing the digested peptides was added to streptavidin-agarose resin (50 µL bead volume) in PBS (5 mL). The mixture was incubated with rotation at room temperature for 2 hr. The beads were pelleted by centrifuging at 2,000 RPM for 2 minutes and washed with 0.2% SDS in PBS (5 mL) followed by PBS (3 X 5 mL). The bound peptides were then eluted with a 2% hydrazine solution in PBS (3 X 30 µL, pH 7.4, 30 minutes-incubation for the first two volumes and a wash for the last). The eluted fractions were combined and then acidified with a 5% formic acid solution. The sample was subjected to zip-tip purification and used for MALDI-TOF/TOF analysis with α-cyano-hydroxycinnamic acid (CHCA) as the matrix.

2.14 Cell culture, differentiation and induction of glutathionylation

Neonatal Rat Ventricular Cardiomyocytes (P1-2) (Lonza, R-CM-561) were cultured on nitrocellulose coated plates by following the company protocol and using the media (Lonza, CC-4515) provided by the company. HL-1 cells (kindly provided by Dr. Karin Przyklenk, WSU) were cultured in Claycomb medium (Sigma, 51800C) supplemented with 10% FBS, 100 U/ml penicillin, 100 µg/ml streptomycin, 0.1 mM norepinephrine and 2 mM L-glutamine in fibronectin–gelatin-coated flasks. A H9c2 cell line was obtained from America Tissue Type Collection (ATTC, CRL-1446), and cultured in Dulbecco's Modified Eagle's Medium (DMEM) supplemented with 10% fetal bovine serum (FBS), 100 units/ml penicillin and 100 µg/ml streptomycin. All the cell lines were cultured at 37^{o}C in a 5% CO_2 humidified atmosphere.

H9c2 cells were sub-cultured when reaching a 70–80% confluence to maintain the differentiation potential of H9c2 cells. H9c2 myoblasts were differentiated by switching to DMEM medium containing 1% FBS with supplementation of trans-retinoic acid (1 μM). A differentiation medium (1% FBS, 1% penicillin/streptomycin, and 1 μM all-trans-retinoic acid) were maintained over 5 days. After differentiation, cells were subjected to DMEM medium containing 2% FBS, and infected with adenovirus-expressing GS M4 (Ad/GS M4) (prepared from Vector Biolabs). Briefly, adenovirus (MOI = 25) was incubated with polybrene (10 μg/mL) in DMEM medium containing 2% FBS for 15 min, and added to differentiated H9c2 cells. The medium containing adenovirus was removed after 6 h. Cells were then incubated for 18 h in 10% FBS complete medium and further incubated with L-azido-Ala (0.6 mM) for 20 h. Cells were then washed and serum starved for 4 h before inducing for glutathionylation with different stimuli, including H_2O_2 and antimycin A respectively. After inducing glutathionylation, cells were lysed with a lysis buffer [100 mM Tris-HCl, 150 mM NaCl, pH 7.4, 0.1% Tween 20, a protease inhibitor cocktail tablet, 100 μM PMSF and 50 mM N-ethylmaleimide (NEM)]. Collected lysates were incubated at 4^oC for 30 min. After centrifugation at 16,000 rpm for 15 min, the supernatant was collected and protein concentration was measured by Bradford assay.

A HEK293 cell line stably expressing GS M4 (HEK 293/GSM4) [128] was maintained in DMEM medium with 10% FBS, 100 units/mL penicillin, 100 μg/mL streptomycin and 100 μg/mL hygromycin B at 37°C in a 5% CO_2 humidified atmosphere. For induction of glutathionylation, HEK293-GSM4 cells were transfected with HA-tagged SMYD2 WT or C13S mutant using PEI-MAX as the transfecting agent.

After 24 h, cells were incubated with azido-Ala (0.6 mM) and induced for glutathionylation by adding antimycin A (2 µg/mL) in glucose-free media for 2 h. Cells were then lysed in a lysis buffer (100 mM Tris-HCl, 150 mM NaCl, pH 7.4, 0.1% Tween 20, a protease inhibitor cocktail tablet, 100 µM PMSF and 50 mM N-ethylmaleimide). Lysates were collected in the same manner to H9c2 cells.

2.15 Click reaction and pull down of glutathionylated proteins

Cell lysates collected after inducing glutathionylation from HEK293-GSM4 or H9c2 expressing GS M4 were incubated with 4X volume of cold acetone for 30 min at -20^{o}C. The precipitated proteins were then centrifuged, and protein pellet was re-dissolved in PBS with a brief sonication. The re-suspended proteins were subjected to click reaction with 0.2 mM biotin-alkyne, rhodamine-alkyne, or Cy5-alkyne, 1 mM CuBr and 0.4 mM Tris[(1-benzyl-1*H*-1,2,3-triazol-4-yl)methyl]amine (TBTA). A click reaction mixture was incubated at room temperature for 1 h, and run on SDS-PAGE for fluorescence detection when using rhodamine-alkyne or Cy5-alkyne. For pull down of glutathionylated proteins, a click reaction mixture with biotin-alkyne was treated again with 4X volume of cold acetone, and incubated for 30 minutes at -20^{o}C. Protein pellet was then completely dissolved in TBS buffer (100 mM Tris-HCl and 150 mM NaCl) containing 10% SDS with sonication for 20 seconds. The re-dissolved proteins were diluted with TBS (100 times dilution) and incubated with pre-washed streptavidin agarose beads for 3 h at room temperature. After washing beads with TBST (5 mL) three times, beads were then eluted with a SDS loading buffer, and eluted proteins were separated from running on SDS-PAGE gel for detection of glutathionylated proteins (SMYD2, or Hsp90) by Western blotting. For SMYD2, blots were probed with mouse

anti-HA antibody (Biolegend, Cat# 901502) or rabbit SMYD2 antibody (Cell Signaling Technology, Cat# 9734). For HSP90, blots were probed with mouse anti-HSP90 (BD transduction, Cat# 610418).

For mass-shift analysis of SMYD2, H9c2 cells, after expressing of GS M4 and incubation of azido-Ala, were treated with antimycin A (2 μg/mL) for 1 h or 12 h. Lysates were subjected to click reaction with 2-kD PEG-alkyne twice to assure the complete conjugation (after first click reaction for 2 h at 37^{o}C, lysates were precipitated by acetone and re-dissolved in a TBST buffer, and re-subjected to the second click reaction for 4 h at 37^{o}C). Cell lysates were then separated on SDS-PAGE gel and were analyzed by Western blotting. The blot was probed with rabbit SMYD2 antibody (Cell Signaling Technology, Cat# 9734) to see a mass shift of SMYD2.

2.16 siRNA mediated knockdown of SMYD2 and MMP-2

H9c2 cells were transfected two times during the differentiation process by using Lipofectamine 3000 with SMYD2 siRNA (100 nM) (Santa Cruz Biotechnology, sc-76530) or MMP-2 siRNA (100 nM) (Santa Cruz Biotechnology, sc-37264). As a negative, control siRNA (Santa Cruz Biotechnology, sc-37007) was used.

2.17 Cell viability assay

SMYD2 WT and C13S were expressed in H9c2 myoblasts by electroporation using Nucleofector^{TM} 2b device (Lonza), according to manufacturer protocols. After electroporation, cells were seeded onto six-well plates at a density of 2.5 x 10^5 cells/well with 10% FBS supplemented DMEM medium (3 mL) for 2 days, and then switched to a differentiation medium (1% FBS, 1% penicillin/streptomycin, and 1 μM all-trans-retinoic acid). Differentiated H9c2 myocytes were treated with H_2O_2 (25 μM), antimycin A (2

μg/mL), nitric oxide donor (NONOate, 100 μM), angiotensin II (1 μM), or DMSO (vehicle) in a serum-free DMEM medium for 24 hrs. Cell viability was then measured by Trypan blue assay. Briefly, after removal of the medium, cells were washed once with PBS, and treated with trypsin to detach cells from plates. Cells were then re-suspended in culture medium, and mixed with 0.4% trypan blue sterile-filtered solution (1 part of trypan blue and 1 part of cell suspension) by gently pipetting up and down for 10 times. 10 μL of the mixture was then loaded into the opening of either chamber on the counting slide (BioRad) and cell number was determined by TC20 automated cell counter (BioRad).

In the same procedure, cell viability was measured for differentiated H9c2 myocytes transfected with empty pcDNA3.1 and pcDNA3.1-HA-SMYD2 WT by electroporation, after inducing glutathionylation by treatment of antimycin A. Similarly, differentiated H9c2 cells were transfected with SMYD2 siRNA, MMP-2 siRNA and control siRNA by using Lipofectamine 3000. Cell viability was measured after incubation of antimycin A (2 μg/mL) for 24 h.

The same approach was used to measure the viability of H9c2 myocyte in the presence of MMP-2 inhibitor (ARP 100) or calpain inhibitor (acetyl-calpastatin). Briefly, cells were pre-incubated with acetyl-calpastatin (5 μM) or ARP 100 (1 μM) for 1 h at 37^{o}C in serum free media before incubation of antimycin A (2 μg/mL) for 24 h. Trypan blue assay was then carried out to analyze the percentage of viable cells compared to total cells.

2.18 Immunofluorescence and immunostaining

Neonatal Rat Ventricular Cardiomyocytes were transfected with SMYD2 or C13S mRNA using Lipofectamine MessengerMAX Transfection Reagent (invitrogen), and mRNA were synthesized using mMESSAGE mMACHINE T7 ULTRA Transcription Kit (Invitrogen). For titin and SMYD2, and α-actinin immunostaining, neonatal rat ventricular cardiomyocytes and differentiated H9c2 cells expressing SMYD2 WT or C13S were incubated with antimycin A (2 µg/mL) for 12 h. Cells were then washed 3 times with cold-PBS and fixed with either 4% paraformaldehyde for 10-20 min at room temperature or ice-cold methanol for 10-15 min at -20^{o}C. After fixation, cells were washed with PBS for 3x times and paraformaldehyde fixed cells were incubated 10-15 min at room temperature in a permeabilization buffer (1x PBS with 0.1% Triton X-100). Cells were then kept on a blocking buffer (1x PBS with 0.1% TWEEN-20 and 3% BSA) for 1 h at room temperature. Subsequently, cells were incubated with primary antibodies in a blocking buffer overnight at 4^{o}C. The following antibodies were used: Titin rabbit antibody (Novus biologicals, Cat# NBP 1-88071, I band region of titin) (1:100 dilution), SMYD2 mouse antibody (Sigma, Cat# SAB1407760) (1:100 dilution), SMYD2 rabbit antibody (Cell Signaling Technology, Cat# 9734) (1:100 dilution), HA-tag (6E2) mouse antibody (conjugated with Alexa Fluor 488) (Cell Signaling Technology, Cat# 2350S) and α-actinin mouse antibody (Abcam, Cat# ab9465) (1:100 dilution). After washing several times with PBS, cells were incubated for 1 h at room temperature with the following Alexa Fluor conjugated secondary antibodies: anti-rabbit Alexa Fluor 647 secondary antibody (Invitrogen, Cat# A-21244), anti-mouse Alexa Fluor 647 secondary antibody (Invitrogen, Cat# A-21235), anti-rabbit Alexa Fluor 488 secondary antibody (Invitrogen, Cat# A-11008) and anti-mouse Alexa Fluor 488 secondary antibody

(Invitrogen, Cat# A-11001). Cells were then washed extensively with 1x PBS, and cover slips were mounted onto the microscopic plate with a DAPI-containing mounting solution. Cells were then analyzed under confocal microscope.

PcDNA3.1-HA-SMYD2 WT or pcDNA3.1-HA-SMYD2 C13S was co-transfected with either pEGFP-C1 beta-actin or pCMV-mCherry-MHC-IIA by electroporation using Nucleofector^{TM} 2b device (Lonza). After electroporation, cells were seeded onto six-well plates at a density of 2.5 x 10^5 cells/well with 10% FBS supplemented DMEM medium (3 mL) for 2 days, and then switched to a differentiation medium (1% FBS, 1% penicillin/streptomycin, and 1 μM all-trans-retinoic acid) for 4 days. Differentiated H9c2 myocytes were then kept on serum-free-medium for 12 hrs. Subsequently, cells were treated with antimycin A (2 μg/mL) for 12 hrs. Cells were then washed 3 times with cold-PBS and fixed with 4% paraformaldehyde for 10 min at room temperature. After washing thoroughly with PBS, cells were incubated on a blocking buffer (1xPBS with 0.1% TWEEN-20 and 3% BSA) for 1 h at room temperature. After washing with PBS, cover slips were mounted onto the microscopic plate after adding a DAPI-containing mounting solution. Cells were then analyzed under confocal microscope.

In all experiments with titin, SMYD2, α-actinin, actin-EGFP, myosin-mCherry, about 30 cells were photographed and observed for a staining pattern of myofibrils: photographed pictures were analyzed by using Fiji-imageJ software with orientation J distribution plugin to count the number of cells that retain aligned myofibrils or misaligned myofibrils [the aligned myofibrils were determined by following definition: Orientation degrees between (+20) and (-20) and Distribution of orientation > 10,000] Volocity 6.3.1 software was utilized to obtain the Pearson's Correlation Coefficient (Rr)

for the colocalization between titin and SMYD2 [the co-localization status was estimated by the Pearson's coefficient values with the following definition: weak correlation = (-0.26)-0.09, moderate correlation = 0.1-0.48, and strong correlation = 0.49-0.84]. All fluorescence images were captured by Zeiss LSM 780 Confocal Microscope using (100X/1.4NA, 63X/1.4NA and 40X/1.3NA) oil objectives. The following laser was used for individual channels: Diode laser (405 nm) for excitation of DAPI (emission: 410-467 nm); Argon laser (488 nm) for excitation of EGFP (emission: 499-552 nm); Diode Pumped Solid State (DPSS) laser (561 nm) for excitation of mCherry (emission: 572-647 nm); HeNe laser (633 nm) for excitation of Alexa 647 (emission: 640-721 nm).

2.19 Immunoblotting analysis

Differentiated H9c2 myocytes or HL-1 cardiomyocytes expressing in SMYD2-HA WT or C13S was serum starved for 12 h, and treated with antimycin A (2 μg/mL). Cells were then washed with cold PBS and lysed with a lysis buffer and protein concentrations were measured by Bradford assay. Cell lysates from each sample were separated on a protein gel and transferred into PVDF membrane. Then membrane was blocked and incubated with primary antibodies, including α-actinin (Abcam, Cat# ab9465) (1:500), Hsp90 (BD transduction, Cat# 610418) (1:1000), actin (Abcam, Cat# ab3280) (1:2000), HA-tag (Biolegend, Cat# 901502) (1:1000), cardiac heavy chain myosin (Abcam, ab50967) (1:200), troponin I (Cell Signaling Technology, Cat#4002S) (1:1000), and β-tubulin (Santa Cruz) (1:1000) diluted in a blocking buffer at $4^{o}C$ overnight. Protein levels were then visualized by chemiluminescence using appropriate HRP-conjugated secondary antibodies.

In a similar experiment, H9c2 myocytes were treated with antimycin A after knockdown of SMYD2 or MMP-2 using siRNA. Western blot was performed and analyzed for α-actinin, troponin I, SMYD2 and MMP-2 using following primary antibodies: SMYD2 (Cell Signaling Technology, Cat# 9734) (1:1000), and MMP-2 (Cell Signaling Technology, Cat#4022S) (1:1000). Similarly, a MMP-2 inhibitor (ARP 100, 10 μM) was incubated with H9c2 myocytes transfected with SMYD2 WT at 37^{o}C for 1 h before treatment of antimycin A, and the α-actinin level was compared in the presence versus absence of antimycin A (2 μg/mL) by Western blotting.

2.20 Co-immunoprecipitation analysis

For co-immunoprecipitation of Hsp90 and SMYD2, HEK293 cells were transfected with plasmids containing SMYD2-HA WT or C13S, using PEI-MAX. After 2 days, cells were incubated with serum-free DMEM for 4 h, and further incubated in glucose-free DMEM (glucose deprivation) with treatment of antimycin A (2 μg/mL) for 2 h. Cells were then lysed at 4^{o}C for 30 min in a lysis buffer (100 mM Tris-HCl pH 7.4, NaCl 150 mM, 0.1% Tween 20 and protease inhibitor cocktail). Cell lysate (1 mg) were mixed with HSP90 antibody (BD Bioscience, Cat# 610418) for 1 h at 4^{o}C. This mixture was then incubated with Protein-G agarose beads (pre-washed with a 1xTBST buffer) for overnight at 4^{o}C. Beads were washed with 3 times with a 1xTBST buffer, and bound proteins were eluted using a SDS loading buffer. Eluted proteins were separated on a SDS-PAGE gel and transferred into PVDF membrane. Membrane was blocked by a blocking buffer (1xTBS with 0.1% TWEEN-20 and 3% BSA) for 1 h at room temperature and incubated with mouse Hsp90 antibody (BD transduction, Cat# 610418) or HA-antibody (Biolegend, Cat# 901502) diluted in a blocking buffer at 4^{o}C for overnight. After

washing 5 times with a TBST buffer, membrane was incubated with HRP-conjugated mouse secondary antibody (GE health care, Cat # NA931) for 1 h at RT. Membrane was then washed 3 times with a TBST buffer and visualized by chemi-luminescence. For N2A-FLAG and SMYD2-HA co-immunoprecipitation, the same approach was used after transfection of a plasmid-containing N2A-FLAG (pcDNA N2A-FLAG). HA-antibody (Biolegend, Cat# 901502) was used for immunoprecipitation in the same manner. For co-immunoprecipitation of SMYD2-HA C13D with Hsp90 or N2A, HA-antibody (Biolegend, Cat# 901502) was used for immunoprecipitation in the same manner.

2.21 Detection of Hsp90 methylation and SMYD2 oxidation (sulfonic acid)

For detection of Hsp90 methylation, differentiated H9C2 myocytes, without or with SMYD2 knockdown, were treated with antimycin A (2 µg/mL). After lysis, Hsp90 was immunoprecipitated, using mouse Hsp90 antibody (BD transduction, Cat# 610418) and then probed with rabbit mono-methyl lysine (me-K) (Cell Signaling Technology, Cat#14679) (1:1000) to analyze the methylation level of HSP90. The rabbit mono-methyl lysine (me-K) antibody was validated, after performing *in vitro* SMYD2 methyl transferase assay with purified Hsp90; Briefly, SMYD2 (200 nM) was incubated with Hsp90 (2 µg) and SAM (25 uM). At different time points, the enzyme activity was quenched by addition of an SDS-loading dye. The samples were separated on a SDS gel, transferred to membrane, and probed with antibodies to Hsp90 and me-K for Western blotting.

For detection of sulfonic acid in SMYD2, differentiated H9c2 myocytes expressing SMYD2-HA WT or C13S was serum starved for 12 h, and treated with antimycin A (2 µg/mL) for 12 h. Cells were then lysed with a lysis buffer containing

iodoacetamide (25 mM). Immunoprecipitation was performed with mouse HA-antibody (Biolegend, Cat# 901502) and blot was probed with rabbit cysteine (sulfonate) antibody (Enzo Life Sciences, Cat# ADI-OSA-820-D), which can detect sulfinic acid or sulfonic acid. The rabbit cysteine (sulfonate) antibody was validated with purified SMYD2 using an in vitro assay; briefly, SMYD2 was incubated with H_2O_2 (10 mM) for 20 min at room temperature or after pretreatment of iodoacetamide (25 mM) to block cysteine oxidation as a negative control. Samples were run on a gel for Western blotting with SMYD2 antibody or cysteine (sulfonate) antibody.

2.22 Dot-blot analysis of titin

Differentiated H9c2 myocytes or HL-1 cardiomyocytes expressing in SMYD2-HA WT or C13S (by SMYD2 or C13S mRNA transfection) was serum starved for 12 h, and treated with antimycin A (2 μg/mL). Titin was immunoprecipitated, following a previously reported method [163, 164]. First, plates were washed 2 times with a PBS buffer containing $MgCl_2$ (2 mM) and EGTA (1 mM) and incubated with an extraction buffer (100 mM KCl, 10 mM Pipes, pH 6.8, 300 mM sucrose, 2 mM $MgCl_2$, 1 mM EGTA, 0.1 mM PMSF, 10 μM E-64, 100 μM leupeptin, protease inhibitor cleavage cocktail and DNase1) containing 0.5% Triton X-100 for 10 min on ice. After collecting the initial extractable fraction, Triton-resistant material was scraped into the cytoskeletal-fraction-removal buffer (the extraction buffer with 2% SDS, 75 mM β-mercaptoethanol and 100 mM NaCl, instead of KCl). Then, scraped portion was heated at 60^{o}C for 10 min, and passed through a 1 mL syringe with a needle for 5-10 times to homogenize the solution. Lysates were diluted with a non-denaturing lysis buffer (20 mM Tris HCl pH 8, 140 mM NaCl, 1% Triton X-100, protease inhibitors and 2 mM EDTA), and dialyzed against the

same non-denaturing lysis buffer containing 0.05% SDS and protease inhibitors. Cell lysates (5 mg) were mixed with titin (E-2) mouse antibody (α-titin-CT) (Santa Cruz, sc271946) for 4 h at 4^{o}C. This mixture was then incubated with Protein-G agarose beads (pre-washed 2 times with a non-denaturing buffer) for overnight at 4^{o}C. Beads were washed 3 times with a non-denaturing buffer, and bound proteins were eluted using a 0.05 % SDS in buffer by boiling the beads at 90^{o}C for 10 min. Eluted proteins were then diluted and blotted onto a PVDF membrane, using Bio-Rad Bio-Dot Blot micro-filtration Apparatus with 96 wells. Membrane was blocked by a blocking buffer (1xTBS with 0.1% TWEEN-20 and 3% BSA) for 1 h at room temperature, and probed with following primary antibodies: titin rabbit antibody (Novus biologicals, Cat# NBP 1-88071)(1:1000) (titin-NT), titin mouse antibody (Santa Cruz, sc271946) (α-titin-CT) (1:1000), HA-antibody (Biolegend, Cat# 901502)(1:1000), and β-tubulin (Santa Cruz) (1:1000) to observe the cleavage or degradation of titin.

2.23 *In vitro* degradation of N2A by matrix metalloproteinase 2 (MMP-2)

Purified N2A (3 µg) was incubated with human recombinant active MMP2 in a buffer (Tris-HCl pH 7.4, 150 mM NaCl and 5 mM $CaCl_2$) at 37^{o}C with an increasing incubation time (1-5 h) or an increasing amount of MMP-2 (0.05, 0.1, 0.15 µg) for 2 h. Each reaction was quenched with a SDS loading dye at 95^{o}C for 5 min. Proteins were then separated by 10% SDS-PAGE gel, and visualized by Coomassie blue stain. In the similar manner, N2A was incubated with MMP-2 at 37^{0}C for 4 h with an increasing amount of SMYD2 (C13S) (a ratio of N2A to SMYD2 was 1:1.5, 1:3 and 1:5), and proteins were resolved on 10% SDS-PAGE gel and analyzed by Coomassie blue stain

2.24 *In vitro* degradation of N2A by calpain 1

Purified N2A (3 µg) was incubated with human recombinant calpain 1 in a buffer (Tris-HCl pH 7.4, 150 mM NaCl, 1 mM $CaCl_2$ and 1 mM beta mercaptoethanol) at room temperature with an increasing incubation time (15-60 min) or an increasing amount of calpain 1 (0.05, 0.5, 1.0 µg) for 1 h. Each reaction was quenched with a SDS loading dye at 95^{o}C for 5 min. Proteins were then separated by 10% SDS-PAGE gel, and visualized by Coomassie blue stain. In the similar manner, N2A was incubated with calpain 1 at room temperature for 2 h with an increasing amount of SMYD2 (C13S) (a ratio of N2A to SMYD2 was 1:0.6, 1:1.5 and 1:3), and proteins were resolved on 10% SDS-PAGE gel and analyzed by Coomassie blue stain.

2.25 Isolation and digestion of myofibrils

C57BL/6 mice were used under the guidelines of protocols approved by the Wayne State University Animal Care and Use Committee. Gastrocnemius muscle of 2-3-month-old mice were rapidly removed after euthanasia and rinsed with ice-cold PBS. The tissue was flash-frozen and stored in liquid nitrogen until use. Skeletal myofibrils were isolated from mouse gastrocnemius muscle according to the method described previously [166]. Initially the frozen muscle was thawed on ice and cut into small pieces, followed by homogenization in a cold lysis buffer [10 mM Tris-HCl, pH 7.0, 5 mM EGTA, 130 mM NaCl, 5 mM KCl, 1 mM $MgCl_2$, 1 mM NaN_3, 1 mM DTT, 0.1 mM PMSF, 10 µM E-64, 100 µM leupeptin and protease inhibitor cleavage cocktail (Thermo Scientific, Cat# A32955)] using an electronic homogenizer. Homogenates were then pelleted at 4^{o}C by centrifuging for 5 min at 2500g. Pellets were then washed in a cold washing buffer [60 mM KCl, 30 mM imidazole (pH 7.0), 2 mM $MgCl_2$, 1 mM DTT, 0.1 mM PMSF,

10 µM E-64, 100 µM leupeptin and protease inhibitor cleavage cocktail] with 0.5% (v/v) Triton X-100 for once and without Triton X-100 for three times.

Myofibrils were then suspended in a cold suspension buffer (20 mM MOPS, pH 7.0, 1 mM EGTA, 5 mM $MgCl_2$, 100 mM KCl, 0.1 mM PMSF, 10 µM E-64, 100 µM leupeptin and protease inhibitor cleavage cocktail), and filtered through a 70 µm pore size nylon mesh (sterile cell strainer) (Fisher Scientific, Cat# 22363548), and stored in 4^oC until its use. Myofibril digestion was performed according to the previous method [167]. Briefly, freshly prepared myofibrils were washed 3 times using a suspension buffer without protease inhibitors, and incubated with human recombinant active MMP-2 (0.4 µg) in a buffer (Tris-HCl pH 7.4, 150 mM NaCl, 2.0 mM $CaCl_2$) at 37^oC with an increasing incubation time (0-30 min). In the same experiment, MMP-2 was pre-incubated with ARP100 (100 nM) for 15 min at 37°C before adding to the myofibril digestion mixture. Alternatively, myofibrils were pre-incubated with excess amount of SMYD2 (25 µg) for 15 min at 37°C, and then subjected to MMP-2 digestion.

2.26 Electrophoresis of titin

The mixture was then denatured using a 2X urea loading buffer (8M urea, 2M thiourea, 3% SDS, 75 mM dithiothreitol, 0.03% bromophenol blue, 25% glycerol and 0.05 M Tris-HCl; pH 6.8). Before loading to the gel, all the samples were mixed with 60% glycerol solution (making glycerol as 25% in the final volume). The proteins were then separated by 1% vertical sodium dodecyl sulfate (SDS)-agarose gel, using a lower buffer (50 mM Tris-base, 0.384 M glycine, and 0.1% SDS) and the same buffer with 10 mM 2-mercaptoethanol as the upper buffer in the Hoefer™ SE 600 Chroma Vertical Electrophoresis System, according to a method described previously [168].

2.27 Statistical analysis

Data are represented as the means ± SD and were statistically analyzed by Student's t test with Welch's correction. The value $p<0.05$ was considered as statistically significant.

CHAPTER 3: RESULTS

Portions of the text in this chapter were reprinted or adapted with permission from: Samarasinghe, K.T. *et al.* A clickable glutathione approach for identification of protein glutathionylation in response to glucose metabolism. *Mol Biosyst* **12**, 2471-2480 (2016)

3.1 Clickable glutathione is catalyzed by enzymes implicated in glutathionylation

In order to analyze the reversible change of protein glutathionylation, we begin to determine whether clickable glutathione can detect the reversible change of glutathionylation[99].

a

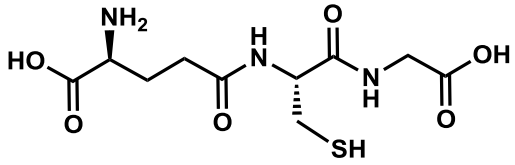

b

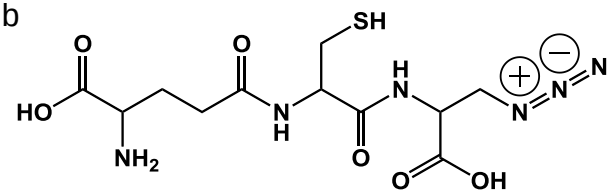

c

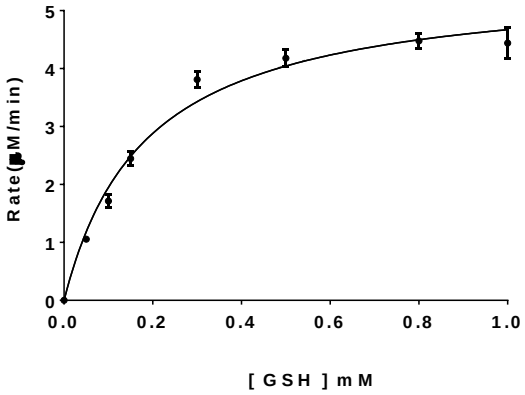

d

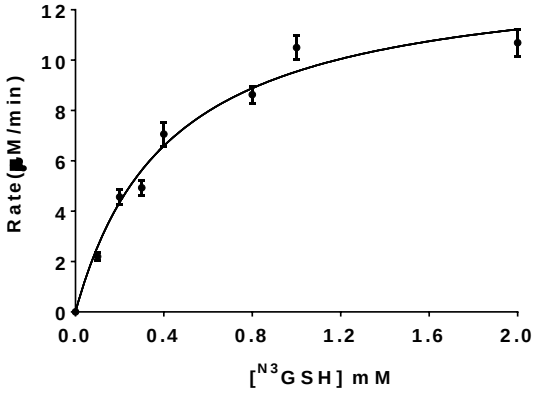

e

Enzyme	Substrate	K_m	k_{cat}	k_{cat}/K_m
Gstp1	GSH	0.184 ±0.02	17.73±0.7	96.35
	^{N3}GSH	0.425±0.06	5.45±0.3	12.82

Figure 3.1. Enzyme kinetic data of clickable GSH substrate catalyzed by Gstp1. (**a**) Endogenous glutathione (**b**) Clickable derivative of glutathione (**c** and **d**) Initial velocity versus substrate concentration plots were fitted to the Michaelis-Menten equation using Graphpad prism 5.01. (**e**) Apparent kinetic constants (K_m, K_{cat} and V_{max}) for GSH and ^{N3}GSH

Glutathionylation can occur by non-enzymatic reactions of protein cysteine residues with glutathione in the presence of ROS. However, redox enzymes may facilitate formation of glutathionylation. Glutathione-S-transferase pi (GSTP) was shown to catalyze formation of glutathionylation[100].

a

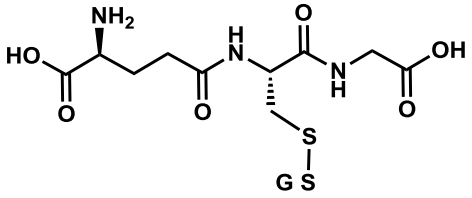

b

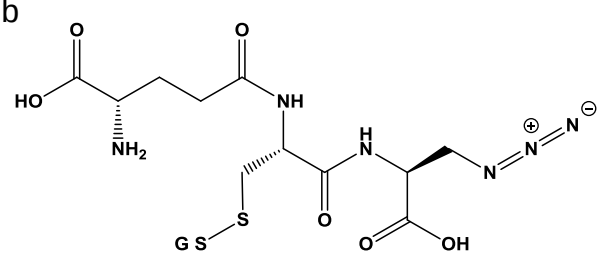

c

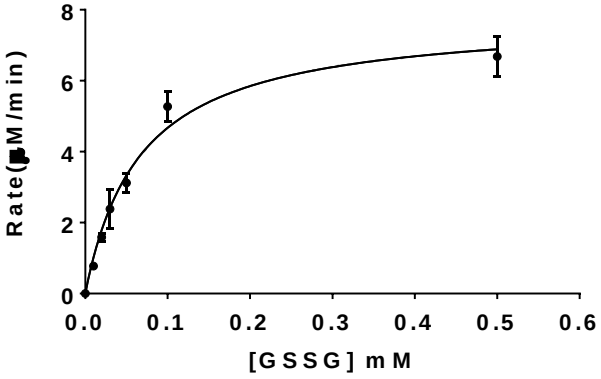

d

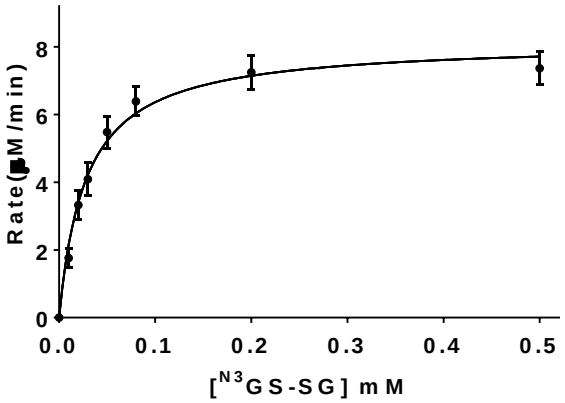

e

Enzyme	Substrate	K_m	k_{cat}	k_{cat}/K_m
GR	GS-SG	0.067 ±0.01	27.7±1.7	413
	^{N3}GS-SG	0.028±0.003	28.83±1.8	1029

Figure 3.2. Enzyme kinetic data of clickable GSH substrate catalyzed by GR. (**a**) Endogenous oxidized glutathione (**b**) Clickable derivative of oxidized glutathione (**c** and **d**) Initial velocity versus substrate concentration plots were fitted to the Michaelis-Menten equation using Graphpad prism 5.01. (**e**) Apparent kinetic constants (K_m, K_{cat} and V_{max}) for GS-SG and ^{N3}GS-SG

Deglutathionylation (reduction of glutathionylation) can occur by non-enzymatic reactions. However, glutaredoxin 1 (Grx1)[169], together with glutathione reductase (GR), catalyzes deglutathionylation with about 1,000- fold higher rate than glutathione alone. Also, glutathione-S-transferase omega (GSTO) was recently shown to catalyze deglutathionylation[101].

a

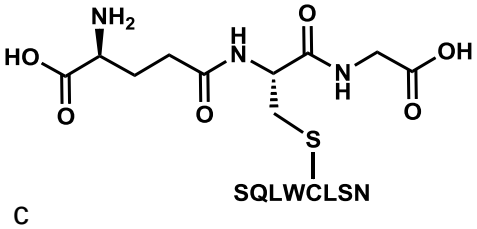

b

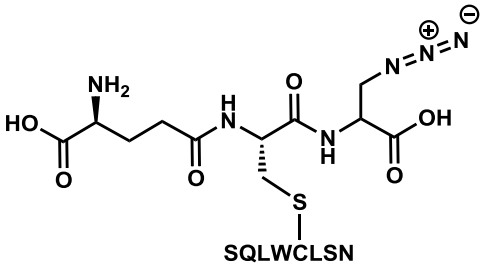

c

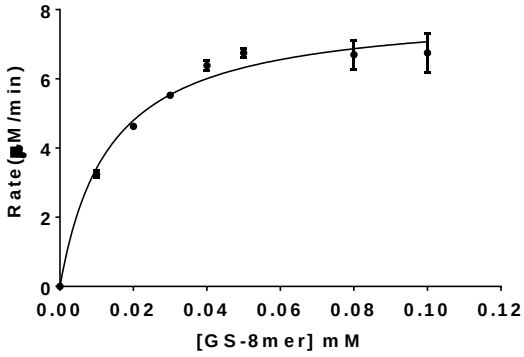

d

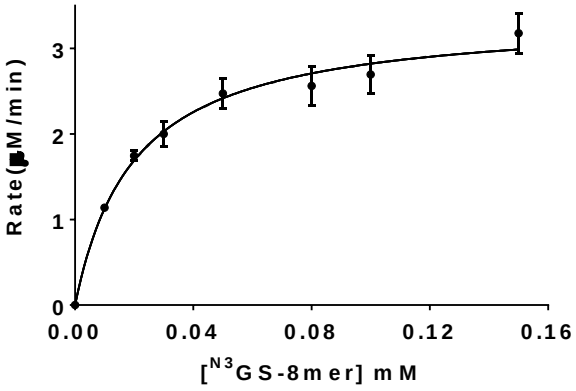

e

Enzyme	Substrate	K_m	k_{cat}	k_{cat}/K_m
Grx1	GS-8mer	0.014 ±0.002	5.68±0.23	405
	^{N3}GS-8mer	0.019±0.002	2.96±0.14	150

Figure 3.3. Enzyme kinetic data of clickable GSH substrate catalyzed by Grx1. (**a**) Glutathionylated peptide (**b**) Glutathionylated peptide with clickable handle (**c** and **d**) Initial velocity versus substrate concentration plots were fitted to the Michaelis-Menten equation using Graphpad prism 5.01. (**e**) Apparent kinetic constants (K_m, K_{cat} and V_{max}) for GS-8mer and ^{N3}GS-8mer.

A few other redox enzymes, such as thioredoxin[170] and sulfiredoxin[171], may contribute to deglutathionylation although their specificity for deglutathionylation is low. Despite the small size of azido-group in glutathione, it may interfere with enzyme-mediated (de)glutathionylation.

a

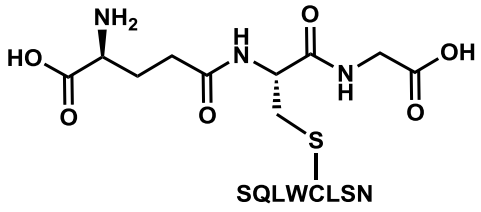

a

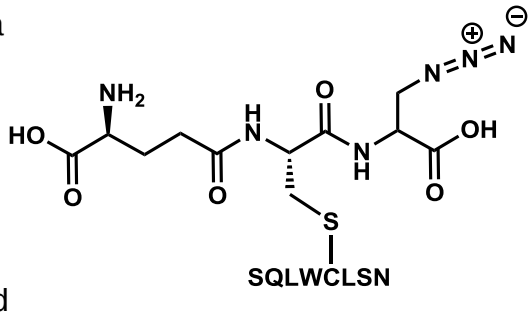

c

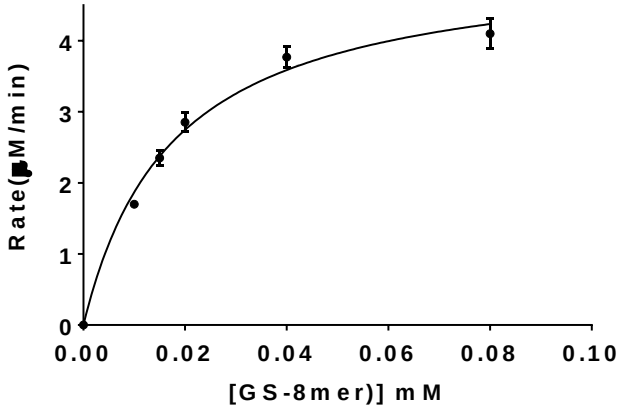

d

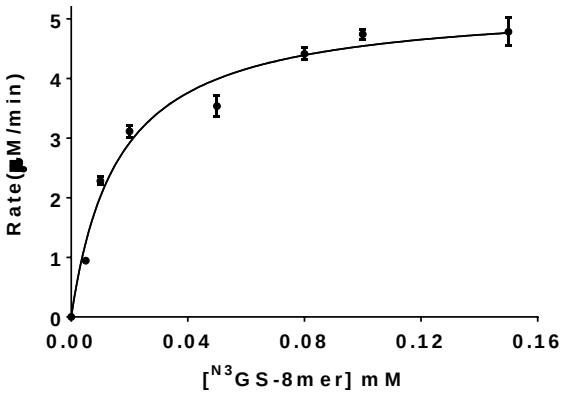

e

Enzyme	Substrate	K_m	k_{cat}	k_{cat}/K_m
GSTO1	GS-8mer	0.017 ±0.002	0.45±0.02	26.45
	^{N3}GS-8mer	0.016±0.002	0.47±0.01	29.38

Figure 3.4. Enzyme kinetic data of clickable GSH substrate catalyzed by GSTO1. (**a**) Glutathionylated peptide (**b**) Glutathionylated peptide with clickable handle (**c** and **d**) Initial velocity versus substrate concentration plots were fitted to the Michaelis-Menten equation using Graphpad prism 5.01. (**e**) Apparent kinetic constants (K_m, K_{cat} and V_{max}) for GS-8mer and ^{N3}GS-8mer.

In order to determine whether azido-glutathione can be used as a substrate of major enzymes involved in glutathionylation, we have prepared substrates of Grx1 (Figure 3.3a and b), GSTO1 (Figure 3.4a and b), GR (Figure 3.2a and b) and GSTP1 (Figure 3.1a and b) that contain either endogenous glutathione (GSH) or azido glutathione (^{N3}GSH) for kinetic comparisons. The model peptides (SQLWCLSN) glutathionylated by GSH or ^{N3}GSH were prepared and assayed for deglutathionylation by Grx1 and GSTO[172]. Disulfides of GSH (GSSG and N3GSSG) were used for substrate of GR. In the kinetic data, it is notable that Grx1 (Figure 3.3c, d and e), GSTO1 (Figure 3.4c, d and e), and GR (Figure 3.2c, d and e) catalyzed both GSH- and ^{N3}GSH -containing substrates with the similar values of K_m and K_{cat}. This shows that the small size of azide-group could be tolerated not only by Grx1 and GSTO1 that have broad substrate specificity, but also by GR that is relatively specific to GSSG. The exception was GSTP (Figure 3.1c, d and e), which showed an 8-fold lower catalytic efficiency with ^{N3}GSH versus GSH. This suggests that GSTP may not catalyze azido-glutathione efficiently. However, note that there is no direct assay for GSTP-mediated glutathionylation, and GSTP assay (1-chloro-2,4-dinitrobenzene alkylation) in this study may not represent the reaction of glutathionylation. Overall, these kinetic data supports that azido-glutathione detects the reversible change of protein glutathionylation in response to ROS.

3.2 Clickable glutathione approach in cells

To extend our data to cardiomyocytes, we applied our clickable glutathione approach to a H9c2 myoblast cell line. GS M4 mutant was expressed into differentiated H9c2 myocytes by treating with adenovirus containing the GS M4 gene (Ad/GS M4) (Figure 3.5a). GS M4 expression did not induce significant cell toxicity or alteration of redox systems, such as a thiol-content or levels of redox enzymes in cells (Figure 3.5b and c).

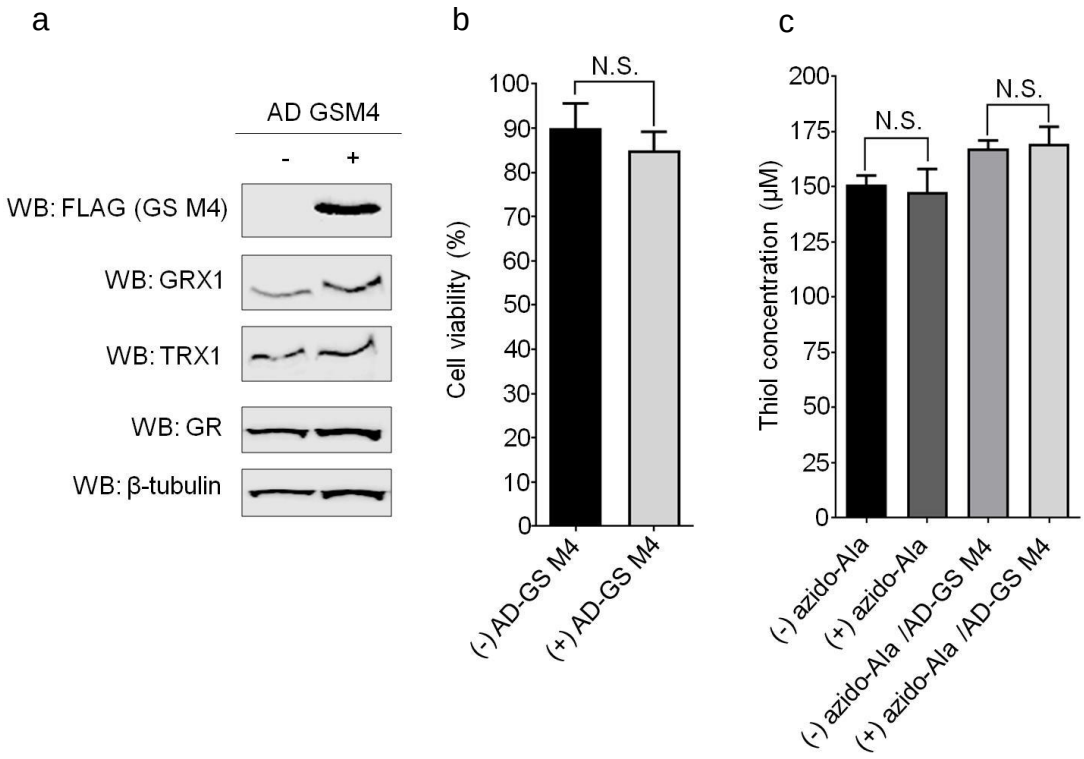

Figure 3.5. A clickable glutathione approach does not induce significant cell toxicity or alteration of redox systems. GS M4 mutant was expressed into differentiated H9c2 myocytes by treating with adenovirus containing the GS M4 gene. (**a**) Level of GS M4 and other redox enzymes.(**b**) Cell viability after expression of GS M4, determine by trypan blue assay. (**c**) A total level of thiols in cells after expression of GS M4 with incubation of azido-Ala. Cells were lysed by freeze-thawing, and protein-free lysates were analyzed for a thiol-concentration by a bromobimane assay. Results represent the mean ± SD, (n=3). Two-tailed Student's unpaired t-test with Welch's correction, *$p < 0.05$ and N.S.= non-significant.

3.3 Clickable GSH approach in H9C2 myocytes for detection of global protein glutathionylation

Initially, GS M4 mutant was expressed into differentiated H9c2 myocytes by treating with adenovirus containing the GS M4 gene (Ad/GS M4). Cells were then incubated with azido-Ala for 20 h, and treated with ROS stimuli. After the click reaction of lysates with rhodamine-alkyne, in-gel fluorescence analysis showed that global glutathionylation were induced by exposure to an increasing concentration of hydrogen peroxide (Figure 3.6a), glucose deprivation (Figure 3.6b) and antimycin A (AMA) (Figure 3.6c), which is known to induce mitochondrial ROS[173].

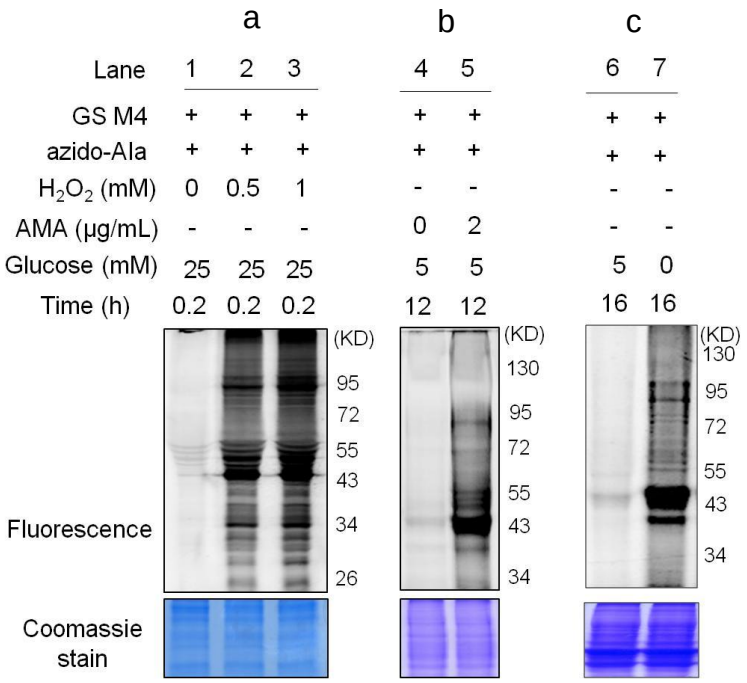

Figure 3.6. Clickable GSH approach in H9C2 myocytes for detection of global protein glutathionylation in response to hydrogen peroxide, ETC blocker and glucose deprivation. A glutathione synthetase mutant (GS M4), which synthesizes azido-glutathione (γGlu-Cys-azido-Ala), was expressed in differentiated H9c2 cells. After incubation of azido-Ala, cells were subjected to ROS. Glutathionylated proteins in

lysates were identified after click reaction.In-gel fluorescence detection of glutathionylated proteins. H9c2 cells expressing GS M4 were incubated with azido-Ala for 20 h and treated with (**a**) H_2O_2, (**b**) AMA and (**c**) glucose deprivation. Collected lysates were then subjected to click reaction with rhodamine-alkyne for fluorescence detection. Results represent (n = 3) experiments.

3.4 Identification of individual protein glutathionylation including SMYD2 through clickable GSH approach

Previously, we found that SMYD2 can be glutathionylated in response to glucose deprivation in HEK293 cells[132]. Then, we applied our clickable glutathione approach to a H9c2 myoblast cell line, which can be differentiated into a cardiac phenotype, to detect SMYD2 glutathionylation in vivo. Initially, GS M4 mutant was expressed into differentiated H9c2 myocytes by treating with adenovirus containing the GS M4 gene (Ad/GS M4). Cells were then incubated with azido-Ala for 20 h, and treated with ROS stimuli. The subsequent pull-down analysis after click reaction of lysates with biotin-alkyne detected glutathionylation of SMYD2 (Figure 3.7a, b and c). In addition, we also detected glutathionylation of other sarcomere-associated proteins, including Hsp90 (Figure 3.7a, b and c), actin, and myosin heavy chain (MHC) (Figure 3.7c).

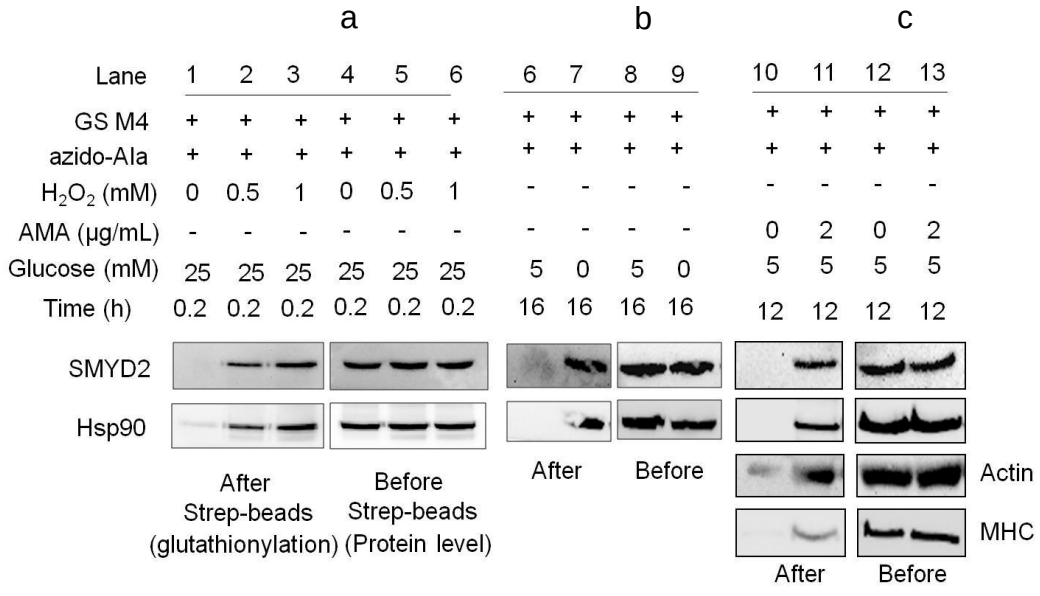

Figure 3.7. Identification of individual protein glutathionylation including SMYD2 through Clickable GSH approach. Identification of individual glutathionylated proteins in response to hydrogen peroxide, ETC blocker and glucose deprivation. H9c2 cells expressing GS M4 were incubated with azido-Ala for 20 h and treated with (**a**) H_2O_2, (**b**) glucose deprivation and (**c**) AMA. Glutathionylated proteins were subjected to click reaction with biotin-alkyne and pull-downs with streptavidin-agarose, and detected by Western blotting with individual antibodies, including SMYD2, Hsp90, actin, and myosin-heavy chain (MHC). Results represent (n = 3) experiments.

3.5 The level of SMYD2 glutathionylation in H9c2 myocytes

To estimate the level of glutathionylation on SMYD2, lysates were subjected to click reaction with 2 kD-polyethyleneglycol-alkyne (PEG-alkyne), which will increase the molecular mass of SMYD2. The subsequent Western blotting analysis found that over 30% of SMYD2 was glutathionylated upon treatment of AMA for 12 h (Figure 3.8a and b). In the same condition, we did not detect any significant signal for irreversible oxidation of SMYD2, such as sulfonic acid formation (Figure 3.8c and d). Overall, these data support that SMYD2 is susceptible to glutathionylation in response to ROS.

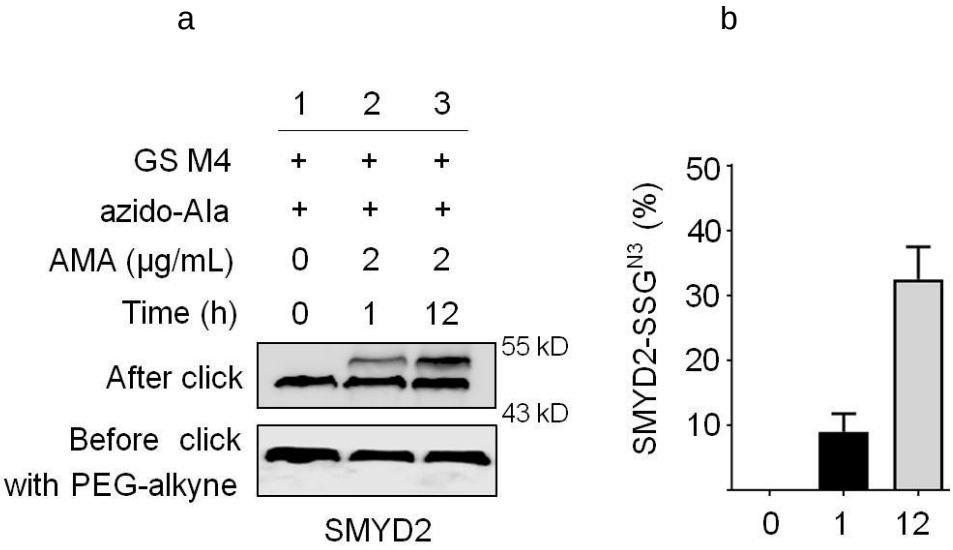

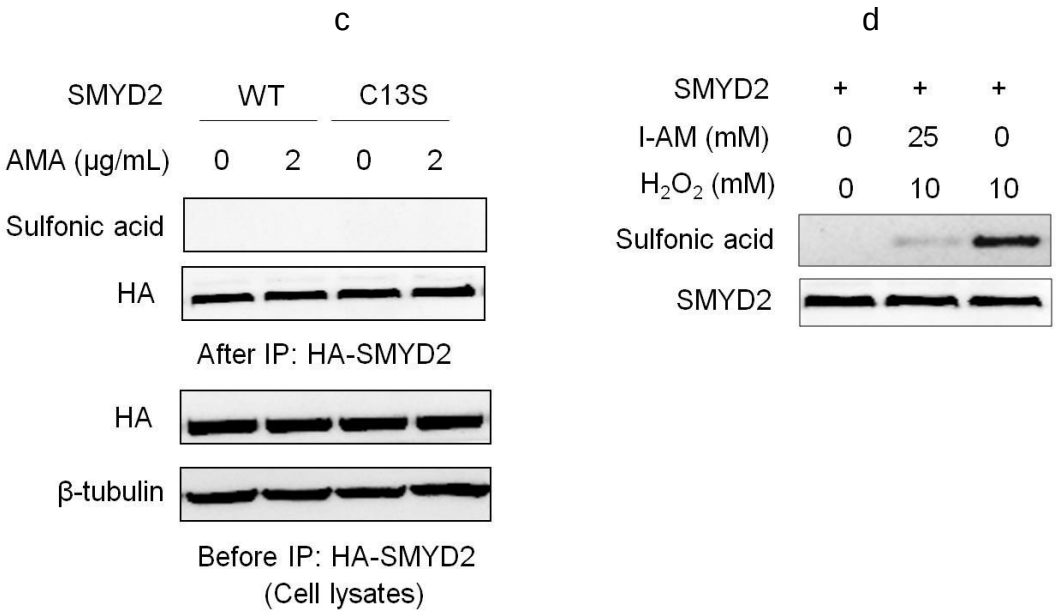

Figure 3.8. The level of SMYD2 glutathionylation *in vivo*. Lysates were subjected to click reaction with 2-kD PEG-alkyne. (a and b)The mass shift of SMYD2 was analyzed by Western blotting. Detection of SMYD2 oxidations by antibodies that detect sulfonic acid. (**c**)H9c2 cells expressing SMYD2 WT or C13S were treated with AMA, and the sulfonic acid formation in SMYD2 was probed by Western blotting after pull-down of SMYD2. (**d**)Validation of the antibody for detection of sulfonic acid. To purified SMYD2 was added H_2O_2 (10 mM) without or with pre-treatment of iodoacetamide (I-AM) that blocks Cys residues. Blots are the representative of at least two replicates. Results represent (n = 3) experiments.

3.6 SMYD2 Cys 13 is a potential candidate for glutathionylation

SMYD2 has 17 cysteine residues, ten of which are bound to three zinc ions in the MYND and Post-SET domains (Figure 3.9a)[174]. SMYD2 structural data (PDB: 3RIB) showed that Cys13 is highly exposed at the protein surface and is surrounded by four basic Arg or Lys residues (Figure 3.9a, right), which may increase its potential reactivity. Cys13 is in the SET-domain (Figure 3.9a, green) and it is close to a S-adenosylmethionine (SAM) binding site (Figure 3.9a). Cys13 in SMYD2 is not

conserved among members of the SMYD2 family (Figure 3.9b), but found in its orthologs (Figure 3.9c).

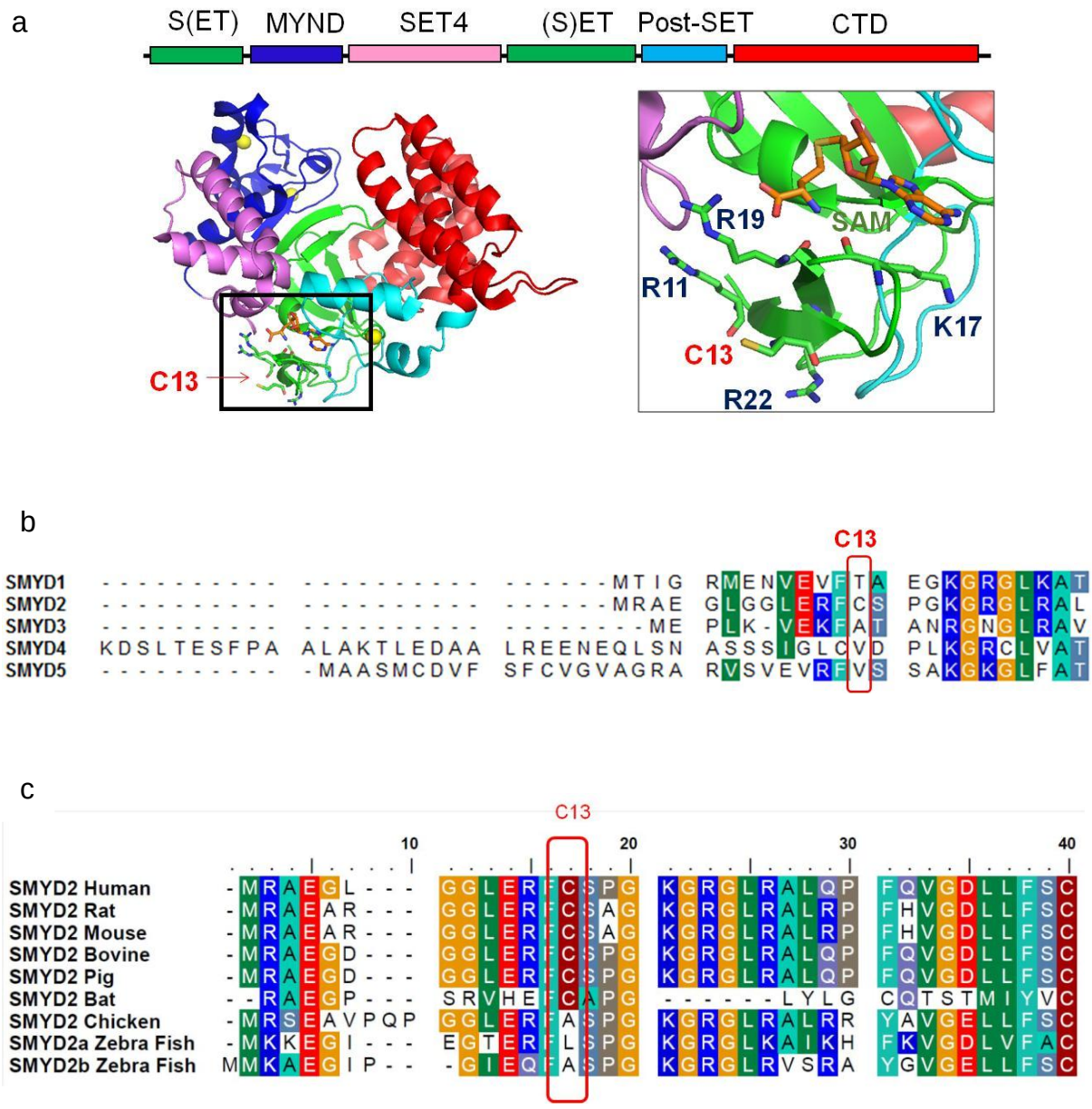

Figure 3.9. SMYD2 Cys 13 is a potential site of glutathionylation (**a**) The structure (PDB: 3RIB) and domains of SMYD2, and an enlarged area around Cys13 in SMYD2. (**b**) Sequence alignment around Cys13 of SMYD2 with other members of the SMYD family. (**c**)The sequence alignment of SMYD2 Cys 13 in SMYD2 orthologs.

3.7 SMYD2 is selectively glutathionylated at Cys13

To determine whether Cys13 is important for SMYD2 glutathionylation, we purified wild-type (WT) and C13S mutant proteins of SMYD2 (Figure 3.10b), and evaluated their glutathionylation with azido-glutathione in vitro.

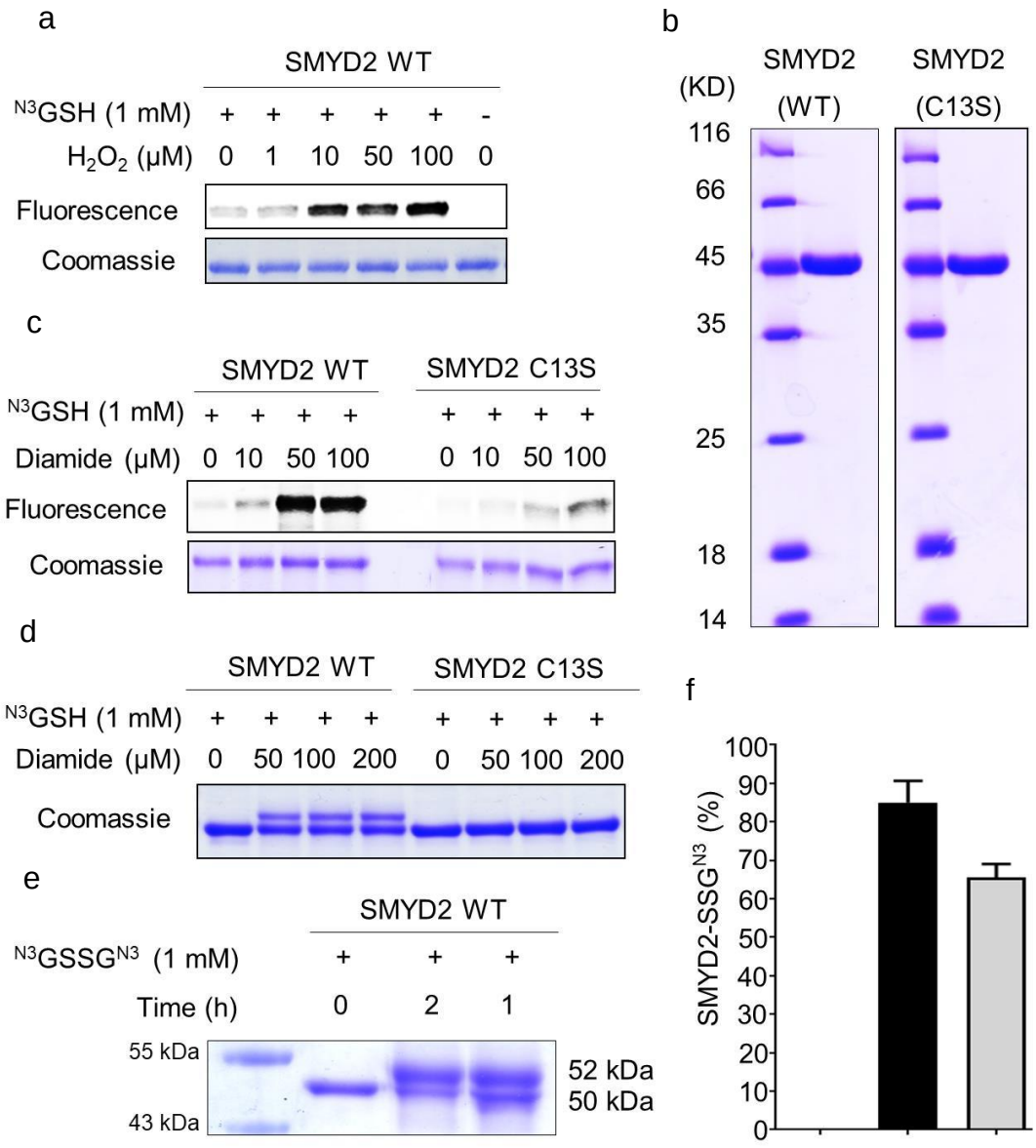

Figure 3.10. Cysteine 13 is important for SMYD2 glutathionylation (**b**)Purified SMYD2 WT or C13S was mixed with azido-glutathione in vitro, and treated with H_2O_2 or diamide for 15 min. SMYD2 glutathionylation was detected by fluorescence (**a** and **c**) or

a mass shift (**d-f**) after click reaction with rhodamine-alkyne or 2-kD PEG-alkyne, respectively. Results represent (n = 3) experiments.

Notably, after click reaction with rhodamine-alkyne, in-gel fluorescence analysis showed that SMYD2 WT was strongly glutathionylated upon addition of H_2O_2 or diamide (Figure 3.10a and c), whereas SMYD2 C13S showed weak signals (Figure 3.10c). In addition, the same result was observed when a click reaction was done with 2-kD PEG-alkyne, showing one Cys modification with SMYD2 WT versus no modification with SMYD2 C13S (Figure 3.10d, e and f).

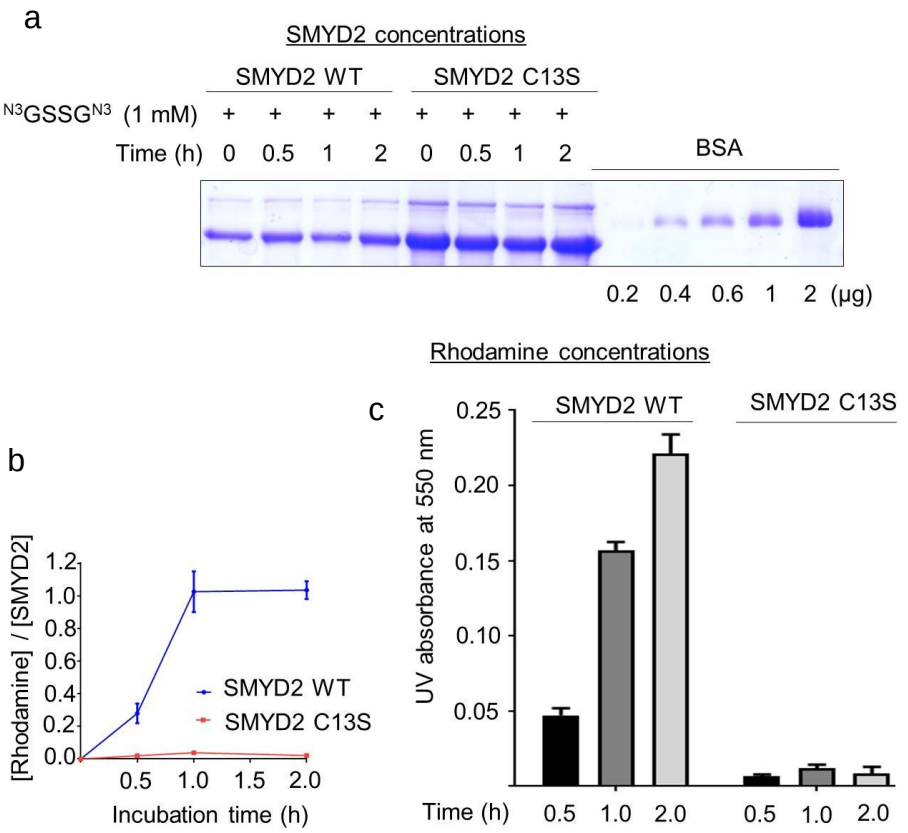

Figure 3.11. Selective glutathionylation of SMYD2 Cys 13 position. (**a-c**) Quantifying the molar ratio of rhodamine to SMYD2 concentrations after incubation of SMYD2 with oxidized azido-glutathione ($^{N3}GSSG^{N3}$) and click reaction with rhodamine-alkyne. Results represent (n = 3) experiments.

Furthermore, the level of glutathionylation was quantified by measuring the molar ratio of rhodamine to SMYD2 concentrations after click reaction with rhodamine-alkyne (Figure 3.11a, b and c). Incubation of SMYD2 with oxidized azido-glutathione (^{N3}GSSG^{N3}) led to an approximately 1:1 molar ratio of rhodamine to SMYD2 (Figure 3.11b, blue). In contrast, almost no modification was observed with SMYD2 C13S (Figure 3.11b, red), showing the selective glutathionylation at Cys13 of SMYD2.

a

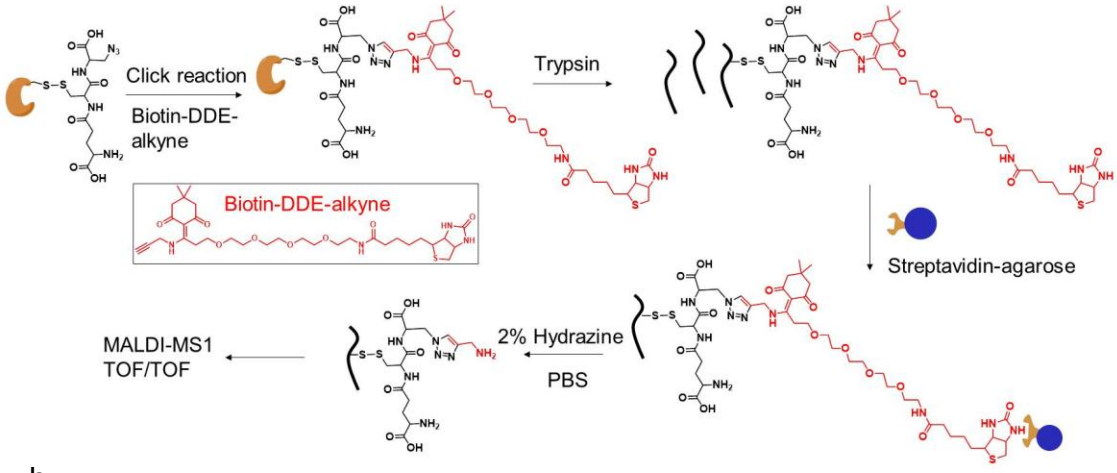

b

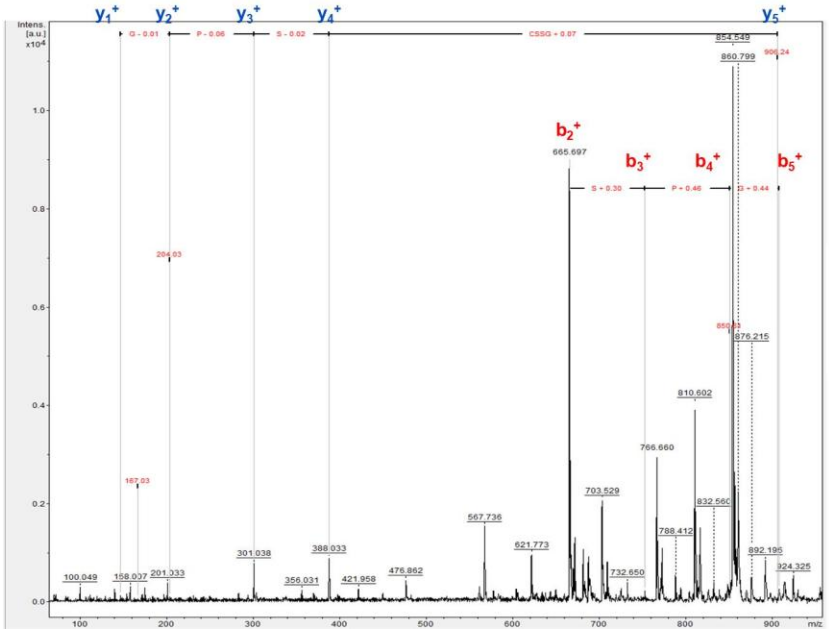

#1	b+	Seq.	y+	#2
1	148.0757	F		6
2	666.0849	C*	906.2282	5
3	753.1169	S	388.2191	4
4	850.1697	P	301.187	3
5	907.1911	G	204.1343	2
6		K	147.1128	1

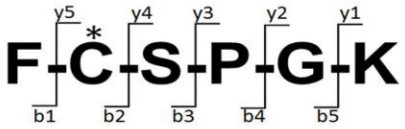

Figure 3.12. Identification of SMYD2 glutathionylation site by a mass analysis. (**a**) A scheme for mass identification of glutathionylated peptides in SMYD2. SMYD2 glutathionylated by azido-glutathione was subjected to click reaction with biotin-DDE-alkyne (click chemistry tools, Inc.), which is cleavable by hydrazine, and digested by trypsin at 37°C overnight. Digested peptides were incubated with streptavidin-agarose for 3 h, and bound peptides were eluted by 2% hydrazine in PBS (pH 7.4) for 30 min (twice). The collected sample was ziptiped and analyzed for MALDI-TOF and TOF/TOF. (**b**) The spectrum of MALDI-TOF/TOF with identified ions, and the predicted mass table for individual ions. Identified y and b ions are highlighted by red and blue colors. The modification on Cys was calculated as 415.14, which adds the mass of azido-glutathione and a fragment cleaved from biotin-DDE-alkyne.

.

3.8 Confirmation of SMYD2 Cys 13 glutathionylation by mass spectrometry.

To directly confirm the modification site, we analyzed glutathionylated SMYD2 by mass spectrometry analysis: SMYD2 was glutathionylated by ^{N3}GSSG^{N3} and conjugated with biotin-alkyne by click reaction and digested by trypsin. The glutathionylated peptides were purified by streptavidin-beads (Figure 3.12a).

a

AEGLGGLERFC_{13}*SPGK

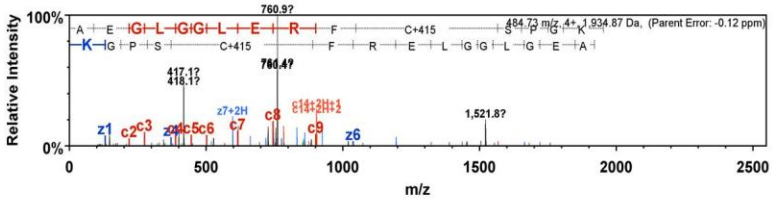

b

SPSELLEIC_{321}*ELS

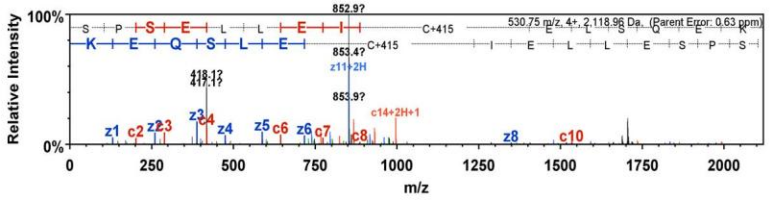

c

QAFYC_{74}*NVECQKEDWPMHK

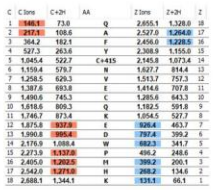

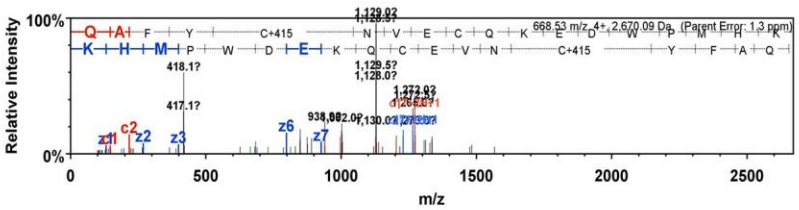

Figure 3.13. **LC-MS/MS (ESI) analysis of glutathionylated SMYD2.** Glutathionylated SMYD2 was analyzed by ESI LC-MS/MS after the same procedure described in (Figure 10a), except glutathionylation was induced by addition of diamide (100 µM) in the presence of azido-glutathione, detecting the peptides glutathionylated at (**a**) Cys13, (**b**)Cys74, and (**c**)Cys321.

MALIDI analysis of eluted samples found one peak that is in precise agreement with the molecular weight of the peptide glutathionylated at Cys13 (m/z 1053.5, FC*SPGK) (Figure 3.12b and Figure 3.13a). LC-MS/MS analysis confirmed this assignment and found two additional peptides glutathionylated at Cys74 (Figure 3.13b) and Cys321 (Figure 3.13c).

3.9 Evaluation of SMYD2 Cys13 glutathionylation in cells

Glutathionylation of SMYD2 at Cys13 was further confirmed in differentiated H9c2 cells (Figure 3.14a) and HEK293 cells (Figure 11b) expressing GS M4. In response to AMA with glucose deprivation[128], SMYD2 WT was strongly glutathionylated while glutathionylation was significantly decreased with SMYD2 C13S. Taken together, our data strongly support that SMYD2 is selectively glutathionylated at Cys13.

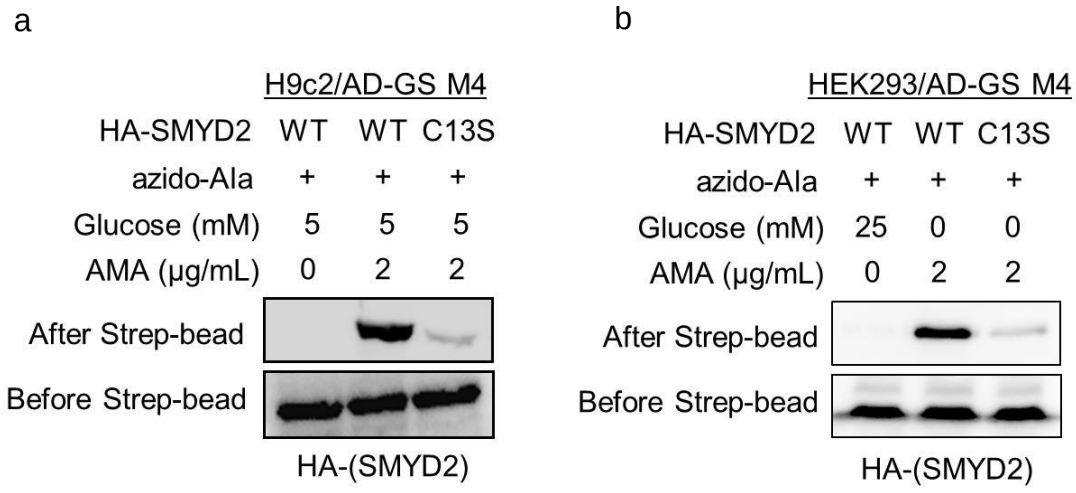

Figure 3.14. Detection of SMYD2 Cys13 glutathionylation in differentiated H9c2 and HEK293 cells expressing GS M4. (**a, b**) After transfection of SMYD2 WT or C13S,

cells were incubated with azido-Ala. After inducing glutathionylation, collected lysates were subjected to click reaction with biotin-alkyne before pull-downs with streptavidin-agarose and Western blotting. Results represent (n = 3) experiments.

3.10 SMYD2 Cys13 glutathionylation decreases cell viability

Despite a dispensable role of SMYD2 in normal heart development[175], we hypothesized that SMYD2 may have an important role in muscle under stressed conditions. To examine the functional significance of SMYD2 Cys13 glutathionylation, we compared cell viability of H9c2 myoblasts following expression of SMYD2 WT versus C13S, differentiation to a cardiomyocyte phenotype, and subsequent exposure to various ROS stimuli (Figure 3.15a, b, c and d).

After differentiation, SMYD2 levels were similar in the two cohorts of cells expressing SMYD2 WT or C13S within 1.7-fold of the endogenous level (Figure 3.15a). Sarcomeric α-actinin was also expressed in a similar level (Figure 3.15b). Differentiated H9c2 cells were then treated with H_2O_2 (25 μM), AMA (2 μg/mL), a nitric oxide donor (NONOate, 100 μM), or angiotensin II (1 μM) (Figure 3.15b and d). Under unstressed conditions, viability was comparable in cells expressing SMYD2 WT or C13S (Figure 3.15d, bars 1-2 and 11-12). However, in all stressed conditions, viability was significantly decreased in cells expressing SMYD2 WT versus C13S (Figure 3.15d, bars 3-10), suggesting that SMYD2 Cys13 glutathionylation decreases cell viability.

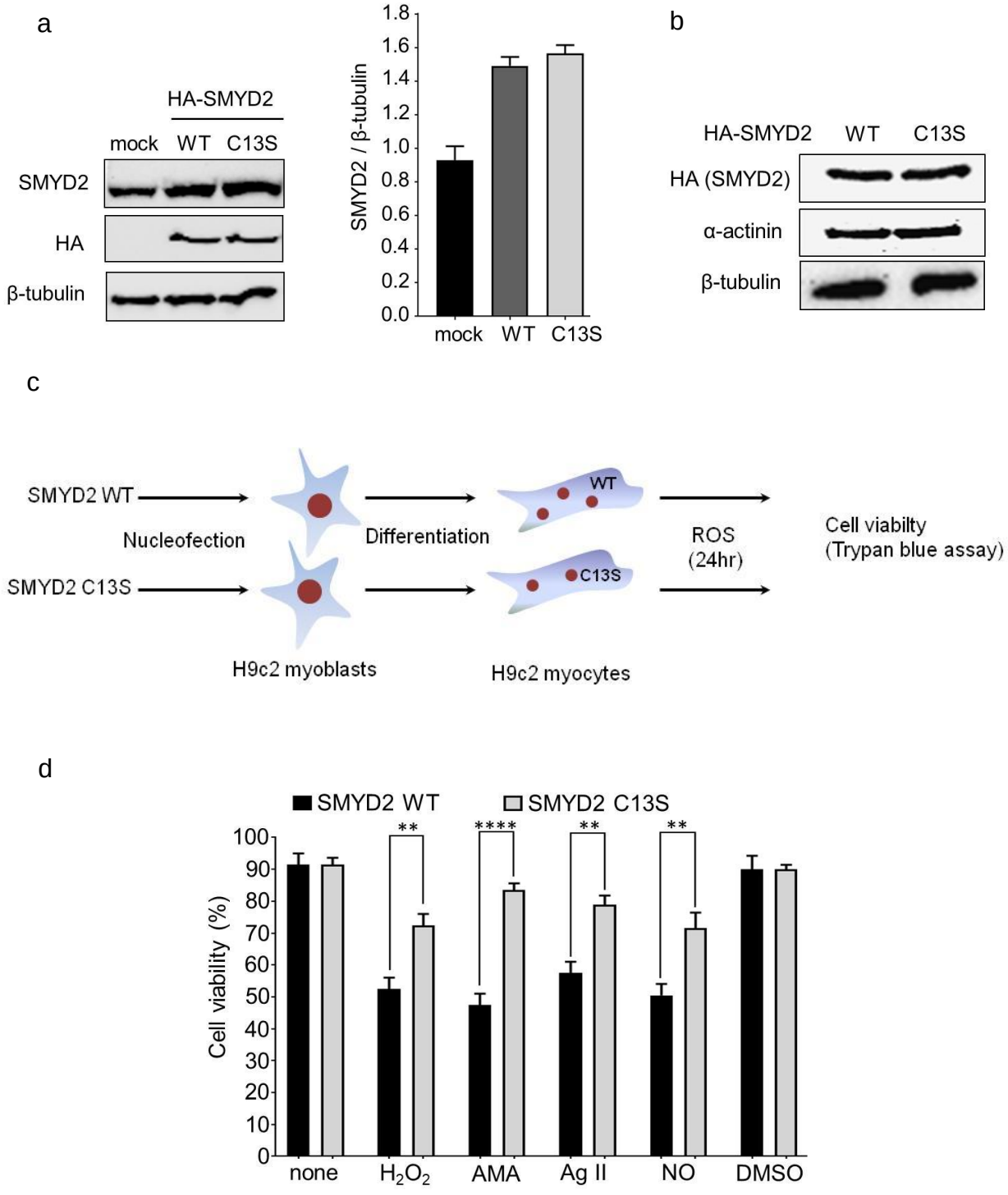

Figure 3.15. SMYD2 Cys13 glutathionylation decreases cell viability. (**a**) Levels of SMYD2 WT and C13S in differentiated H9c2 cells. **(b**) Protein levels of SMYD2 and α-actinin in H9c2 myocytes after differentiation. SMYD2 WT or C13S plasmids were electroporated to H9c2 myoblasts. Cells were then differentiated for 5 days. After differentiation, cells were lysed for comparing the protein levels by Western blotting. (**c and d**) Viability of differentiated H9c2 cells expressing SMYD2 WT or C13S after

exposure to H_2O_2 (25 µM), AMA, (2 µg/mL), angiotensin II (Ag II, 1 µM), or a nitric oxide (NO) donor (NONOate, 100 µM) for 24 h. Results represent the mean ± SD, (n = 3). Two-tailed Student's unpaired t-test with Welch's correction, *p < 0.05

To corroborate these findings, we examined cell viability after SMYD2 overexpression or knockdown. There is no difference of cell viability in an unstressed condition after SMYD2 overexpression (Figure 3.16a, bars 1 vs. 2). However, SMYD2 overexpression rescued viability of cells treated with AMA in a modest but statistically significant level (Figure 3.16a, bars 3 vs. 4). Conversely, in an unstressed condition (without AMA), there is a modest reduction of cell viability after SMYD2 knockdown (Figure 3.16b, bars 1 vs. 3). However, SMYD2 knockdown induced more significant reduction of cell viability after treatment of AMA (Figure 3.16b, bars 2 vs. 4). Overall, these results support the hypothesis that SMYD2 plays a protective role under cellular stress, and SMYD2 Cys13 glutathionylation in response to ROS decreases viability of H9c2 cells.

3.11SMYD2 Cys13 glutathionylation induces a loss of myofibril integrity

Because SMYD2 is reportedly involved in sarcomere stabilization[176], we proposed that the reduced cell viability may be associated with altered sarcomere stability upon SMYD2 glutathionylation. To monitor myofibril structure under stress, we examined rat neonatal cardiomyocytes treated with AMA. Immunostaining of titin, with antibody that binds to the N-terminal region of titin (α-titin-NT) (Figure 3.17a), showed a parallel array of striated myofibrils in unstressed cardiomyocytes (Figure 3.17b, top left). The directionality analysis showed uniform orientation of myofibrils (Figure 3.18a)

a

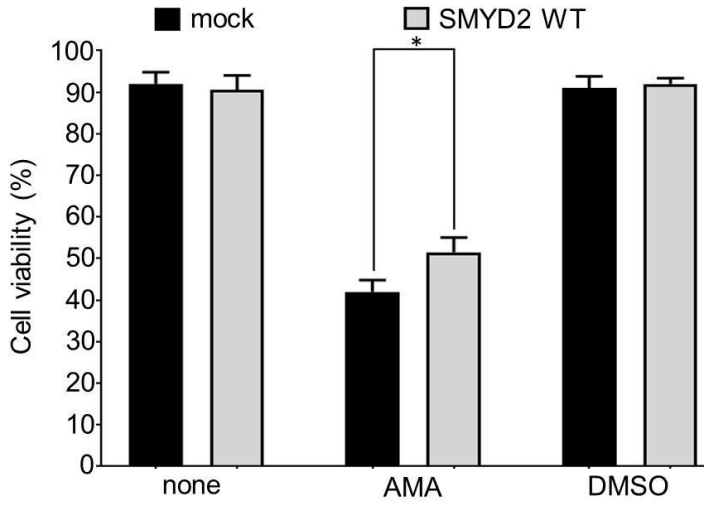

b

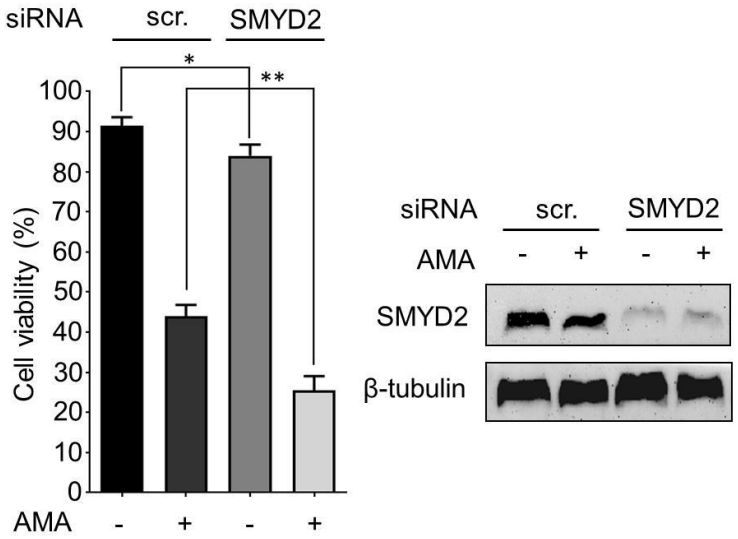

Figure 3.16. Correlation between SMYD2 protein level and viability of H9c2 myocytes ubnder stress conditions. (**a and b**) Viability of differentiated H9c2 cells with overexpression (**a**) or knockdown (**b**) of SMYD2 after treatment of AMA (2 µg/mL) for 24 h. Results represent the mean ± SD, (n = 3). Two-tailed Student's unpaired t-test with Welch's correction, *p < 0.05

In contrast, upon incubation of AMA, myofibrils are highly misaligned with a complete loss of directionality (Figure 3.17a, bottom left). The directionality analysis confirmed the same result (Figure 3.18a), showing a loss of myofibrillar structural

integrity. Immunostaining of SMYD2, which binds to the N2A domain of titin, showed the same pattern while showing high levels of co-localization with titin (Figure 3.17a, right).

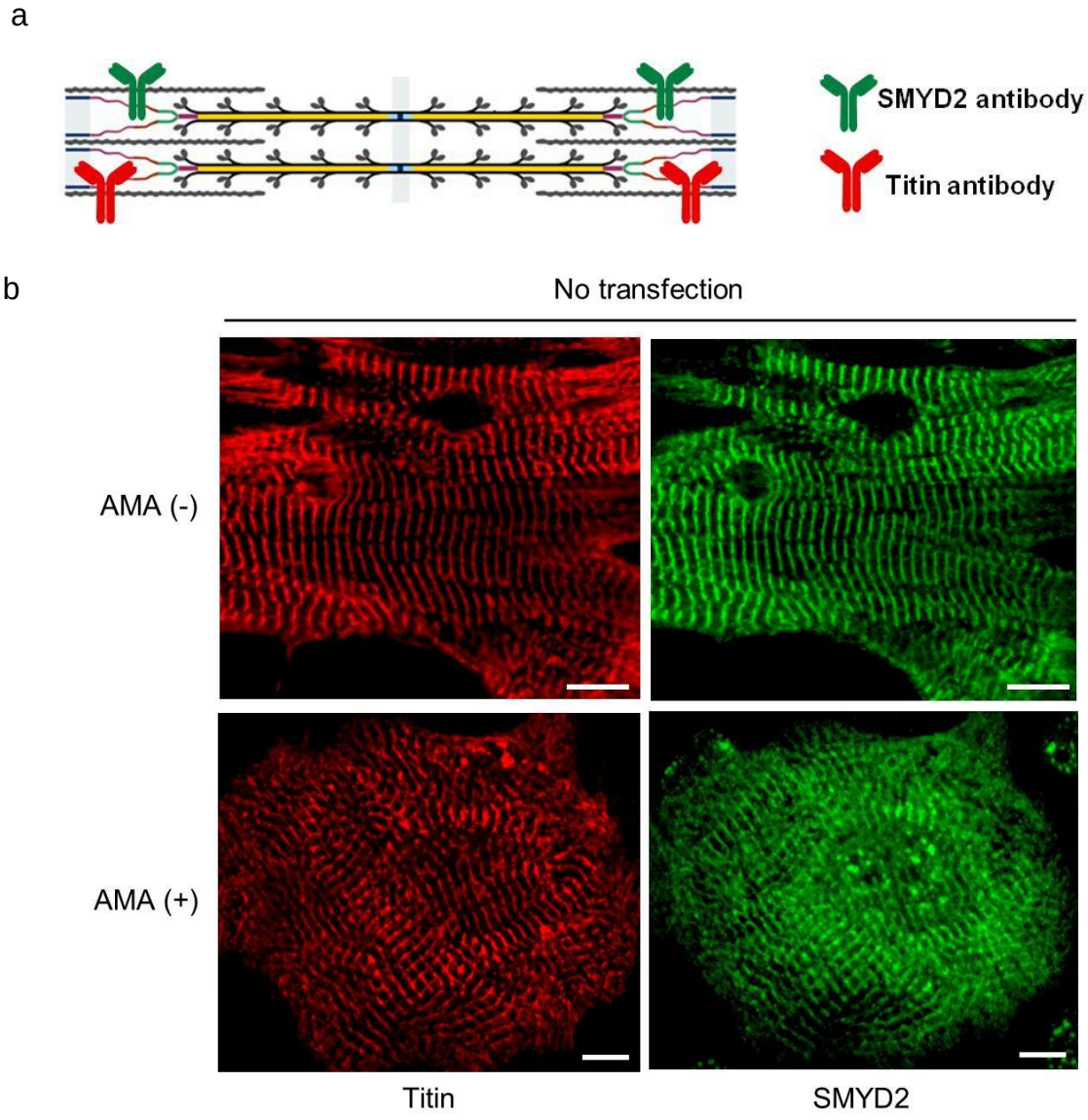

Figure 3.17. Antimycine A treatment induces a loss of myofibril integrity in rat neonatal cardiomyocytes. (**a)** Localization of SMYD2 and titin antibodies on sarcomere**. (b**) Monitoring the myofibril alignment in rat neonatal cardiomyocytes upon incubation of AMA (2 µg/mL) for 12 h. Immunostainings were done by using antibodies to SMYD2 (green) titin (α-titin-NT, red). About 30 cells were photographed and examined for myofibril alignment or directionality by using ImageJ software. Images represent the major myofibril structure in individual conditions. Scale bars, 10 µm.

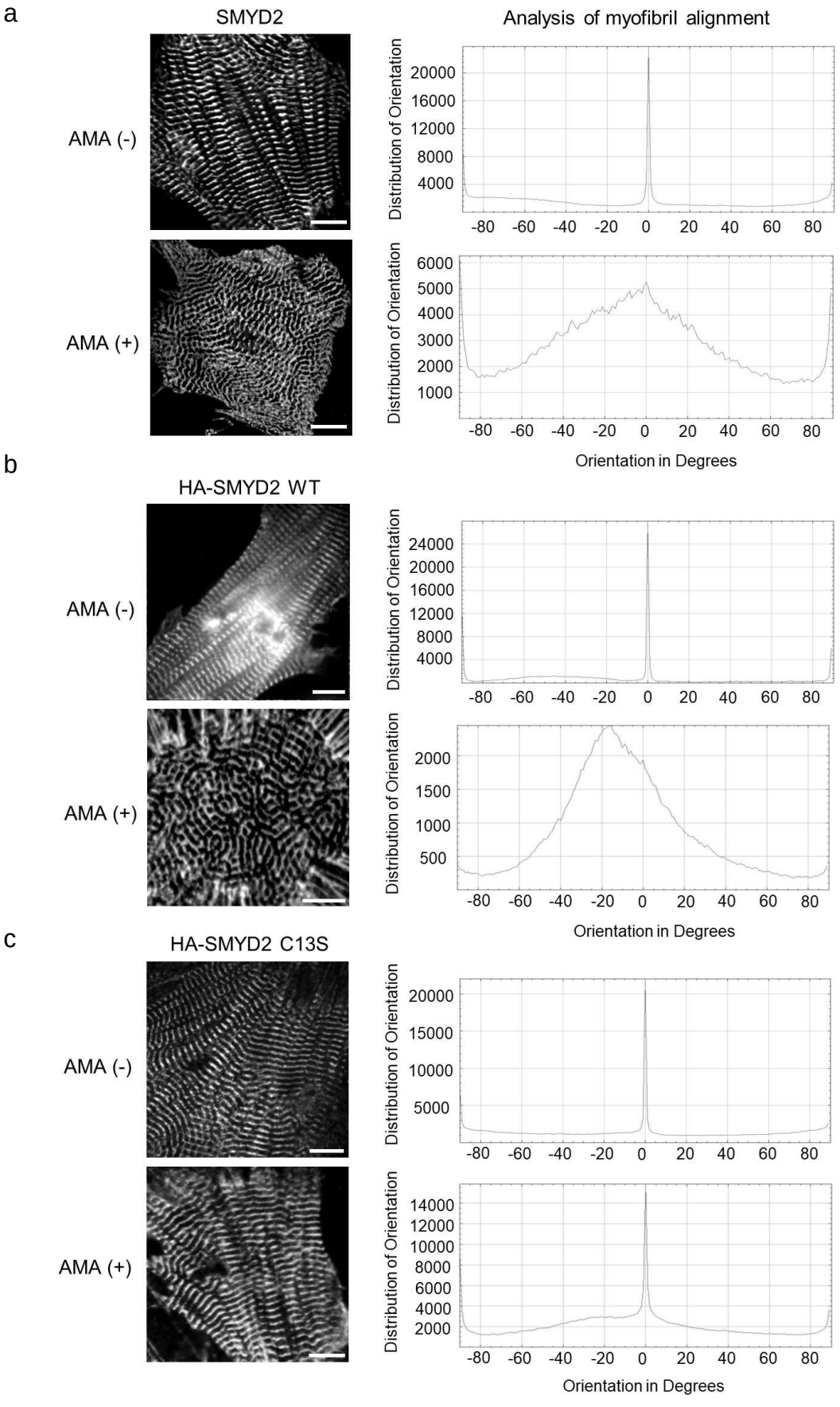
a
SMYD2
Analysis of myofibril alignment
AMA (-)
AMA (+)
Distribution of Orientation
Orientation in Degrees
b
HA-SMYD2 WT
AMA (-)
AMA (+)
Distribution of Orientation
Orientation in Degrees
c
HA-SMYD2 C13S
AMA (-)
AMA (+)
Distribution of Orientation
Orientation in Degrees

Figure 3.18. Analyses of directionality of myofibrils. Rat neonatal cardiomyocytes without expression of SMYD2 (**a**), or with expression of SMYD2 WT (**b**) or C13S (**c**) were treated with AMA for 12 h. About 30 cells were photographed and analyzed for orientation of myofibrils by ImageJ program. Images are representatives of cells in individual conditions. Cells were counted as 'aligned' when 'orientation in degree' stays between -20 to 20 with a 'distribution of orientation' more than 10,000.Scale bars, 10 μm.

3.12 SMYD2 C13S recovers myofibril integrity under oxidative stressed conditions.

To examine the importance of SMYD2 Cys13 glutathionylation for myofibrillar structure, we repeated experiments upon expression of SMYD2 WT or C13S to rat neonatal cardiomyocytes. Without treatment of AMA, both cells expressing SMYD2 WT or C13S showed parallel striated myofibrils stained by titin or HA antibodies (Figure 3.19a, top rows,). The directionality analysis showed uniform orientation of myofibrils (Figure 3.19b and c) (Figure 3.19b, bars 3 and 5, n = 30, triplicate). However, after incubation of AMA for 12 h, cells with SMYD2 WT showed disoriented and misaligned myofibrils (Figure 3.19b, bottom, columns 1-2). The directionality analysis confirmed the same result (Figure 3.19b). Strikingly, cells with SMYD2 C13S retained parallel and regular arrangement of myofibrils in a similar pattern to that seen in the unstressed condition (Figure 3.19c) (Figure 3.19a, bottom, columns 3-4). Directionality analyses of myofibrils in individual cells showed that treatment of AMA induced misaligned myofibrils in a high number of cells expressing SMYD2 WT versus a low number of cells with SMYD2 C13S (Figure 3.19b bars 4 vs 6, cells with aligned myofibrils: 36.7 ± 3.3% vs 63.3 ± 3.3% for SMYD2 WT and C13S respectively, n = 30 cells, triplicate,).

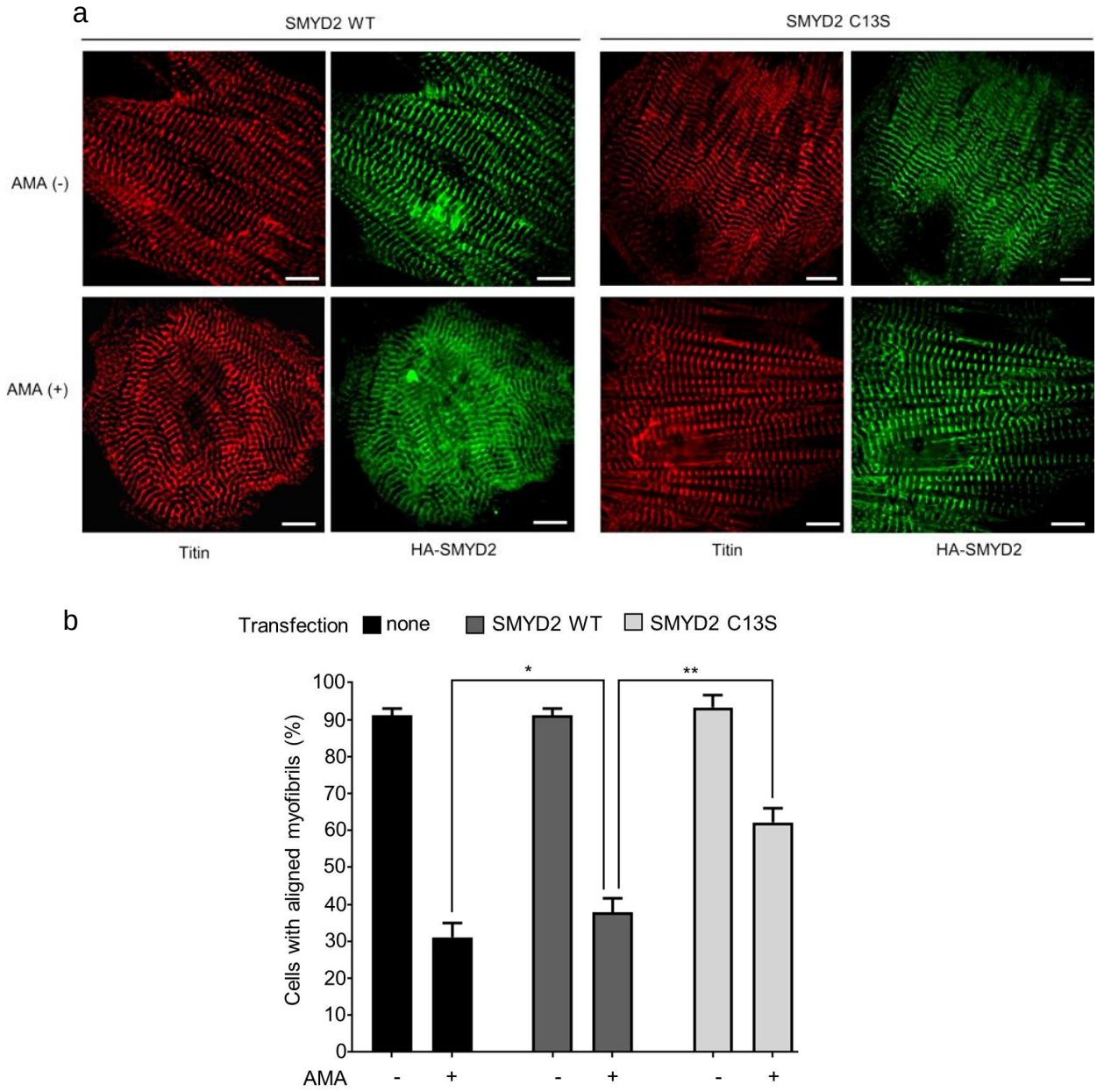

Figure 3.19. SMYD2 Cys13 glutathionylation induces a loss of myofibril integrity. Monitoring the myofibril alignment in rat neonatal cardiomyocytes upon incubation of AMA (2 µg/mL) for 12h: (**a**) ectopic expression of SMYD2 WT or C13S. Immunostainings were done by using antibodies to HA (green) and titin (α-titin-NT, red). About 30 cells were photographed and examined for myofibril alignment or directionality by using ImageJ software. Images represent the major myofibril structure in individual conditions. Scale bars, 10 µm. (**b**) The percentage of cells that have a parallel array of myofibrils in cardiomyocytes. Results represent the mean ± SD, (n = 3). Two-tailed Student's unpaired t-test with Welch's correction, *p < 0.05

a

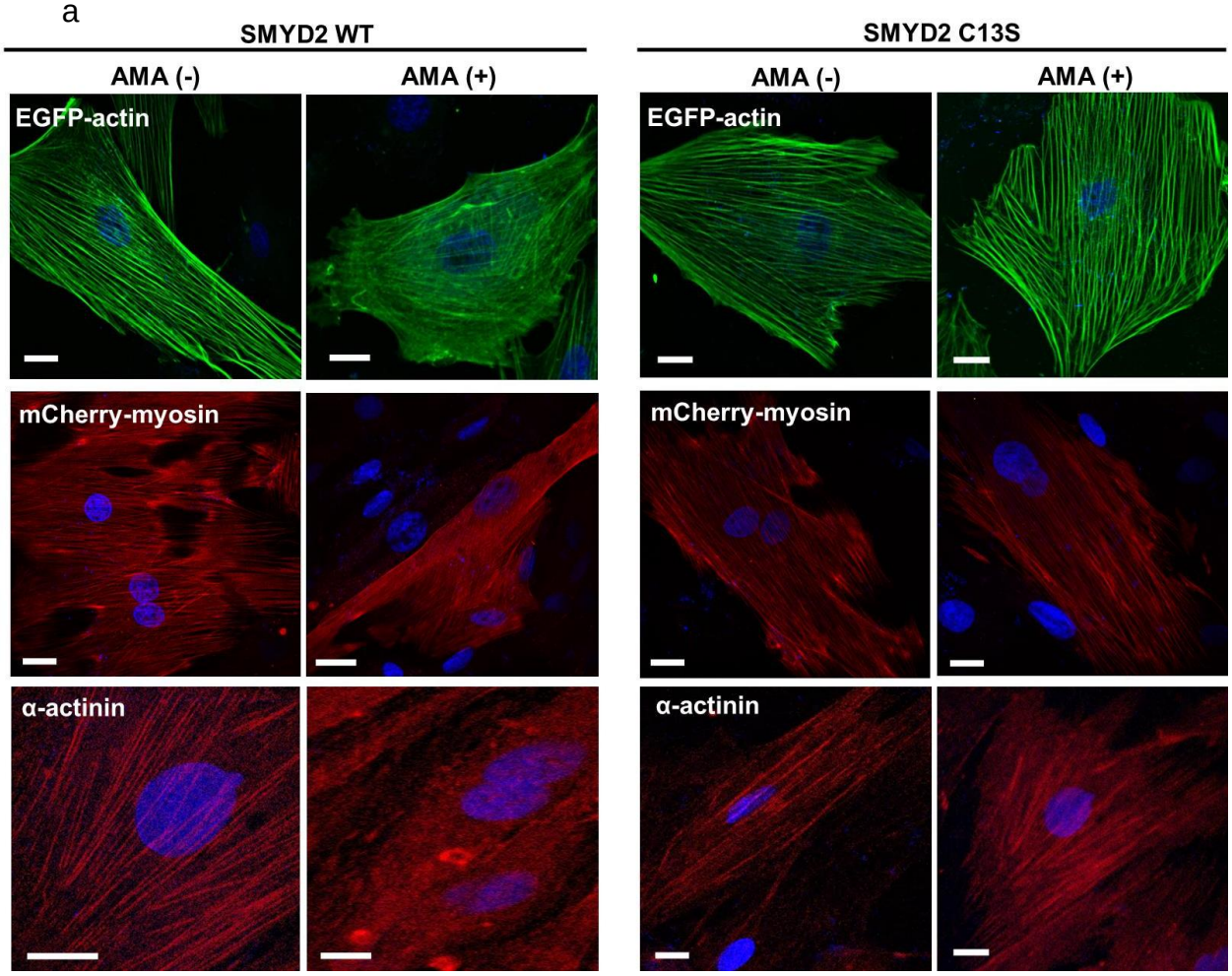
SMYD2 WT
SMYD2 C13S
AMA (-)
AMA (+)
AMA (-)
AMA (+)
EGFP-actin
EGFP-actin
mCherry-myosin
mCherry-myosin
α-actinin
α-actinin

b

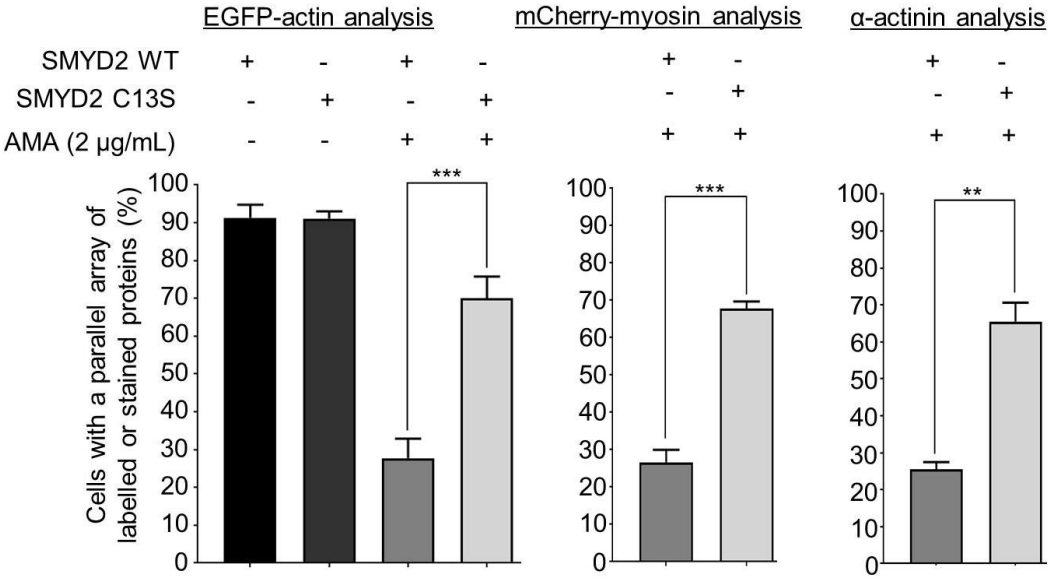
EGFP-actin analysis
mCherry-myosin analysis
α-actinin analysis
SMYD2 WT + - + - + - + -
SMYD2 C13S - + - + - + - +
AMA (2 µg/mL) - - + + + + + +
Cells with a parallel array of labelled or stained proteins (%)
100
90
80
70
60
50
40
30
20
10
0
***
***
**

Figure 3.20. Fluorescence imaging of sarcomeric proteins in differentiated H9c2 cells expressing SMYD2 WT or C13S. (**a**) After co-expression of SMYD2 WT or C13S with EGFP-actin or mCherry-myosin to H9c2 cells, cells were differentiated. Cells were then treated with antimycin A (AMA) for 12 h. H9c2 cells expressing SMYD2 WT or C13S were imaged by EGFP-actin, mCherry-myosin, or α-actinin immunostaining. About 30 cells were photographed and examined for directionality of labeled or stained proteins by using ImageJ software. (**b**) The percentage of cells that showed a parallel array of labelled or stained proteins. Results represent the mean ± SD, (n = 3). Two-tailed Student's unpaired t-test with Welch's correction, *p < 0.05. Scale bars, 20 μm.

In a similar manner, we also examined the structural integrity of differentiated H9c2 cells by fluorescence imaging of EGFP-actin, mCherry-MHC, and α-actinin immunostaining. All analyses showed the same pattern that upon treatment of AMA, cells expressing SMYD2 WT showed a loss of structural integrity, whereas cells with SMYD2 C13S maintained the similar structural integrity to ones in the unstressed condition (Figure 3.20a and b). Overall, these data support the concept that SMYD2 Cys13 glutathionylation is responsible for misalignment or destabilization of myofibrils.

3.13 SMYD2 Cys13 glutathionylation leads to degradation of sarcomeric proteins

The loss of stability or integrity of myofibrils is likely due to degradation of sarcomeric proteins. Therefore, we compared protein levels in H9c2 myocytes (Figure 3.21a) and HL-1 cardiomyocytes (Figure 3.21b) expressing SMYD2 WT versus C13S. Before treatment with AMA, the protein level of α-actinin was similar in differentiated H9c2 cells and HL-1 cardiomyocytes expressing SMYD2 WT or C13S. Exposure to AMA resulted in a decreased level of α-actinin and troponin I in cells with SMYD2 WT (Figure 3.21a, lane 1 vs. 2) (Figure 3.21b, lane 1 vs. 2), but had no effect in cells with SMYD2 C13S (Figure 3.21a, lane 3 vs. 4) (Figure 3.21b, lane 3 vs. 4). Under the same condition, treatment with AMA had no effect on the expression levels of actin, MHC, SMYD2, and Hsp90 in cells with SMYD2 WT or C13S (Figure 3.21a). Interestingly, we

also found that cardiac ankyrin repeat protein (CARP), transcription cofactor that is involved in muscle remodeling[177], is highly elevated in cells with SMYD2 WT versus C13S (Figure 3.21c).

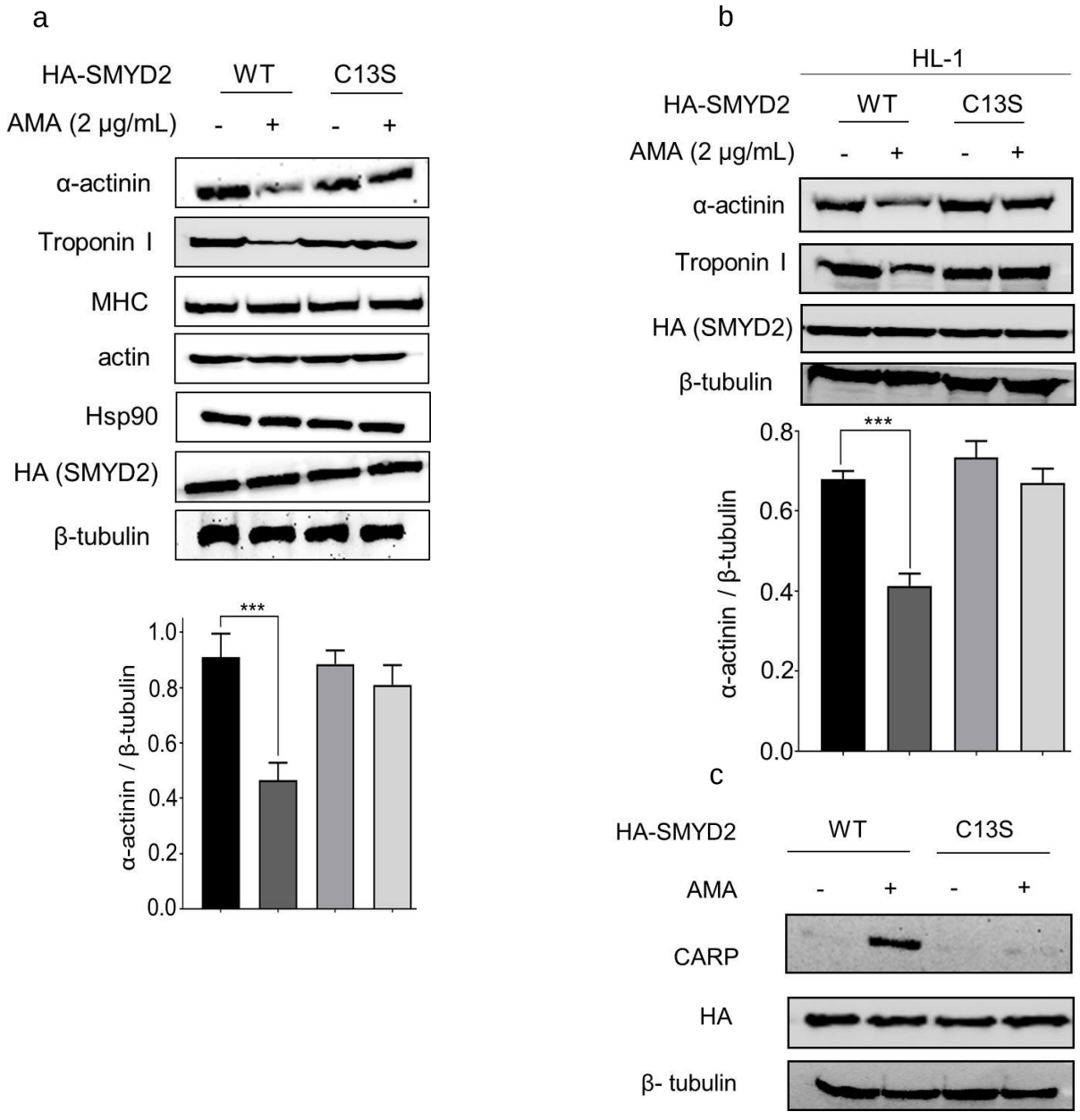

Figure 3.21. SMYD2 Cys13 glutathionylation leads to degradation of sarcomeric proteins. (**a** and **b**) Sarcomeric protein levels in H9c2 myocytes and HL-1 cardiomyocytes in response to AMA. H9c2 and HL-1 cells expressing SMYD2 WT or C13S were treated with AMA (2 µg/mL) for 12 h. Protein levels were determine by

Western blotting. (**c**) The level of CARP in differentiated H9c2 cells in response to AMA treatment. After incubation of AMA for 12 h, lysates were analyzed by Western blotting. Results represent the mean ± SD, (n = 3). Two-tailed Student's unpaired t-test with Welch's correction, *p < 0.05

In addition, we probed the cleavage or degradation of titin by dot-blot analysis: the blot was probed with α-titin-NT antibody, which recognizes an N-terminal region of titin, after pull-down of titin with α-titin-CT antibody, which binds to a C-terminal region of titin (Figure 3.22a).

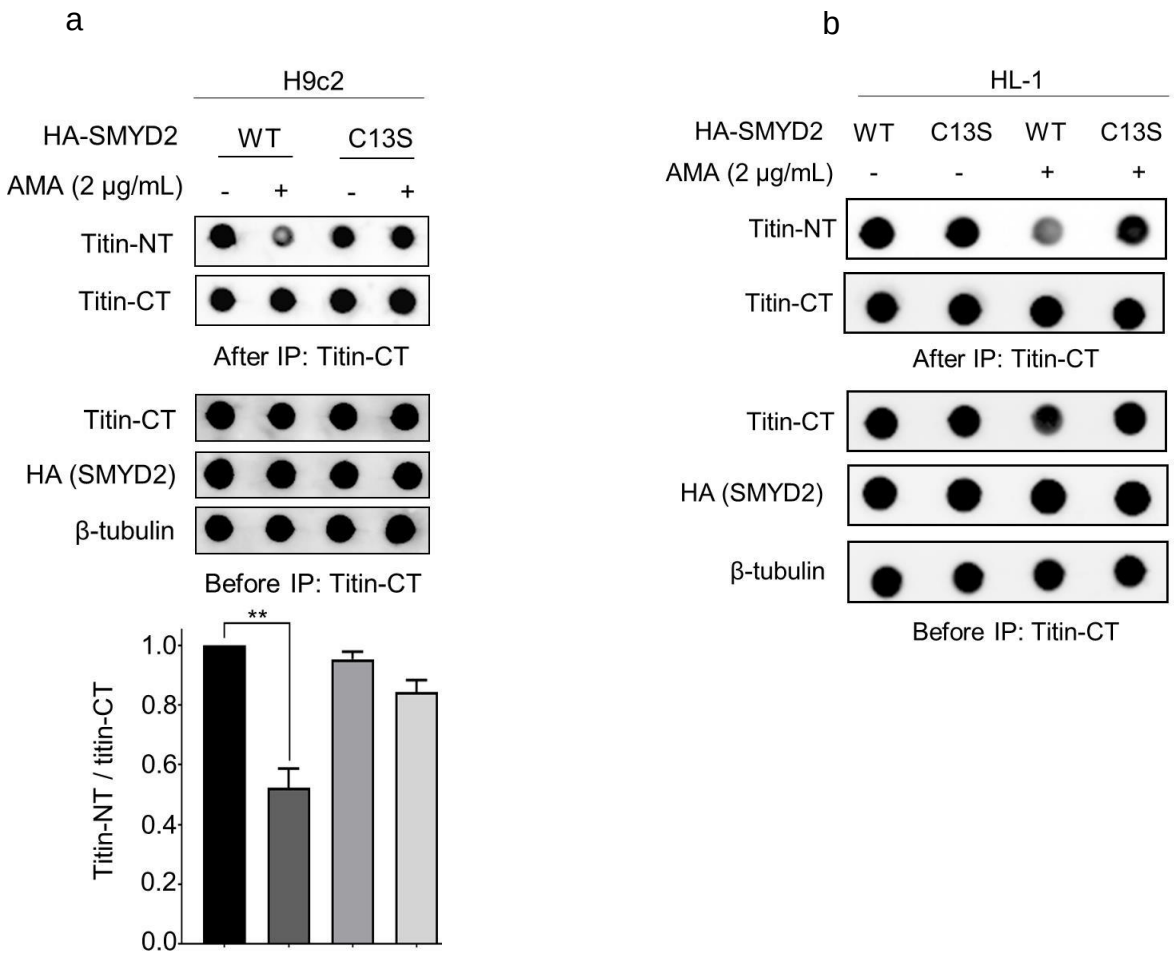

c

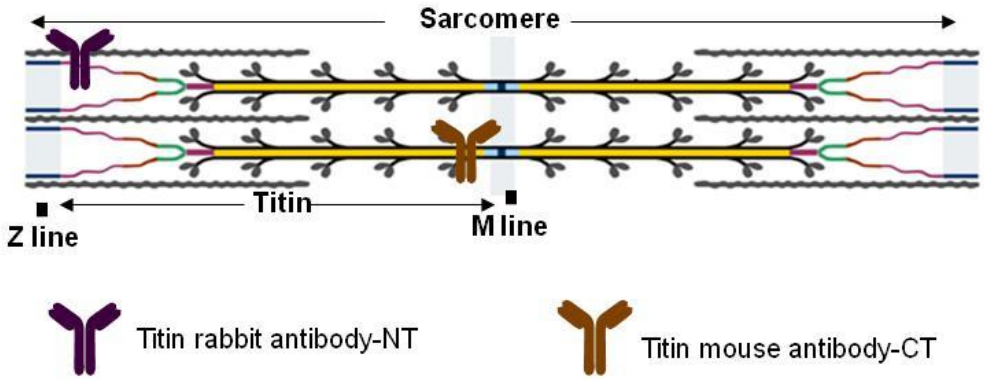
Sarcomere
Titin
Z line
M line
Titin rabbit antibody-NT
Titin mouse antibody-CT

d

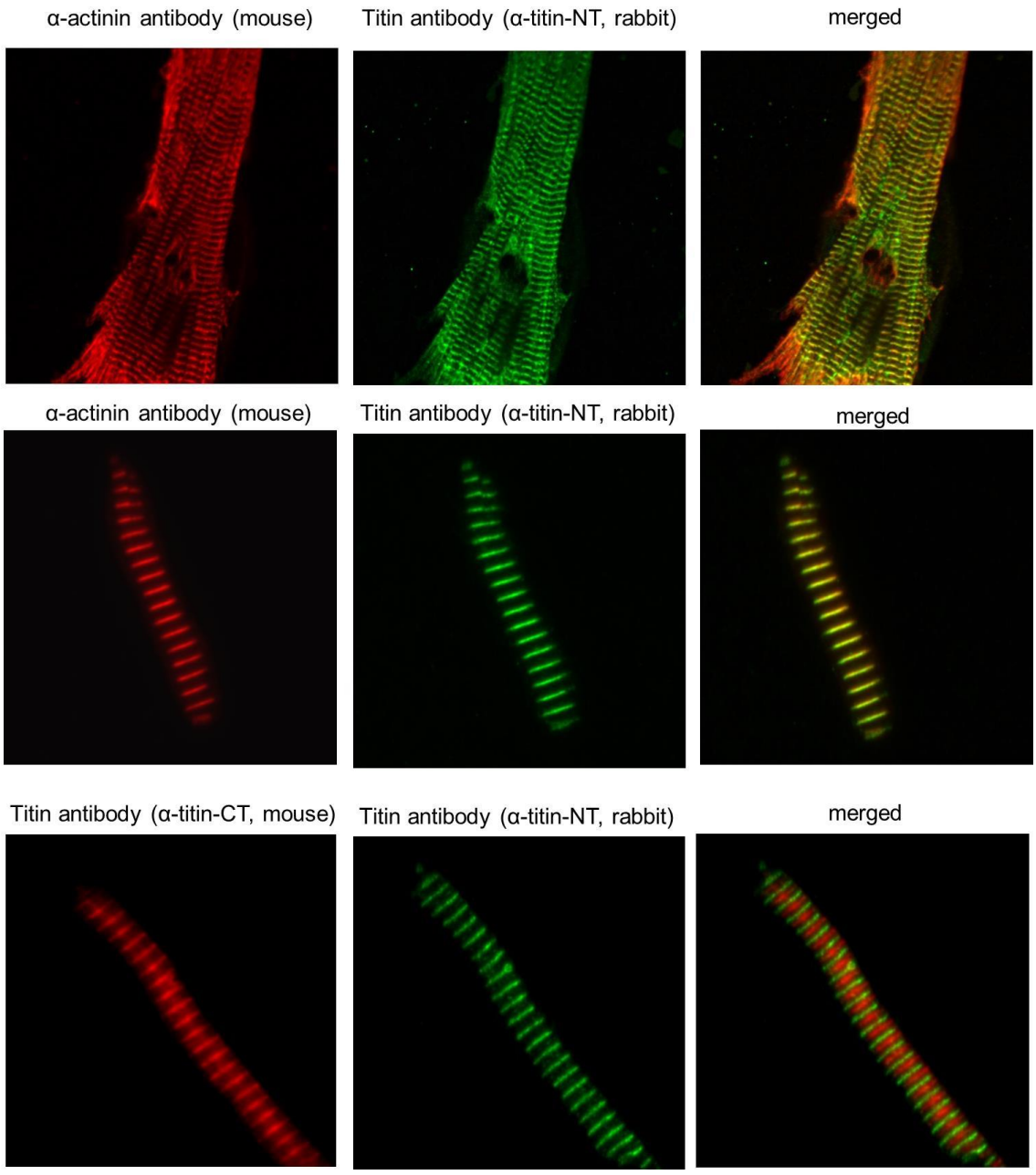
α-actinin antibody (mouse)
Titin antibody (α-titin-NT, rabbit)
merged
α-actinin antibody (mouse)
Titin antibody (α-titin-NT, rabbit)
merged
Titin antibody (α-titin-CT, mouse)
Titin antibody (α-titin-NT, rabbit)
merged

Fgure 3.22. SMYD2 Cys13 glutathionylation leads to degradation or cleavage of titin protein. (**a** and **b**) Dot blot analysis of titin. To monitor the cleavage or degradation of titin, titin was pull-downed with antibody that binds to a C-terminal region of titin (α-titin-CT), followed by Western blotting with antibody that binds to an N-terminal region of titin (α-titin-NT). (**c**) Localization of titin antibodies on sarcomere. (**d**)Validation of titin antibody (α-Titin-NT). α-Titin-NT antibody recognizes the N-terminus of an I-band region (Ig7-8) of titin. Immunostaining of rat neonatal cardiomyocytes (top) or isolated myofibrils (from mouse gastrocnemius) (bottom) with α-titin-NT antibody shows a high co-localization pattern with α-actinin antibody that stains the Z-disk of sarcomere. (**d**) Validation of titin antibody (α-titin-CT). α-Titin-CT antibody recognizes the C-terminal region of titin. Immunostaining of isolated myofibrils (from mouse gastrocnemius) with α-titin-NT and α-titin-CT shows the alternating staining pattern. Results represent the mean ± SD, (n = 3). Two-tailed Student's unpaired t-test with Welch's correction, *p < 0.05

Upon treatment of AMA, the level of titin detected by α-titin-NT was decreased in cells expressing SMYD2 WT (Figure 3.22a, lane 1 vs. 2), whereas it was unchanged in cells expressing SMYD2 C13S (Figure 3.22a, lane 3 vs. 4). In addition to H9c2 cells, we also examined HL-1 mouse cardiac muscle cells upon ectopic expression of SMYD2 WT or C13S. Similarly, reduced levels of titin was observed in cells expressing SMYD2 WT (Figure 3.22b, lane 1 vs. 2), whereas no changes were observed in cells with SMYD2 C13S (Figure 3.22b, lane 3 vs. 4).

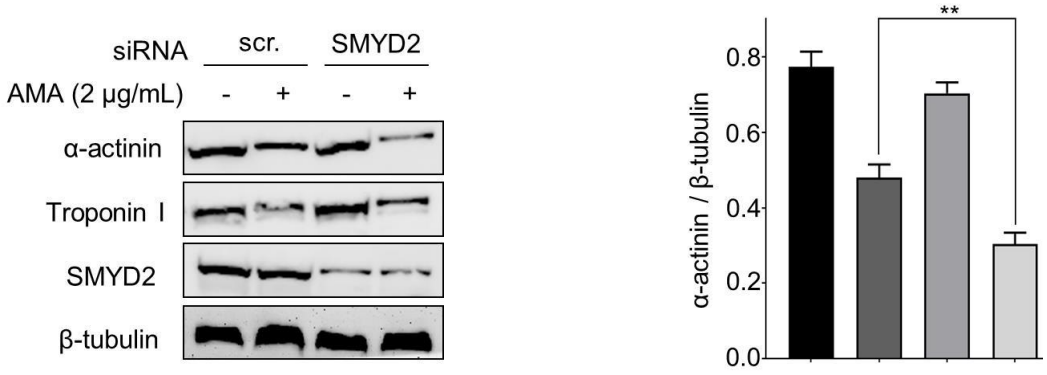

Figure 3.23. SMYD2 knockdown induces more significant reduction of α-actinin and troponin I. Sarcomeric protein levels in response to AMA after SMYD2

knockdown. Results represent the mean ± SD, (n = 3). Two-tailed Student's unpaired t-test with Welch's correction, *p < 0.05

Supporting these findings, without treatment of AMA, levels of α-actinin or troponin I remain similar upon SMYD2 knockdown (Figure 3.23, lane 1 vs. 3). However, SMYD2 knockdown induced more significant reduction of α-actinin and troponin I levels upon treatment of AMA (Figure 3.23, lane 2 vs. 4), which correlates with the data that SMYD2 knockdown induces more significant reduction of cell viability upon incubation of AMA. These data support that SMYD2 Cys13 glutathionylation leads to reduced levels of several sarcomeric proteins, such as α-actinin, troponin I, and titin.

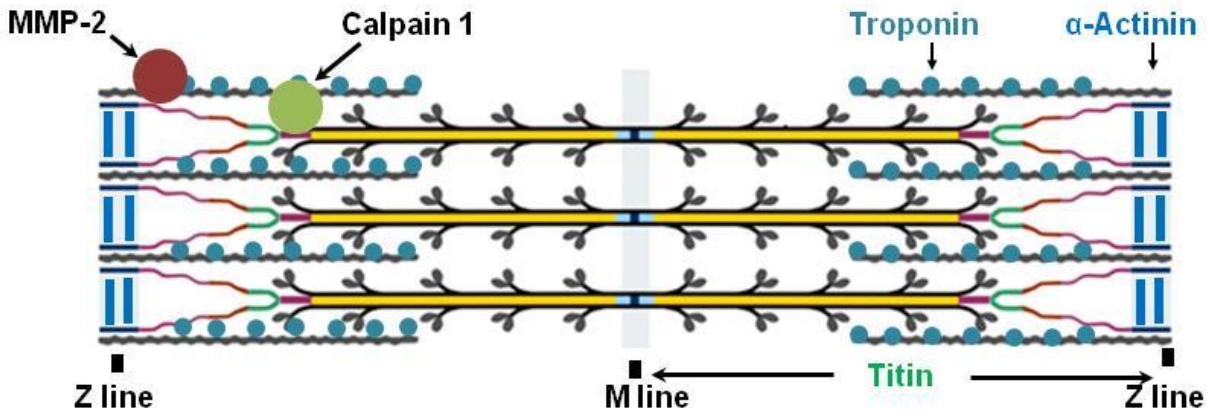

Figure 3.24. Proteases responsible for sarcomeric protein degradation. MMP-2 and calpain 1 are localized on sarcomere.

3.14 MMP-2 and calpain 1 are responsible for sarcomeric protein degradation under stressed conditions

Previously, calpain 1/3 and MMP-2 have been found to play a role in degradation of sarcomeric proteins, including α-actinin and titin (Figure 3.24). Therefore, we

evaluated whether calpain and MMP-2 contribute to sarcomeric protein degradation in our model. The decreased levels of α-actinin and troponin I in the presence of AMA was restored upon incubation with an MMP-2 inhibitor (ARP-100) (Figure 3.25a, lane 2 vs. 4) or MMP-2 knockdown (Figure 3.25b, lane 2 vs. 4), while there was no effect on the expression levels of other proteins, including actin and SMYD2 (Figure 3.25a).

a

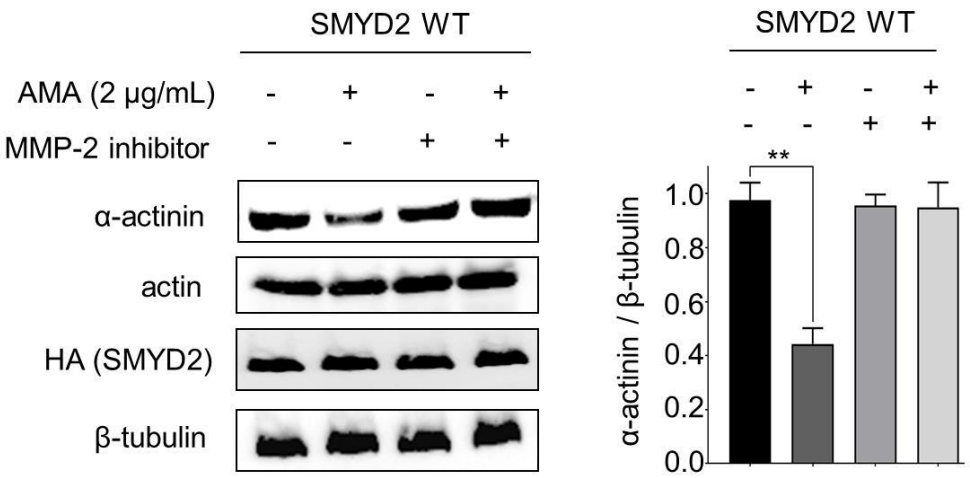

b

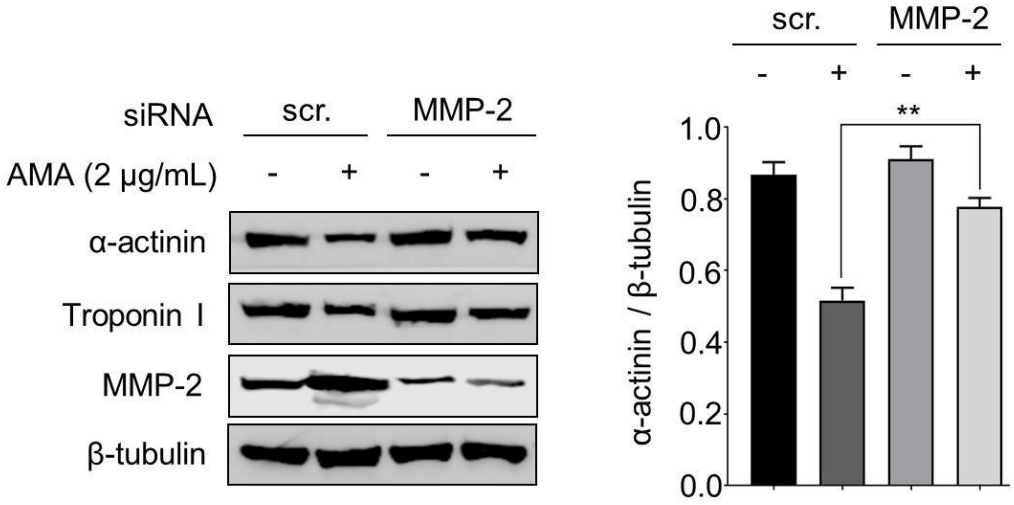

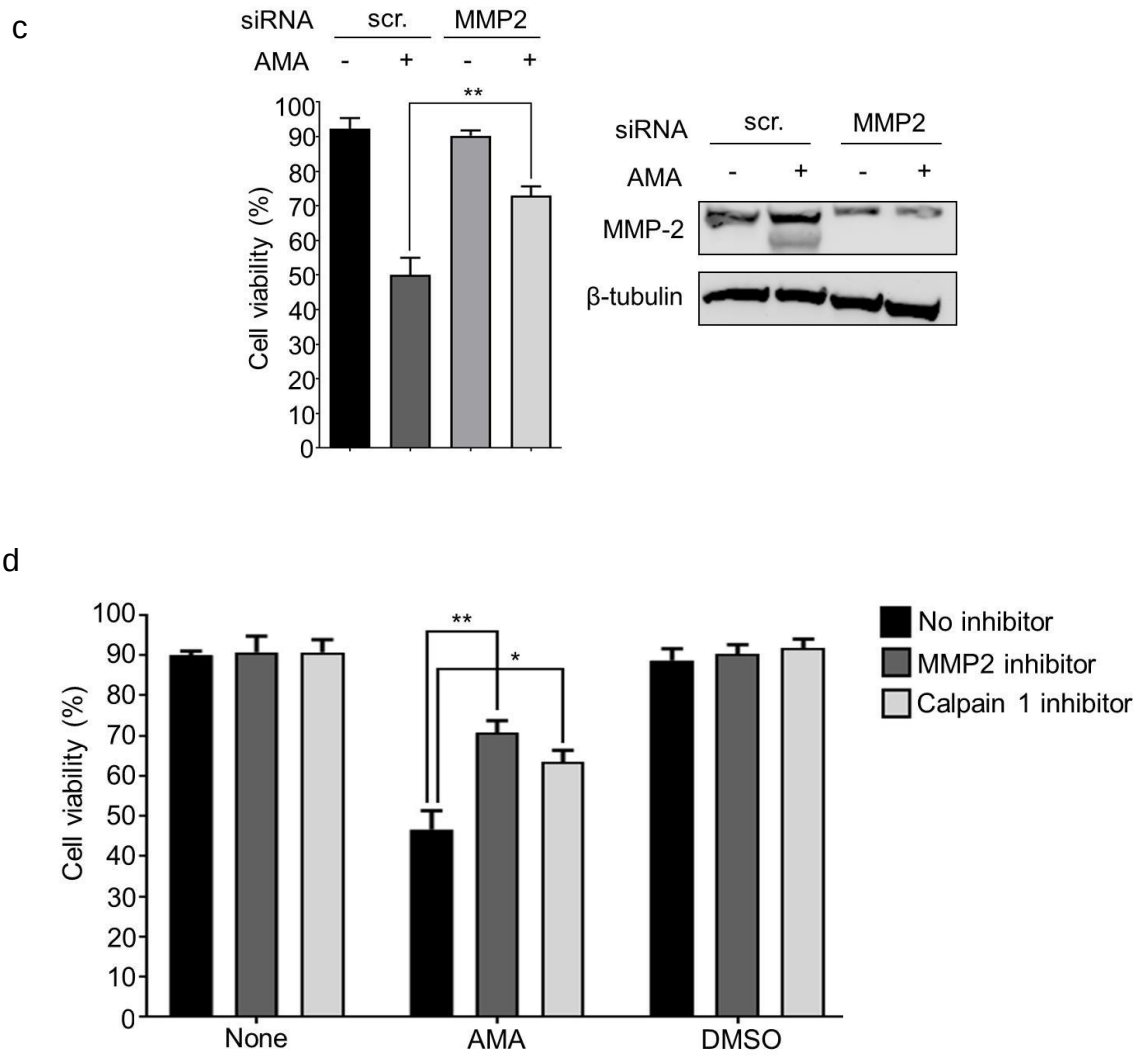

Figure 3.25. SMYD2 C13S is protective against sarcomeric proteins degradation and cell death in oxidatively stressed conditions. Sarcomeric protein levels in response to AMA after incubation of ARP-100 (MMP-2 inhibitor) (**d**), or MMP-2 knockdown (**e**). (**f**-**g**) The cell viability in response to AMA after incubation of ARP-100 (1 µM) or calpastatin (calpain 1 inhibitor, 5 µM) (**f**) or MMP-2 knockdown (**g**). In all conditions, differentiated H9c2 cells were treated with AMA (2 µg/mL) for 12 h. Lysates were analyzed by Western blotting. Cell viability was analyzed by Trypan blue assay. Results represent the mean ± SD, (n = 3). Two-tailed Student's unpaired t-test with Welch's correction, *$p < 0.05$

We further evaluated H9c2 cell viability upon exposure to inhibitors of MMP-2 (ARP-100) and calpain 1 (acetyl-calpastatin) (Figure 3.25d) or MMP-2 knockdown (Figure 3.25c). As expected, viability of H9c2 cells was significantly decreased after

treatment of AMA (Figure 3.25c and d). This effect was mitigated by treatment with either the MMP-2 or calpain 1 inhibitor (Figure 3.25d, bars 4 vs. 5 and 6) or MMP-2 knockdown (Figure 3.25c, bars 2 vs. 4), suggesting that calpain 1 and MMP-2 contribute to the stressor-induced reduction of cell viability and degradation of α-actinin and troponin I. Overall, these data reveal that SMYD2 C13S is protective against sarcomeric proteins degradation and cell death in oxidatively stressed conditions, and that SMYD2 Cys13 glutathionylation is an important molecular event involved in degradation of sarcomeric proteins mediated by MMP-2 and/or calpain-1.

3.15 Preparation and characterization of glutathionylated SMYD2

In myocytes, SMYD2 is involved in mono-methylation of Hsp90, which increases Hsp90 chaperone activity. SMYD2 then forms a complex with mono-methylated Hsp90. This complex binds to N2A, a domain of titin, which has been implicated to be important for sarcomere stabilization.

a

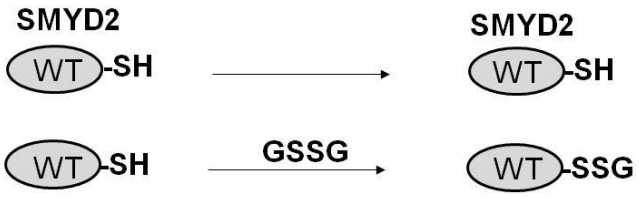

c

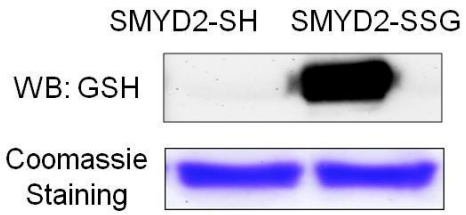

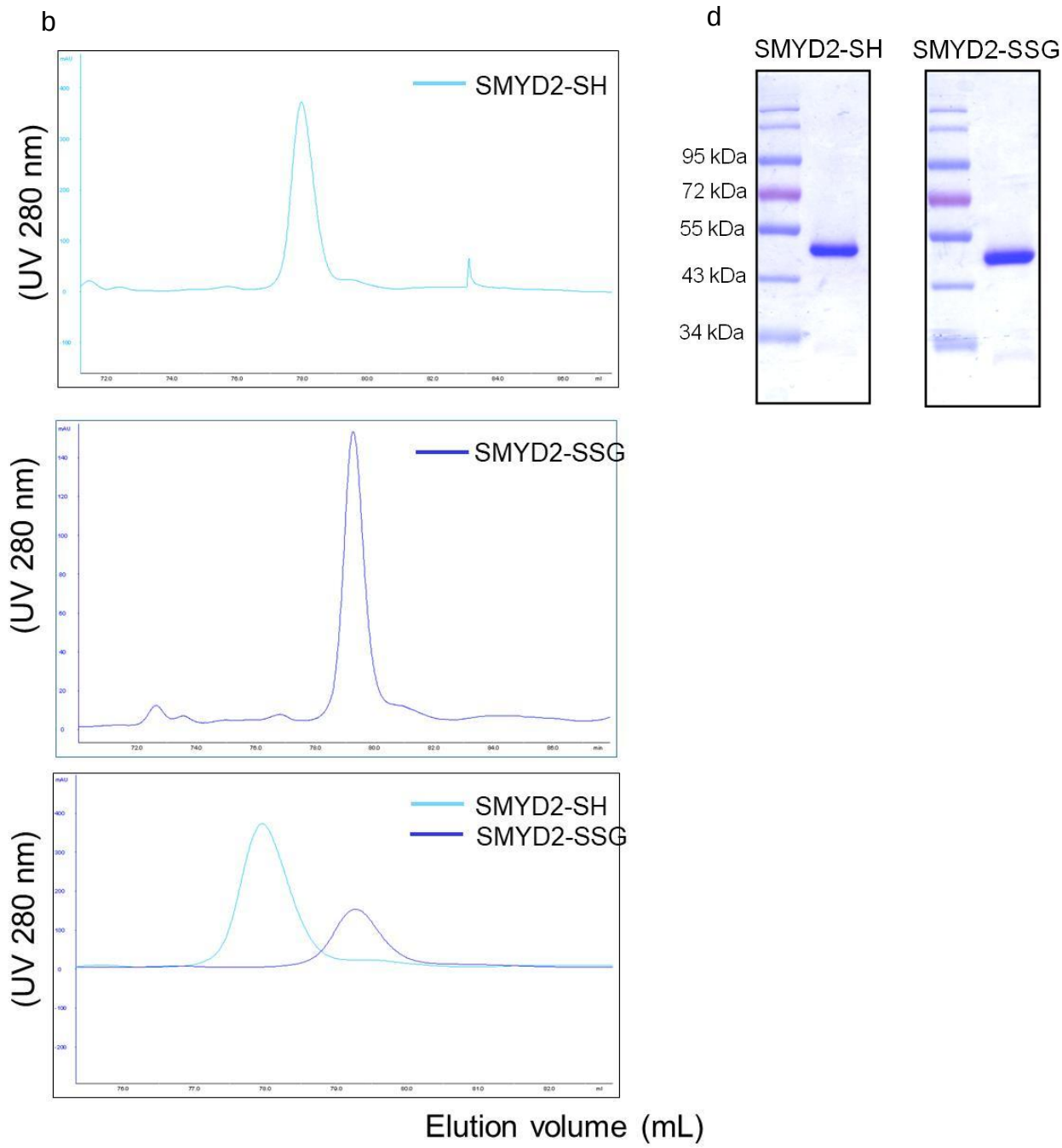

Figure 3.26. Preparation of SMYD2 glutathionylated version to characterize the SMYD2:HSP90:N2A interactions (**a**) A scheme for preparing non-glutathionylated SMYD2 (SMYD2-SH) and glutathionylated SMYD2 (SMYD2-SSG). (**b**) Chromatograms of ion-exchange column purification of SMYD2-SH and SMYD2-SSG. (**d**) Gel analysis and purity after purification of SMYD2-SH and SMYD2-SSG. (**c**) Western blotting that shows glutathionylation of SMYD2.

Therefore, we investigated whether glutathionylation of SMYD2 changes its enzymatic activity or interaction with Hsp90 or the N2A domain. To interrogate the effect of glutathionylation on SMYD2 in vitro, purified SMYD2 WT was glutathionylated by incubating with oxidized glutathione (GSSG) (Figure 3.26a). Note that similar incubation of SMYD2 with oxidized azido-glutathione (^{N3}GSSG^{N3}) induced selective glutathionylation of SMYD2 at Cys13. SMYD2 WT (SMYD2-SH) and glutathionylated SMYD2 (SMYD2-SSG) were further purified (Figure 3.26b and d). SMYD2-SH and SMYD2-SSG show the same partial digestion pattern by trypsin (Figure 3.27), suggesting their similarly folded structures.

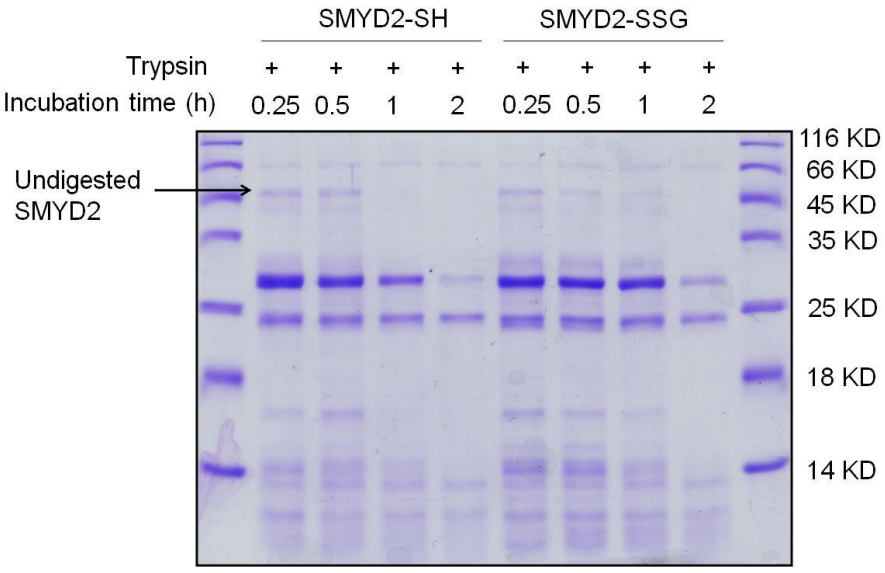

Figure 3.27. Characterization of SMYD2-SH and SMYD2-SSG. The partial trypsin digestion of SMYD2-SH and SMYD2-SSG. Purified SMYD2-SH or SMYD2-SSG was incubated with trypsin, quenched at the indicated time, and resolved on a SDS-PAGE gel.

3.16 SMYD2 glutathionylation does not affect its methyl transferase activity

SMYD2 enzymatic activity was then examined by LC-MS methylation analysis (Figure 3.28b). In this assay, when using Hsp90 as a substrate, SAH production was

decreased by approximately 50% with SMYD2-SSG versus SMYD2-SH (the rate of SAH production: 13.2 ± 1.6 nM min^{-1} for SMYD2-SH vs. 7.4 ± 1.0 nM min^{-1} for SMYD2-SSG) (Figure 3.28b).

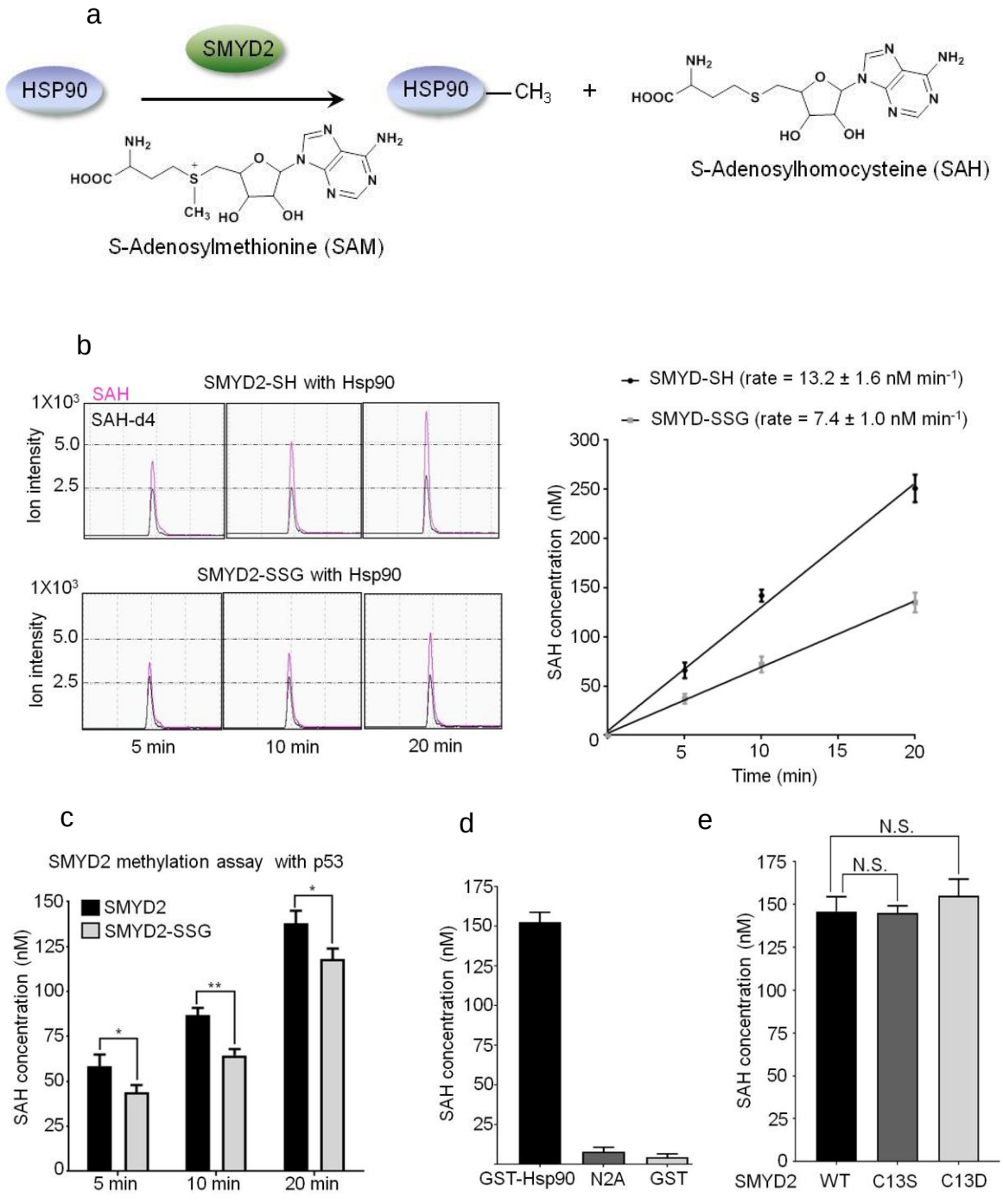

Figure 3.28. Enzyme activity of SMYD2 and glutathionylated SMYD2. (**a**) A scheme of protein methyl transferase reaction catalyzes by SMYD2 and utilization of SAM as

the methyl donor while production of SAH as the byproduct. The amount of SAH was quantified by comparing to the amount of deuterium-labelled SAH (SAH-D4) as an internal standard in LC-MS analysis. (**b** and **c**) Enzyme activity of SMYD2-SH or SMYD2-SSG with Hsp90 (**b**) or 11-mer p53 peptide (HSSHLKSKKGQ) (**c**) as substrates. SMYD2-SH or SMYD2-SSG (200 nM) was mixed with Hsp90 (4 µM) or p53 peptide (25 µM) and SAM (25 µM) in TBST (pH 7.4). The SAH formation was quantified in a time-dependent manner. (**d**) Enzyme activity of SMYD2 with different substrates. SMYD2 (200 nM) was mixed with GST-Hsp90, N2A, or GST (all 4 µM). (**e**) Enzyme activity of SMYD2 (WT, C13S and C13D) with Hsp90 as a substrate. Results represent the mean ± SD, (n = 3). Two-tailed Student's unpaired t-test with Welch's correction, *p < 0.05

In comparison, when p53 peptide was used as a substrate, SAH production was less significantly decreased with SMYD2-SSG versus SMYD2-SH (Figure 3.28c). A decrease of Hsp90 methylation, but not p53 methylation, with SMYD2-SSG suggests that the complex formation between Hsp90 and SMYD2 may be disrupted upon SMYD2 glutathionylation.

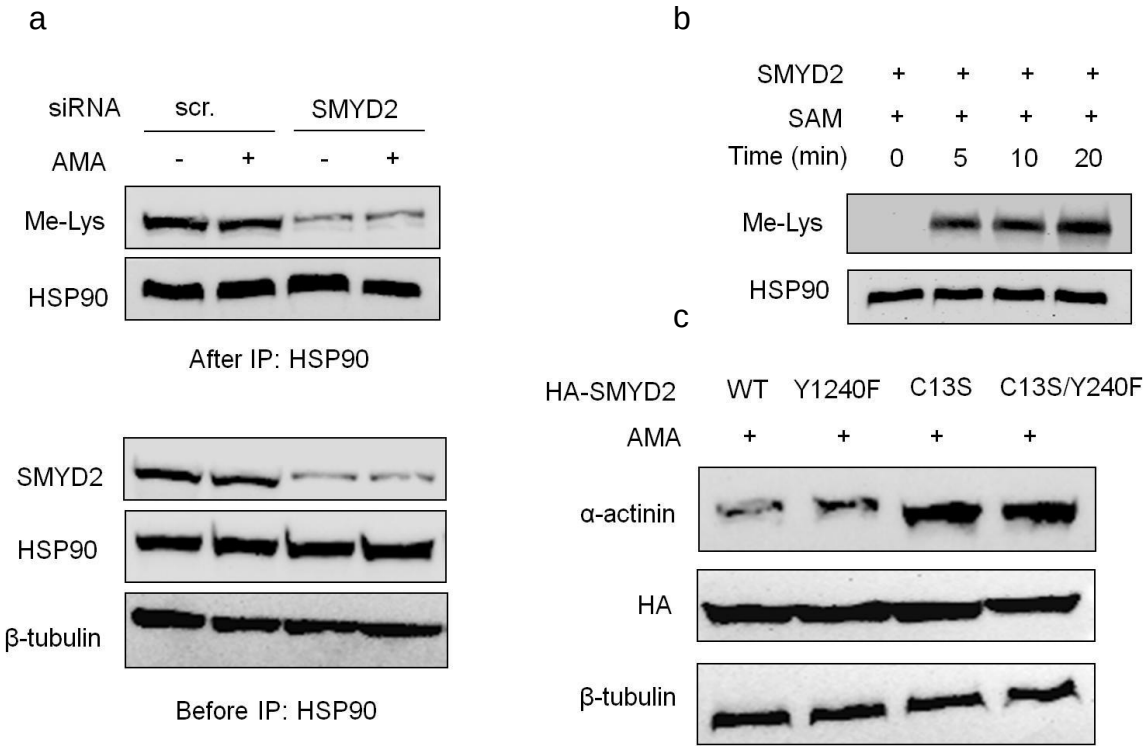

Figure 3.29. SMYD2 glutathionylation does not change methylation levels of Hsp90 in cells, and SMYD2 enzyme activity is not responsible for degradation of sarcomeric proteins. (**a**) Levels of mono-methyl lysine (Me-Lys) in Hsp90 in cells in

response to AMA. After incubation of AMA to differentiated H9c2 cells for 12 h, Hsp90 was immunoprecipitated and probed for its level of Me-Lys. There is no change of methylation levels in Hsp90 upon incubation of AMA (lane 1 vs. 2), whereas SMYD2 knockdown decreases Hsp90 methylation level (lane 1-2 vs. 3-4). (**b**) Valuation of an antibody to Me-Lys. Purified Hsp90 was methylated by incubation of SMYD2 and SAM, detecting methylation of Hsp90. (**c**) SMYD2 enzyme activity is not necessary for degradation of sarcomeric proteins. Differentiated H9c2 cells expressing SMYD2 WT and catalytically inactive mutants (Y1240F) were treated with AMA for 12 h. The level of α-actinin was analyzed by Western blotting, showing no difference between enzymatically active SMYD2 and inactive SMYD2.

Despite the modest reduction of SMYD2 enzymatic activity upon glutathionylation in vitro, the level of Hsp90 methylation was unchanged in cells upon treatment of AMA (Figure 3.29a), suggesting a low or no change of SMYD2 enzyme activity upon glutathionylation. Importantly, a catalytic inactive SMYD2 Y240F mutant could also lead to degradation of α-actinin in the same manner to SMYD2 WT (Figure 3.29c), suggesting that SMYD2 enzyme activity is not responsible for sarcomeric protein degradation.

3.17 SMYD2 Cys13 glutathionylation induces dissociation of SMYD2 from N2A and Hsp90

Next, we analyzed whether SMYD2-Hsp90-N2A interactions can be disrupted upon SMYD2 glutathionylation. A binding assay showed that GST-Hsp90 binds to SMYD2-SH more strongly than SMYD2-SSG (Figure 3.30b), showing that SMYD2 glutathionylation decreases the SMYD2-Hsp90 interaction. This result was further confirmed by co-immunoprecipitation (co-IP) in HEK293 cells expressing SMYD2 WT or C13S (Figure 3.30c): SMYD2 WT binding with Hsp90 was significantly decreased in stressed conditions (AMA and glucose deprivation) (Figure 3.30c, lane 1 vs. 2). In contrast, SMYD2 C13S interaction with Hsp90 did not change in identical stressed

conditions (Figure 3.30c, lane 3 vs.4). Similarly, the N2A domain was examined for binding with SMYD2 (Figure 3.30d and e).

a

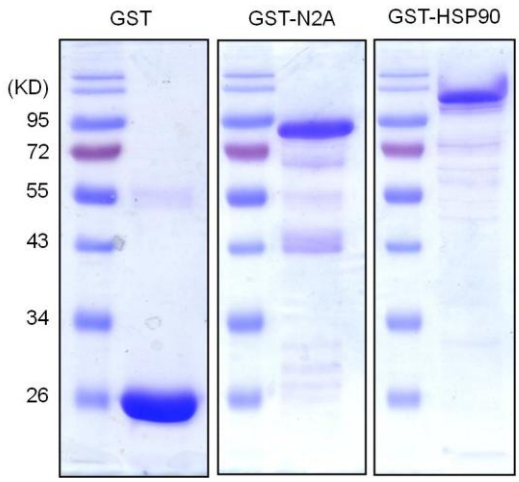

b

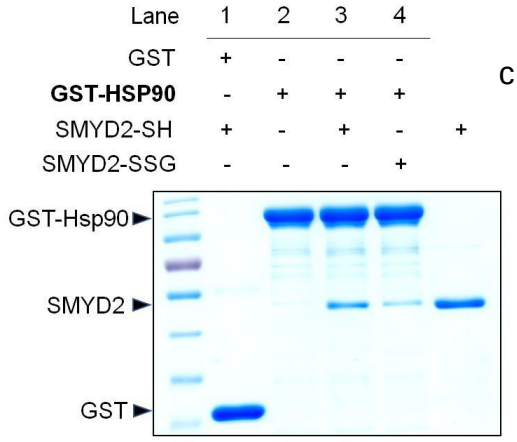

c

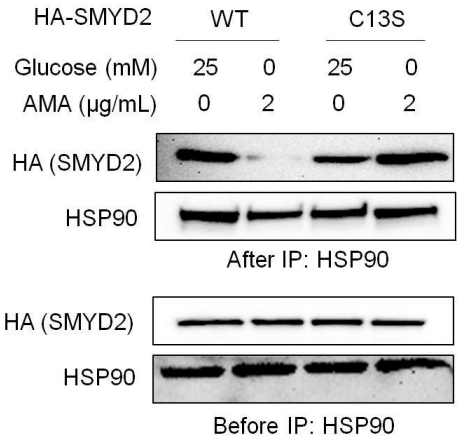

d

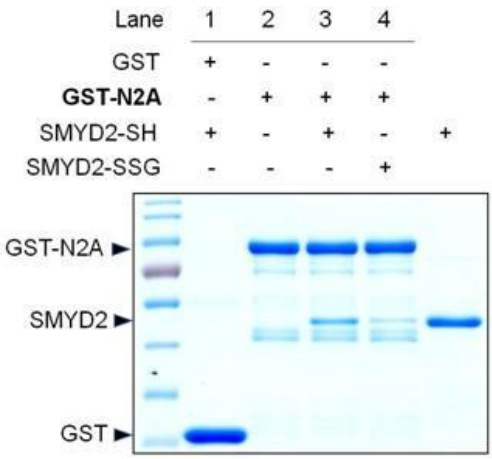

e

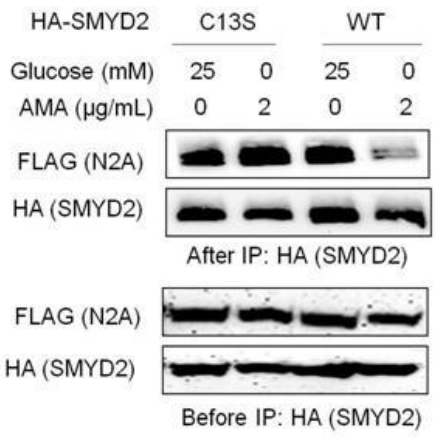

Figure 3.30. SMYD2 Cys13 glutathionylation induces dissociation of SMYD2 from N2A and Hsp90. (**a**) GST, GST-N2A, and GST-Hsp90 were expressed in E. coli and purified by affinity-column (glutathione-agarose). (**b** and **c**) SMYD2 glutathionylation disrupts its interaction with Hsp90. (**b**) Purified SMYD2-SH and SMYD2-SSG were incubated with GST-Hsp90 bound to glutathione beads, and eluted sample was analyzed. (**c**) Hsp90 was co-immunoprecipitated with SMYD2 WT or C13S from HEK293 cells in response to AMA with glucose deprivation. (**d** and **e**) SMYD2 glutathionylation disrupts its interaction with N2A. (**d**) Purified SMYD2-SH and SMYD2-SSG were incubated with GST-N2A bound to glutathione beads, and eluted sample was analyzed. (**e**) FLAG-N2A was co-immunoprecipitated with SMYD2 WT or C13S in HEK293 cells in response to AMA with glucose deprivation.

N2A binding to SMYD2 was decreased with SMYD2-SSG versus SMYD2-SH (Figure 3.30d). Similarly, co-IP confirmed that SMYD2 WT lost its interaction with N2A in the presence of stressors (Figure 3.30e, lane 3 vs. 4) while SMYD2 C13S retained its interaction (Figure 3.30e, lane 1 vs. 2).

3.18 SMYD2 Cys13 glutathionylation induces dissociation of SMYD2 from titin in rat neonatal cardiomyocytes.

To further demonstrate that SMYD2 dissociates from the N2A domain or titin upon SMYD2 glutathionylation, we examined co-localization of SMYD2 and titin in the sarcomeres of rat neonatal cardiomyocytes expressing SMYD2 WT or C13S. Consistently, immunostaining showed high levels of SMYD2 co-localized with titin in the absence of AMA (Figure 3.31a). However, co-localization of SMYD2 with titin was decreased upon incubation of AMA (Figure 3.31a, and 3.31d, n = 30, Pearson Coefficient 0.80 ± 0.03 and 0.32 ± 0.04 without and with AMA, respectively). Notably, co-localization of SMYD2 with titin was also decreased in cells expressing SMYD2 WT after incubation of AMA (Figure 3.31b and 3.31d, n = 30, Pearson Coefficient 0.75 ± 0.05 and 0.43 ± 0.04 without and with AMA, respectively), whereas co-localization remains high in cells expressing SMYD2 C13S (Figure 3.31c and 3.31d, n = 30)

Pearson Coefficient 0.77 ± 0.05 and 0.67 ± 0.06 without and with AMA, respectively).

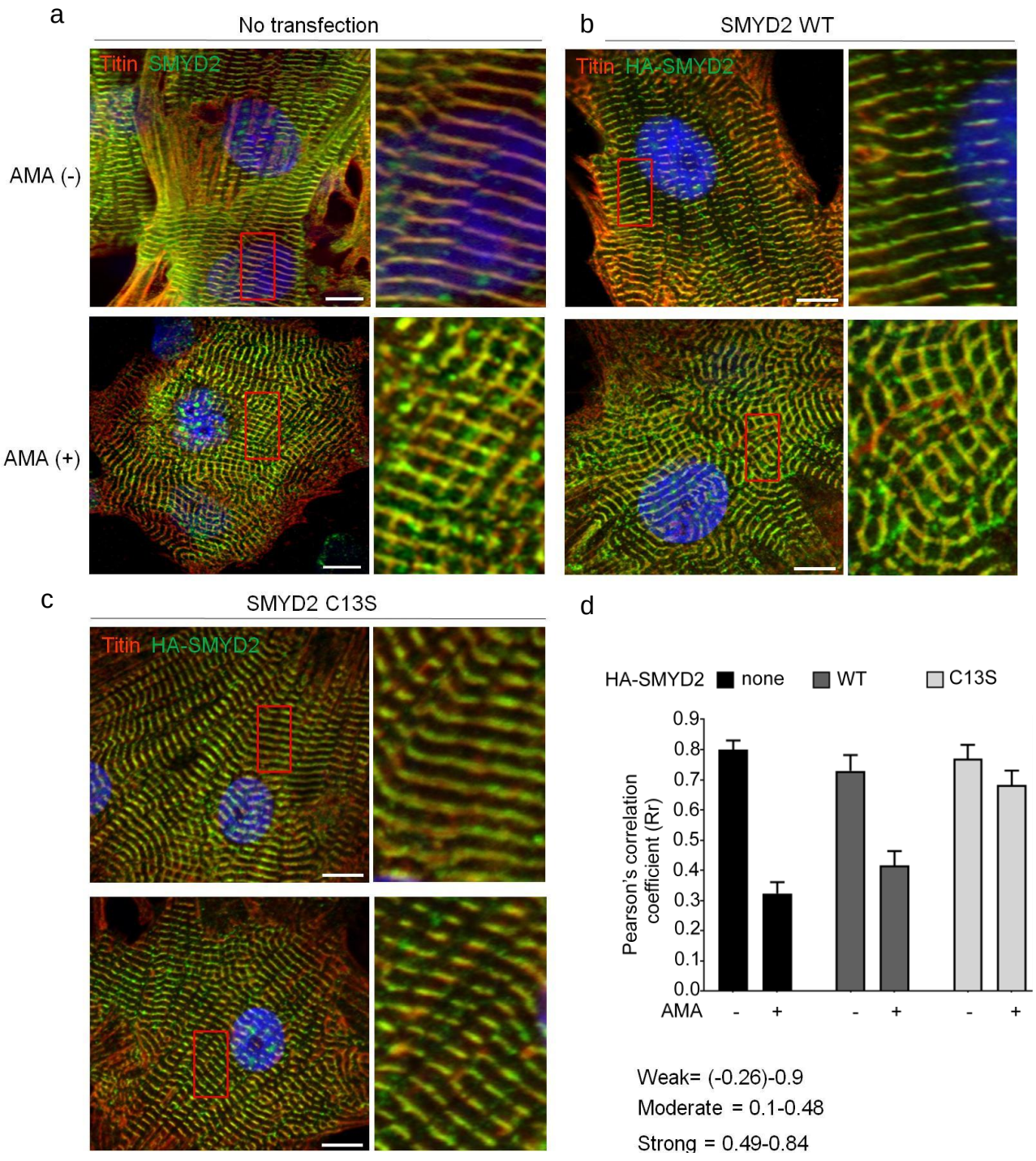

Figure 3.31. Co-localization of titin and SMYD2 decreases upon incubation of AMA in rat neonatal cardiomyocytes expressing SMYD2 WT versus C13S. (**a-c**)Immunostainings of cardiomyocytes with antibodies to titin (α-titin-NT, red), HA, or

SMYD2 (green) are shown with enlarged areas for details (the red boxes). (**d**)Pearson's correlation coefficients were calculated to estimate co-localization of titin and SMYD2. Images represent the major co-localization pattern in individual experiments. Scale bars, 10 µm. Results represent the mean ± SD, (n = 3). Two-tailed Student's unpaired t-test with Welch's correction, *p < 0.05.

Taken together, these data provide evidence that SMYD2 Cys13 glutathionylation disrupts the SMYD2 interaction with Hsp90 and N2A of titin, and induces dissociation of SMYD2 from titin and the sarcomere.

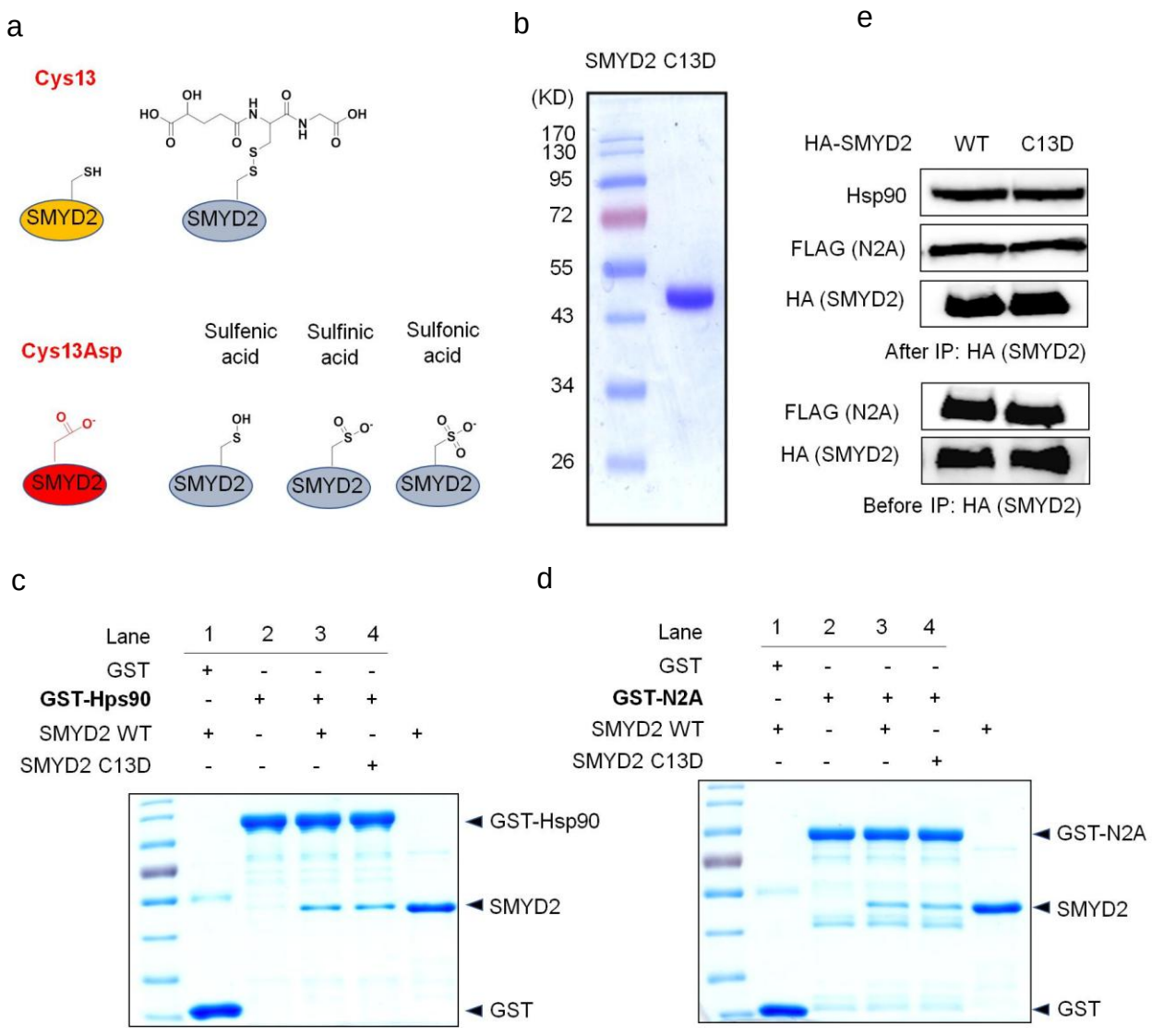

Figure 3.32. SMYD2 C13D mutation retains the interaction with Hsp90 and N2A. (**a**) A rationale for expressing SMYD2 C13D: The size and charge of Asp are similar to ones of oxidative cysteine modifications, such as sulfinic acid. (**b**) Gel analysis of SMYD2 C13D after purification. (**c**-**d**) Purified SMYD2 WT and C13D were incubated with GST-Hsp90 (**c**) or GST-N2A (**d**) bound to glutathione beads, and eluted samples were analyzed by Coomassie stains. (**e**) SMYD2 C13D mutant retains the interaction with Hsp90 and N2A. Hsp90 or FLAG-N2A was co-immunoprecipitated with SMYD2 WT or C13D from HEK293 cells.

3.19 SMYD2 C13D mutation doesn't affect its HSP90 or N2A interactions

In addition to glutathionylation, cysteine oxidation in proteins involves formation of sulfenic acid, sulfinic acid, and sulfonic acid, which are relatively smaller size modifications in comparison to glutathionylation (Figure 3.32a). Although we did not detect sulfonic acid formation in SMYD2, we examined potential effects of these oxidations on the interaction of SMYD2 with Hsp90 and N2A. To mimic a small size oxidative modification in SMYD2 at Cys13, we expressed SMYD2 C13D in which Asp serves as a close mimic of sulfinic acid at Cys13 with respect to both size and charge (Figure 3.32a).

In vitro binding assays showed that similar levels of SMYD2 WT and C13D were bound to Hsp90 and N2A (Figure 3.32c and d). Co-IP experiments confirmed these results, showing that SMYD2 WT and C13D maintain the similar level of binding with both Hsp90 and N2A (Figure 3.32e). These data suggest that glutathionylation of SMYD2, rather than small size oxidative modifications, is likely responsible for disrupting SMYD2 interactions with Hsp90 and N2A.

3.20 Dissociation between SMYD2 and N2A leads to degradation of sarcomeric proteins

3.20.1 SMYD2 C13S protects N2A from MMP-2 mediated degradation

Next, we attempted to examine whether the dissociation between SMYD2 and N2A is responsible for sarcomere degradation. We hypothesized that the N2A domain or its proximal region in titin may contain the cleavage sites of MMP-2 or calpain-1, which could be protected when SMYD2 binds to N2A, whereas the SMYD2-N2A dissociation may expose N2A for degradation.

a

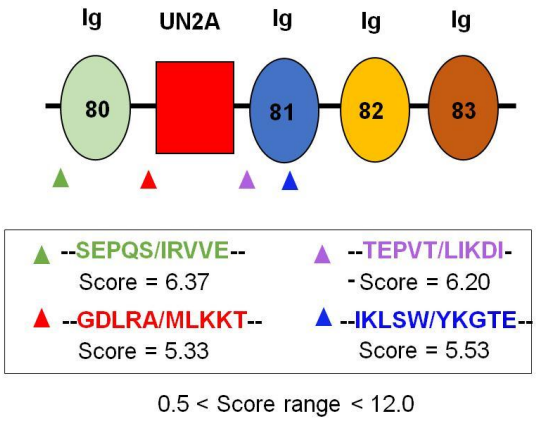

b

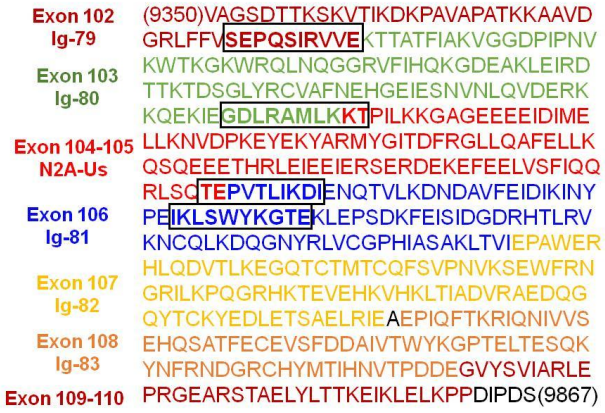

c

Predicted MMP2 cleavage sites in N2A domain

	P1	Cleaved-seq	Score	N-mass	C-mass
	23	VAPAT-KKAAV	1.97	2284.25	57189.62
▲	40	SEPQS-IRVVE	6.37	4144.23	55329.64
▲	137	GDLRA-MLKKT	5.33	15154.93	44318.94
	159	IDIME-LLKNV	1.62	17638.18	41835.69
	183	TDFRG-LLQAF	2.22	20525.61	38948.26
	222	EELVS-FIQQR	3.28	25294.91	34178.96
▲	235	TEPVT-LIKDI	6.2	26822.71	32651.16
▲	268	IKLSW-YKGTE	5.53	30720.73	28753.14
	325	IEPAW-ERHLQ	2.9	37168.98	22304.89
	378	HKVHK-LTIAD	1.25	43420.13	16053.74
	383	LTIAD-VRAED	2.34	43933.41	15540.46
	404	ETSAE-LRIEA	1.54	46349.45	13124.42
	413	AEPIQ-FTKRI	2.91	47399.02	12074.85
	420	KRIQN-IVVSE	2.5	48286.51	11187.36
	444	AIVTW-YKGPT	2.21	50979.75	8494.12
	450	KGPTE-LTESQ	4.91	51655.06	7818.81
	498	RSTAE-LYLTT	1.44	57161.64	2312.23

Fragment sizes

(4KD and 55 KD)
(15KD and 45 KD)

(27KD and 33 KD)
(31KD and 29 KD)

d

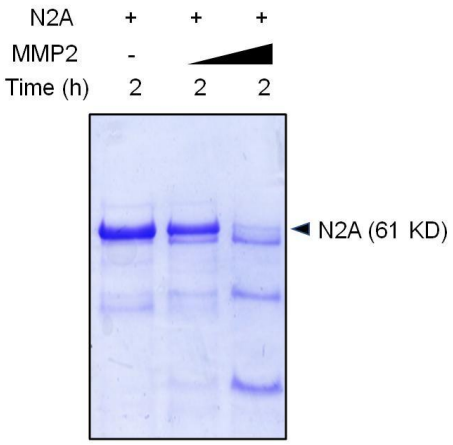

Figure 3.32. Predicted N2A cleavage sites by MMP2 protease. The potential cleavage site(s) were predicted by using the MMP cleavage site prediction tool (CleavPredict). (**a**) N2A sub-domains (I80-UN2A-I81-I82-I83, Ig: Immunoglobulin domain; UN2A: a unique sequence in N2A) with potential cleavage sites that have a high score of probability. The potential cleavage sequences are shown with their positions in N2A indicated by arrow head. (**b**) The peptide sequence of N2A. N2A sub-domains are shown in different colors, and the MMP-2 cleavage sites with a high score are shown in box. (**c**) The potential MMP2 cleavage site with different scores and the resulting mass after cleavage. These are results from the MMP cleavage site prediction tool (CleavPredict). (**d**) Gel analysis of N2A degradation upon incubation of MMP-2 with an increasing amount of MMP-2. The blot is a representative of at least three replicates.

Notably, several domains of titin in the I-band of sarcomere, which can be unfolded during contraction and relaxation, were suggested to contain MMP-2 cleavage sites. However, it is unknown whether N2A contains the cleavage site. The N2A domain is composed of four immunoglobulin domains (Ig80-83) and a unique sequence region, called N2A-Us (also called UN2A), between Ig80 and Ig81 (Figure 3.32a).

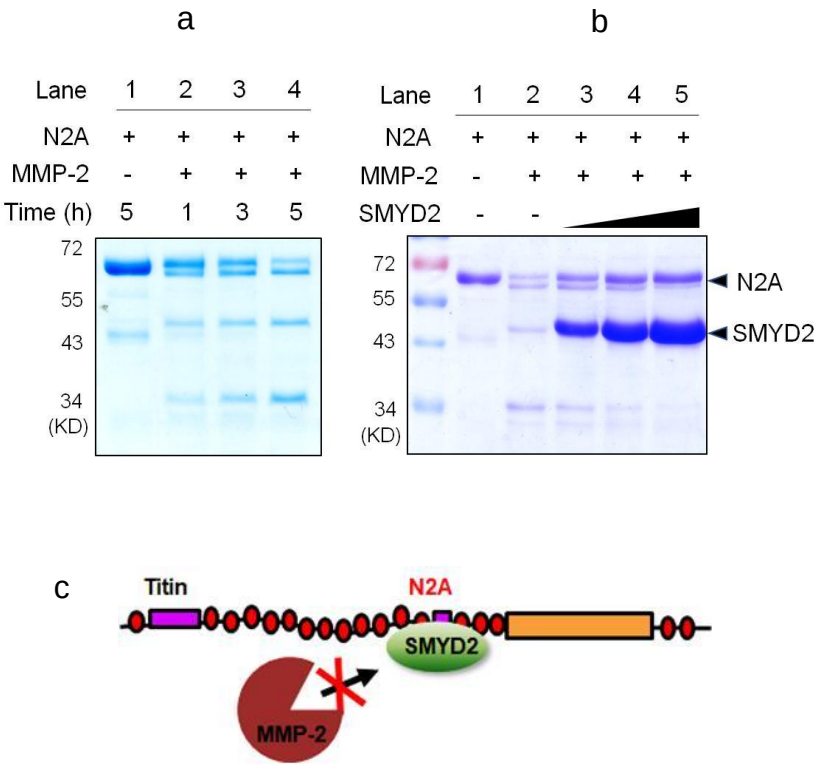

Figure 3.33. Dissociation between SMYD2 and N2A leads to degradation of sarcomeric proteins by MMP-2. N2A is degraded by MMP-2, and SMYD2 protects

N2A from degradation. Purified N2A was incubated with active MMP-2 in (**a**)a time-dependent manner or (**b**) with an increasing amount of SMYD2 . (**c**) Binding of SMYD2 protects the N2A domain from MMP-2 degradtion.

We analyzed whether N2A contains the MMP-2 cleavage site by using the MMP cleavage site prediction tool (CleavPredict). The tool predicted the presence of several MMP-2 cleavage sequences in N2A, including high probability of cleavage sites around N2A-Us (Figure 3.32b and c).

a

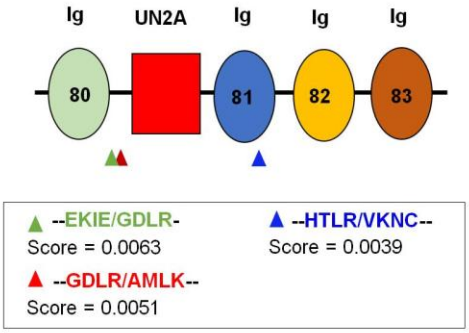

b

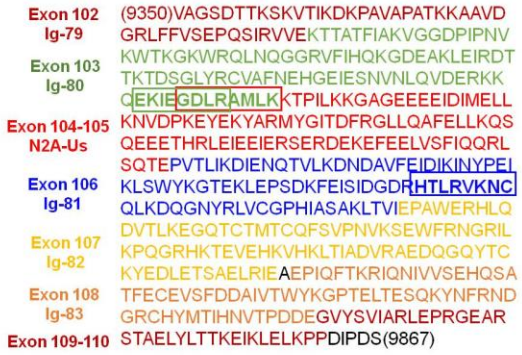

c

Predicted calpain cleavage sites in N2A domain

	P1	Cleaved-seq	Score	Fragment sizes
	146	PILK-KGAG	0.0067	
	24	PATK-KAAV	0.0067	
	56	AKVG-GDPI	0.0065	
▲	132	EKIE-GDLR	0.0063	(16KD and 45 KD)
▲	136	GDLR-AMLK	0.0051	(16KD and 45 KD)
	385	ADVR-AEDQ	0.0049	
▲	293	HTLR-VKNC	0.0039	(26KD and 35 KD)

d

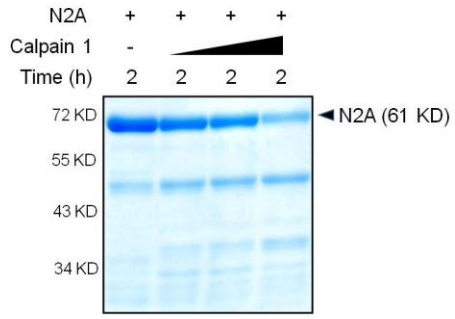

e

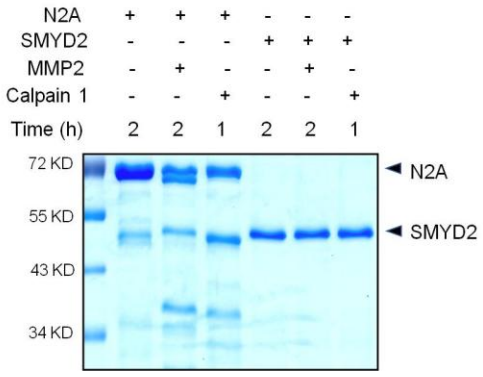

Figure 3.34. Predicted N2A cleavage sites by calpain 1. The potential cleavage site(s) were predicted by using the calpain cleavage site prediction tool (LabCas). (**a**) N2A sub-domains (I80-UN2A-I81-I82-I83, Ig: Immunoglobulin domain; UN2A: a unique sequence in N2A) with potential cleavage sites that have a high score of probability. The potential cleavage sequences are shown with their positions in N2A indicated by arrow head. (**b**) The peptide sequence of N2A. N2A sub-domains are shown in different colors, and the relevant calpain 1 cleavage sites are shown in a box. (**c**) The potential calpain 1 cleavage site with different scores and the resulting mass after cleavage. (**d**) Gel analysis of N2A degradation upon incubation of calpain 1 with an increasing amount of calpain 1. (**e**) Gel analysis of N2A degradation by MMP-2 or calpain 1 in the same gel, which shows the similar size of cleaved products. SMYD2 is not degraded by MMP-2 or calpain 1. Blots are representative of at least three replicates.

Indeed, purified N2A was cleaved upon incubation with active MMP-2 (Figure 3.32d and 3.33a). The sizes of the cleaved products (~approximately 50kD and 35kD) appear to correlate with the potential cleavage in domains around N2A-Us. Notably, addition of SMYD2 C13S, which binds to the N2A domain, decreased degradation of N2A by MMP-2 in a dose-dependent manner (Figure 3.33b).

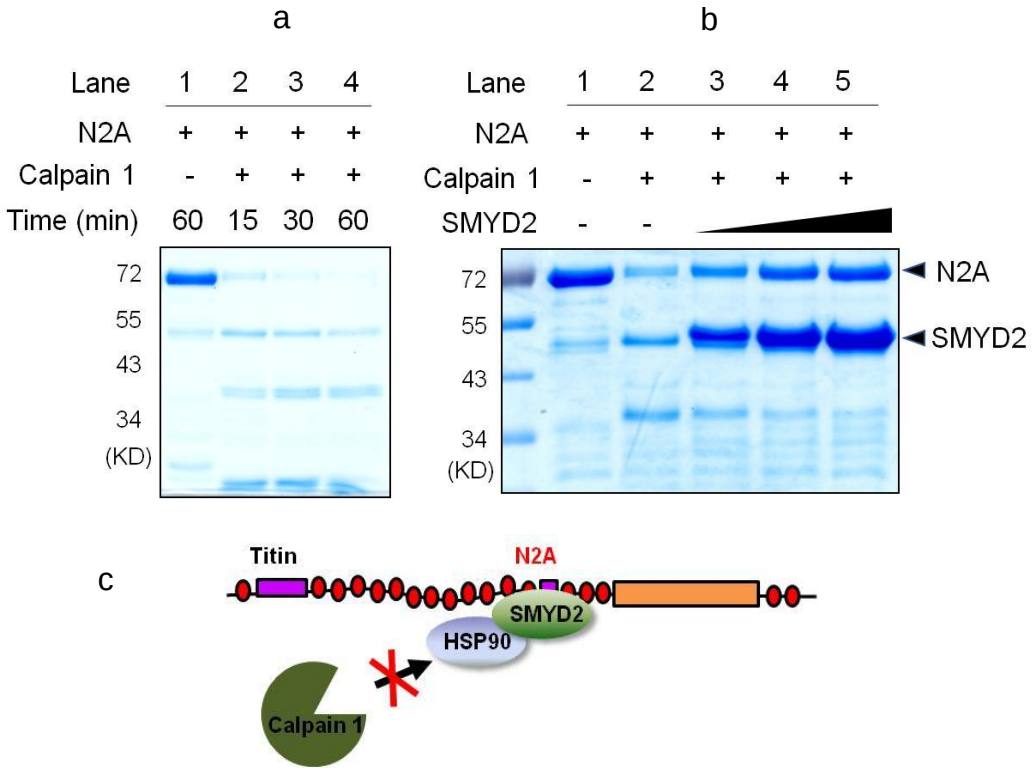

Figure 3.35. Dissociation between SMYD2 and N2A leads to degradation of sarcomeric proteins by calpain1. N2A is degraded by calpain 1, and SMYD2 protects N2A from degradation. Purified N2A was incubated with calpain 1 in (**a**) a time-dependent manner or (**b**) with an increasing amount of SMYD2. (**c**) Binding of SMYD2 protects the N2A domain from MMP-2 degradtion. Data are representative of at least 4 independent experiments.

3.20.2 SMYD2 C13S protects N2A from calpain 1 mediated degradation

Similarly, N2A was predicted to have the calpain 1 cleavage site (Figure 3.34a, b and c). N2A was also susceptible to degradation by calpain 1 (Figure 3.34d and Figure 3.35a). Incubation with SMYD2 C13S protected N2A degradation from calpain 1 (Figure 3.35b). Interestingly, both MMP-2 and calpain 1 resulted in cleaved products of N2A that are of similar sizes (Figure 3.35e), suggesting that N2A has a local motif vulnerable to degradation by both proteases.

3.20.3 SMYD2 C13S protects titin in myofibrils from MMP-2 mediated degradation

To further support our hypothesis, we performed the similar experiments in which N2A was replaced by myofibrils isolated from mouse gastrocnemius muscle that has an N2A-titin isoform (Figure 3.36a). Incubation of fresh myofibrils with active MMP-2 induced degradation of titin, decreasing the level of N2A-titin (T1) while increasing the level of T2 (Figure 3.36b), a degraded product of titin[165] (Figure 3.36c, lane 2 vs. 3, and 34d). Notably, incubation of SMYD2 protected titin from MMP-2 mediated degradation (Figure 3.36c, lane 3 vs. 4, and 34d). Titin degradation was also inhibited upon an addition of ARP-100 (Figure 3.36c, lane 3 vs. 5, and 34d). In these experiments, there was no apparent degradation of MHC (Figure 3.36c). These data support our model that the SMYD2 binding interaction with N2A, titin, or sarcomeric proteins confers the

protection against proteases, whereas SMYD2 dissociation upon glutathionylation contributes to degradation of sarcomeric proteins (Figure 4.1)

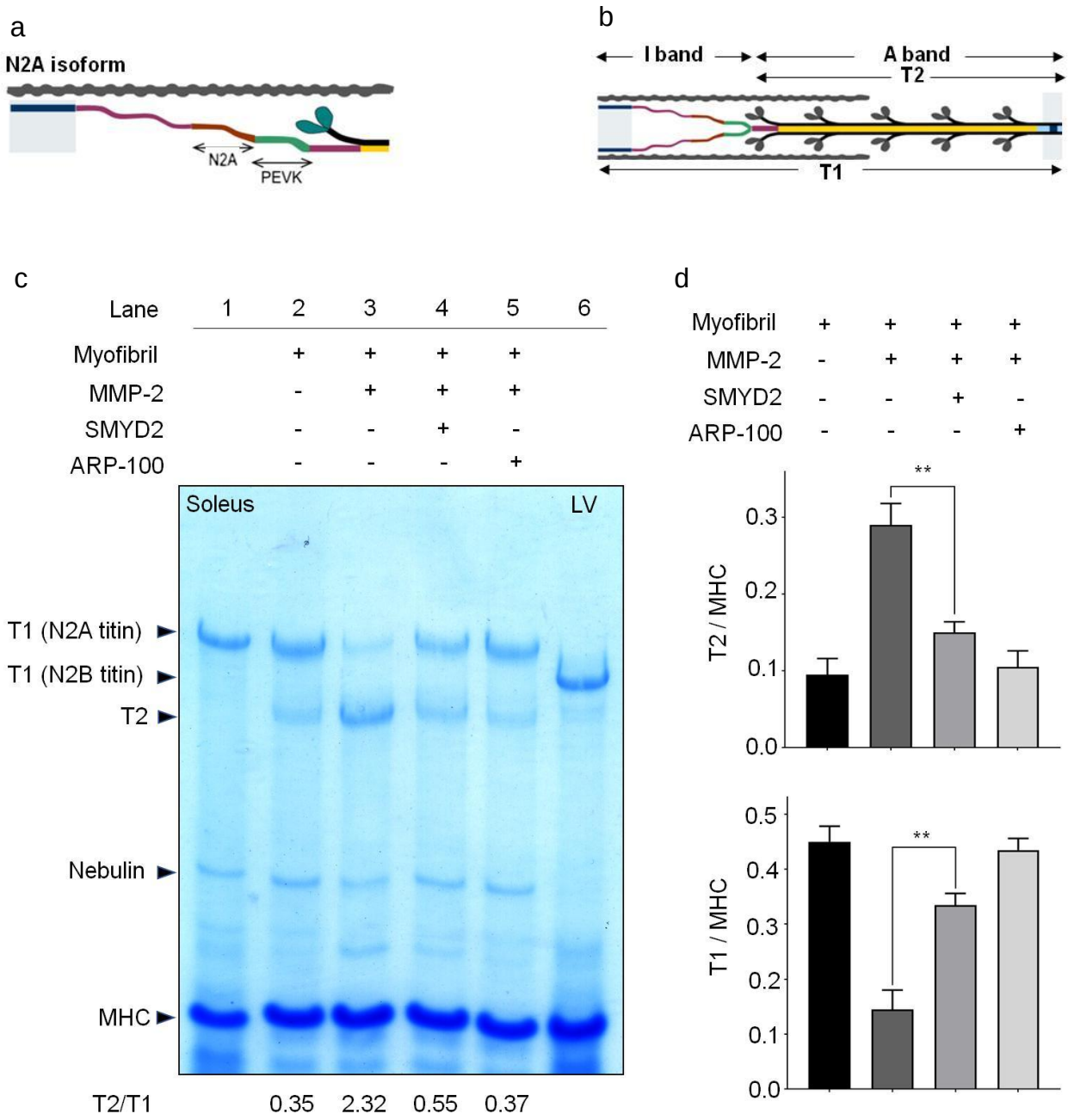

Figure 3.36. Titin in isolated myofibrils is degraded by MMP-2, and SMYD2 protects titin from degradation. (**a**) Titin N2A isoform (**b**) Titin degradation product T2. (**c**) Myofibrils isolated from mouse gastrocnemius muscle were incubated with active MMP-2 in the absence and presence of SMYD2. Extracts of soleus muscle and left

ventricle (LV) isolated from 6.5-months old rat were used as standards (lane 1 and lane 6) to show the position of N2A-titin or N2B-titin isoforms, respectively. (**d**) Levels of titin degradation by measuring the ratio of T1 or T2 to MHC. Results represent the mean ± SD, (n = 3). Two-tailed Student's unpaired t-test with Welch's correction, *$p < 0.05$

CHAPTER 4: DISCUSSION

The detrimental role of ROS in cardiac muscle has been extensively analyzed in ischemia-reperfusion injuries that are well-known to cause a burst of mitochondrial ROS and contribute to muscle damage.[178] One direct effect of ROS in muscle is the reduction of myofilament contraction, which is attributed to alteration in calcium transient, reduced calcium sensitivity of myofilament, or reduced maximal peak force of myofilament contraction.[143-145] Many of these ROS effects partially result from oxidative modifications of sarcomeric or myofibrillar proteins.[138, 140, 141, 179, 180] For example, ROS elevated during ischemic reperfusion cause glutathionylation and carbonylation of actin,[138] glutathionylation of troponin subunits,[139] and disulfide formation in tropomyosin,[140] nitration of myosin,[141] many of which result in the reduced contractile force of myofilaments. Titin is also oxidized in multiple regions. For example, the N2B domain of titin forms disulfide, which increases muscle stiffness.[142] The cryptic cysteine residues in Ig-domains of titin at the I-band are also glutathionylated, which reduces passive stiffness.[123] The detrimental role of ROS in cardiac muscle has been extensively analyzed in ischemia-reperfusion injuries that are well-known to cause a burst of mitochondrial ROS and contribute to muscle damage.[178] One direct effect of ROS in muscle is the reduction of myofilament contraction, which is attributed to alteration in calcium transient, reduced calcium sensitivity of myofilament, or reduced maximal peak force of myofilament contraction.[143-145] Many of these ROS effects partially result from oxidative modifications of sarcomeric or myofibrillar proteins.

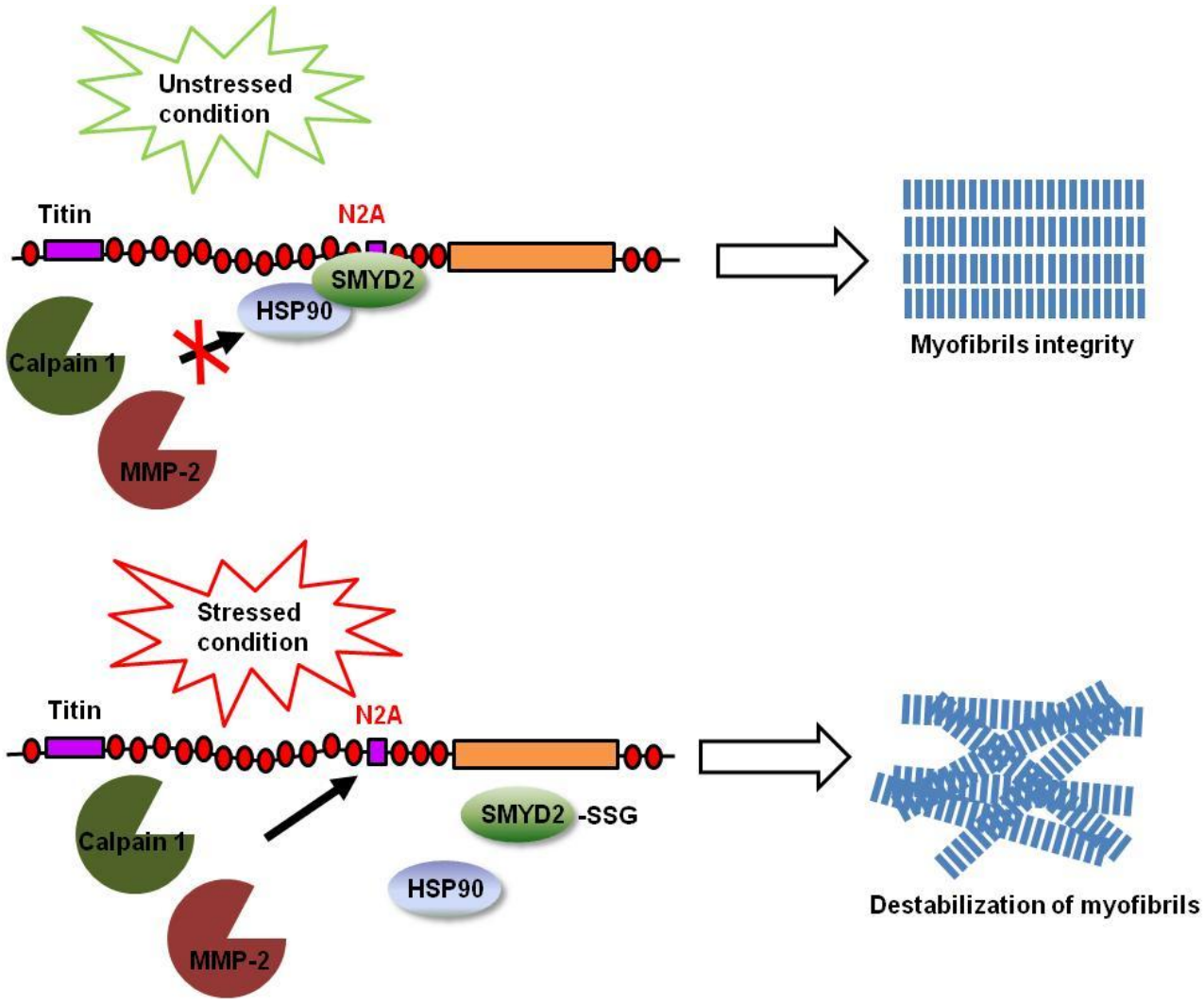

Figure 4.1. A proposed mechanism of sarcomere destabilization upon SMYD2 glutathionylation. Under unstressed conditions, SMYD2-Hsp90 binds with and protects N2A in titin from MMP2 or calpain 1 mediated degradation (top). Under stressed conditions, SMYD2 is glutathionylated and dissociated from N2A or titin, allowing for sarcomeric protein degradation (bottom).

For example, ROS elevated during ischemic reperfusion cause glutathionylation and carbonylation of actin,[138] glutathionylation of troponin subunits,[139] and disulfide formation in tropomyosin,[140] nitration of myosin,[141] many of which result in the reduced contractile force of myofilaments. Titin is also oxidized in multiple regions. For example,

the N2B domain of titin forms disulfide, which increases muscle stiffness.[142] The cryptic cysteine residues in Ig-domains of titin at the I-band are also glutathionylated, which reduces passive stiffness.[123]

In addition to reduction of myofilament contraction, numerous data support that cellular stress during ischemic-reperfusion or nutrient starvation causes proteolysis of sarcomeric and myofibrillar proteins,[181, 182] which eventually causes reduced muscle mass and a loss of contractility. There is emerging evidence that the highly ordered structure of sarcomere is maintained in a dynamic process that involves an intricate balance between assembly and degradation of sarcomeric proteins by the action of many chaperones and proteases.[183] While proteolytic systems, including the ubiquitin-proteasome system (UPS) and calpains, are largely responsible for sarcomeric and myofibrillar protein degradation,[183] the molecular link between sarcomeric protein oxidative modification and the action of the protease system is not well-characterized. In this report, we showed that glutathionylation of sarcomere-associated SMYD2 serves as a potential mechanism of ROS that contributes to degradation of sarcomeric proteins.

Glutathionylation plays an important role in regulating protein function in cellular stress.[127] In this report, we used our clickable glutathione approach to detect glutathionylation of multiple proteins, including SMYD2, under stressed conditions. A key idea of our approach is routing glutathione biosynthesis to clickable glutathione by using a mutant of a glutathione biosynthetic enzyme.[147] An azide-tag on glutathione can be replaced by other bioorthogonal functional groups, including terminal-alkene.[129] A modified clickable glutathione is an efficient substrate of glutathione disulfide reductase (GR) (Figure 3.2), glutaredoxin 1 (Grx1) (Figure 3.3), glutathione transferase omega

(GSTO) (Figure 3.4), and is tolerated in cells without significant disturbance of the redox system (Figure 3.5),[129, 148] all of which support that our approach is suitable for investigating glutathionylation in response to cellular stress.

We confirmed glutathionylation of SMYD2 in various stressed conditions (Figure 3.7) and found selective glutathionylation at Cys13 (Figure 3.10, 3.11, 3.12 and 3.14). While there are 17 Cys residues in SMYD2, many of them are bound to zinc atoms or buried inside SMYD2, thus may not be accessible for glutathionylation. In our experiments, we did not detect sulfonic acid formation in SMYD2 (Figure 3.8). However, other oxoforms, such as sulfenic acid, may form. It is also possible to form Cys modifications with other electrophiles, such as 4-hydroxynonenal[184] and fumarate,[185] which may induce a similar cellular phenotype to glutathionylation, due to their relatively large size.

A key observation in our report is that myofibril integrity is significantly lost in cells expressing SMYD2 WT in response to ROS, whereas SMYD2 C13S protects myofibrils from degradation (Figure 3.19 and 3.20), showing a critical role of SMYD2 glutathionylation in myofibril integrity or sarcomere stability. While our data may suggest a pathologic consequence of SMYD2 glutathionylation in muscle, sarcomere degradation or disassembly is not only found in pathologic conditions, such as cardiomyopathy[186] and chronic hibernating cardiomyocytes.[187] Sarcomere degradation is also observed in physiologic processes during muscle growth or remodeling that requires a partial degradation of sarcomeres or myofibrils in order to form a higher mass of muscle.[188] Indeed, the beneficial role of sarcomere proteolysis is well-recognized in skeletal muscle growth and stress adaptation.[188] It is notable that SMYD2 expression is

peaked in fetus and neonates, but reduced in adult mice.[175] In addition, during fetal and neonatal periods, N2BA titin that contains N2A is abundant in cardiomyocytes, while it decreases in adult cardiomyocytes.[189] Therefore, it is interesting to correlate that both N2BA titin and SMYD2, which are implicated in sarcomere degradation in our study, are abundant in fetal and neonatal cardiomyocytes in which sarcomeres are more dynamic during developmental growth and remodeling.[190] More importantly, N2BA titin and fetal genes increase in cardiac diseases,[191, 192] while SMYD2 expression may be induced under stress.[193] Therefore, it will be interesting to investigate SMYD2 expression and its glutathionylation in pathological conditions in future studies.

Another important finding is that protein interaction between SMYD2 and the N2A domain of titin contributes to modulating myofibril or sarcomere degradation (Figure 3.21 and 3.22). Indeed, protein-protein interactions at titin's extensible domains, including N2B, PEVK, and N2A at the I-band, plays a central role in stress-signaling.[149] For example, the N2B domain has four Ig-domains and one extensible unique sequence region (N2B-Us). A small chaperone, αB-crystallin, binds to N2B-Us for stabilization or protection of sarcomere from stress.[150] N2B-Us also interacts with signaling complexes, including four-and-a-half-LIM-domain protein (FHL2) that can translocate to the nucleus to participate in gene expression.[149] Similarly, N2A has four Ig-domains and one extensible unique sequence (N2A-Us). Hsp90-SMYD2 chaperone complex binds to N2A, mainly with N2A-Us.[176] Our data showed that the SMYD2-N2A interaction protects N2A from degradation by MMP-2 and calpain 1 (Figure 3.34 and 3.35), and SMYD2 also protect titin in myofibrils from MMP-2 mediated cleavage (Figure 3.36). Therefore, our data support the concept that N2A is an important domain of titin where the SMYD2-

Hsp90 chaperone complex interacts for stabilization or protection of sarcomeres (Figure 3.31). Notably, it is interesting to find that N2A can be cleaved by MMP-2 and calpain 1 in our data (Figure 3.34 and 3.35). While titin is known to be degraded by MMP-2 and calpain 1,[165, 194] the exact cleavage sites of titin are unknown and difficult to confirm due to a large size of titin (>3 MD). Our data suggest that titin can be cleaved at the N2A domain that interacts with SMYD2.

While our data support the importance of SMYD2-N2A dissociation for myofibril disassembly, the results may explain a part of the complex mechanisms by which SMYD2 glutathionylation contributes to sarcomere degradation. Notably, N2A-Us also interacts with CARP,[195] which acts as a transducer that translocate to the nucleus during mechanical stress and is upregulated in ischemic-reperfusion injury or nutrition starvation.[195] Our data showed that CARP is up-regulated under stress in cells with SMYD2 WT versus C13S (Figure 3.21), suggesting that SMYD2 glutathionylation is in part responsible for stabilization of CARP. Because CARP is implicated in activating or suppressing many fetal genes involved in muscle remodeling, it will be interesting to find which genes are modulated upon SMYD2 glutathionylation.

APPENDIX - COPYRIGHT PERMISSIONS

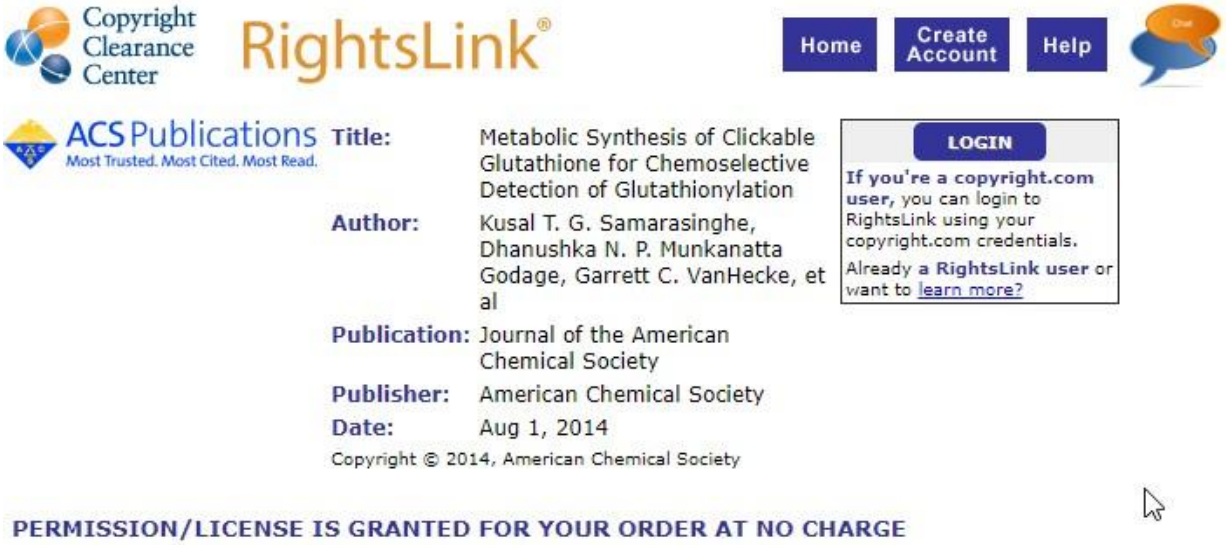

Copyright Clearance Center RightsLink®

Home | Create Account | Help

ACS Publications
Most Trusted. Most Cited. Most Read.

Title: Metabolic Synthesis of Clickable Glutathione for Chemoselective Detection of Glutathionylation

Author: Kusal T. G. Samarasinghe, Dhanushka N. P. Munkanatta Godage, Garrett C. VanHecke, et al

Publication: Journal of the American Chemical Society

Publisher: American Chemical Society

Date: Aug 1, 2014

Copyright © 2014, American Chemical Society

LOGIN

If you're a copyright.com user, you can login to RightsLink using your copyright.com credentials.

Already a RightsLink user or want to learn more?

PERMISSION/LICENSE IS GRANTED FOR YOUR ORDER AT NO CHARGE

This type of permission/license, instead of the standard Terms & Conditions, is sent to you because no fee is being charged for your order. Please note the following:

- Permission is granted for your request in both print and electronic formats, and translations.
- If figures and/or tables were requested, they may be adapted or used in part.
- Please print this page for your records and send a copy of it to your publisher/graduate school.
- Appropriate credit for the requested material should be given as follows: "Reprinted (adapted) with permission from (COMPLETE REFERENCE CITATION). Copyright (YEAR) American Chemical Society." Insert appropriate information in place of the capitalized words.
- One-time permission is granted only for the use specified in your request. No additional uses are granted (such as derivative works or other editions). For any other uses, please submit a new request.

Order Completed

Thank you for your order.

This Agreement between Wayne State University, Department of Chemistry -- Dhanushka Munkanatta Godage ("You") and Springer Nature ("Springer Nature") consists of your license details and the terms and conditions provided by Springer Nature and Copyright Clearance Center.

Your confirmation email will contain your order number for future reference.

printable details

License Number	4366300463726
License date	Jun 12, 2018
Licensed Content Publisher	Springer Nature
Licensed Content Publication	Nature Medicine
Licensed Content Title	Sudden Cardio Arrest: Oxidative stress irritates the heart
Licensed Content Author	Gordon F Tomaselli, Andreas S Barth
Licensed Content Date	Jun 1, 2010
Licensed Content Volume	16
Licensed Content Issue	6
Type of Use	Thesis/Dissertation
Requestor type	academic/university or research institute
Format	print and electronic
Portion	figures/tables/illustrations
Number of figures/tables/illustrations	1
High-res required	no
Will you be translating?	no
Circulation/distribution	<501
Author of this Springer Nature content	no
Title	FUNCTIONAL STUDY OF SMYD2 GLUTATHIONYLATION IN CARDIOMYOCYTES
Instructor name	Dr. YOUNG-HOON AHN
Institution name	Wayne State University, Department of Chemistry
Expected presentation date	Jul 2018
Portions	Figure 1
Requestor Location	Wayne State University, Department of Chemistry 5101, Cass ave, DETROIT, MI 48202 United States Attn: Dhanushka Nalin Munkanatta Godage
Billing Type	Invoice
Billing address	Wayne State University, Department of Chemistry 5101, Cass ave, DETROIT, MI 48202 United States Attn: Dhanushka Nalin Munkanatta Godage
Total	0.00 USD

Arquivos Brasileiros de Cardiologia
Print version ISSN 0066-782X

Arq. Bras. Cardiol. vol.96 no.4 São Paulo Apr. 2011 Epub Feb 25, 2011

http://dx.doi.org/10.1590/S0066-782X2011005000023

The role of titin in the modulation of cardiac function and its pathophysiological implications

Ricardo Castro-Ferreira; Ricardo Fontes-Carvalho; Inês Falcão-Pires; Adelino F. Leite-Moreira

Serviço de Fisiologia Faculdade de Medicina da Universidade do Porto, Portugal

Mailing address

ABSTRACT

Titin is a giant sarcomeric protein that extends from the Z-line to the M-line. Due to its location, it represents an important biomechanical sensor, which has a crucial role in the maintenance of the sarcomere structural integrity. Titin works as a "bidireactional spring" that regulates the sarcomeric length and performs adequate adjustments of passive tension whenever the length varies. Therefore, it determines not only ventricular rigidity and diastolic function, but also systolic cardiac function, modulating the Frank-Starling mechanism.

The myocardium expresses two isoforms of this macromolecule: the N2B, more rigid and the isoform N2BA, more compliant. The alterations in the relative expression of the two titin isoforms or alterations in their state of phosphorylation have been implicated in the pathophysiology of several diseases, such as diastolic heart failure, dilated cardiomyopathy, ischemic cardiomyopathy and aortic stenosis.

The aim of this study is to describe, in brief, the structure and location of titin, its association with different cardiomyopathies and understand how alterations in this macromolecule influence the pathophysiology of diastolic heart failure, emphasizing the therapeutic potential of the manipulation of this macromolecule.

Keywords: Protein isoforms; atrial myosins; heart failure; cardiomyopathy, dilated.

Mailing address:
Ricardo Luis Castro Silva Ferreira
Serviço de Fisiologia, Faculdade de Medicina da Universidade do Porto
Alameda Prof. Hernâni Monteiro - 4200-219 - Porto
E-mail: amoreira@med.up.pt

Manuscript received September 16, 2009; revised manuscript received November 05, 2009; accepted January 26, 2010.

Order Completed

Thank you for your order.

This Agreement between Wayne State University, Department of Chemistry -- Dhanushka Munkanatta Godage ("You") and Elsevier ("Elsevier") consists of your license details and the terms and conditions provided by Elsevier and Copyright Clearance Center.

Your confirmation email will contain your order number for future reference.

printable details

License Number	4366541128054
License date	Jun 12, 2018
Licensed Content Publisher	Elsevier
Licensed Content Publication	Elsevier Books
Licensed Content Title	Advances in Protein Chemistry
Licensed Content Author	Henk L. Granzier,Siegfried Labeit
Licensed Content Date	Jan 1, 2005
Licensed Content Pages	31
Type of Use	reuse in a thesis/dissertation
Portion	figures/tables/illustrations
Number of figures/tables/illustrations	1
Format	both print and electronic
Are you the author of this Elsevier chapter?	No
Will you be translating?	No
Original figure numbers	1
Title of your thesis/dissertation	FUNCTIONAL STUDY OF SMYD2 GLUTATHIONYLATION IN CARDIOMYOCYTES
Publisher of new work	Wayne State University, Department of Chemistry
Author of new work	Dr. YOUNG-HOON AHN
Expected completion date	Jul 2018
Estimated size (number of pages)	1
Requestor Location	Wayne State University, Department of Chemistry 5101, Cass ave, DETROIT, MI 48202 United States Attn: Dhanushka Nalin Munkanatta Godage
Publisher Tax ID	98-0397604
Total	0.00 USD

Int. J. Mol. Sci. **2015**, *16*(1), 1406-1428; https://doi.org/10.3390/ijms16011406 Open Access Review

Structure and Function of SET and MYND Domain-Containing Proteins

Nicholas Spellmon [1], **Joshua Holcomb** [1], **Laura Trescott** [1], **Nualpun Sirinupong** [2] and **Zhe Yang** [1,*]

[1] Department of Biochemistry and Molecular Biology, Wayne State University School of Medicine, 540 East Canfield Street, Detroit, MI 48201, USA

[2] Nutraceuticals and Functional Food Research and Development Center, Prince of Songkla University, Hat-Yai, Songkhla 90112, Thailand

[*] Author to whom correspondence should be addressed.

Academic Editor: Charles A. Collyer

Received: 5 December 2014 / Accepted: 5 January 2015 / Published: 8 January 2015

(This article belongs to the Special Issue Protein Crystallography in Molecular Biology 2015)

Abstract

SET (Suppressor of variegation, Enhancer of Zeste, Trithorax) and MYND (Myeloid-Nervy-DEAF1) domain-containing proteins (SMYD) have been found to methylate a variety of histone and non-histone targets which contribute to their various roles in cell regulation including chromatin remodeling, transcription, signal transduction, and cell cycle control. During early development, SMYD proteins are believed to act as an epigenetic regulator for myogenesis and cardiomyocyte differentiation as they are abundantly expressed in cardiac and skeletal muscle. SMYD proteins are also of therapeutic interest due to the growing list of carcinomas and cardiovascular diseases linked to SMYD overexpression or dysfunction making them a putative target for drug intervention. This review will examine the biological relevance and gather all of the current structural data of SMYD proteins. View Full-Text

Keywords: SMYD (SET and MYND domain-containing proteins); structure and function; SET (Suppressor of variegation, Enhancer of Zeste, Trithorax); MYND (Myeloid-Nervy-DEAF1)

▼ Figures

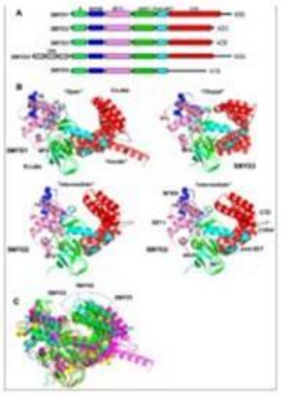

Figure 1

Order Completed

Thank you for your order.

This Agreement between Wayne State University, Department of Chemistry -- Dhanushka Munkanatta Godage ("You") and Springer Nature ("Springer Nature") consists of your license details and the terms and conditions provided by Springer Nature and Copyright Clearance Center.

Your confirmation email will contain your order number for future reference.

printable details

License Number	4366550370250
License date	Jun 12, 2018
Licensed Content Publisher	Springer Nature
Licensed Content Publication	Cellular and Molecular Life Sciences
Licensed Content Title	α-Actinin structure and regulation
Licensed Content Author	B. Sjöblom, A. Salmazo, K. Djinović-Carugo
Licensed Content Date	Jan 1, 2008
Licensed Content Volume	65
Licensed Content Issue	17
Type of Use	Thesis/Dissertation
Requestor type	academic/university or research institute
Format	print and electronic
Portion	figures/tables/illustrations
Number of figures/tables/illustrations	1
Will you be translating?	no
Circulation/distribution	<501
Author of this Springer Nature content	no
Title	FUNCTIONAL STUDY OF SMYD2 GLUTATHIONYLATION IN CARDIOMYOCYTES
Instructor name	Dr. YOUNG-HOON AHN
Institution name	Wayne State University, Department of Chemistry
Expected presentation date	Jul 2018
Portions	1
Requestor Location	Wayne State University, Department of Chemistry 5101, Cass ave, DETROIT, MI 48202 United States Attn: Dhanushka Nalin Munkanatta Godage
Billing Type	Invoice
Billing address	Wayne State University, Department of Chemistry 5101, Cass ave, DETROIT, MI 48202 United States Attn: Dhanushka Nalin Munkanatta Godage
Total	0.00 USD

Title: Exercise-Induced Cardiac Troponin Elevation Evidence, Mechanisms, and Implications
Author: Rob Shave,Aaron Baggish,Keith George,Malissa Wood,Jurgen Scharhag,Gregory Whyte,David Gaze,Paul D. Thompson
Publication: Journal of the American College of Cardiology
Publisher: Elsevier
Date: 13 July 2010

Order Completed

Thank you for your order.

This Agreement between Wayne State University, Department of Chemistry -- Dhanushka Munkanatta Godage ("You") and Elsevier ("Elsevier") consists of your license details and the terms and conditions provided by Elsevier and Copyright Clearance Center.

Your confirmation email will contain your order number for future reference.

printable details

License Number	4366551192543
License date	Jun 12, 2018
Licensed Content Publisher	Elsevier
Licensed Content Publication	Journal of the American College of Cardiology
Licensed Content Title	Exercise-Induced Cardiac Troponin Elevation Evidence, Mechanisms, and Implications
Licensed Content Author	Rob Shave,Aaron Baggish,Keith George,Malissa Wood,Jurgen Scharhag,Gregory Whyte,David Gaze,Paul D. Thompson
Licensed Content Date	Jul 13, 2010
Licensed Content Volume	56
Licensed Content Issue	3
Licensed Content Pages	8
Type of Use	reuse in a thesis/dissertation
Portion	figures/tables/illustrations
Number of figures/tables/illustrations	1
Format	both print and electronic
Are you the author of this Elsevier article?	No
Will you be translating?	No
Original figure numbers	1
Title of your thesis/dissertation	FUNCTIONAL STUDY OF SMYD2 GLUTATHIONYLATION IN CARDIOMYOCYTES
Publisher of new work	Wayne State University, Department of Chemistry
Author of new work	Dr. YOUNG-HOON AHN
Expected completion date	Jul 2018
Estimated size (number of pages)	1
Requestor Location	Wayne State University, Department of Chemistry 5101, Cass ave, DETROIT, MI 48202 United States Attn: Dhanushka Nalin Munkanatta Godage
Publisher Tax ID	98-0397604
Total	0.00 USD

Keywords: cardiac ischemia-reperfusion, mitochondria, permeability transition pore, calcium, ROS, pH

Citation: Javadov S (2015) The calcium-ROS-pH triangle and mitochondrial permeability transition: challenges to mimic cardiac ischemia-reperfusion. *Front. Physiol.* **6**:83. doi: 10.3389/fphys.2015.00083

Received: 19 February 2015; **Accepted:** 03 March 2015;
Published: 18 March 2015.

Edited by:
Miguel A. Aon, Johns Hopkins University School of Medicine, USA

Reviewed by:
Paolo Bernardi, University of Padova, Italy
Elizabeth Ann Jonas, Yale University, USA

***Correspondence:** Sabzali Javadov, sabzali.javadov@upr.edu

Order Completed

Thank you for your order.

This Agreement between Wayne State University, Department of Chemistry -- Dhanushka Munkanatta Godage ("You") and Oxford University Press ("Oxford University Press") consists of your license details and the terms and conditions provided by Oxford University Press and Copyright Clearance Center.

Your confirmation email will contain your order number for future reference.

printable details

License Number	4366570818328
License date	Jun 12, 2018
Licensed Content Publisher	Oxford University Press
Licensed Content Publication	Cardiovascular Research
Licensed Content Title	Matrix metalloproteinase-2 and myocardial oxidative stress injury: beyond the matrix
Licensed Content Author	Kandasamy, Arulmozhi D.; Chow, Ava K.
Licensed Content Date	Aug 4, 2009
Licensed Content Volume	85
Licensed Content Issue	3
Type of Use	Thesis/Dissertation
Requestor type	Educational Institution/Non-commercial/ Not for-profit
Format	Print and electronic
Portion	Figure/table
Number of figures/tables	3
Will you be translating?	No
Title	FUNCTIONAL STUDY OF SMYD2 GLUTATHIONYLATION IN CARDIOMYOCYTES
Instructor name	Dr. YOUNG-HOON AHN
Institution name	Wayne State University, Department of Chemistry
Expected presentation date	Jul 2018
Portions	1,2 and 5
Requestor Location	Wayne State University, Department of Chemistry 5101, Cass ave, DETROIT, MI 48202 United States Attn: Dhanushka Nalin Munkanatta Godage
Publisher Tax ID	GB125506730
Billing Type	Invoice
Billing address	Wayne State University, Department of Chemistry 5101, Cass ave, DETROIT, MI 48202 United States Attn: Dhanushka Nalin Munkanatta Godage
Total	0.00 USD

Journal List › Cell J › v.13(2); Summer 2011 › PMC3584455

CELL JOURNAL (Yakhteh)
ROYAN INSTITUTE
Home | Submit a Manuscript | Alerts

Cell J. 2011 Summer; 13(2): 65–72.
Published online 2011 Aug 24.

PMCID: PMC3584455
PMID: 23507938

Role of Calpain in Apoptosis

Hamid Reza Momeni, Ph.D.*

Author information ► Article notes ► Copyright and License information ▼ Disclaimer

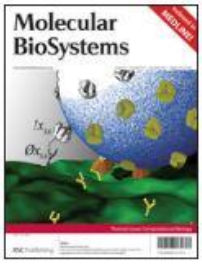

Title: A clickable glutathione approach for identification of protein glutathionylation in response to glucose metabolism
Author: Kusal T. G. Samarasinghe,Dhanushka N. P. Munkanatta Godage,Yani Zhou,Fidelis T. Ndombera,Eranthie Weerapana,Young-Hoon Ahn
Publication: Molecular BioSystems
Publisher: Royal Society of Chemistry
Date: May 10, 2016

Order Completed

Thank you for your order.

This Agreement between Wayne State University, Department of Chemistry -- Dhanushka Munkanatta Godage ("You") and Royal Society of Chemistry ("Royal Society of Chemistry") consists of your license details and the terms and conditions provided by Royal Society of Chemistry and Copyright Clearance Center.

Your confirmation email will contain your order number for future reference.

printable details

License Number	4366590301216
License date	Jun 12, 2018
Licensed Content Publisher	Royal Society of Chemistry
Licensed Content Publication	Molecular BioSystems
Licensed Content Title	A clickable glutathione approach for identification of protein glutathionylation in response to glucose metabolism
Licensed Content Author	Kusal T. G. Samarasinghe,Dhanushka N. P. Munkanatta Godage,Yani Zhou,Fidelis T. Ndombera,Eranthie Weerapana,Young-Hoon Ahn
Licensed Content Date	May 10, 2016
Licensed Content Volume	12
Licensed Content Issue	8
Type of Use	Thesis/Dissertation
Requestor type	academic/educational
Portion	figures/tables/images
Number of figures/tables/images	1
Distribution quantity	1
Format	print and electronic
Will you be translating?	no
Order reference number	
Title of the thesis/dissertation	FUNCTIONAL STUDY OF SMYD2 GLUTATHIONYLATION IN CARDIOMYOCYTES
Expected completion date	Jul 2018
Estimated size	1
Requestor Location	Wayne State University, Department of Chemistry 5101, Cass ave, DETROIT, MI 48202 United States Attn: Dhanushka Nalin Munkanatta Godage
Billing Type	Invoice
Billing address	Wayne State University, Department of Chemistry 5101, Cass ave, DETROIT, MI 48202 United States Attn: Dhanushka Nalin Munkanatta Godage
Total	0.00 USD

Order Completed

Thank you for your order.

This Agreement between Wayne State University, Department of Chemistry -- Dhanushka Munkanatta Godage ("You") and Springer Nature ("Springer Nature") consists of your license details and the terms and conditions provided by Springer Nature and Copyright Clearance Center.

Your confirmation email will contain your order number for future reference.

printable details

License Number	4366790286817
License date	Jun 12, 2018
Licensed Content Publisher	Springer Nature
Licensed Content Publication	Nature Medicine
Licensed Content Title	Sudden Cardio Arrest: Oxidative stress irritates the heart
Licensed Content Author	Gordon F Tomaselli, Andreas S Barth
Licensed Content Date	Jun 1, 2010
Licensed Content Volume	16
Licensed Content Issue	6
Type of Use	Thesis/Dissertation
Requestor type	academic/university or research institute
Format	print and electronic
Portion	figures/tables/illustrations
Number of figures/tables/illustrations	1
High-res required	no
Will you be translating?	no
Circulation/distribution	<501
Author of this Springer Nature content	no
Title	FUNCTIONAL STUDY OF SMYD2 GLUTATHIONYLATION IN CARDIOMYOCYTES
Instructor name	Dr. YOUNG-HOON AHN
Institution name	Wayne State University, Department of Chemistry
Expected presentation date	Jul 2018
Portions	1
Requestor Location	Wayne State University, Department of Chemistry 5101, Cass ave, DETROIT, MI 48202 United States Attn: Dhanushka Nalin Munkanatta Godage
Billing Type	Invoice
Billing address	Wayne State University, Department of Chemistry 5101, Cass ave, DETROIT, MI 48202 United States Attn: Dhanushka Nalin Munkanatta Godage
Total	0.00 USD

REFERENCE

1. Klein, L. & Hsia, H. Sudden cardiac death in heart failure. *Cardiology clinics* **32**, 135-144, ix (2014).
2. Tomaselli, G.F. & Zipes, D.P. What Causes Sudden Death in Heart Failure? *Circ Res* **95**, 754-763 (2004).
3. Steinberg, S.F. Oxidative stress and sarcomeric proteins. *Circ Res* **112**, 393-405 (2013).
4. Sugamura, K. & Keaney, J.F., Jr. Reactive oxygen species in cardiovascular disease. *Free Radic Biol Med* **51**, 978-992 (2011).
5. Pastore, A. & Piemonte, F. Protein Glutathionylation in Cardiovascular Diseases. *International Journal of Molecular Sciences* **14**, 20845 (2013).
6. Stojkov, D. *et al.* ROS and glutathionylation balance cytoskeletal dynamics in neutrophil extracellular trap formation. *The Journal of cell biology* **216**, 4073-4090 (2017).
7. Sanger, J.W., Ayoob, J.C., Chowrashi, P., Zurawski, D. & Sanger, J.M. Assembly of myofibrils in cardiac muscle cells. *Advances in experimental medicine and biology* **481**, 89-102; discussion 103-105 (2000).
8. Gautel, M. & Djinović-Carugo, K. The sarcomeric cytoskeleton: from molecules to motion. *The Journal of Experimental Biology* **219**, 135-145 (2016).
9. Willis, M.S., Schisler, J.C., Portbury, A.L. & Patterson, C. Build it up-Tear it down: protein quality control in the cardiac sarcomere. *Cardiovascular research* **81**, 439-448 (2009).

10. Tajsharghi, H. & Oldfors, A. Myosinopathies: pathology and mechanisms. *Acta neuropathologica* **125**, 3-18 (2013).

11. LeWinter, M.M. & Granzier, H. Cardiac titin: a multifunctional giant. *Circulation* **121**, 2137-2145 (2010).

12. Elzinga, G., Peckham, M. & Woledge, R.C. The sarcomere length dependence of the rate of heat production during isometric tetanic contraction of frog muscles. *The Journal of physiology* **357**, 495-504 (1984).

13. Woodhead, J.L., Zhao, F.Q. & Craig, R. Structural basis of the relaxed state of a Ca2+-regulated myosin filament and its evolutionary implications. *Proceedings of the National Academy of Sciences of the United States of America* **110**, 8561-8566 (2013).

14. Squire, J.M. Muscle myosin filaments: cores, crowns and couplings. *Biophysical reviews* **1**, 149 (2009).

15. van Dijk, S.J., Bezold, K.L. & Harris, S.P. Earning stripes: myosin binding protein-C interactions with actin. *Pflugers Archiv : European journal of physiology* **466**, 445-450 (2014).

16. Hitchcock-DeGregori, S.E. & Barua, B. Tropomyosin Structure, Function, and Interactions: A Dynamic Regulator. *Sub-cellular biochemistry* **82**, 253-284 (2017).

17. LeWinter, M.M., Wu, Y., Labeit, S. & Granzier, H. Cardiac titin: structure, functions and role in disease. *Clinica chimica acta; international journal of clinical chemistry* **375**, 1-9 (2007).

18. Granzier, H.L. & Labeit, S. The giant protein titin: a major player in myocardial mechanics, signaling, and disease. *Circ Res* **94**, 284-295 (2004).

19. Tskhovrebova, L. & Trinick, J. Properties of titin immunoglobulin and fibronectin-3 domains. *The Journal of biological chemistry* **279**, 46351-46354 (2004).

20. Castro-Ferreira, R., Fontes-Carvalho, R., Falcao-Pires, I. & Leite-Moreira, A.F. The role of titin in the modulation of cardiac function and its pathophysiological implications. *Arquivos brasileiros de cardiologia* **96**, 332-339 (2011).

21. Tskhovrebova, L. & Trinick, J. Titin: properties and family relationships. *Nature reviews. Molecular cell biology* **4**, 679-689 (2003).

22. Maruyama, K. Connectin/titin, giant elastic protein of muscle. *FASEB journal : official publication of the Federation of American Societies for Experimental Biology* **11**, 341-345 (1997).

23. Granzier, H. & Labeit, S. Cardiac titin: an adjustable multi-functional spring. *The Journal of physiology* **541**, 335-342 (2002).

24. Eckels, E.C., Tapia-Rojo, R., Rivas-Pardo, J.A. & Fernandez, J.M. The Work of Titin Protein Folding as a Major Driver in Muscle Contraction. *Annual review of physiology* **80**, 327-351 (2018).

25. Zhou, T. *et al.* CARP interacts with titin at a unique helical N2A sequence and at the domain Ig81 to form a structured complex. *FEBS letters* **590**, 3098-3110 (2016).

26. Lun, A.S., Chen, J. & Lange, S. Probing muscle ankyrin-repeat protein (MARP) structure and function. *Anatomical record (Hoboken, N.J. : 2007)* **297**, 1615-1629 (2014).

27. Garvey, S.M., Rajan, C., Lerner, A.P., Frankel, W.N. & Cox, G.A. The muscular dystrophy with myositis (mdm) mouse mutation disrupts a skeletal muscle-specific domain of titin. *Genomics* **79**, 146-149 (2002).

28. Raynaud, F. *et al.* Calpain 1-titin interactions concentrate calpain 1 in the Z-band edges and in the N2-line region within the skeletal myofibril. *The FEBS journal* **272**, 2578-2590 (2005).

29. Miller, M.K. *et al.* The muscle ankyrin repeat proteins: CARP, ankrd2/Arpp and DARP as a family of titin filament-based stress response molecules. *Journal of molecular biology* **333**, 951-964 (2003).

30. Donlin, L.T. *et al.* Smyd2 controls cytoplasmic lysine methylation of Hsp90 and myofilament organization. *Genes & development* **26**, 114-119 (2012).

31. Voelkel, T. *et al.* Lysine methyltransferase Smyd2 regulates Hsp90-mediated protection of the sarcomeric titin springs and cardiac function. *Biochimica et biophysica acta* **1833**, 812-822 (2013).

32. Jin, J.P. Titin-thin filament interaction and potential role in muscle function. *Advances in experimental medicine and biology* **481**, 319-333; discussion 334-315 (2000).

33. Rivas-Pardo, J.A. *et al.* Work Done by Titin Protein Folding Assists Muscle Contraction. *Cell reports* **14**, 1339-1347 (2016).

34. Granzier, H.L. & Labeit, S. Titin and its associated proteins: the third myofilament system of the sarcomere. *Advances in protein chemistry* **71**, 89-119 (2005).

35. Granzier, H. & Labeit, S. Structure-function relations of the giant elastic protein titin in striated and smooth muscle cells. *Muscle & nerve* **36**, 740-755 (2007).

36. Cazorla, O. *et al.* Differential expression of cardiac titin isoforms and modulation of cellular stiffness. *Circ Res* **86**, 59-67 (2000).

37. Wu, Y., Labeit, S., Lewinter, M.M. & Granzier, H. Titin: an endosarcomeric protein that modulates myocardial stiffness in DCM. *Journal of cardiac failure* **8**, S276-286 (2002).

38. Freiburg, A. *et al.* Series of exon-skipping events in the elastic spring region of titin as the structural basis for myofibrillar elastic diversity. *Circ Res* **86**, 1114-1121 (2000).

39. Helmes, M., Trombitas, K. & Granzier, H. Titin develops restoring force in rat cardiac myocytes. *Circ Res* **79**, 619-626 (1996).

40. Linke, W.A. *et al.* I-band titin in cardiac muscle is a three-element molecular spring and is critical for maintaining thin filament structure. *The Journal of cell biology* **146**, 631-644 (1999).

41. Spellmon, N., Holcomb, J., Trescott, L., Sirinupong, N. & Yang, Z. Structure and function of SET and MYND domain-containing proteins. *Int J Mol Sci* **16**, 1406-1428 (2015).

42. Wu, J. *et al.* Biochemical characterization of human SET and MYND domain-containing protein 2 methyltransferase. *Biochemistry* **50**, 6488-6497 (2011).

43. Xu, S., Zhong, C., Zhang, T. & Ding, J. Structure of human lysine methyltransferase Smyd2 reveals insights into the substrate divergence in Smyd proteins. *J Mol Cell Biol* **3**, 293-300 (2011).

44. Huang, J. *et al.* Repression of p53 activity by Smyd2-mediated methylation. *Nature* **444**, 629-632 (2006).

45. Cho, H.S. *et al.* RB1 methylation by SMYD2 enhances cell cycle progression through an increase of RB1 phosphorylation. *Neoplasia (New York, N.Y.)* **14**, 476-486 (2012).

46. Zhang, X. *et al.* Regulation of estrogen receptor alpha by histone methyltransferase SMYD2-mediated protein methylation. *Proceedings of the National Academy of Sciences of the United States of America* **110**, 17284-17289 (2013).

47. Hamamoto, R., Toyokawa, G., Nakakido, M., Ueda, K. & Nakamura, Y. SMYD2-dependent HSP90 methylation promotes cancer cell proliferation by regulating the chaperone complex formation. *Cancer letters* **351**, 126-133 (2014).

48. Olsen, J.B. *et al.* Quantitative Profiling of the Activity of Protein Lysine Methyltransferase SMYD2 Using SILAC-Based Proteomics. *Molecular & cellular proteomics : MCP* **15**, 892-905 (2016).

49. Du, S.J., Tan, X. & Zhang, J. SMYD proteins: key regulators in skeletal and cardiac muscle development and function. *Anatomical record (Hoboken, N.J. : 2007)* **297**, 1650-1662 (2014).

50. Gottlieb, P.D. *et al.* Bop encodes a muscle-restricted protein containing MYND and SET domains and is essential for cardiac differentiation and morphogenesis. *Nature genetics* **31**, 25-32 (2002).

51. Diehl, F. *et al.* Cardiac deletion of Smyd2 is dispensable for mouse heart development. *Plos One* **5**, e9748 (2010).

52. Sajjad, A. *et al.* Lysine methyltransferase Smyd2 suppresses p53-dependent cardiomyocyte apoptosis. *Biochimica et biophysica acta* **1843**, 2556-2562 (2014).

53. Sjoblom, B., Salmazo, A. & Djinovic-Carugo, K. Alpha-actinin structure and regulation. *Cellular and molecular life sciences : CMLS* **65**, 2688-2701 (2008).

54. Ribeiro Ede, A., Jr. *et al.* The structure and regulation of human muscle alpha-actinin. *Cell* **159**, 1447-1460 (2014).

55. Parmacek, M.S. & Leiden, J.M. Structure, function, and regulation of troponin C. *Circulation* **84**, 991-1003 (1991).

56. Shave, R. *et al.* Exercise-induced cardiac troponin elevation: evidence, mechanisms, and implications. *Journal of the American College of Cardiology* **56**, 169-176 (2010).

57. Takeda, S. Crystal structure of troponin and the molecular mechanism of muscle regulation. *Journal of electron microscopy* **54 Suppl 1**, i35-41 (2005).

58. Marin-Garcia, J. & Goldenthal, M.J. [The mitochondrial organelle and the heart]. *Revista espanola de cardiologia* **55**, 1293-1310 (2002).

59. Dorn, G.W., 2nd, Vega, R.B. & Kelly, D.P. Mitochondrial biogenesis and dynamics in the developing and diseased heart. *Genes & development* **29**, 1981-1991 (2015).

60. Park, S.Y. *et al.* Cardiac, skeletal, and smooth muscle mitochondrial respiration: are all mitochondria created equal? *American journal of physiology. Heart and circulatory physiology* **307**, H346-352 (2014).

61. Gustafsson, A.B. & Gottlieb, R.A. Heart mitochondria: gates of life and death. *Cardiovascular research* **77**, 334-343 (2008).

62. Huss, J.M. & Kelly, D.P. Mitochondrial energy metabolism in heart failure: a question of balance. *The Journal of clinical investigation* **115**, 547-555 (2005).

63. Dorn, G.W., 2nd Mitochondrial dynamics in heart disease. *Biochimica et biophysica acta* **1833**, 233-241 (2013).

64. Ong, S.B., Hall, A.R. & Hausenloy, D.J. Mitochondrial dynamics in cardiovascular health and disease. *Antioxidants & redox signaling* **19**, 400-414 (2013).

65. Heinz, S. *et al.* Mechanistic Investigations of the Mitochondrial Complex I Inhibitor Rotenone in the Context of Pharmacological and Safety Evaluation. *Scientific reports* **7**, 45465 (2017).

66. Bleier, L. & Drose, S. Superoxide generation by complex III: from mechanistic rationales to functional consequences. *Biochimica et biophysica acta* **1827**, 1320-1331 (2013).

67. Javadov, S. The calcium-ROS-pH triangle and mitochondrial permeability transition: challenges to mimic cardiac ischemia-reperfusion. *Frontiers in physiology* **6**, 83 (2015).

68. Ma, X. *et al.* Mitochondrial electron transport chain complex III is required for antimycin A to inhibit autophagy. *Chemistry & biology* **18**, 1474-1481 (2011).

69. Tsutsui, H., Kinugawa, S. & Matsushima, S. Oxidative stress and heart failure. *American journal of physiology. Heart and circulatory physiology* **301**, H2181-2190 (2011).

70. Dietl, A. & Maack, C. Targeting Mitochondrial Calcium Handling and Reactive Oxygen Species in Heart Failure. *Current heart failure reports* **14**, 338-349 (2017).

71. Giordano, F.J. Oxygen, oxidative stress, hypoxia, and heart failure. *The Journal of clinical investigation* **115**, 500-508 (2005).

72. Lenaz, G. *et al.* Role of mitochondria in oxidative stress and aging. *Annals of the New York Academy of Sciences* **959**, 199-213 (2002).

73. Heymes, C. *et al.* Increased myocardial NADPH oxidase activity in human heart failure. *Journal of the American College of Cardiology* **41**, 2164-2171 (2003).

74. Meneshian, A. & Bulkley, G.B. The physiology of endothelial xanthine oxidase: from urate catabolism to reperfusion injury to inflammatory signal transduction. *Microcirculation (New York, N.Y. : 1994)* **9**, 161-175 (2002).

75. Lambeth, J.D. NOX enzymes and the biology of reactive oxygen. *Nature reviews. Immunology* **4**, 181-189 (2004).

76. Dhalla, N.S., Temsah, R.M. & Netticadan, T. Role of oxidative stress in cardiovascular diseases. *Journal of hypertension* **18**, 655-673 (2000).

77. Lefer, D.J. & Granger, D.N. Oxidative stress and cardiac disease. *The American journal of medicine* **109**, 315-323 (2000).

78. Tomaselli, G.F. & Barth, A.S. Sudden cardio arrest: oxidative stress irritates the heart. *Nature medicine* **16**, 648-649 (2010).

79. Cervantes Gracia, K., Llanas-Cornejo, D. & Husi, H. CVD and Oxidative Stress. *Journal of clinical medicine* **6** (2017).

80. Violi, F., Cangemi, R. & Brunelli, A. Oxidative stress, antioxidants, and cardiovascular disease. *Arteriosclerosis, thrombosis, and vascular biology* **25**, e37; author reply e37 (2005).

81. Siti, H.N., Kamisah, Y. & Kamsiah, J. The role of oxidative stress, antioxidants and vascular inflammation in cardiovascular disease (a review). *Vascular pharmacology* **71**, 40-56 (2015).

82. Sachidanandam, K., Fagan, S.C. & Ergul, A. Oxidative stress and cardiovascular disease: antioxidants and unresolved issues. *Cardiovascular drug reviews* **23**, 115-132 (2005).

83. Duguez, S., Bartoli, M. & Richard, I. Calpain 3: a key regulator of the sarcomere? *The FEBS journal* **273**, 3427-3436 (2006).

84. Ali, M.A. *et al.* Titin is a target of matrix metalloproteinase-2: implications in myocardial ischemia/reperfusion injury. *Circulation* **122**, 2039-2047 (2010).

85. Kandasamy, A.D., Chow, A.K., Ali, M.A. & Schulz, R. Matrix metalloproteinase-2 and myocardial oxidative stress injury: beyond the matrix. *Cardiovascular research* **85**, 413-423 (2010).

86. Baghirova, S., Hughes, B.G., Poirier, M., Kondo, M.Y. & Schulz, R. Nuclear matrix metalloproteinase-2 in the cardiomyocyte and the ischemic-reperfused heart. *Journal of molecular and cellular cardiology* **94**, 153-161 (2016).

87. Ali, M.A. & Schulz, R. Activation of MMP-2 as a key event in oxidative stress injury to the heart. *Frontiers in bioscience (Landmark edition)* **14**, 699-716 (2009).

88. Schulz, R. Intracellular targets of matrix metalloproteinase-2 in cardiac disease: rationale and therapeutic approaches. *Annual review of pharmacology and toxicology* **47**, 211-242 (2007).

89. Suzuki, K., Hata, S., Kawabata, Y. & Sorimachi, H. Structure, activation, and biology of calpain. *Diabetes* **53 Suppl 1**, S12-18 (2004).

90. Strobl, S. *et al.* The crystal structure of calcium-free human m-calpain suggests an electrostatic switch mechanism for activation by calcium. *Proceedings of the*

National Academy of Sciences of the United States of America **97**, 588-592 (2000).

91. Momeni, H.R. Role of calpain in apoptosis. *Cell journal* **13**, 65-72 (2011).
92. Smith, M.A. & Schnellmann, R.G. Calpains, mitochondria, and apoptosis. *Cardiovascular research* **96**, 32-37 (2012).
93. Grek, C.L., Zhang, J., Manevich, Y., Townsend, D.M. & Tew, K.D. Causes and consequences of cysteine S-glutathionylation. *The Journal of biological chemistry* **288**, 26497-26504 (2013).
94. Xiong, Y., Uys, J.D., Tew, K.D. & Townsend, D.M. S-glutathionylation: from molecular mechanisms to health outcomes. *Antioxidants & redox signaling* **15**, 233-270 (2011).
95. Janssen-Heininger, Y.M. *et al.* Emerging mechanisms of glutathione-dependent chemistry in biology and disease. *Journal of cellular biochemistry* **114**, 1962-1968 (2013).
96. Martinez-Ruiz, A. & Lamas, S. Signalling by NO-induced protein S-nitrosylation and S-glutathionylation: convergences and divergences. *Cardiovascular research* **75**, 220-228 (2007).
97. Tao, L. & English, A.M. Protein S-glutathiolation triggered by decomposed S-nitrosoglutathione. *Biochemistry* **43**, 4028-4038 (2004).
98. Giustarini, D. *et al.* S-nitrosation versus S-glutathionylation of protein sulfhydryl groups by S-nitrosoglutathione. *Antioxidants & redox signaling* **7**, 930-939 (2005).

99. Gallogly, M.M. & Mieyal, J.J. Mechanisms of reversible protein glutathionylation in redox signaling and oxidative stress. *Current opinion in pharmacology* **7**, 381-391 (2007).

100. Tew, K.D. Redox in redux: Emergent roles for glutathione S-transferase P (GSTP) in regulation of cell signaling and S-glutathionylation. *Biochemical pharmacology* **73**, 1257-1269 (2007).

101. Menon, D. & Board, P.G. A role for glutathione transferase Omega 1 (GSTO1-1) in the glutathionylation cycle. *The Journal of biological chemistry* **288**, 25769-25779 (2013).

102. Deponte, M. Glutathione catalysis and the reaction mechanisms of glutathione-dependent enzymes. *Biochimica et biophysica acta* **1830**, 3217-3266 (2013).

103. Chen, C.A., De Pascali, F., Basye, A., Hemann, C. & Zweier, J.L. Redox modulation of endothelial nitric oxide synthase by glutaredoxin-1 through reversible oxidative post-translational modification. *Biochemistry* **52**, 6712-6723 (2013).

104. Morgan, B. *et al.* Multiple glutathione disulfide removal pathways mediate cytosolic redox homeostasis. *Nature chemical biology* **9**, 119-125 (2013).

105. Lo Conte, M. & Carroll, K.S. The redox biochemistry of protein sulfenylation and sulfinylation. *The Journal of biological chemistry* **288**, 26480-26488 (2013).

106. Saurin, A.T., Neubert, H., Brennan, J.P. & Eaton, P. Widespread sulfenic acid formation in tissues in response to hydrogen peroxide. *Proceedings of the National Academy of Sciences of the United States of America* **101**, 17982-17987 (2004).

107. Mallis, R.J., Buss, J.E. & Thomas, J.A. Oxidative modification of H-ras: S-thiolation and S-nitrosylation of reactive cysteines. *The Biochemical journal* **355**, 145-153 (2001).

108. Rozenberg, O. & Aviram, M. S-Glutathionylation regulates HDL-associated paraoxonase 1 (PON1) activity. *Biochemical and biophysical research communications* **351**, 492-498 (2006).

109. Mallis, R.J. *et al.* Irreversible thiol oxidation in carbonic anhydrase III: protection by S-glutathiolation and detection in aging rats. *Biological chemistry* **383**, 649-662 (2002).

110. Borges, C.R., Geddes, T., Watson, J.T. & Kuhn, D.M. Dopamine biosynthesis is regulated by S-glutathionylation. Potential mechanism of tyrosine hydroxylast inhibition during oxidative stress. *The Journal of biological chemistry* **277**, 48295-48302 (2002).

111. Casagrande, S. *et al.* Glutathionylation of human thioredoxin: a possible crosstalk between the glutathione and thioredoxin systems. *Proceedings of the National Academy of Sciences of the United States of America* **99**, 9745-9749 (2002).

112. Manevich, Y., Feinstein, S.I. & Fisher, A.B. Activation of the antioxidant enzyme 1-CYS peroxiredoxin requires glutathionylation mediated by heterodimerization with pi GST. *Proceedings of the National Academy of Sciences of the United States of America* **101**, 3780-3785 (2004).

113. Ralat, L.A., Manevich, Y., Fisher, A.B. & Colman, R.F. Direct evidence for the formation of a complex between 1-cysteine peroxiredoxin and glutathione S-

transferase pi with activity changes in both enzymes. *Biochemistry* **45**, 360-372 (2006).

114. Dalle-Donne, I., Rossi, R., Giustarini, D., Colombo, R. & Milzani, A. S-glutathionylation in protein redox regulation. *Free Radic Biol Med* **43**, 883-898 (2007).

115. Cabiscol, E. & Levine, R.L. The phosphatase activity of carbonic anhydrase III is reversibly regulated by glutathiolation. *Proceedings of the National Academy of Sciences of the United States of America* **93**, 4170-4174 (1996).

116. Adachi, T. *et al.* S-glutathiolation of Ras mediates redox-sensitive signaling by angiotensin II in vascular smooth muscle cells. *The Journal of biological chemistry* **279**, 29857-29862 (2004).

117. Klatt, P. *et al.* Redox regulation of c-Jun DNA binding by reversible S-glutathiolation. *FASEB journal : official publication of the Federation of American Societies for Experimental Biology* **13**, 1481-1490 (1999).

118. Lee, S.R., Kwon, K.S., Kim, S.R. & Rhee, S.G. Reversible inactivation of protein-tyrosine phosphatase 1B in A431 cells stimulated with epidermal growth factor. *The Journal of biological chemistry* **273**, 15366-15372 (1998).

119. Fratelli, M. *et al.* Identification by redox proteomics of glutathionylated proteins in oxidatively stressed human T lymphocytes. *Proceedings of the National Academy of Sciences of the United States of America* **99**, 3505-3510 (2002).

120. Pineda-Molina, E. *et al.* Glutathionylation of the p50 subunit of NF-kappaB: a mechanism for redox-induced inhibition of DNA binding. *Biochemistry* **40**, 14134-14142 (2001).

121. Passarelli, C. *et al.* Myosin as a potential redox-sensor: an in vitro study. *Journal of muscle research and cell motility* **29**, 119-126 (2008).

122. Chen, F.C. & Ogut, O. Decline of contractility during ischemia-reperfusion injury: actin glutathionylation and its effect on allosteric interaction with tropomyosin. *American journal of physiology. Cell physiology* **290**, C719-727 (2006).

123. Alegre-Cebollada, J. *et al.* S-glutathionylation of cryptic cysteines enhances titin elasticity by blocking protein folding. *Cell* **156**, 1235-1246 (2014).

124. Pan, K.T. *et al.* Mass spectrometry-based quantitative proteomics for dissecting multiplexed redox cysteine modifications in nitric oxide-protected cardiomyocyte under hypoxia. *Antioxidants & redox signaling* **20**, 1365-1381 (2014).

125. Steinberg, S.F. Oxidative Stress and Sarcomeric Proteins. *Circ Res* **112**, 393-405 (2013).

126. Beckendorf, L. & Linke, W.A. Emerging importance of oxidative stress in regulating striated muscle elasticity. *Journal of muscle research and cell motility* **36**, 25-36 (2015).

127. Mieyal, J.J., Gallogly, M.M., Qanungo, S., Sabens, E.A. & Shelton, M.D. Molecular mechanisms and clinical implications of reversible protein S-glutathionylation. *Antioxidants & redox signaling* **10**, 1941-1988 (2008).

128. Samarasinghe, K.T., Munkanatta Godage, D.N., VanHecke, G.C. & Ahn, Y.H. Metabolic synthesis of clickable glutathione for chemoselective detection of glutathionylation. *Journal of the American Chemical Society* **136**, 11566-11569 (2014).

129. Kekulandara, D.N., Samarasinghe, K.T.G., Godage, D.N.P.M. & Ahn, Y.H. Clickable glutathione using tetrazine-alkene bioorthogonal chemistry for detecting protein glutathionylation. *Organic & Biomolecular Chemistry* **14**, 10886-10893 (2016).

130. Lu, S.C. Glutathione synthesis. *Biochimica et biophysica acta* **1830**, 3143-3153 (2013).

131. Lu, S.C. Regulation of glutathione synthesis. *Molecular aspects of medicine* **30**, 42-59 (2009).

132. Samarasinghe, K.T. *et al.* A clickable glutathione approach for identification of protein glutathionylation in response to glucose metabolism. *Mol Biosyst* **12**, 2471-2480 (2016).

133. Burgoyne, J.R., Mongue-Din, H., Eaton, P. & Shah, A.M. Redox signaling in cardiac physiology and pathology. *Circ Res* **111**, 1091-1106 (2012).

134. Smith, M.A. & Reid, M.B. Redox modulation of contractile function in respiratory and limb skeletal muscle. *Respiratory physiology & neurobiology* **151**, 229-241 (2006).

135. Miura, H. *et al.* Role for hydrogen peroxide in flow-induced dilation of human coronary arterioles. *Circ Res* **92**, e31-40 (2003).

136. Kalogeris, T., Bao, Y. & Korthuis, R.J. Mitochondrial reactive oxygen species: a double edged sword in ischemia/reperfusion vs preconditioning. *Redox biology* **2**, 702-714 (2014).

137. Tidball, J.G. & Wehling-Henricks, M. The role of free radicals in the pathophysiology of muscular dystrophy. *Journal of applied physiology (Bethesda, Md. : 1985)* **102**, 1677-1686 (2007).

138. Chen, F.C. & Ogut, O. Decline of contractility during ischemia-reperfusion injury: actin glutathionylation and its effect on allosteric interaction with tropomyosin. *American Journal of Physiology-Cell Physiology* **290**, C719-C727 (2006).

139. Mollica, J.P. *et al.* S-Glutathionylation of troponin I (fast) increases contractile apparatus Ca2+ sensitivity in fast-twitch muscle fibres of rats and humans. *Journal of Physiology-London* **590**, 1443-1463 (2012).

140. Canton, M., Neverova, I., Menabo, R., Van Eyk, J. & Di Lisa, F. Evidence of myofibrillar protein oxidation induced by postischemic reperfusion in isolated rat hearts. *American Journal of Physiology-Heart and Circulatory Physiology* **286**, H870-H877 (2004).

141. Polewicz, D. *et al.* Ischemia induced peroxynitrite dependent modifications of cardiomyocyte MLC1 increases its degradation by MMP-2 leading to contractile dysfunction. *Journal of Cellular and Molecular Medicine* **15**, 1136-1147 (2011).

142. Grutzner, A. *et al.* Modulation of Titin-Based Stiffness by Disulfide Bonding in the Cardiac Titin N2-B Unique Sequence. *Biophysical Journal* **97**, 825-834 (2009).

143. Kusuoka, H., Porterfield, J.K., Weisman, H.F., Weisfeldt, M.L. & Marban, E. Pathophysiology and Pathogenesis of Stunned Myocardium - Depressed Ca-2+ Activation of Contraction as a Consequence of Reperfusion-Induced Cellular Calcium Overload in Ferret Hearts. *Journal of Clinical Investigation* **79**, 950-961 (1987).

144. Macfarlane, N.G. & Miller, D.J. Depression of Peak Force without Altering Calcium Sensitivity by the Superoxide Anion in Chemically Skinned Cardiac-Muscle of Rat. *Circ Res* **70**, 1217-1224 (1992).

145. Ferdinandy, P., Danial, H., Ambrus, I., Rothery, R.A. & Schulz, R. Peroxynitrite is a major contributor to cytokine-induced myocardial contractile failure. *Circ Res* **87**, 241-247 (2000).

146. Linke, W.A. Sense and stretchability: the role of titin and titin-associated proteins in myocardial stress-sensing and mechanical dysfunction. *Cardiovascular research* **77**, 637-648 (2008).

147. Samarasinghe, K.T.G. & Ahn, Y.H. Synthesizing Clickable Glutathione by Glutathione Synthetase Mutant for Detecting Protein Glutathionylation. *Synlett* **26**, 285-293 (2015).

148. Samarasinghe, K.T.G. *et al.* A clickable glutathione approach for identification of protein glutathionylation in response to glucose metabolism. *Mol Biosyst* **12**, 2471-2480 (2016).

149. Linke, W.A. Sense and stretchability: The role of titin and titin-associated proteins in myocardial stress-sensing and mechanical dysfunction. *Cardiovascular research* **77**, 637-648 (2008).

150. Bullard, B. *et al.* Association of the chaperone alpha B-crystallin with titin in heart muscle. *Journal of Biological Chemistry* **279**, 7917-7924 (2004).

151. Watanabe, N. & Mitchison, T.J. Single-molecule speckle analysis of actin filament turnover in lamellipodia. *Science (New York, N.Y.)* **295**, 1083-1086 (2002).

152. Dulyaninova, N.G., House, R.P., Betapudi, V. & Bresnick, A.R. Myosin-IIA heavy-chain phosphorylation regulates the motility of MDA-MB-231 carcinoma cells. *Molecular biology of the cell* **18**, 3144-3155 (2007).

153. Caccuri, A.M. *et al.* Properties and utility of the peculiar mixed disulfide in the bacterial glutathione transferase B1-1. *Biochemistry* **41**, 4686-4693 (2002).

154. Winther, J.R. & Thorpe, C. Quantification of Thiols and Disulfides. *Biochimica et biophysica acta* **1840**, 10.1016/j.bbagen.2013.1003.1031 (2014).

155. Tew, K.D. *et al.* The Role of Glutathione S-transferase P in signaling pathways and S-glutathionylation in Cancer. *Free radical biology & medicine* **51**, 299-313 (2011).

156. Gronwald, J.W. & Plaisance, K.L. Isolation and Characterization of Glutathione S-Transferase Isozymes from Sorghum. *Plant Physiology* **117**, 877-892 (1998).

157. Menon, D. & Board, P.G. A Role for Glutathione Transferase Omega 1 (GSTO1-1) in the Glutathionylation Cycle. *The Journal of biological chemistry* **288**, 25769-25779 (2013).

158. Greetham, D. *et al.* Thioredoxins function as deglutathionylase enzymes in the yeast Saccharomyces cerevisiae. *BMC Biochemistry* **11**, 3-3 (2010).

159. Fruscione, F. *et al.* Differential role of NADP+ and NADPH in the activity and structure of GDP-D-mannose 4,6-dehydratase from two chlorella viruses. *The Journal of biological chemistry* **283**, 184-193 (2008).

160. Bulger, J.E. & Brandt, K.G. Yeast glutathione reductase. I. Spectrophotometric and kinetic studies of its interaction with reduced nicotinamide adenine dinucleotide. *The Journal of biological chemistry* **246**, 5570-5577 (1971).

161. Wang, L. *et al.* Structure of human SMYD2 protein reveals the basis of p53 tumor suppressor methylation. *The Journal of biological chemistry* **286**, 38725-38737 (2011).

162. Krijt, J., Duta, A. & Kozich, V. Determination of S-Adenosylmethionine and S-Adenosylhomocysteine by LC-MS/MS and evaluation of their stability in mice tissues. *Journal of chromatography. B, Analytical technologies in the biomedical and life sciences* **877**, 2061-2066 (2009).

163. Isaacs, W.B., Kim, I.S., Struve, A. & Fulton, A.B. Biosynthesis of titin in cultured skeletal muscle cells. *The Journal of cell biology* **109**, 2189-2195 (1989).

164. Isaacs, W.B., Kim, I.S., Struve, A. & Fulton, A.B. Association of titin and myosin heavy chain in developing skeletal muscle. *Proceedings of the National Academy of Sciences of the United States of America* **89**, 7496-7500 (1992).

165. Ali, M.A.M. *et al.* Titin is a Target of Matrix Metalloproteinase-2 Implications in Myocardial Ischemia/Reperfusion Injury. *Circulation* **122**, 2039-U2106 (2010).

166. Gunther, L.K. *et al.* Effect of N-Terminal Extension of Cardiac Troponin I on the Ca(2+) Regulation of ATP Binding and ADP Dissociation of Myosin II in Native Cardiac Myofibrils. *Biochemistry* **55**, 1887-1897 (2016).

167. Zhang, Z., Biesiadecki, B.J. & Jin, J.P. Selective deletion of the NH2-terminal variable region of cardiac troponin T in ischemia reperfusion by myofibril-associated mu-calpain cleavage. *Biochemistry* **45**, 11681-11694 (2006).

168. Chung, C.S. *et al.* Shortening of the elastic tandem immunoglobulin segment of titin leads to diastolic dysfunction. *Circulation* **128**, 19-28 (2013).

169. Gallogly, M.M., Starke, D.W. & Mieyal, J.J. Mechanistic and kinetic details of catalysis of thiol-disulfide exchange by glutaredoxins and potential mechanisms of regulation. *Antioxidants & redox signaling* **11**, 1059-1081 (2009).

170. Greetham, D. *et al.* Thioredoxins function as deglutathionylase enzymes in the yeast Saccharomyces cerevisiae. *BMC Biochemistry* **11**, 3 (2010).

171. Park, J.W., Mieyal, J.J., Rhee, S.G. & Chock, P.B. Deglutathionylation of 2-Cys peroxiredoxin is specifically catalyzed by sulfiredoxin. *The Journal of biological chemistry* **284**, 23364-23374 (2009).

172. Peltoniemi, M.J., Karala, A.R., Jurvansuu, J.K., Kinnula, V.L. & Ruddock, L.W. Insights into deglutathionylation reactions. Different intermediates in the glutaredoxin and protein disulfide isomerase catalyzed reactions are defined by the gamma-linkage present in glutathione. *The Journal of biological chemistry* **281**, 33107-33114 (2006).

173. Chen, Y.R. & Zweier, J.L. Cardiac Mitochondria and Reactive Oxygen Species Generation. *Circ Res* **114**, 524-537 (2014).

174. Xu, S.T., Zhong, C., Zhang, T.L. & Ding, J.P. Structure of human lysine methyltransferase Smyd2 reveals insights into the substrate divergence in Smyd proteins. *J Mol Cell Biol* **3**, 293-300 (2011).

175. Diehl, F. *et al.* Cardiac Deletion of Smyd2 Is Dispensable for Mouse Heart Development. *Plos One* **5** (2010).

176. Voelkel, T. *et al.* Lysine methyltransferase Smyd2 regulates Hsp90-mediated protection of the sarcomeric titin springs and cardiac function. *Bba-Mol Cell Res* **1833**, 812-822 (2013).

177. Kojic, S., Radojkovic, D. & Faulkner, G. Muscle ankyrin repeat proteins: their role in striated muscle function in health and disease. *Crit Rev Cl Lab Sci* **48**, 269-294 (2011).

178. Chouchani, E.T. *et al.* A Unifying Mechanism for Mitochondrial Superoxide Production during Ischemia-Reperfusion Injury. *Cell Metabolism* **23**, 254-263 (2016).

179. Avner, B.S. *et al.* Myocardial infarction in mice alters sarcomeric function via post-translational protein modification. *Molecular and Cellular Biochemistry* **363**, 203-215 (2012).

180. Pan, K.T. *et al.* Mass Spectrometry-Based Quantitative Proteomics for Dissecting Multiplexed Redox Cysteine Modifications in Nitric Oxide-Protected Cardiomyocyte Under Hypoxia. *Antioxidants & redox signaling* **20**, 1365-1381 (2014).

181. Kandasamy, A.D., Chow, A.K., Ali, M.A.M. & Schulz, R. Matrix metalloproteinase-2 and myocardial oxidative stress injury: beyond the matrix. *Cardiovascular research* **85**, 413-423 (2010).

182. Letavernier, E. *et al.* The role of calpains in myocardial remodelling and heart failure. *Cardiovascular research* **96**, 38-45 (2012).

183. Willis, M.S., Schisler, J.C., Portbury, A.L. & Patterson, C. Build it up-Tear it down: protein quality control in the cardiac sarcomere. *Cardiovascular research* **81**, 439-448 (2009).

184. Castro, J.P., Jung, T., Grune, T. & Siems, W. 4-Hydroxynonenal (HNE) modified proteins in metabolic diseases. *Free Radical Biology and Medicine* **111**, 309-315 (2017).

185. Ternette, N. *et al.* Inhibition of Mitochondrial Aconitase by Succination in Fumarate Hydratase Deficiency. *Cell reports* **3**, 689-700 (2013).

186. Hein, S. *et al.* Deposition of nonsarcomeric alpha-actinin in cardiomyocytes from patients with dilated cardiomyopathy or chronic pressure overload. *Experimental & Clinical Cardiology* **14**, E68-E75 (2009).

187. Dispersyn, G.D., Geuens, E., Donck, L.V., Ramaekers, F.C.S. & Borgers, M. Adult rabbit cardiomyocytes undergo hibernation-like dedifferentiation when co-cultured with cardiac fibroblasts. *Cardiovascular research* **51**, 230-240 (2001).

188. Bell, R.A.V., Al-Khalaf, M. & Megeney, L.A. The beneficial role of proteolysis in skeletal muscle growth and stress adaptation (vol 6, 16, 2016). *Skeletal Muscle* **6** (2016).

189. Lahmers, S., Wu, Y.M., Call, D.R., Labeit, S. & Granzier, H. Developmental control of titin isoform expression and passive stiffness in fetal and neonatal myocardium. *Circ Res* **94**, 505-513 (2004).

190. Walker, J.S. & de Tombe, P.P. Titin and the developing heart. *Circ Res* **94**, 860-862 (2004).

191. Nagueh, S.F. *et al.* Altered titin expression, myocardial stiffness, and left ventricular function in patients with dilated cardiomyopathy. *Circulation* **110**, 155-162 (2004).

192. Akazawa, H. & Komuro, I. Roles of cardiac transcription factors in cardiac hypertrophy. *Circ Res* **92**, 1079-1088 (2003).

193. Liu, T. *et al.* Master redox regulator Trx1 upregulates SMYD1 & modulates lysine methylation. *Biochimica Et Biophysica Acta-Proteins and Proteomics* **1854**, 1816-1822 (2015).

194. Lim, C.C. *et al.* Anthracyclines induce calpain-dependent titin proteolysis and necrosis in cardiomyocytes. *Journal of Biological Chemistry* **279**, 8290-8299 (2004).

195. Miller, M.K. *et al.* The muscle ankyrin repeat proteins: CARP, ankrd2/Arpp and DARP as a family of titin filament-based stress response molecules. *Journal of molecular biology* **333**, 951-964 (2003).

ABSTRACT

FUNCTIONAL STUDY OF SMYD2 GLUTATHIONYLATION IN CARDIOMYOCYTES

by

DHANUSHKA MUNKANATTA GODAGE

August 2018

Advisor: Dr. Young-Hoon Ahn

Major: Chemistry (Biochemistry)

Degree: Doctor of Philosophy

Reactive oxygen species (ROS) are important signaling molecules that contribute to the etiology of multiple muscle-related diseases, including cardiomyopathy and heart failure. There is emerging evidence that cellular stress can lead to destabilization of sarcomeres, the contractile unit of muscle. However, it is not completely understood how cellular stress or ROS induce structural destabilization of sarcomeres or myofibrils. Protein glutathionylation is one of the major protein cysteine oxidative modifications that play an important role in redox signaling and oxidative stress. In this report, we used a clickable glutathione approach in a cardiomyocyte cell line, and found that SET and MYND Domain Containing 2 (SMYD2), lysine methyltransferase, can be selectively glutathionylated at Cys13. Functional studies showed that SMYD2 Cys13 glutathionylation serve as a key molecular event that leads to a loss of myofibril integrity and degradation of sarcomeric proteins mediated by matrix metalloprotease 2 (MMP-2) and calpain 1. Biochemical analysis demonstrated that SMYD2 glutathionylated at Cys13 loses its interaction with Hsp90 and N2A, a domain of titin that is important for

stress-sensing. Upon dissociation from SMYD2, N2A or titin was susceptible to degradation by MMP-2, suggesting a protective role of SMYD2 in sarcomere stability. Taken together, our results identify SMYD2 glutathionylation as a novel molecular mechanism by which ROS contribute to sarcomere destabilization and potentially muscle dysfunction.

AUTOBIOGRAPHICAL STATEMENT

DHANUSHKA MUNKANATTA GODAGE

EDUCATION

- Wayne State University, Detroit, MI **2013 -2018**
  Ph.D. in Chemistry (Biochemistry Major), GPA 3.89
  Advisor: Prof. Young-Hoon Ahn

- University of Colombo, Department of Chemistry, Sri Lanka **2007 - 2011**
  B.Sc. (Pharmacy special), GPA 3.29 Second class honors, upper division

AWARDS AND HONORS

- Outstanding Biological Chemistry student award, Department of Chemistry, Wayne State University, **2018**
- Poster presentation (1st place), Graduate and Postdoctoral Research Symposium, Wayne State University, **March 2018**
- Three-minute thesis (3MT) talk (3rd place), Graduate and Postdoctoral Research Symposium, Wayne State University, **March 2018**
- Poster presentation (2nd place), C.P. Lee Endowed Graduate Student Research Day, School of Medicine, Wayne State University, **October 2017**
- Rumble Fellowship, Department of Chemistry, Wayne State University, **2017-2018**
- Graduate Student Professional Travel Award, Wayne State University, **2017**
- Poster presentation (3rd place), Graduate and Postdoctoral Research Symposium, Wayne State University, **March 2017**
- Rumble Fellowship, Department of Chemistry, Wayne State University, **2016-2017**
- Graduate School Citation for Excellence in Teaching, **2016**

PUBLICATIONS

- **Munkanatta Godage, D. N. P.**; VanHecke, G. C.; Samarasinghe, K. T. G.; Feng, H.; Hiske, M.; Holcomb, J.;Yang, Z.; Jin, J. P.;Chung, C. S.; Ahn Y. H. SMYD2 glutathionylation leads to degradation of sarcomeric proteins. *Nature Communications* (under review)

- Kekulandara, D. N.; Samarasinghe, K. T. G.; **Munkanatta Godage, D. N. P.**; Ahn Y. H. Clickable glutathione using tetrazine-alkene bioorthogonal chemistry for detecting protein glutathionylation. *Org. Biomol. Chem.* **2016**, 14, 10886-10893.

- Samarasinghe, K. T. G.; **Munkanatta Godage, D. N. P.**; Zhou, Y.; Ndombera, F. T.; Weerapona, E.; Ahn, Y. H. Identification of protein glutathionylation in response to glucose metabolism. *Mol. Biosyst.* **2016**, 12, 2471-2480.

- Samarasinghe, K. T. G.; **Munkanatta Godage, D. N. P.**; VanHecke, G. C.; Ahn, Y. H. Metabolic Synthesis of Clickable Glutathione for Chemoselective Detection of Glutathionylation. *J. Am. Chem. Soc.* **2014**, 136, 11566-11569.